Annex 1 to final report under
ISTC Project No. 3690

PRE- AND POST-TEST CALCULATIONS OF PARAMETER-SF EXPERIMENTS UNDER ISTC PROJECT #3690

2009

List of abbreviations accepted

core – the core (fuel rod section from 0 to 1275 mm with tantalum heaters)
ECCS – emergency core cooling system
FA – fuel assembly
LTS – length of transition section
NPP – nuclear reactor plant
SOCRAT – system of branch codes for calculational analysis of severe accidents
TC – thermocouple
TS – test section

Computer code	Legend designation in Figures
SOCRAT	SOCRAT
ICARE/CATHARE	ICARE
RELAP/SCDAPSIM MOD3.2	RELAP
PARAM-TG	PARAM-TG
ATHLET-CD	ATHLET-CD
SCDAP/RELAP/FZK-PSI	RELAP/IRS

Contents

Introduction

According to the Work Plan for ISTC Project No.3690 the pre- and post-test calculations were planned in support of experimental program. The given report deals with the results of the corresponding calculational and analytical work. For numerical simulation of the experiments the widely used computer codes for NPP safety evaluation (SOCRAT, ICARE/CATHARE, RELAP/SCDAPSIM MOD3.2) were applied as well as engineering code PARAM-TG developed directly for numerical analysis of PARAMETER facility. The Project collaborators from GRS (Germany) applying the code ATHLET-CD, and also from PSI (Switzerland) applying the code SCDAP/RELAP/FZK-PSI took part in calculational studies. The main objective of pre-test calculations was justification of experiment scenarios and elaboration of recommendations on performing the experiments. At the stage of post-test calculations the applicability of the used nodalizations and models was checked and evaluation of the facility uncertainties was made.

In the course of the Project the calculational and analytical work on codes verifications against data of experiments of PARAMETER-SF series was proposed to the participants of the Project and supported by the collaborators. The pre-test calculation of PARAMETER-SF3 experiment carried out according to the developed specification [1] can be considered as a “blind” phase of codes verification that makes it possible to examine the ability the codes to predict the main characteristics. The post-test calculations allow, on the one hand, obtaining the more objective picture of experimental data reproducibility (and thus, of their reliability and self-consistency) and, on the other hand, allow considering the calculations as a component of verification and cross-verification of the codes.

It should be noted that since 1998 in Forschungzentrum Karlsruhe (FZK), Germany, a series of the experiments has been conducted under QUENCH program that are aimed at studying the hydrogen source term at flooding phase when the overheated assembly of PWR and VVER reactors are quenched with water [2,3,4,5]. The conditions of these experiments reproduce the conditions of the initial stage of severe accident when the core drying, its heating-up and the reflooding with water in case of recovery of ECCS occur. These experimental data are widely used for verification of computer codes. However, in all the experiments performed under this program only bottom flooding of the assembly was studied.

In the experiments of PARAMETER-SF series [6,7,8,9] performed at PARAMETER facility in FSUE SRI SIA "LUCH", 19-rod FAs that are identical to those used in VVER-1000 with respect to materials and dementions (fuel pellets, claddings, spacer grids) were studied under the conditions of top and bottom flooding. The conditions of these experiments reproduce the conditions of the initial stage of severe accident when the core drying occurs, then its heating-up and the reflooding with water in case of recovery of ECCS.

In PARAMETER-SF1 experiment the behaviour of VVER-1000 assembly overheated to 2000ºC was studied for the first time under top flooding conditions. In another experiment PARAMETER-SF2 hydrogen production was studied as well as efficiency of the combined flooding – from top and bottom simultaneously - of VVER-1000 assembly overheated up to 1500ºC (one of the specific features of VVER design is a possibility of the core reflooding from top and bottom). In PARAMETER-SF3 experiment the maximum temperatures were 1600ºC and the top flooding was studied only.

The first part of the report deals with the results of numerical post-test analysis of PARAMETER-SF2 experiment with the combined top and bottom flooding.

The pre-test PARAMETER-SF3 calculations included into the second part of the report were preceded by the work on evaluation of the facility uncertain parameters. For evaluation of the facility uncertain parameters the multi-variant post-test calculations of PARAMETER-SF2 experiment were performed.

The third concluding part of the given report is devoted to the post-test calculational study of PARAMETER-SF3 experiment with top flooding.

1 POST-TEST CALCULATIONS OF PARAMETER-SF2 EXPERIMENT. EVALUATION OF THE FACILITY UNCERTAINTIES

The pre-test numerical analysis of PARAMETER-SF3 experiment was preceded by the work on evaluation of the facility uncertain parameters (values of external resistance, of heat loss through the shroud). In this case the generally accepted practice provides for tuning the poorly determined values, performing a lot of runs, and finally the values are derived from runs in which the best coincidence of calculated and experimental data are obtaind. Thus, the multi-variant post-test calculations of PARAMETER-SF2 experiment were performed. The given section deals with the main results of calculations of Russian groups on calculations using the computer codes SOCRAT, ICARE/CATHARE, RELAP/SCDAPSIM MOD3.2, PARAM-TG, as well as calculations of the project collaborators using the computer codes ATHLET-CD, SCDAP/RELAP/FZK-PSI.

1.1 MAIN PHENOMENA AND PROCESSES STUDIED IN THE EXPERIMENTS OF SF SERIES

The main physical-and-chemical and thermohydraulic phenomena and processes that usually occur during the experiments with the reflooding are presented below (Table 1.1). Correletions (in three levels) between the phenomena and the PARAMETER-SF2 and PARAMETER-SF3 experiments are given in the matrix as well.

Consideration of the above-mentioned Table 1.1 convinces that the modelled experiments cover a wide spectrum of various physical-and-chemical processes. These processes occur in the course of severe accident in VVER and, finally, govern the accident scenario.

Two-phase flowing during top flooding is a complicated process interesting for studying. In particular, in the given conditions counter-current flow limitation can occur when water flow downward is difficult due to steam flow upwards in the assembly channel.

Another phenomenon of interest is radiative heat transfer in hexahedral FA geometry. As known, due to higher density of the assembly of hexahedral type, as, for instance, compared to square lattice, the radiative heat transfer in hexahedral lattice is somewhat weaker than in square one. To obtain the adequate spatial temperature distribution in FA the correct treatment of radiative heat transfer is needed in the geometry interested. The correct treatment means the adequate calculation of view factors and optical lengths in the groupe of rods enclosed into shroud.

In PARAMETER-SF3 experiment, as in PARAMETER-SF2, one more interesting thermomechanical process was observed – intensive spallation of oxide scale on zirconium rods and shroud. As a result, a considerable mass of zirconium dioxide scale, separated from rods and shroud, was accumulated in FA by the end of the experiments.

Table 1.1. Main physical-and-chemical and thermohydraulic phenomena and processes in the experiments of SF series

Phenomena or processes versus test: + – occurring - – not occurring 0 – phenomenon or process does not play a noticeable role	Experimental facility, experiment	
Typical phenomena and processes	PARAMETER facility, PARAMETER-SF2 experiment	PARAMETER facility, PARAMETER-SF3 experiment
Counter-current flow limitation under flooding	+	+
Oxidation of fuel rod claddings and zirconium-bearing structural components, including:	+	+
a) oxidation at the stage of flooding	+	+
b) low-temperature oxidation	+	+
Hydrogen absorption (hydrogenation) for zirconium-bearing structural components	+[10]	+
Oxidation at the stage of cooling with water or saturated steam	+	+
Eutectic interactions of the core materials ((UO_2-Zr(solid), Zr-SS, B_4C-SS	-	-
Deformation and failure of fuel rod claddings	+	+
Dissolution of fuel and zirconium dioxide with liquid metal zirconium	-	-
Oxidation of steel structures	0	0
Oxidation of control rod material B4C (Ag/In/Cd)	-	-
Spallation of zirconium dioxide scale	+	+
Radiative heat transfer, including:	+	+
Radiative heat transfer in the intact geometry of rods	+	+
Radiative heat transfer in the distorted geometry	-	-
Formation of porous debris in the core	0	0
Thermohydraulics of porous debris	-	-
Oxidation of porous debris	-	-
Melt formation in the core	-	-
Melt relocation downward and spreading	-	-
Melt interaction with the core components and shroud	-	-
Melt oxidation	-	-

1.2 DESCRIPTION OF NODALIZATIONS

1.2.1 Nodalization for SOCRAT computer code

All processes that occure in the test selected were classified into 3 groups:

– the most important phenomena that need to simulate thoroughly and accurately;

– less important or not significantly ones that influence on the result within the range of the assigned accuracy;

– the other processes and phenomena.

Simplifications and assumptions used to simulate the processes from the first group are presented in Table 1.2.

Description of assumption to simulate the processes from the second group is given in Table 1.3. For detailed simulation of these processes, substantial sophistication of the nodalization would be needed.

Table 1.2. Simplifications and assumptions used to simulate the main processes

Process and phenomenon	Simplifications and assumptions
Electric heating of simulators	Detail simulation of subcircuit over -800÷1900 mm elevation including Ta heater and part of electrods; simplidied simulation of resistances of remaining part of electrods, contact, and leads by introduction of additional resistance R_{add}. Calculation of current through each fuel rod considering its resistance depending on temperature and constant resistance R_{add}.
Local heat release due to electric heating and oxidation	Length of mesh varies from 100 mm in the lower part (below the steam and argon inlet location) to 25 mm at the elevation of 1000÷1300 mm
Radiative heat transfer	In radial direction only
Heat loss into body in the upper part	Parametrical consideration of radiative heat fluxes
Influence of spacer grid on heat transfer	Limitation of radiation flow (due to reradiation) and convective flow at the location of spacer grid
Influence of spacer grid on top flooding	Reducing of flow area by increasing the local resistance at the location of spacer grid

Table 1.3. Simplifications and assumptions used to simulate the processes from the second group

Process and phenomenon	Simplifications and assumptions
Argon and steam mixing	Argon has the same temperature as steam
Oxidation of spacer grid	Two upper grids are simulated only
Assembly flow area inhomogeneity, steam-argon mixture temperature nonuniformity over bundle cross-section	Not considered
Availability of thermocouples	One thermocouple is simulated at the elevation of 1250 mm for evaluation of difference in thermocouple readings and real cladding temperature and also for evaluation of its oxidation
Availability of peripheral pressure sensors and thermocouples	Simulated by zirconium rods for evaluation of their oxidation
Heater of the lower section	Heat flux is applied to the lower section external surface
Path from outlet to hydrogen measurement device location	Simulated in a simplified manner to take into account time delay connected with gas transport from the assembly to the device
Inlet nozzles	Not simulated. The source was modelled directly in LP element. Temperature of steam-argon mixture, starting from the time moment of 4000 s, was assumed equel to 660 K that allow the adequate calculation of cladding temperatures at the elevations of 0÷300 mm

Nodalization for calculation of the experiment is based on the facility design and presented in Figure 1.1. Hydraulic component of the model of the experimental facility test section can be conventionally divided into three parts:

– bottom part of the bundle (simulated length is 1124 mm from the lower part bottom (elevation -1264) to the lower edge of thermal insulation (elevation -140);

– central part (simulated length is 1490 mm and corresponds to the length of thermal insulation from the elevation of -140 mm to the elevation of 1350 mm (heated part at the elevations from 0 to 1275 mm));

– top part of the bundle (simulated length is 595 mm from the elevation of 1350 mm and above).

Hydraulic cells of unbranched network are simulated with the elements of CHANNEL type (they are rectangles in Figures 1.1). Their length along the coolant flow within the heated part of the test section is 0,1 or 0,05 mm, in the remaining part from 0,1 to 0,3 m. For branching the hydraulic network the element of CHAMBER type is used (the element with rounded boundaries). The outlet element EXIT is intended for consideration of transport delay. Boundary conditions of two types are used for the hydraulic network (element BOUNDARY): 2 – mass flow rate, 5 – pressure and temperature of the environment.

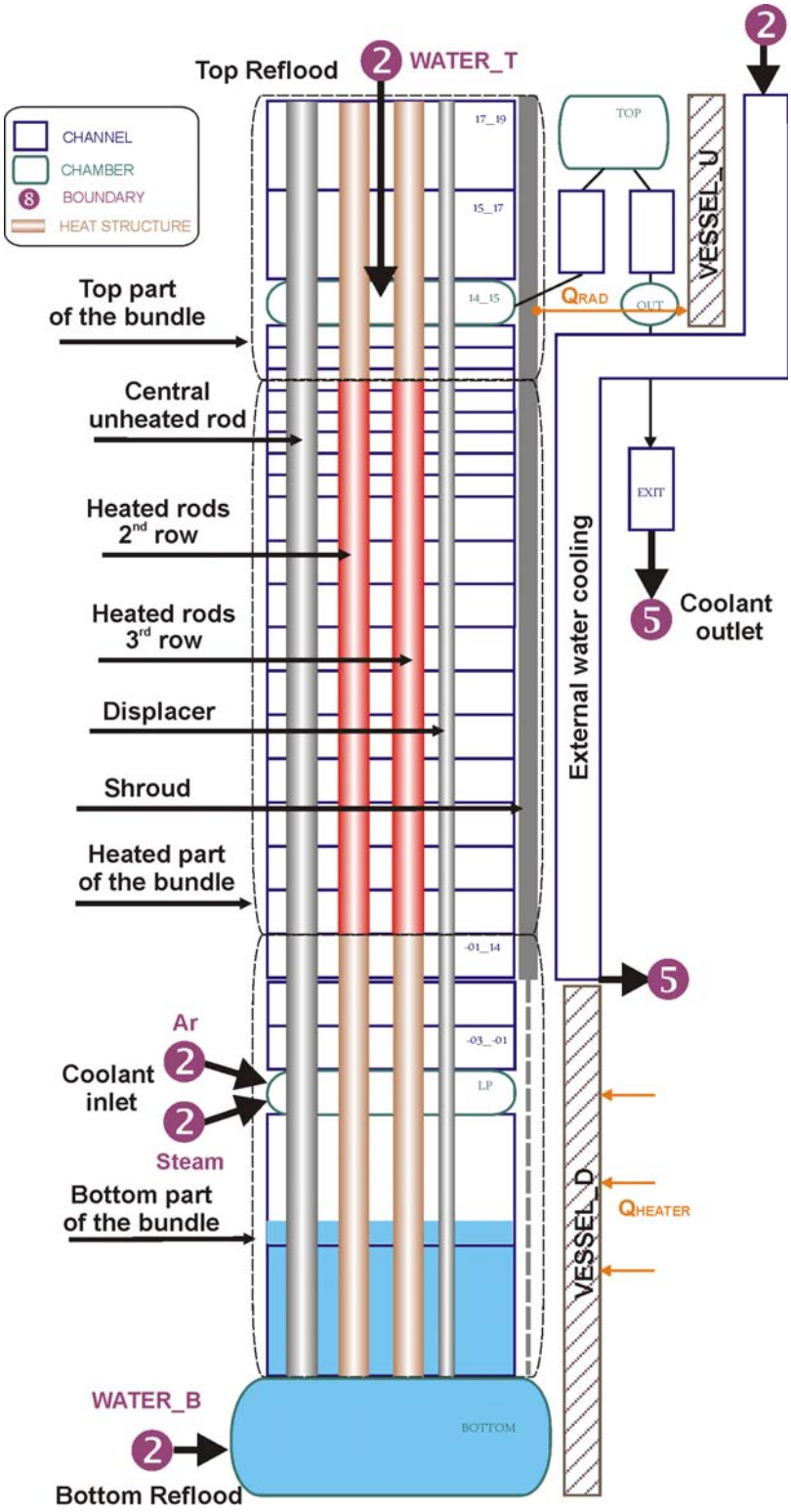

Figure1.1. Nodalization of the test section for SOCRAT computer code. PARAMETER-SF2 experiment. Post-test calculations.

Heat elements of the test section (fuel rod simulators, periphery pressure sensors and thermocouples, shroud, insulation, body) have the axial-ring nodalization. Over the height the elements are divided into 49 cells, over the radius – into five rings:

– HEAT_1 – central rod,
– HEAT_2 – 6 heated fuel rod simulators of the inner (second) row,
– HEAT_3 – 12 heated fuel rod simulators of the outer (third) row,
– DISP – 3 pressure sensors and 3 thermocouples ∅4 mm,
– SHROUD – the bundle shroud together with the thermal insulation and the body.

For evaluation of hydrogen production one thermocouples and two upper spacer grids are simulated.

It should be stressed that the external structures (the shroud, the thermal insulation, the thermal insulation shroud, and the test section body) along heated length are not simulated in details; they are modelled as a single SHROUD heat element with layered structure (Figure 1.2). Below the lower edge of thermoinsulation, the element SHROUD is represented with dummy cells, and above the upper edge of thermoinsulation the element simulates the guid tube of water injection system. This is caused by limitations of radiation model that applies to the elements of similar length only.

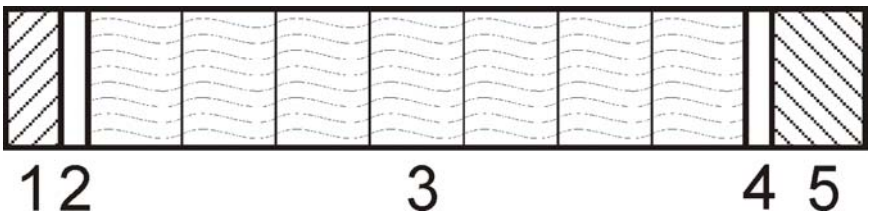

1 - shroud (zirconium);
2 - process gap (Ar);
3 - insulation (ZYFB3);
4 - process gap (Ar);
5 - thermal insulation shroud and body (steel);

Figure1.2. SHROUD element structure. PARAMETER-SF2 experiment. Post-test calculations.

SOCRAT computer code is intended for reactor calculations. For the analysis of experiments at PARAMETER facility in which heating-up of fuel rods is caused by Joule heating, electric heating model is available in the code. For PARAMETER-SF2 bundle, the electric heating model is applied only to the subcircuit with length of 2700 mm that consists of the tantalum heaters (with length of 1275 mm) and a portion of upper and lower electrodes. The rest part of electric circuit is simulated in a simplified manner by a constant resistance R_{add}. Figure 1.3 shows the corresponding electric circuit: constant resistance R_{add} (tuned parameter), length 0÷1275 mm corresponds to the tantalum heater, lengths -800÷0 and 1275÷1900 mm (marked with blue) simulate parts of electrodes.

Figure1.3. Fuel rod electric circuit model. PARAMETER-SF2 experiment. Post-test calculations.

The value of additional resistance was identified from the runs in which the best coincidence of calculated and experimental data in SF2 experiment within the range of “cold” temperatures (300-1000 K) was obtained because the influence of the heat losses at higher temperatures is not so substantial.

1.2.1.1 Initial and boundary conditions

The initial conditions of PARAMETER-SF2 experiment include the values of temperatures of the bundle, the shroud, the insulation, the body at the beginning of the experiment (t=0) corresponding to indoor temperature, axial and, generally speaking, angle (if absence of axial symmetry is considered) dependences (profiles) of these temperatures. The same time moment (t=0) is assumed as the beginning of simulation by SOCRAT computer code.

The exact experimental data of PARAMETER-SF2 on the supplied electric power (Figure 1.19) were used as the boundary conditions.

For mass flow rates of steam and argon the averaging was applied (Figures 1.20 and 1.21).

Water flow rates of top and bottom flooding were assumed equal to 40 and 130 g/s, respectively, the time of flooding switching on and switching off was in exact correspondence with the experimental value, a delay of water entering was not simulated.

Coolant temperature at the test section inlet was assigned proceeding from the thermal balance (equilibrium for mixture) considering heat losses at inlet sleeves (see Table 1.3)

Flow rate of water for cooling the test section was assumed to be constant and equal to 40 g/s.

1.2.2 Nodalization for RELAP/SCDAPSIM computer code

Nodalization (Figure 1.4) is broken down into three parts:

– lower part (1167 mm) from the level of leads to the elevation –177 mm from the beginning of the heated part;

– central part with power release: 1275 mm tantalum electrodes, 158 mm above and 177 mm below with molybdenum electrodes;

– upper part with the length of 600 mm from the end of central part.

Central part of the test section nodalization includes heat elements for simulation of the central rod (element *fuel*), 6 heated fuel rod simulators of the internal row (element *cora*), 12 heated fuel rod simulators of the external row (element *cora*), the shroud and external structures (element SHROUD), spacing grids (6 pieces) located in the central part.

Inlet nozzles, the path upstream of hydrogen detector were not included into the test section nodalization.

Structure of heat element SHROUD is presented in Figure 1.5. The heat element SHROUD is simulated in the heated part only.

Presence of spacing grids was considered both in hydraulic processes, and during oxidation. Presence of thermocouples and channels for pressure measurement was not considered. Argon and steam mixing was assumed to be ideal. Radiant heat transfer was simulated in radial direction only.

Due to limitations of the given code version it is impossible to breakdown the elements *cora*, simulating the fuel rods over the height, into more than 20 elements and to use more than 2 types of materials for heaters. Therefore presence of simulators outside the central section was simulated only by means of their consideration in the channel flow area. Tantalum electric heater was simulated along the assembly heated part length of 1275 mm, as well as a part of leads (along the length of 177 mm down of tantalum heater and 158 mm above it. Power losses in the leads not simulated, as well as in electric wires from the generator terminals to current leads, were considered by means of introducing the additional electric resistance (7 mΩ per a simulator). In calculation of resistance of the simulated section the temperature dependence is considered.

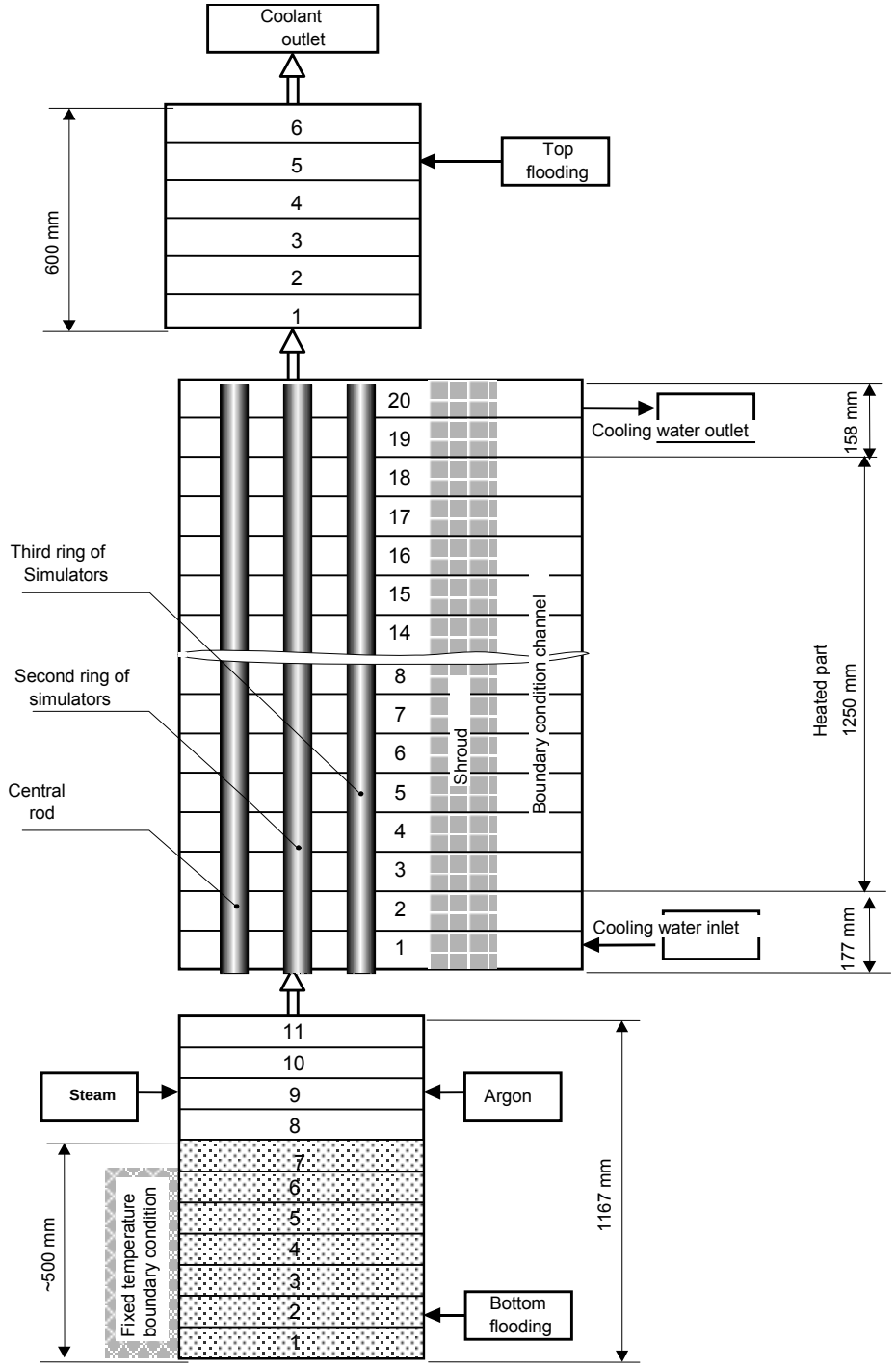

Figure 1.4. Nodalization for RELAP/SCDAPSIM MOD3.2 computer code. PARAMETER-SF2 experiment. Post-test calculations.

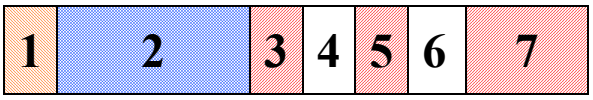

1 - shroud (zirconium);
2 - insulation;
3 - insulation housing;
4 - air gap;
5 - water cooling housing;
6 - air gap;
7 - steel vessel

Figure 1.5. Structure of the heat element SHROUD. PARAMETER-SF2 experiment. Post-test calculations.

1.2.2.1 Initial and boundary conditions

Boundary conditions for electric power, temperature, flow rate of steam, argon, water of top and bottom flooding correspond exactly to the experimental ones.

For simulation of heat transfer between the vessel and air environment of the room the constant temperature is assigned as the boundary condition on the housing outer surface. With this aim the channel with high water flow rate is connected to its outer surface to maintain the constant temperature of the wall of about 70ºC.

In the bundle lower part from the lower current leads to the inlet nozzles the wall temperature and water level in this channel are maintained constant. During the time of calculation the level of water that cools the current leads decreases by less than 0.5%, and hence does not influence the behaviour of the heated part.

Beginning of water supply for flooding is assigned not by the time but by reaching the maximum temperature of claddings that makes possible to avoid the bundle overheating or underheating in the calculations. A delay is simulated for actuation of bottom flooding that corresponds to the experimental delay because the water level in the lower part is close to the experimental value (exceeds by 50 mm).

1.2.2.2 Database on material properties

The following database on material properties is used: for the shroud materials – according to the data on experimental facility, for fuel, heaters and cladding – from the standard library of RELAP/SCDAPSIM MATPRO.

1.2.3 Nodalization for ICARE/CATHARE V1 computer code

For simulation in ICARE/CATHARE V1 computer code the detailed nodalization is applied. With this, separate FA elements are fixed to the geometry of breakdown into radial and vertical cells.

Figures 1.6 and 1.7 present the scheme of model of FA working area in two sections.

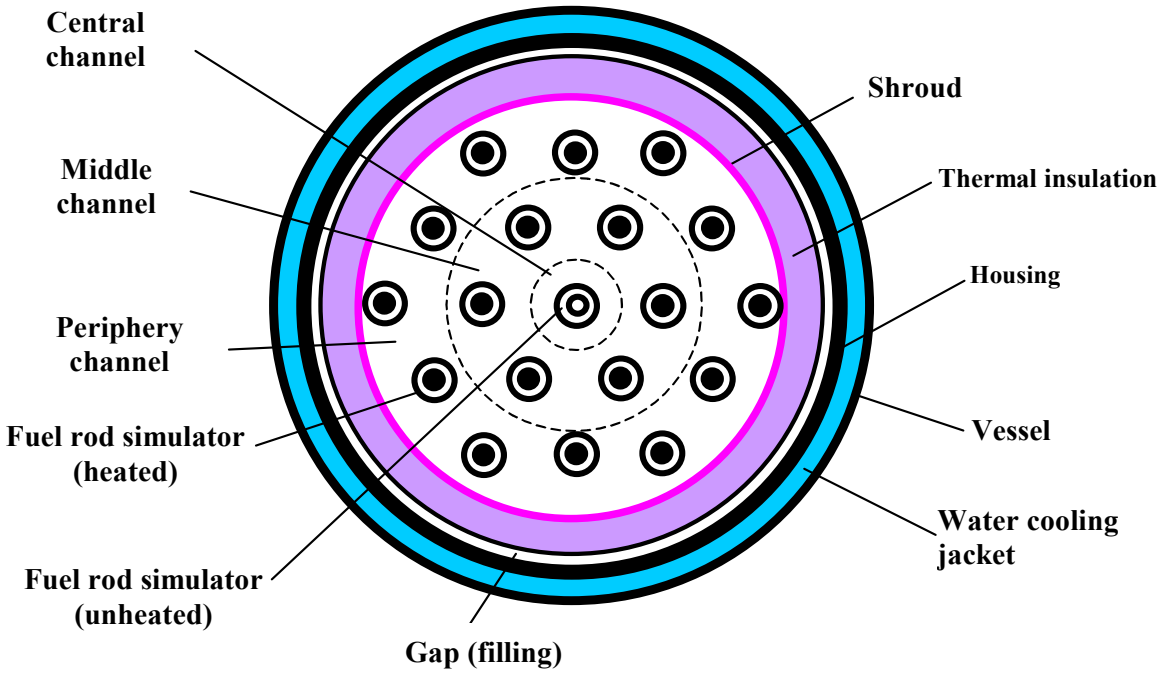

Figure 1.6. Scheme of model FA arrangement in radial section.

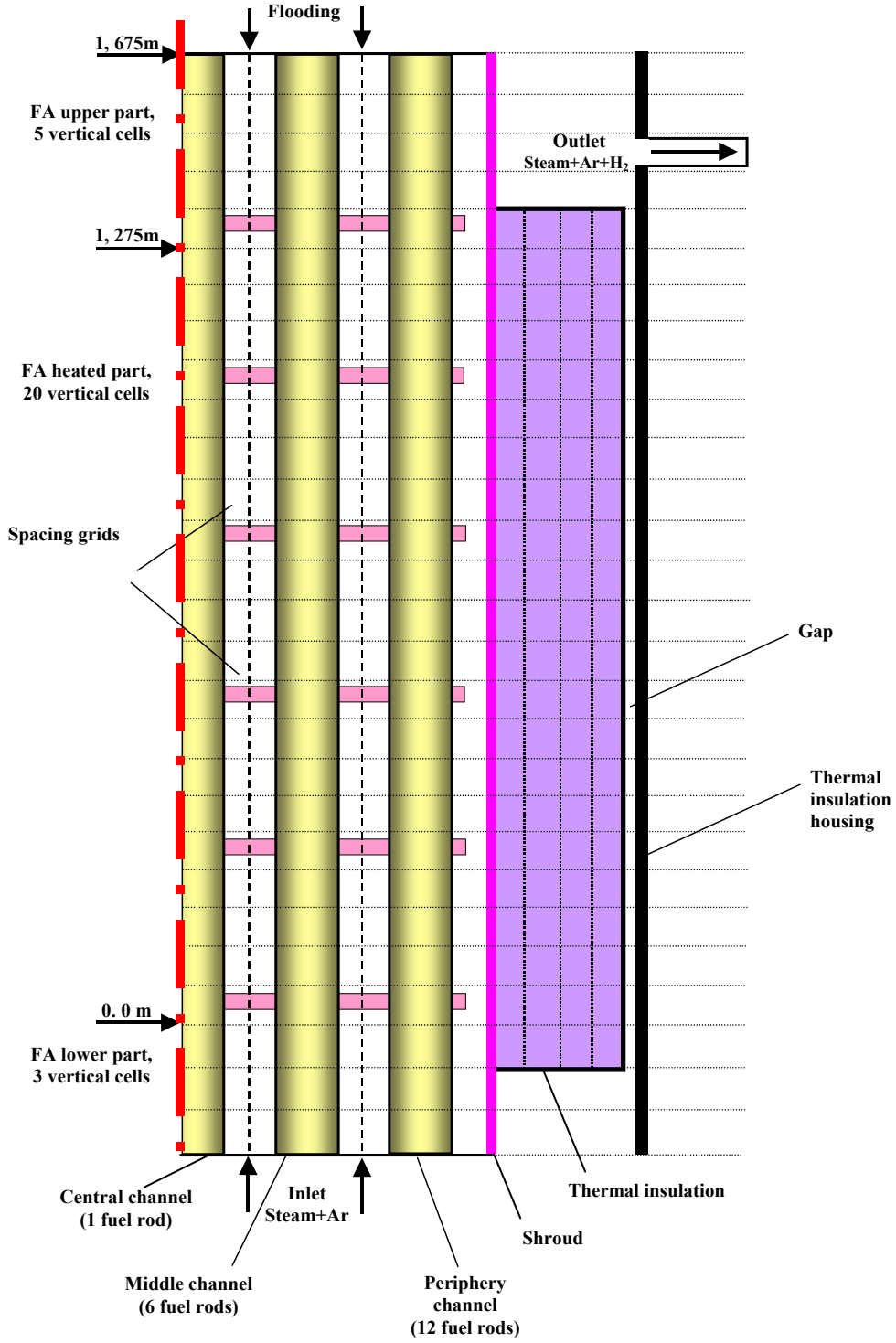

Figure 1.7. Scheme of model FA arrangement in vertical section (right side).

Figure 1.6 shows radial breakdown of FA hydraulic channel at PARAMETER facility into three parts (cells) covering the central fuel rod simulator, six middle fuel rod simulators and 12 periphery simulators, respectively. With this, among the periphery displacers two groups by six fuel rod simulators are picked out with different distance to the centre for detailed consideration of radiative heat transfer. In the scheme there are six displacers (thermocouples and pressure pick-ups).

The shroud and thermal insulation in the model (see Figure 1.6) are represented with conical rings. In all radial concentric structures the heat conduction transfer is simulated up to the water cooling jacket. Additionally for the region of the gap with filling the model of radiative heat transfer is applied.

As shown in Figure 1.7, the FA hydraulic channel of PARAMETER facility is broken down in vertical direction into 28 cells and there are three typical parts:

– lower part – upstream of the heated zone beginning;

– central part including the heated zone;
– upper part.

During simulation the nodalization is applied with small axial cell spacing (up to 6 cm in the heated zone). Proceeding from the previous calculations of 12 experiments on reflooding using ICARE/CATHARE V1 computer code, such breakdown provides for satisfactory accuracy of the flooding front motion simulation.

1.2.3.1 Initial and boundary conditions

Time dependencies of the loaded electric power, flow rates of steam, argon, water of top and bottom flooding are assigned in the calculations with the use of ICARE/CATHARE code according to the experimental data. In addition, for post-test SF2 calculation the experimental values of the housing insulation temperatures were used as the boundary conditions.

The heater components of molybdenum within the frame of numerical scheme (Figure 1.7) are presented partially. General external resistance was found out in the course of the preceding work on SF1 test for pre-test calculations of SF2. It was corrected in the course of the current post-test calculation of SF2 and was found out to be $4.0 \cdot 10^{-4}$ Ω.

1.2.3.2 Database on material properties

For the majority of materials (UO2, Fe, Zr-phase, etc.) the standard database is applied with the addition of properties of the tantalum element used as the heater material. Starting from the post-test calculation of SF2 experiment for zirconium oxidation the correlations are applied that were developed in IBRAE on the basis of processing a number of experimental data and adapted to ICARE/CATHARE computer code [11].

1.2.4 Nodalization for PARAM-TG computer code

The engineering computer code PARAM-TG is developed in SRI SIA "LUCH" especially for the PARAMETER test facility intended to define modes of electric power supply and flow rates of steam and gas mixtures to satisfy a designed temperature scenario. The code was used for all tests performed at the PARAMETER test facility with the assemblies made up of one, 19 and 37 fuel rods.

The nodalization of the code makes possible to consider the majority of structural components of PARAMETER test section. The nodalization used for calculations of SF2 and SF3 experiments is presented in Figures 1.8, 1.9. Figure 1.8 gives the axial nodalization the test section. In the nodalization almost the whole geometry and materials are taken into account along the length of the test section: claddings, pellets, heaters, periphery rods (pressure sensors), shroud, thermal insulation, thermal insulation shroud, bodies. Spacer grids were not considered.

Fuel rods heating is treated by electric heating model. Simulation of the electric circuit in PARAMETER-SF2, SF3 experiments is made in details along the whole length of the simulator from the lower to the upper supplying buses taking into account the actual sizes and materials of the heater and electrodes.

Heat losses througth the shroud were calculated for all layers and all actual gaps, beginning with the shroud and ending with the cooling jacket, considering the convective, contact, molecular and radiative heat conduction.

Heating of the body lower part to the temperature of 145-150°C, made at the beginning of the experiment before the moment of steam swithing on, was simulated with the help of introducing the dummy path 5 (Figure 1.8) filled with water at temperature of 160°C.

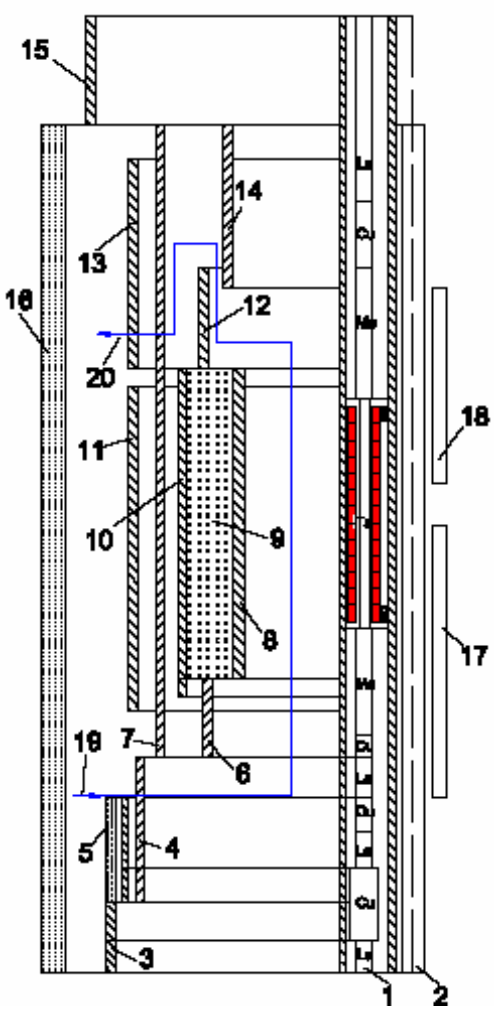

1 – heated fuel rod (with the heater), 2 – central fuel rod, displacers, 3 – body 203x2, 4 – body 156x6, 5 – path to model heating of body 4 with insulation, 6 – bellows simulator, 7 – body 133x6, 8 – shroud, 9 – thermoinsulation ZYFB-3, 10 – thermal insulation shroud, 11 – housing of cooling jacket in the middle section, 12 – cilinder, 13 – housing of cooling jacket in the upper section, 14 – guide tube, 15 – upper water tank wall, 16 – room wall, 17, 18 – thermocouples inserted from bottom and from top, 19, 20 – inlet and outlet.

Figure 1.8. Axial nodalization of the test section for PARAM-TG code.

Figure 1.9 presents the cross-section of the test section with no thermocouples. The coolant area is broken down into separate paths (channels) by boundaries of solid bodies and fictitious lines. The section is broken down into 36 paths. In the periphery paths 25 – 36 the displacers are shown.

In the code the system of heat conduction equations for solid bodies and equations of hydraulics and heat transfer for liquids are solved.

In calculation of temperatures the radiative heat transfer in the section is considered. In the code the radiation view factors between separate bodies are calculated.

Along the length the test bundle is divided into meshes with similar geometry and composition of materials. The number of meshes along the length is arbitrary. For instance, in SF2 test calculations the number of meshes is 28. The time step is assigned and can be change in the course of calculation. Convergence is assured by iterations at each time step.

In the course of calculation the heat release in the heater of each model fuel rod was calculated on the basis of Ohm's law considering the dependence of electric resistance of heaters and current leads on the temperature.

In gas gaps between the shroud and thermal insulation, and between thermal insulation and the thermal insulation shroud the radiative transfer is considered.

Oxidation correlation proposed by VNIINM is used for calculation of oxidation heat and thickness of formed zirconium oxide.

Steam-gas mixture flows upwards from steam inlet 19 up to lower edge of guide tube 14 (Figure 1.8), as well as in the gap between the cilinder 12 and the body 7. Guide tube 14 is assumed

to fill with the stagnant argon. Regions of stagnant argon are also between the guide tube 14 and the body 7 above the upper end of cilinder 12 and below steam inlet 19 in the lower part of the test section down to the level of water filled into the lower part of the test section.

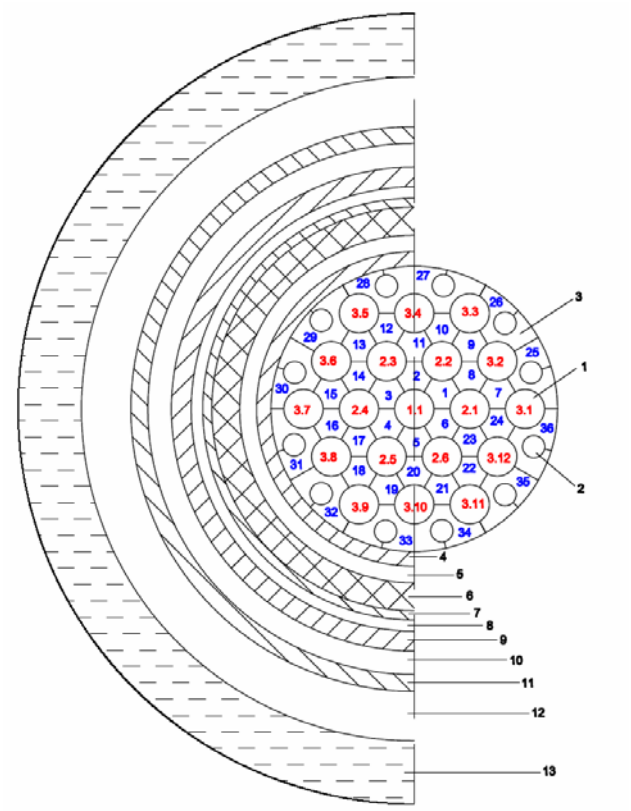

1 – fuel rods, 2 – displacers, 3 – paths (channels), 4 – shroud (8), 5 – gas gap between insulation and shroud, 6 – insulation ZYFB-3 (9), 7 – thermal insulation shroud (10), 8 – gas gap between thermal insulation shroud and body, 9 – test-section body 156x6(7), 10 – cooling path in cooling jacket, 11 – external tube of the cooling jacket (11), 12 – gas atmosphere in room, 13 – room wall (16). The digit in brackets is No. of element in Figure 1.8.

Figure 1.9. Scheme of the PARAMETER facility model in radial section.

1.2.4.1 Description of initial and boundary conditions

Initial conditions

The values of indoor temperatures (290 K for all materials of the test section) were used as the initial conditions.

Boundary conditions

In post-test calculations of SF2 and SF3 experiments the values of temperatures and flow rates of steam and argon at the test section inlet, as well as of temperatures and flow rates of water for cooling the test section body depending on time were taken to be their experimental values, and for the pre-test calculations – those measured in the course of starting-up and adjustment.

Boundary conditions for heat flux are applied at boundaries of solid bodies/flows to treat heat transfer. Steam-gas mixture at the inlet (19, Figure 1.8) was assume to be ideal mixing.

1.2.4.2 Parameters of the nodalization in post-test calculations of SF2 test

Parameters of the nodalization correspond, in the main, to those described in the "Protocol of results of PARAMETER-SF2 experiment (3 April, 2007)" [7]). The main parameters of the test section used in the post-test calculations of SF2 are presented in Table 1.4.

Table 1.4. Main parameters of the test section in the post-test calculations of SF2

Inner radii of the test bundle layers over heated zone, mm, and their materials (in brackets – No. of a layer in Figure 1.9)	Value, material
Shroud (4)	33, Zr1%Nb

Gas gap (5)		35, argon
Thermal insulation (6)		35.2; ZYFB3
Thermal insulation shroud (7)		58, steel
Gas gap (8)		59, argon
Test section body (9)		60.5; steel
Cooling path in cooling jacket (10)		66.5; water
External tube of cooling jacket (11)		68.5; steel
Gas atmosphere in room (12)		69.5; nitrogen
Room wall (13)		1000, steel
Some parameters along the bundle length		
Coordinate of the steam and argon inlet, mm (0 mm elevation corresponds to the lower edge of heated zone)		-372
Coordinate of the steam and argon outlet, mm		1425
Coordinates of the lower and upper edges of modelled length of the test section, mm		-1272: 2165
Total number of heat structures (from…to) Solid Gaseous or liquid		 21 – 49 37 – 49
Total number of cells along the length and within the heated zone		179 : 67
Material of the heaters and electrodes (from the test section bottom)		
Material	Length, mm	Diameter, mm
Brass *)	50	4.71
Copper **)	390	9.13
Brass	230	6
Copper cable	150	6
Copper	22	6
Brass	130	6
Molybdenum	300	6
Tantalum	1275	4
Molybdenum	300	6
Copper	20	6
Brass	570	6
In the calculations 6 displacers are modelled to be located in paths 25, 27, 29, 31, 33, 35 (Figure 1.9)		
In the calculations 10 upper thermocouples are modelled to be located in paths 7, 11, 12, 15, 22, 26, 29, 30, 35, 36 (Figure 1.9): T2111, T2411, T3311, T2312.5, T2612.5, T31112.5, T3113, T3513, T3713, T2314		
Coordinates of cooling path of the middle section and water flow rate: - 270 mm, 1300 mm, 50 g/s		
Coordinates of cooling path of the upper section and water flow rate: 1354 mm, 1873 mm, 50 g/s		
Water level in the test section bottom part, mm		-550
Coordinates of insulation, mm	-165	1325

*) rod-by-rod division is made conventionally for common brass current lead
**) copper current lead outside fuel rod

1.2.5 Nodalization for ATHLET-CD computer code

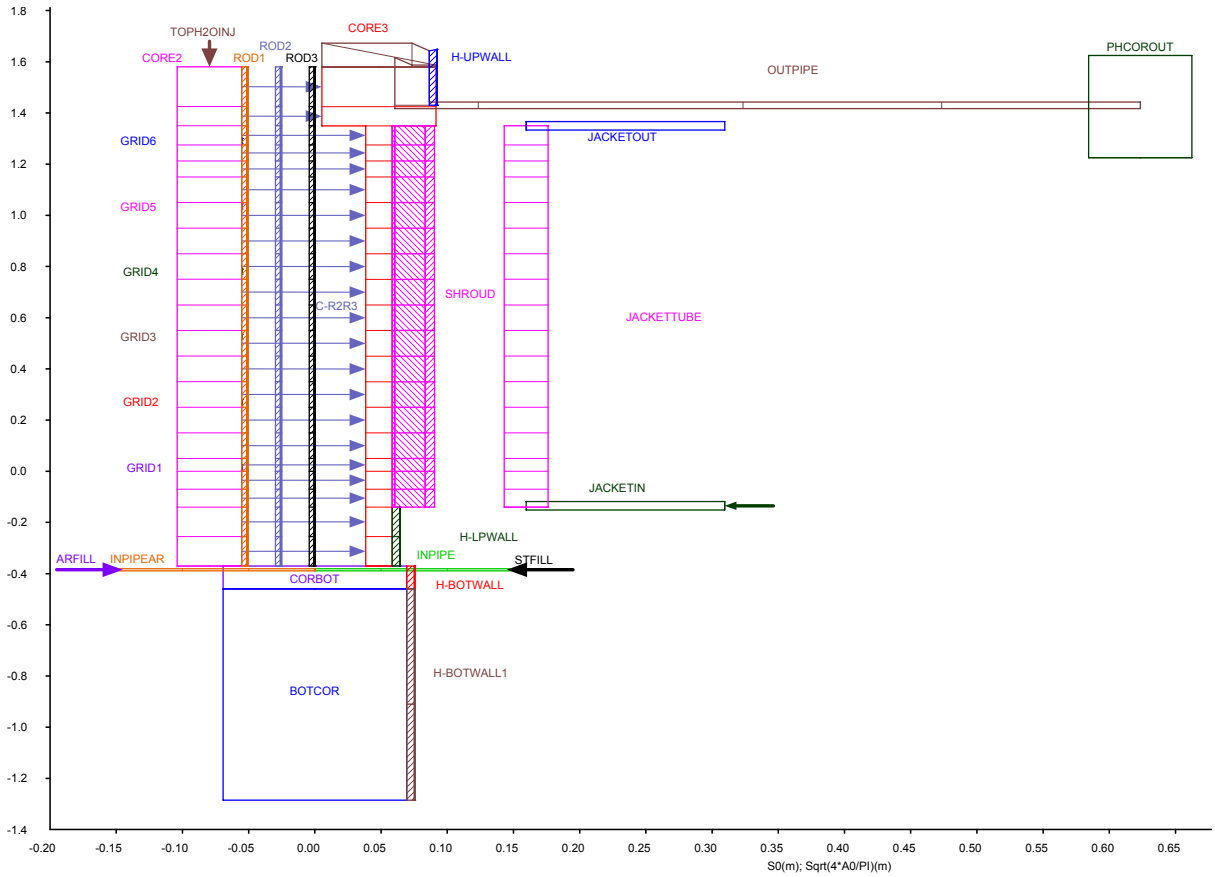

Figure 1.10. Nodalization for ATHLET-CD computer code. PARAMETER-SF2 experiment. Post-test calculations.

Flow Channels [12]:
- Central Bundle 85.7 %
- Outer Bypass 14.3 %
- Cooling Jacket

Structures
- Rods:
  - ROD1 (1)
  - ROD2 (6)
  - ROD3 (12)
- Grids (6)
- Shroud / Insulation
- Cooling Jacket Walls

Cladding oxidation model: Leistikow / Prater-Courtright correlation was used (IOXMOD = 19) instead of recommended Sokolov correlation (WWER: Zr1%Nb) (IOXMOD = 18)

- Electrical resistance of electrodes defined corresponding to given temperature dependency of Mo, Ta; Brass not considered in calculations (below / above simulated core region). External resistance 1 mΩ/rod

- Default values for interfacial friction parameters are used
- Hydraulic diameter in core region: $D_H=3.8\cdot10^{-3}$ m (=D_H at grid positions)

1.2.6 Nodalization for SCDAP/RELAP/FZK-PSI computer code

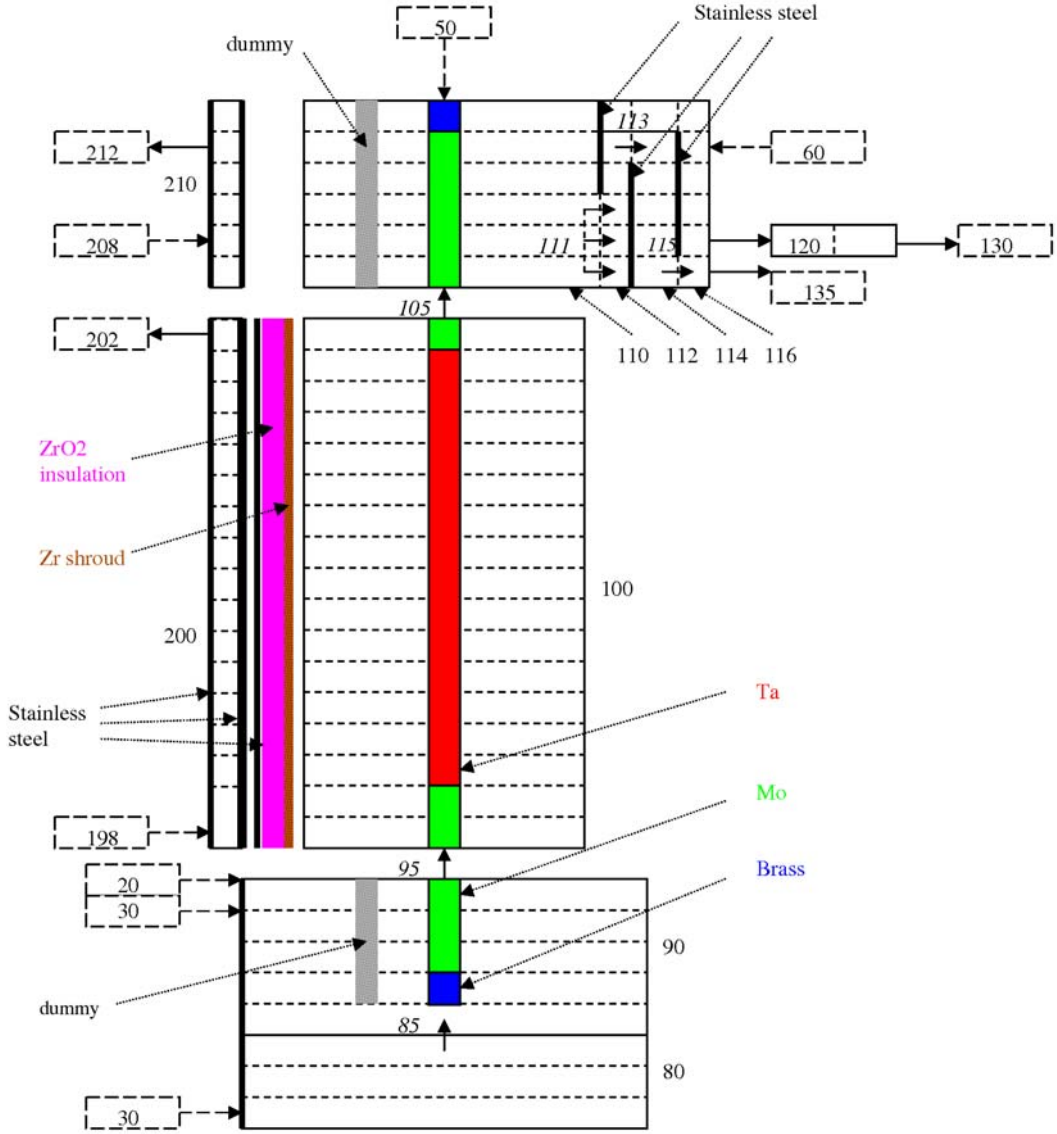

Figure 1.11. Nodalization for SCDAP/RELAP/FZK-PSI. computer code. PARAMETER-SF2 experiment. Post-test calculations.

Experimental boundary conditions [13]:
- pressure, steam and Ar flows, inlet temperatures (experimental)
- power history (experimental)
- cooling jacket conditions (experimental)
- top and bottom injection (experimental)
- dummy components defined to suppress “unphysical” insulation

Initial conditions:
- temperature elevated to ca. 410 K to avoid code instability due to condensation

Heater rod (best guesstimate):
- external resistance 8.5 mΩ/rod
- hydraulic diameter 3.4 mm in bundle

Sensitivity studies
- numerous calculations performed

Many cases calculated with a variety of trial models
SF2 calculations complete as far as current code limitations allow
− all calculations performed with SCDAP/RELAP5/FZK-PSI
− SCDAPSim has more flexibility to represent shroud/insulation but cannot accommodate enough axial nodes in bundle successful analysis will depend on support from code supplier

1.3 CALCULATIONAL ANALYSIS

1.3.1 Comments of participants of calculations

1.3.1.1 SOCRAT

The main purpose of simulation of SF2 experiment at PARAMETER facility was the accurate solution of thermal task (to reproduce experimental temperature evolution at different elevations). Calculated data connected with oxidation prossess are derivative and allowed evaluation the consistency of measurement of temperatures, hydrogen production (Figure 1.22) and thickness of zirconium oxide on cladding surface at the end of the experiment (Figure 1.23).

In performing the first post-test calculations it became clear that alongside with the accurate assigning of boundary conditions for power and flow rates of steam and argon, it is very important to consider the behaviour of the test section components above and below the heated zone. For instance, experimental data on temperature of fuel rod simulators at the elevations of 0÷300 mm can be reproduced in the calculation if the facility lower part is simulated adequately, including the flanges and the body (element VESSEL_D in Figure 1.1). Heat transfer between gas and the body along the length from the inlet nozzle up to the lower edge of tantalum heaters leads to decrease in temperature of steam and claddings at the lower edge of heated zone by ~100-150 K (see Figure 1.39).

Radial radiative heat transfer between the claddings and the shroud is simulated in the calculations (complete radiative heat transfer model initialization results in considerable increase in calculation time (several times) while axial radiative heat transfer effect is significantly weaker than radial one). To treat radiative heat transfer between the claddings and the elements in the upper part of the test section (above 1300 mm elevation) including the body a parametric model of heat fluxes through the surface of cells in radial direction is applied (Qrad in Figure 1.1). On the whole, such an approach made it possible to take into account adequately heat removal from the upper edge of the assembly heated part.

Models of SOCRAT code allowed very accurate description of the assembly temperature behaviour, except for two points:

– Calculated temperature SHROUD at the elevation of 1300 mm does not coincide with that measured by thermocouple, probably due to heat sink from the end of the element which depends on steam condensate presence on insulating membrane (not simulated directly in SOCRAT code but assigned parametrically through the internal surface of the last axial cell with thermal insulation);

– The temperature “hump” (local maximum) within the interval of 10000-12000 s was not reproduced.

It should be noted that this temperature “hump” (local maximum) can be obtained in the calculation by considerable change in boundary conditions and/or thermal-and-physical properties of components, however with such assumptions temperature evolution calculated and experimental are not in a good agrreement within the later interval of 13000-17500 s.

Calculated value of hydrogen production due to oxidation of the simulated components was 24 g (16.4 g – due to oxidation of simulator claddings, 2.6 g – due to oxidation of shroud, 1.3 g – due to oxidation of spacer grids, 3.6 – due to oxidation of three pressure sensors and three periphery thermocouples with diameter of 4 mm). It is a good agreement with the measured mass (25 g). To evaluate hydrogen production due to oxidation of other thermocouples, the model of one thermocouple at the elevation of 1250 mm was added into the nodalization. The calculated mass of hydrogen from its oxidation was ~0.08 g. If we assume that 15 thermocouples located in the hottest zone (from 1000 to 1300 mm) are ixidized the same as well as the oxidation reaction is not steam limited, the hydrogen mass due to oxidation of the thermocouples can be evaluated to be ~1 g.

Calculated profile of oxide scale thickness on fuel rod claddings along heated part (0-1275 mm) is in a good agreement with the measured one (Figure 1.23). A difference between the experimental and calculated value of zirconium dioxide thickness at the elevation of 1300 mm is 25% and caused by underestimation of temperature at this elevation connected probably with the assumption on heat transfer in the upper part of the test section.

Analysising code capability to describe the reflood phase it should be considered that calculated temperatures correspond to the temperatures of cladding surfaces, while the experimental temperatures correspond to thermocouples readings and their thermal response time is rather long at the quick transient. Figure 1.12 presents the comparison of the calculated values of cladding temperatures and thermocouple readings at the flooding stage. It follows from the Figure that SOCRAT code gives quite exact moment of the beginning of wetting both in the facility upper part (top flooding), and in the middle part (combined flooding); the calculated time of thermocouple cooling at the elevation of 1250 mm, obtained by SOCRAT code, is 25 s, for the simulator it is 40 s, while the time interval of decrease in readings of the thermocouple T2513.5 from 1750 K to 600 K is 22 s.

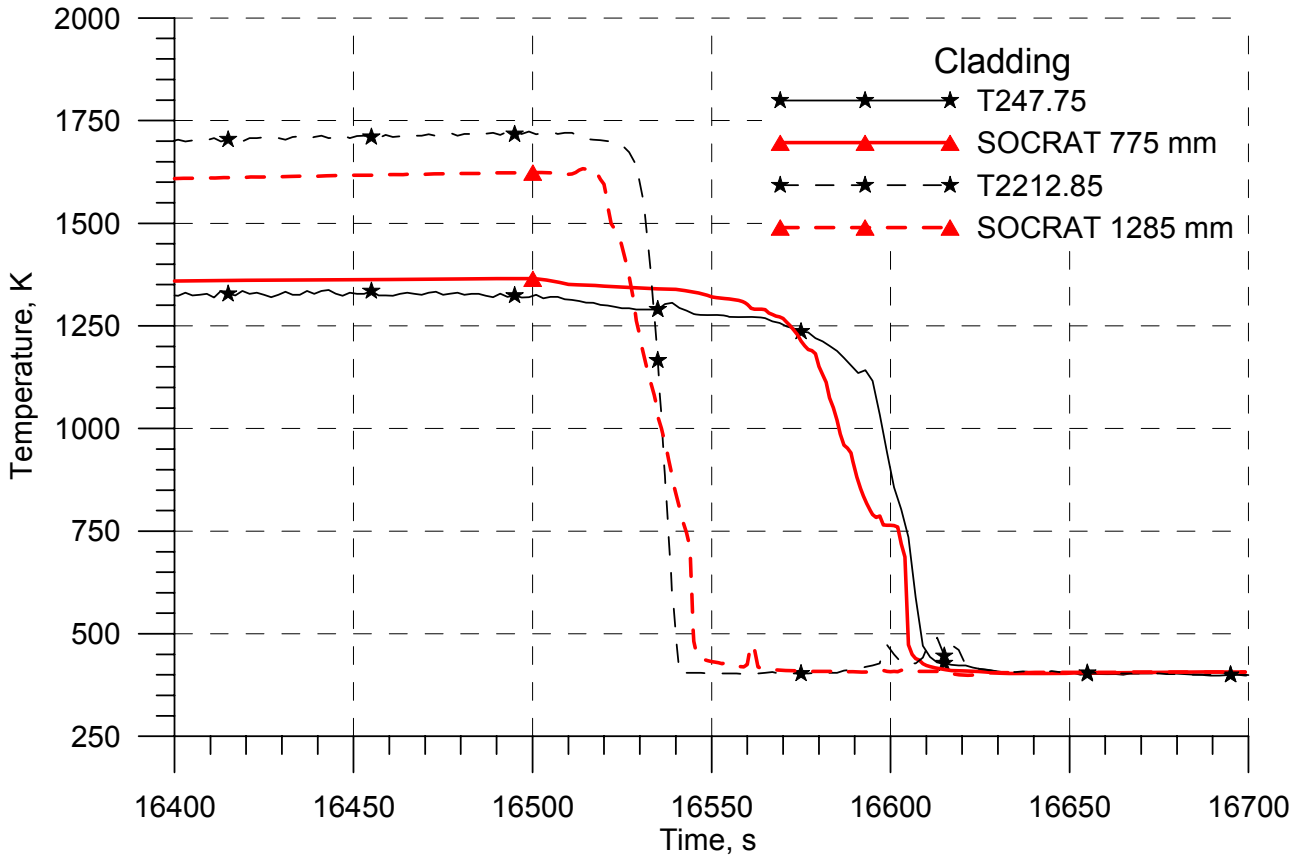

Figure 1.12. Comparison of experimental and calculated cooling front propagation. PARAMETER-SF2 experiment. Post-test calculations.

1.3.1.2 RELAP/SCDAPSIM

The main purpose in constructing the nodalization was obtaining the most accurate model in the temperature region of 1000-2000 K.

The assembly heating-up from indoor temperature to 700 K differs from the experiment because for the sake of numerical stability and simplicity of simulation it was decided not to pay much attention to this negligible region that is required to obtain better agreement with the experiment. The cooling housing model with the use of gas gaps can also give underestimation of losses through the shroud at low temperatures.

By the moment when temperatures reach the value of 900 K the calculational model is in good agreement with the experiment as seen from the Figures.

The temperature at the assembly top is overestimated that is caused by edge effects because outside the central part the simulators are not modelled from the viewpoint of heat transfer. On the whole, the temperature field is in agreement with the experimental data. At the first 4000 s there is a small disagreement with the experimental temperatures. From a comparison of calculated data on power released in the heated part it can be supposed that the main cause is the higher value of additional resistance. Further on, both the character of change, and the temperature values are in

agreement with the experimental data, except for the situation when temperatures at the elevations above 1250 mm are higher than in the experiment due to edge effect (the model of axial heat losses is not available). Maximum temperature at the pre-oxidation stage is 1570 K, maximum temperature before flooding is 1800 K, the hottest zone is located at the elevation of 1250 mm.

On the whole, the best agreement with the experiment is achieved for the simulators of the 2nd row and central rod. Temperatures of the 3rd row are overestimated in comparison with experiment. At the stage of heating-up (4000-12000 s) the discrepancy with the experiment for the simulators of the 2nd row does not exceed 50 K, and for the 3rd row it is not more than 100 K. At the pre-oxidation stage the calculation gives the overestimated temperatures for the simulator of the 3rd row and central rod. Such a discrepancy can be caused by the radiation model due to the fact that the hexahedral geometry is to be simulated using the code developed for the square geometry. The rate of temperature rise at the stage of heating-up to 1800 K coincides with the experimental value. Beginning from the elevation of ~1300 mm the calculation gives a highly overestimated temperature value (the explanation is given above). The discrepancy with the experiment is 300 K.

Full amount of hydrogen is higher than in the experiment by 3 g due to higher oxidation within the time interval of 13000-16000 s. As the calculation gives some overestimation of temperatures for fuel rods of the 3rd row the maximum temperature before flooding is reached 300 s earlier in comparison with the experiment. Due to the fact that instrumentation zirconium tubes of 4 mm in diameter, arranged on the assembly periphery, are not simulated their oxidation should be considered. The estimation is based on the situation that zirconium surface of Shroud is approximately three times less than the surface of 19 fuel rods, however hydrogen release from it is four times less. As to the surface size the instrumentation tubes are equivalent approximately to three fuel rods, each fuel rod gives 1.4 g of hydrogen. So, taking into account the arrangement of tubes the hydrogen mass from their oxidation is estimated as 2.5 g.

Up to the elevation of 900 mm the thickness of oxide scales on claddings is in good agreement both with the experimental data, and with other codes. At the section of 900-1400 mm the thickness of oxide scales is less than in the experiment. The elevation with maximum thickness follows the position of maximum temperature. Maximum calculated thickness of oxide scale (300 μm) differs from the measured value (450 μm) by 150 μm. In spite of underestimation of zirconium dioxide thickness on claddings the calculated integral hydrogen mass exceeds the experimental value because the high contribution into the calculated hydrogen mass is made by the shroud oxidation (8 g).

Crossing of cooling fronts under flooding occurs at the elevation of about 1000-1200 mm (see Figure 1.13), the same as in the experiment (see Figure 26, 25 of Protocol of SF2 experiment [7]).

On the whole, the results of calculation with the use of RELAP/SCDAPSIM code are in good agreement with the experiment both qualitatively, and quantitatively. Integral characteristics of the experiment (hydrogen production, maximum temperature, position of hot spot), alongside with the behaviour of temperature field of the heated fuel rods on the heated section, are reproduced satisfactory in the calculation. Thermal insulation temperature exceeds the experimental value considerably. The profile of oxide scale thickness on fuel rods is underestimated as compared to the experiment.

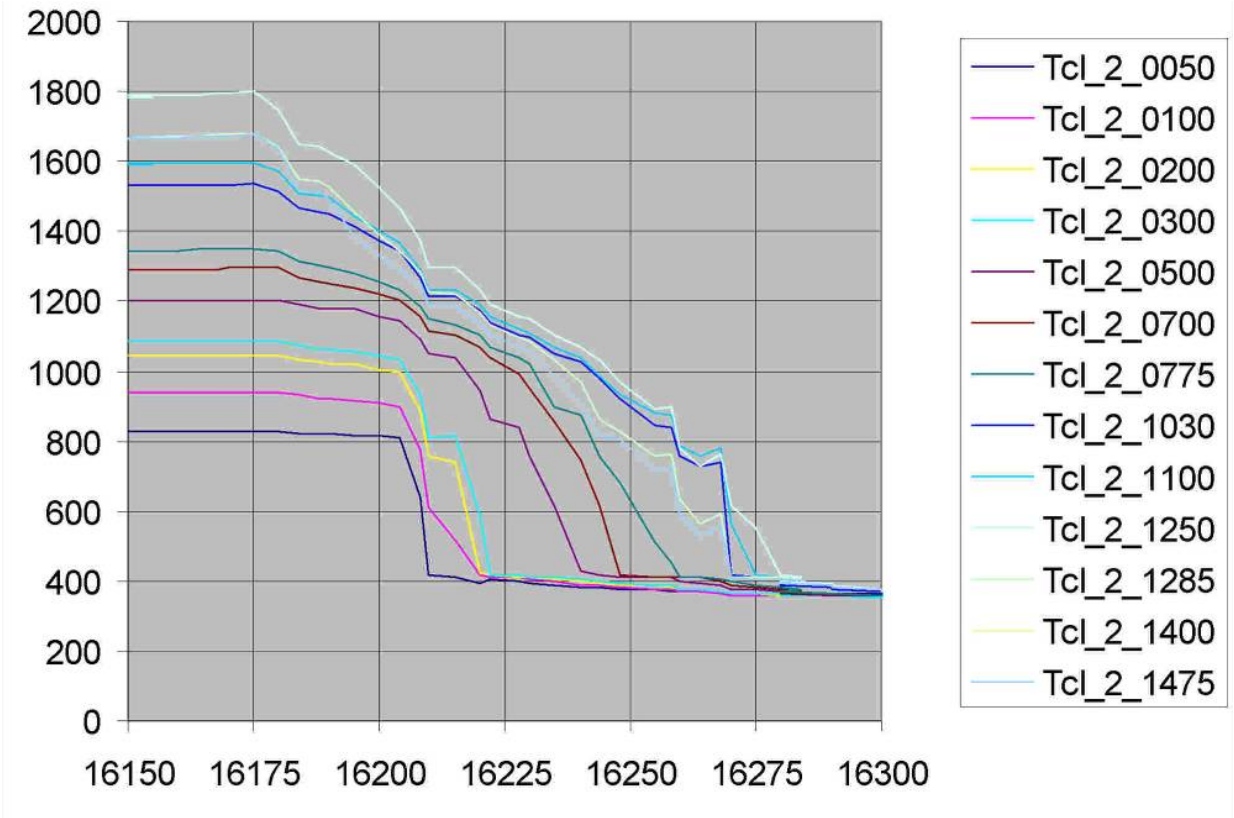

Figure 1.13. Calculated temperatures of thermocouples on the second ring of the simulators under flooding. PARAMETER-SF2 experiment.

Full mass of hydrogen is close to the experimental value: the difference is less than 8% for the measurement using SOV-3 system, and by 3% for the system of measurements using sampling. The above mentioned analysis showed that absence of the model of displacers results in underestimation of the integral hydrogen mass by ~2 g, and the overestimated shroud oxidation, as compared to other codes, gives excessively ~5 g. It could be supposed that elimination of deficiencies of the applied models and nodalization will lead to reducing an error in the integral hydrogen mass.

The code is capable to simulate all typical phenomena occurred in the experiment: oxidation of claddings, of spacing grids, of shroud, radiant heat transfer. The deficiencies in simulation of heat transfer between the assembly components in the periphery part need to be studied, and modification was made later on at the stage of the calculations of SF3 experiment.

1.3.1.3 ICARE/CATHARE

Calculations with the use of ICARE/CATHARE code give a satisfactory reproduction of the main experimental data of PARAMETR-SF2 test as to the following key parameters:

– Behaviour of temperatures of simulators and housing under heating and subsequent cooling;

– Hydrogen production.

With this, temperature behaviour of the assembly components corresponds to the experimental values, and maximum temperatures in the calculation are obtained at the elevation 1250 mm – 1716 K at 16414 second. The only exception is a small temperature peak at the upper elevations in the region of 12000 s, that is caused probably by the time-dependent local irregularity of heat flux.

Hydrogen production of 25.4 g is close to the measured 25 g. Probably, a small discrepancy in time-dependent behaviour of hydrogen production is caused by transport delay of measurement under flooding. It can be noted that hydrogen production due to oxidation of simulator claddings is 60%, of the assembly housing – 30%, of pressure pick-up and spacing grids – 10%.

The predicted maximum thickness of zirconium oxide external scale (319 μm per 1250 mm) is in agreement with the lower limit of the measured value, and at the elevations below

1000 mm it is close to the average value. Possible causes of discrepancy in calculated and measured values of maximum ZrO_2 thickness could be the following:

Too high calculated value of α-Zr(O) phase in zirconium cladding.

As it was already noted, in ICARE/CATHARE code database a new version of correlations was used for oxidation of claddings of VVER materials. These correlations were tested in a number of experiments both for separate rods in FZK program (separate effect tests FZK, SETs), and for integral (bundle experiments) – CORA-VVER, CODEX. At present the testing of correlations can be considered to be finished practically. The most uncertain value for testing was the value of α-Zr(O) because in the experimental material available on oxidation of Zr1%Nb there is a large scatter in data both on thickness of oxide, and on thickness of α-Zr(O) with good agreement of gain in weight.

Therefore it can be supposed that the calculated value of α-Zr(O), smaller in comparison with the experimental value, will lead to increase in oxide thickness. However even in the limit of zero thickness of α-Zr(O) the calculated increase in oxide thickness can not exceed 30% of oxide thickness that is below the observed value.

Approaching of calculated and experimental oxide thickness can be influenced by specifying the procedure of evaluation of experimental thickness in its comparison with the calculation.

Evidently, in the course of the experiment some temperature irregularities took place in the cladding over the radius of a separate cladding and along the assembly radius. That is indicated by scatter in measurements of oxide thickness in the region of maximum heating (±200 μm corresponding approximately to ±70 K). Specifying the procedure can include using of weight characteristics for different thicknesses measured that can make the results of experiment and calculation closer, while in the calculation there is a small temperature irregularity governed by the place of electric power application.

In the current analysis the evaluation of experimental thickness was applied proceeding from the measured remaining metal part and the initial cladding thickness that is defined strictly with the constant geometry of fuel rod. Therefore the finite error of measurements could increase considerably due to neglecting the deformation of fuel rods occurring under temperature heating. Probably the procedure should be specified by a comparison of results for the chosen test rods and the remaining oxide layer not separated.

Results of simulation of SF2 experiment were presented at the International Seminar on ICARE/CATHARE computer code [14].

1.3.1.4 SCDAP/RELAP/FZK-PSI

The result of a large number of test calculations carried out gave a good agreement of calculated temperatures of heated rods and experiments data. Nevertheless in the calculations some distortion of axial temperature profile was found out (location of a “hot spot” occurred about 100 mm below the measured data). Some discrepancy of calculated and experimental data was noted also for the shroud and insulation, and at the same time temperature head through the insulation was satisfactory reproduced in the calculations.

Hydrogen production was underestimated in the calculations. The cause of discrepancies can be erroneous kinetics of oxidation reaction in the code or underestimation of temperatures in the assembly upper part.

On the whole, the results look as giving hope but still not adequate enough because they can not allow to make a conclusion on the assured reproduction of all important parameters.

By the results of PARAMETER-SF2 simulation the following conclusions can be also made on the code capabilities:

– all calculations were made using the version SCDAP/RELAP/FZK-PSI;

– SCDAPSim is capable of high flexibility to reproduce the shroud/insulation structure but can not assure a sufficient number of axial nodes in the assembly;

– successful analysis depends on the support of the code developers.

1.3.1.5 PARAM-TG

SF2 test till power increase from 4.1 kW to 5.1 kW was performed according to the calculated diagram except for the fact that the first power plato was 816 s longer than in calculation (for matching the time scales the zero time point in calculation is shifted 1910 s ahead in Figure 1.14). Then to avoid the quick heating-up after reaching the temperature of 1000°C a step of power increase did not exceed 0.5 kW.

In PARAM-TG computer code provided a possibility to make a comparison of the results of calculated and experimental value of temperature on claddings of those fuel rods wherein thermocouples are placed. On the whole, the agreement is satisfactory, some "excursions" in readings of thermocouples of the 2nd and 3rd rows are observed at the beginning of temperature plato at 1200°C. For instance, in Figure 1.56 these "excursions" are distinctly seen in comparison of the calculated values of cladding temperature of fuel rod 2.1 at the elevation of 1100 mm and of fuel rod 2.6 at the elevation of 1250 mm with the corresponding readings of thermocouples T2111 (tungsten-rhenium) and T2612,5 (Chromel-alumel). It may be caused by insufficient account in the code of power of steam-zirconium reaction on weakly oxidized cladding surface. After formation of quite thick oxide scale on zirconium surfaces (of claddings, shroud, thermocouples sheath) the power of steam-zirconium reaction reduces and temperatures are equalized.

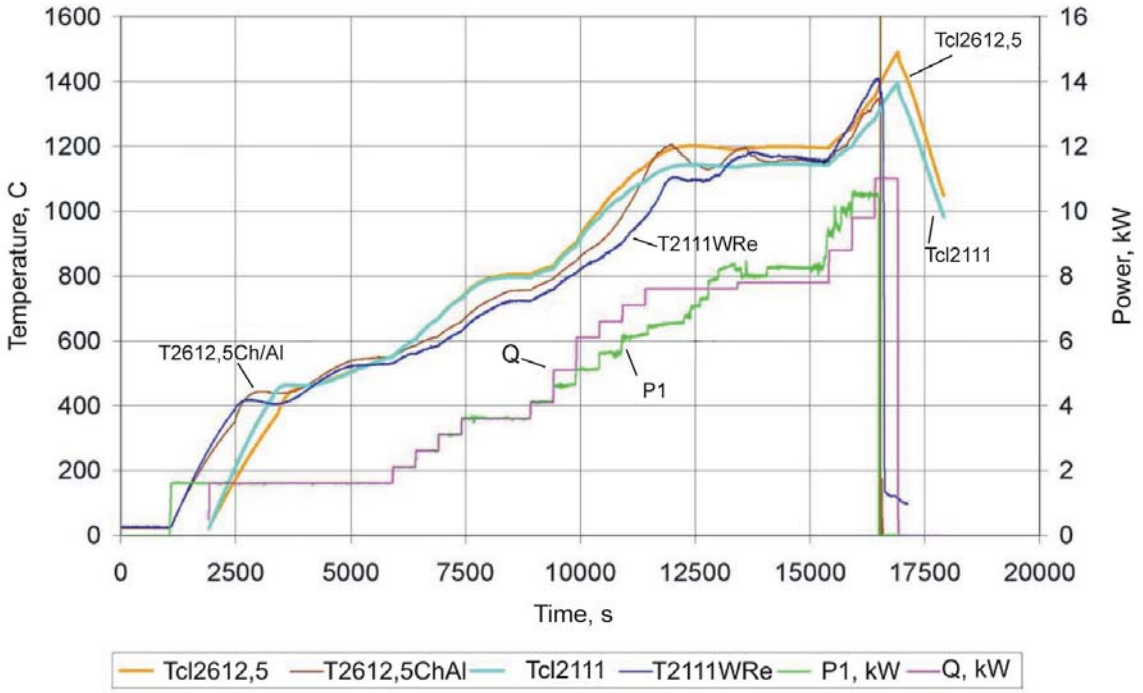

Figure 1.14. Power calculated (Q) and experimental (P1). Calculated temperatures of claddings (Тст – pre-test calculation) and thermocouples readings (T).

It can be pointed out also small but systematic temperature overestimation at the lower elevations (z = 0, 100 and 200 mm) after steam swithing on. Moreover, at the lower elevations this deviation increases by the end of the test. Figures 1.15 and 1.16 provide a comparison of calculated and experimental temperature at the elevations of 0 and 1250 mm.
This effect can be explained most likely by evaporation of water droplets in steam flow.

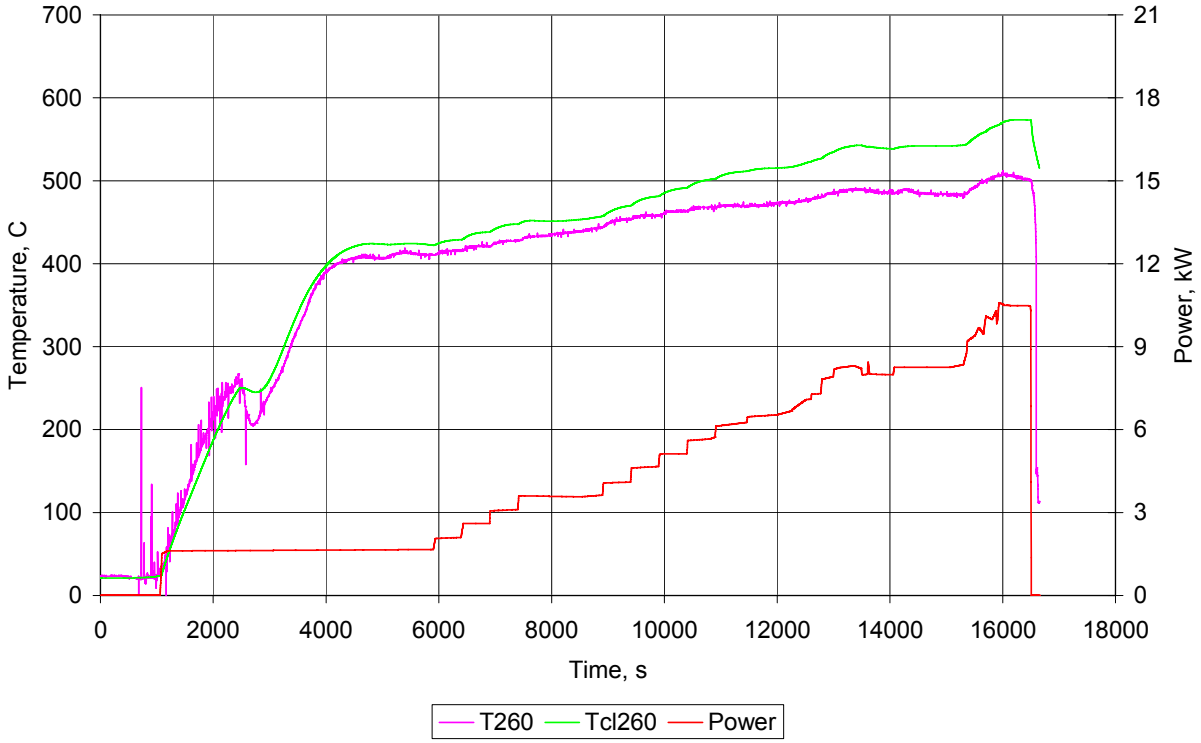

Figure 1.15. Comparison of calculated cladding temperature and thermocouple reading for fuel rod 2.6 at the elevation of 0 mm.

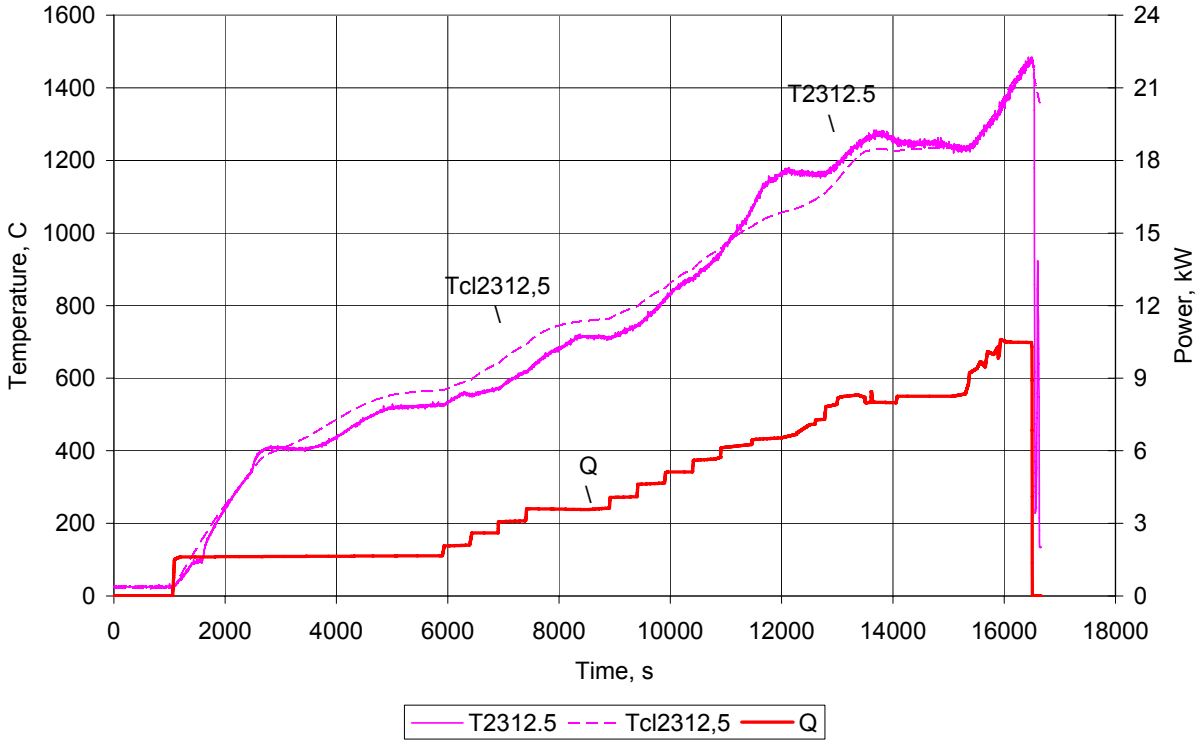

Figure 1.16. Comparison of calculated cladding temperature and thermocouple reading for fuel rod 2.3 at the elevation of 1250 mm.

Five tungsten-rhenium and 29 Chromel-alumel thermocouples (their diameters are 2.8 and 1.5 mm, respectively) were inserted in SF2 test section, they influence temperature field. Therefore, for the first time in the calculations the detailed analysis was made for differences between cladding temperature and thermocouple readings considering the concept of their attachment to fuel rod claddings and effect of their detachment from cladding in the course of the experiment. The thermocouples effect on temperature field due to decrease the flow area at their location in the

model assembly was analyzed. It is shown that the thermocouple of Ch/Al type attached to the cladding can introduce an error of not more than 12-15°C at the place of junction, and the thermocouple of WRe5/ WRe20 type – 20 - 22°C for temperatures not exceeding 1200°C for Ch/Al thermocouples, and 1600°C – for tungsten-rhenium thermocouples. If junctions of thermocouple detach off the claddings in the course of the experiment these errors increase but not so much, to ~20 and 30°C, respectively.

Calculated values of temperatures on the shroud are higher than the experimental values, on the whole. On the contrary, time the calculated temperature of the external surface of the thermo insulation are lower than the experimental date. Perhaps, it is due to somewhat higher thermal conductivity of thermal insulation in comparison with the value given in the certificate that is caused by process of installing the thermal insulation into the cavity (its cutting, placing, etc.). Considerable difference between thermocouples readings located on the shroud and external surface of thermal insulation at the elevation of 1300 mm and fit calculated values might be caused by substantial increase in thermal insulation heat conduction that can be explained by shrinkage of thermal insulation over the assembly height.

1.3.2 Correctness of heat loss estimation due to resistance

According to Figure 1.3 the rod resistance R is determined by the sum of resistances of tantalum heater $R_{tantalum,}$ electrods $R_{electrod}$ and additional resistance R_{add}.

$$R = R_{\tan talum} + R_{electrod} + R_{add} \quad (1)$$

Power P, supplied to fuel rod, is determined as

$$P = U^2 / R, \quad (2)$$

here U – voltage on the generator terminals.

Power released over tantalum heaters length -

$$P_{\tan talum} = \left[\frac{U}{R}\right]^2 R_{\tan talum} \quad (3)$$

The parameters measured in SF2 were the total current and voltage on the generator terminals. However, for numerical analysis the most important value is the value of power released over heated section, i.e. to simulate correctly fuel rod heating the exact data on ohmic resistance of electrodes and external leads and contact zones in “cold” state, on changes of contact resistances versus temperature and time should be known, however such data for SF2 are not available within the full scope.

To prove correctness of calculations of heat loss due to resistance, the measurements of electric characteristics were made at the methodical test bench in SRI SIA "LUCH" and power distribution along the length of a fuel rod at different temperatures was obtained.

A tested electrical subcircuit was identical to that used inside fuel rod simulator in PARAMETER-SF tests with respect to dimensions, materials and fabrication technique but without UO_2 pellets. Tantalum heater and electrodes made of molybdenum, copper, brass were connected to each other by welding (Ta-Mo) or by thread (Mo-Cu-brass). The tested electrical subcircuit was arranged horizontally.

Registration of voltage difference at different zones was made with the use of voltmeter M2017 (accuracy class 0,2), registration of current through the heating element was made with the use of a shunt with millivoltmeter M1105 (accuracy class 0,2). Registration of temperature at sections was made with the use of precise converter “Tercon” (temperature registration error ±0.2°C).

It was found out that fraction of power released on tantalum heater within the temperature range of 20–1000°C is approximately constant and corresponds to the value of 80%. For instance, in Figure 1.17 the experimental data on distribution of the released energy are presented for different zones at full released power of 650 W.

The fraction of power calculated by the electric heating model, described in item 1.1.1 for SOCRAT code for SF2 experiment, is presented in Figure 1.18. From the Figure one can see that within the verified temperatures, except for the range of very lower temperatures (20-200°C, the time interval of 1000-2500 s), the model calculates energy released over heated zone reasonably

good – calculated fraction of the released power corresponds to 77-83% (the time interval of 2500-11000 s).

Usefulness the measured electric characteristics for evaluation of the model adequacy at low temperatures (20-200°C) is not obvious because conditions of fuel rod keeping in the test and in SF2 test is not evident. Low power should be suppied for a long time and the tested electrical subcircuit should be kept under the conditions identical to SF2 test ones with respect to temperature gradient along the fuel rod length).

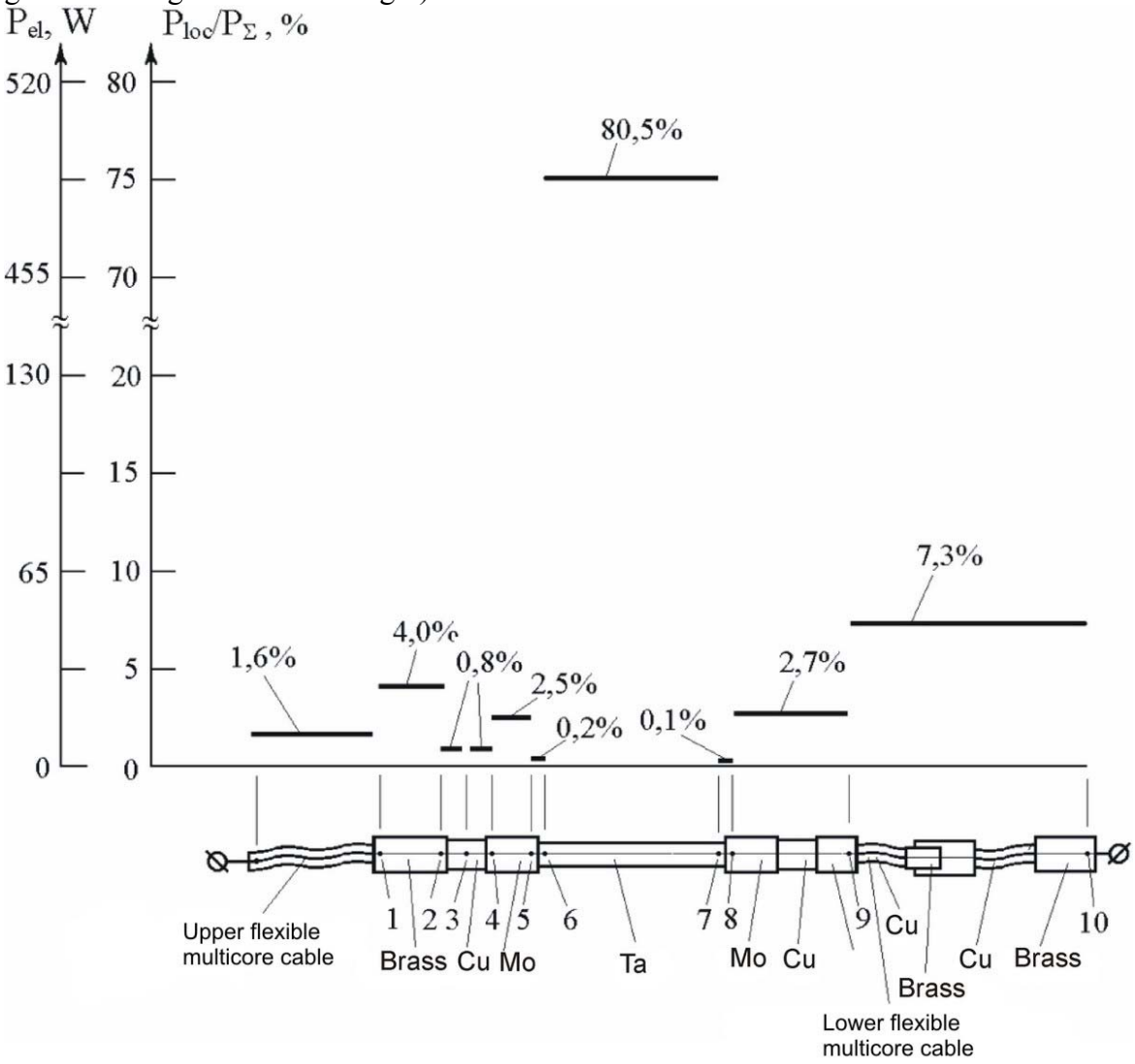

Figure 1.17. Power loss at different zones of electrical subcircuit at full released power of 650 W.

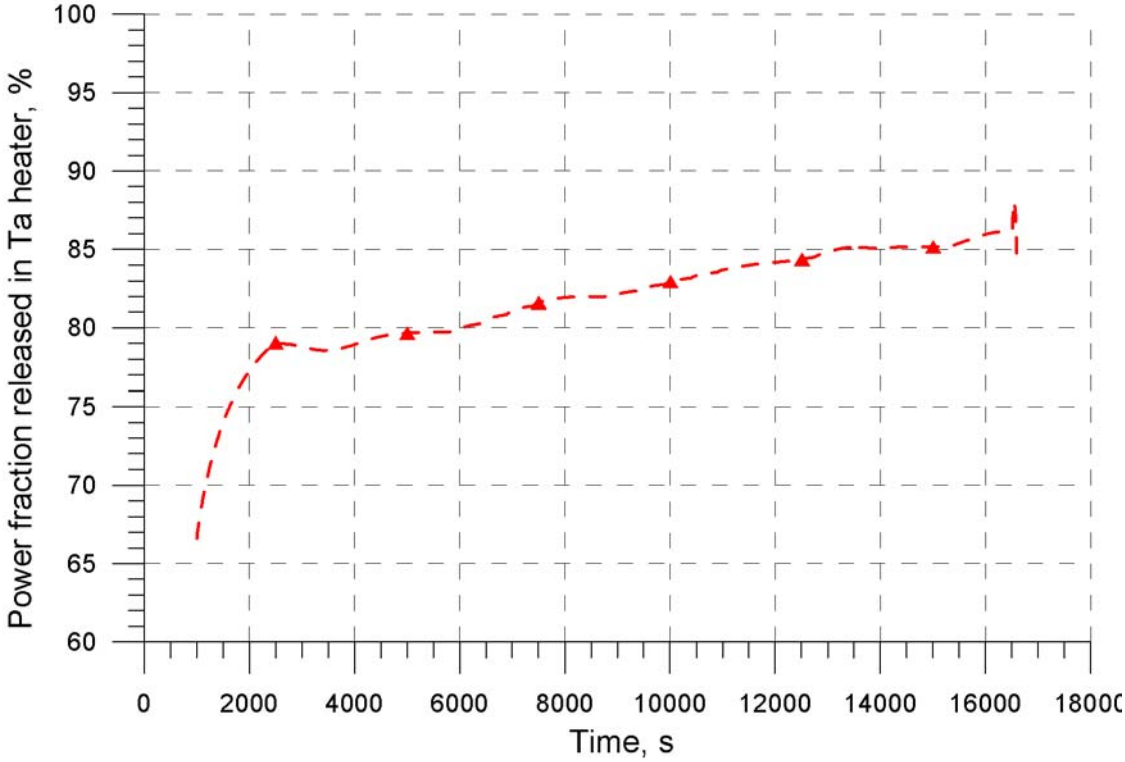

Figure 1.18. Fraction of power released over the heated zone 0÷1275 mm in SF2 experiment calculated by SOCRAT code.

1.3.3 Assessment of the facility parameters uncertainties

Figures 1.36-1.58 present the temperature behaviour of fuel rod claddings at different elevations. One can see that practically all the codes give good reproducibility of the temperature behaviour of fuel rod claddings throughout the whole experiment, except for local maximum at the time moment of 12000 s in the upper part (1030-1300 mm) of the heated zone. The truth of this temperature "hump" registered by thermocouples but no reproduced by the codes is confirmed by increase in the hydrogen generation rate registered experimentally (Figure 1.22). Most of the codes predict location of the hottest zone at the elevation of 1250 mm at the pre-oxidation stage, and this corresponds to thermocouple readings. In the calculations by RELAP/SCDAPSIM code the axial radiative heat transfer is not simulated and it results in overestimation of temperatures in the upper unheated part of the assembly (1400-1500 mm). In SCDAP/RELAP/FZK-PSI code the shroud top is also simulated poorly, so the location of maximum temperature zone is shifted approximately 100 mm below. Maximum calculated temperatures before flooding onset correspond to the experimental values (1770 K). Calculations with the use of RELAP/SCDAPSIM code show very strong temperature escalation at the transient stage due to neglecting the axial heat transfer and, thus, the user ought to switch off electric power earlier to get the experimental maximum temperature before flooding onset.

The shroud temperature behaviour is described satisfactory by the codes. From the Figures 1.32-1.35 one can see that the calculated temperatures either correspond to the experimental values or slightly (not more than by 130 K) overestimated at the pre-oxidation stage and transient phase to maximum temperature. At the elevation of 1300 mm (Figure 1.35) the shroud reveals pronounced instable temperature. Such instability could be considered as local effect caused by additional shroud cooling with whater which condense on the isolating membrane at the upper edge of thermal insulation.

A good agreement of calculated and experimental data is obtained on coolant temperature (see Figures 1.29-1.31). At the elevations of 1030 mm, 1285 mm the weak local maximum (12000s) not reproduced by the codes can be seen. It reflects the pronounced but not reproduced local maximum in temperature behaviour of claddings in the middle and upper part of the heated zone.

As seen from Figures 1.36-1.58, three codes ICARE/CATHARE, SOCRAT, ATHLET-CD give a good reproducing of temperature behaviour of claddings and shroud over the whole height of

the assembly (heated and unheated upper part). The values of total hydrogen mass (Figure 1.24) correspond to each other (23-25 g). For comparison indications of the SOV-3 hydrogen measuement device recommended by experimentators for verification as reliable data are plotted in the Figure. It should be noted that the device measures the hydrogen content in steam-gas atmosphere at the assembly outlet. Material studies [10] showed hydrogen presence in the remaining metal part of the shroud (integral mass is estimated to be about 2 g). Calculated values correspond to the hydrogen production caused by oxidation without hydrogen absorption treatment. So, the experimental mass of 27 g should be compared with the calculated total hydrogen mass. As seen from the Figure, the codes ICARE/CATHARE, SOCRAT, ATHLET-CD slightly underestimate the total mass, however in the calculations oxidation of non-prototype materials didn't take into account (thermocouples for codes ICARE/CATHARE, SOCRAT; periphery pressor sensors and thermocouples for ATHLET-CD code). Underestimation of hydrogen production in the calculations by SCDAP/RELAP/FZK-PSI code is caused probably by rather low calculated temperatures near the shroud upper edge elevation.

All codes show no hydrogen production at the flooding stage. Insignificant rise in experimental hydrogen mass at this phase probably results from time delay connected with hydrogen transport from the source to the SOV-3 hydrogen measurement device.

Figure 1.23 presents the calculated data on zirconium dioxide thickness on claddings over heated part. For a comparison the experimental data are presented in the plot [10], that were obtained by calculation using the remaining metal part of claddings (considering Pilling-Bedworth factors). Maximum measured thickness of zirconium dioxide of ~450 μm corresponds to the elevation of 1250 mm. The calculated data on zirconium dioxide in relation to location of the hottest zone are in agreement with the experimental data though there are differences in thickness. Thicknesses calculated with codes SOCRAT and ATHLET-CD are the most close to the experimental thicknesses. From comparison of calculated data on the total hydrogen mass and the data on thicknesses of oxide scales on fuel rod claddings one can conclude that in the calculations by RELAP/SCDAPSIM and ICARE/CATHARE codes contribution of hydrogen mass due to the shroud oxidation in total mass production is greater than in calculations by other codes.

The performed calculations allow analysis the effect of different thermohydraulic and physical-and-chemical processes on the assembly temperature response.

The major source of the assembly heating is Joule heat. The values of external resistances for the SF2 assembly, as discussed above, are determined poorly. The values tuned by the users are different. Heat loss along electrodes and leads zone is estimated to be 0.7-1.4 kW at the stage of pre-oxidation, 0.8-1.8 kW at the transient stage. So, there is a scatter in the calculated Joule heating power in heated zone to be about 1 kW (see Figures 1.19 and 1.25).

Another heat source is zirconium oxidation exothermic reaction (see Figure 1.28). At the stage of pre-oxidation its contribution into heat balance is insignificant. Most of the codes show the oxidation power of 0.5-1 kW to be released. As temperature rises at the transient stage, the oxidation power increases but does not exceed 30% of the Joule heating power.

As seen from a comparison of Figures 1.26 and 1.27, the convective heat transfer is the main mechanism of the assembly cooling at the pre-oxidation and the transient phases. Calculations show that at these phases the coolant removes from heated zone about 85÷90% of Joule heating power. Radial heat loss through the shroud brings a considerable contribution into heat balance over the heated part at the beginning of the experiment as heating the assembly up to temperatures 750 K (the first 6000 s) occurs. With the assembly heating-up this heat loss increases but not so high as the convective heat transfer and is estimated by the codes with close values: ~1 kW at the pre-oxidation phase (RELAP/SCDAPSIM, ATHLET-CD, SOCRAT, PARAM-TG,) and to 1.2-1.5 kW at the transient phase.

From the presented analysis of results of SF2 experiment modelling one can see that the main source of uncertainties is uncertain values of external resistance. This causes a scatter in calculated power released over the assembly heated part, to be about 1 kW. Scatter in power of radial heat loss at the pre-oxidation and transient phase is less considerable in respect of both absolute value, and their contribution into the heat balance.

1.3.4 Comparison of calculation results with the experimental data

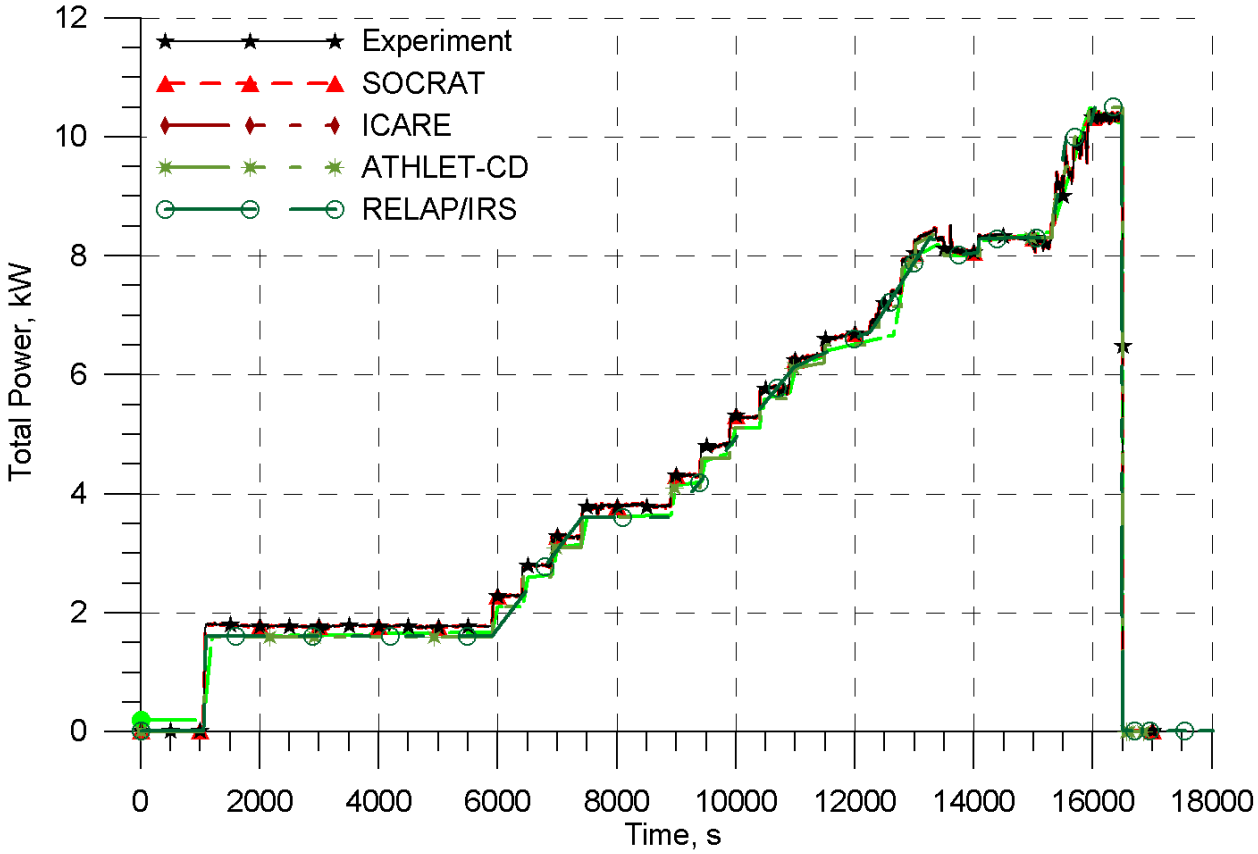

Figure 1.19. Electric power supplied. PARAMETER-SF2 experiment. Post-test calculations.

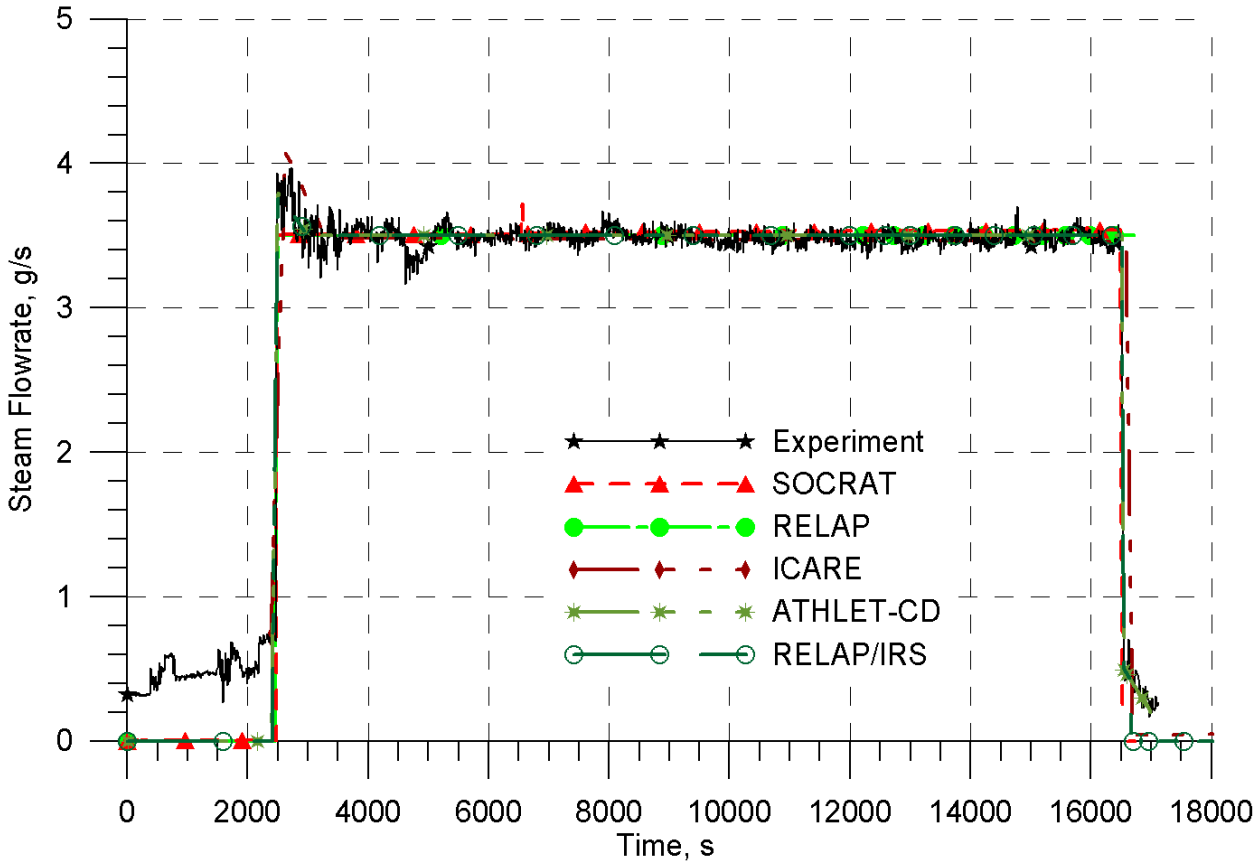

Figure 1.20. Steam flow rate at the test section inlet. PARAMETER-SF2 experiment. Post-test calculations.

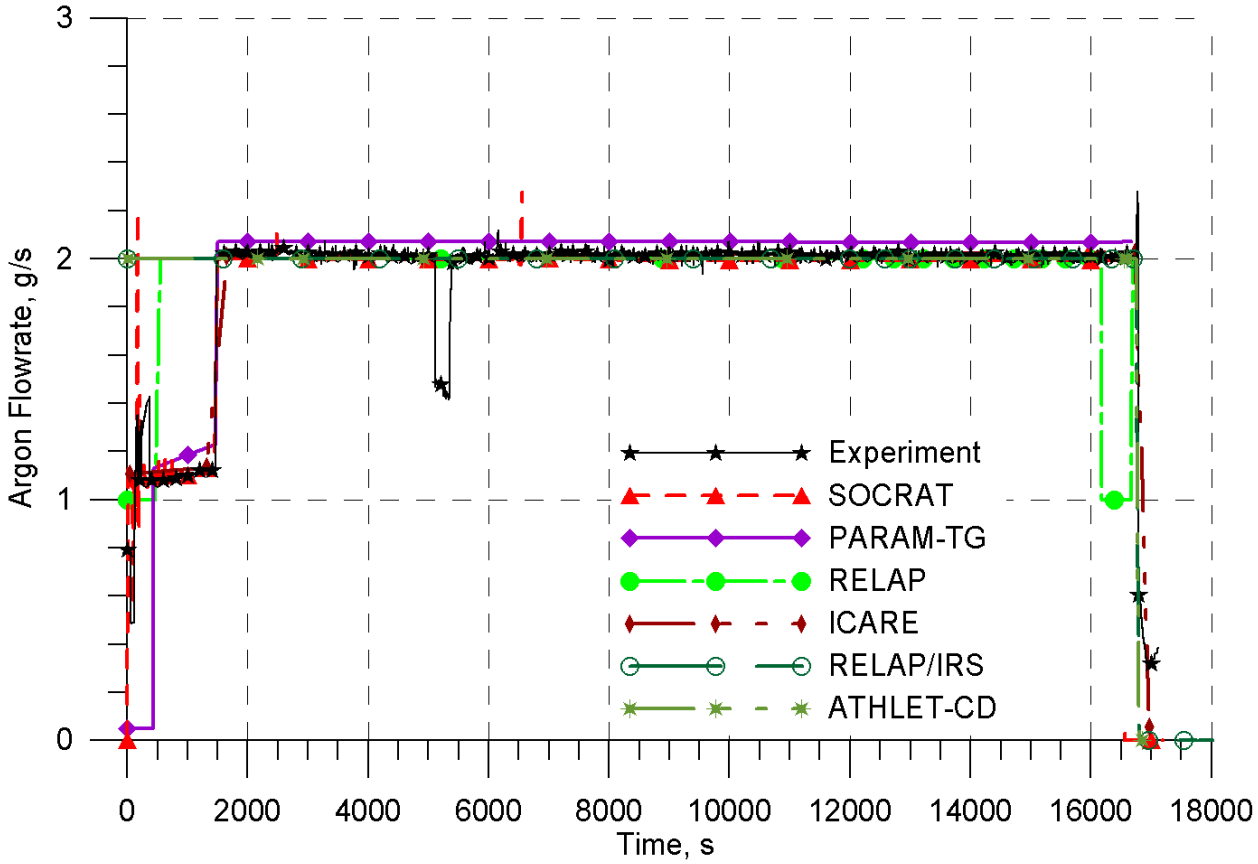

Figure 1.21. Argon flow rate at the test section inlet. PARAMETER-SF2 experiment. Post-test calculations.

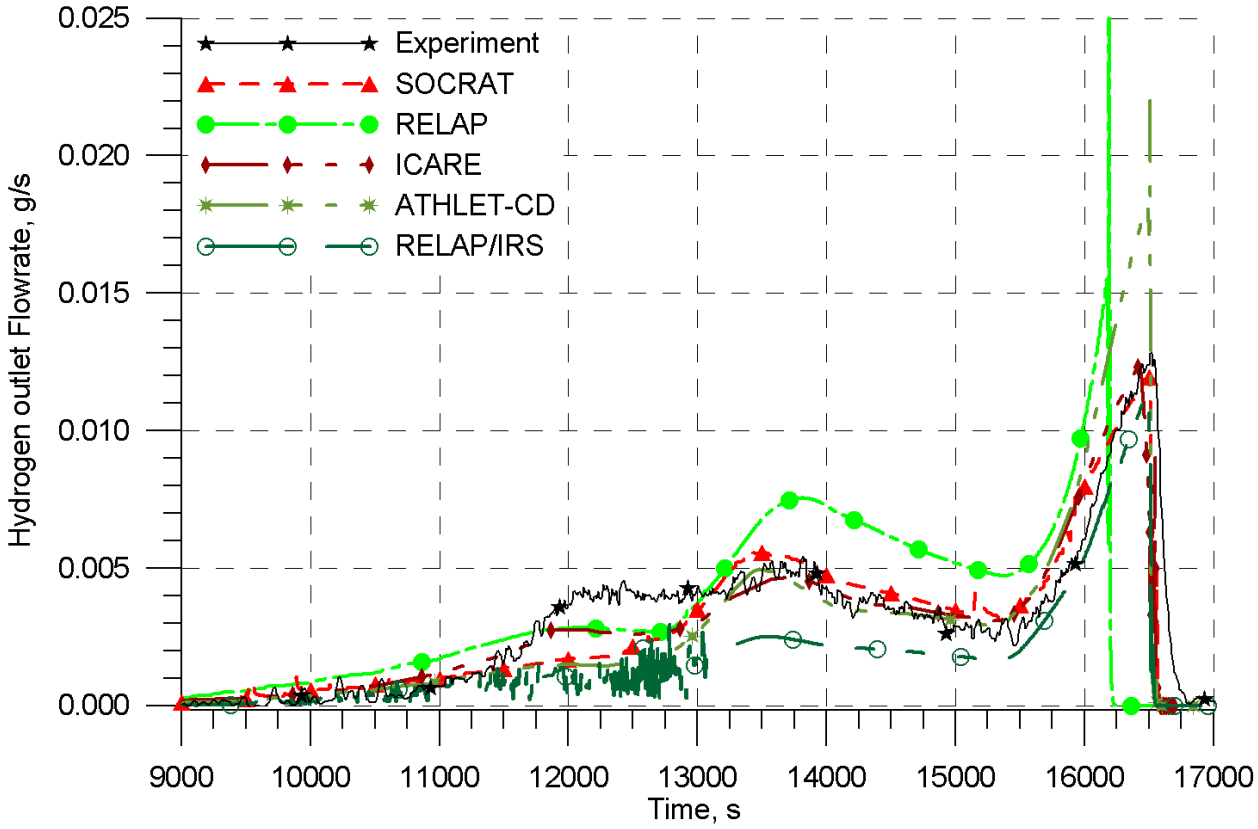

Figure 1.22. Hydrogen flowrate released. PARAMETER-SF2 experiment. Post-test calculations.

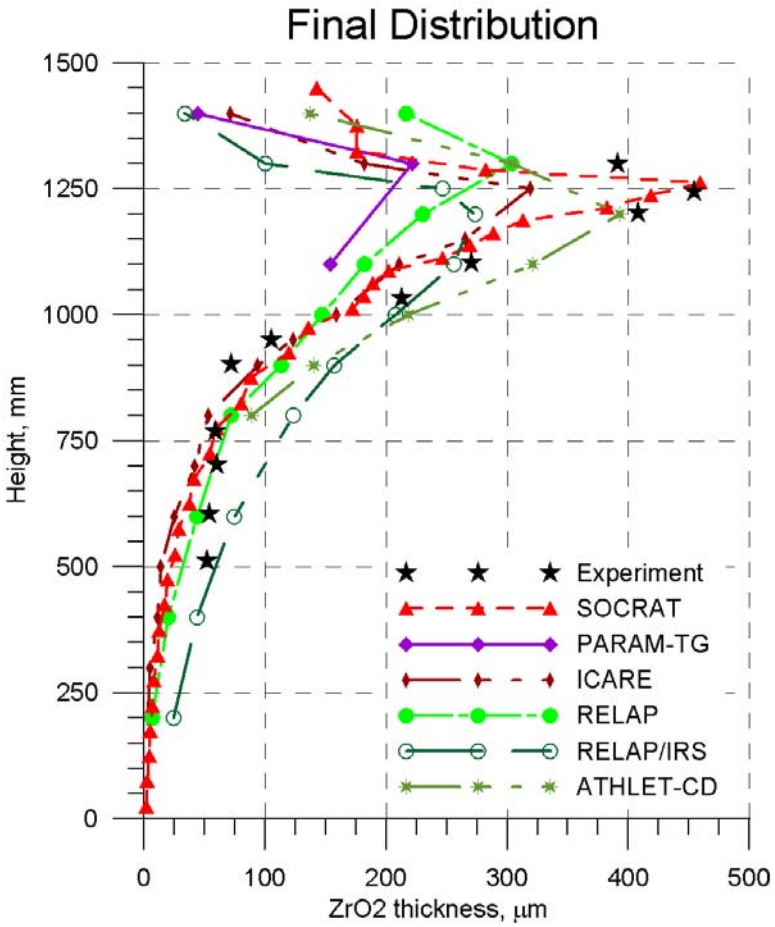

Figure 1.23. Distribution of cladding oxide scale thickness over heated zone. PARAMETER-SF2 experiment. Post-test calculations.

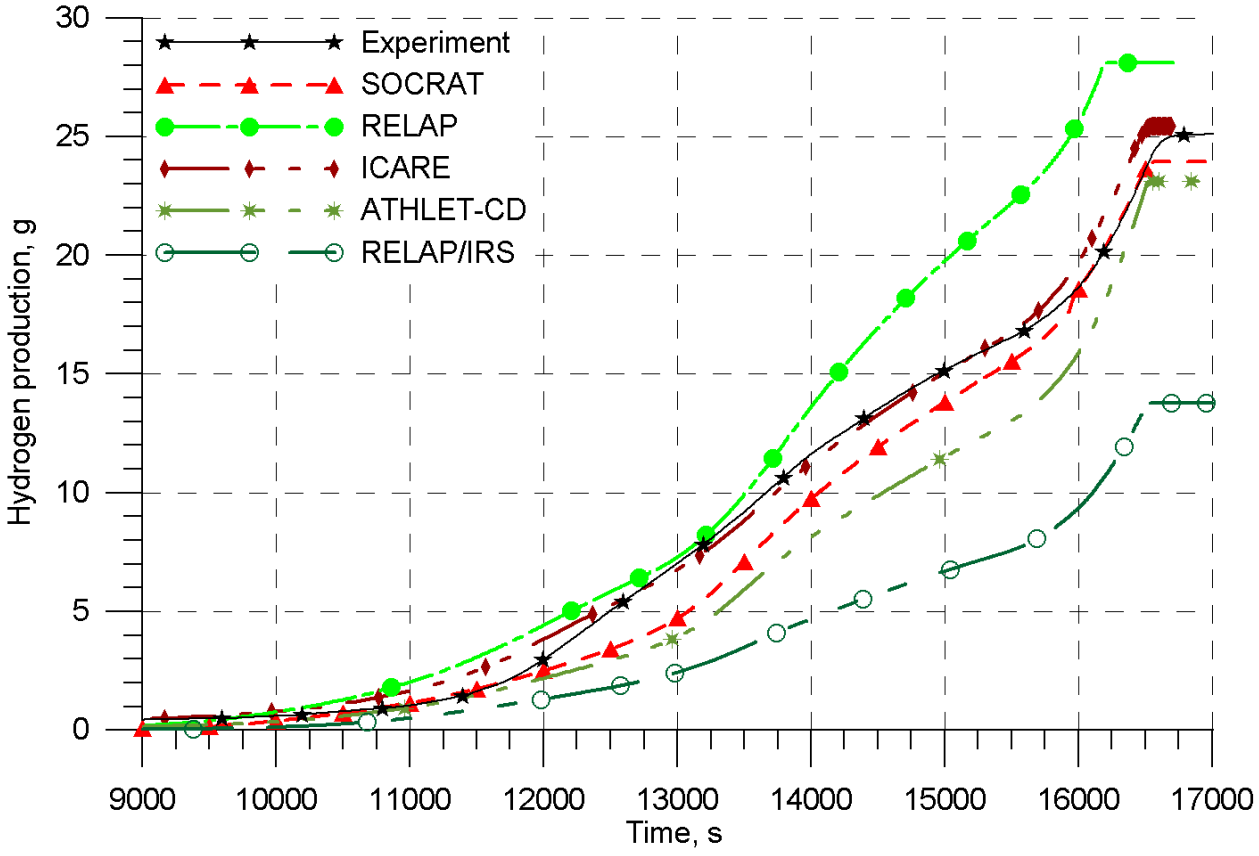

Figure 1.24. Total hydrogen mass. PARAMETER-SF2 experiment. Post-test calculations.

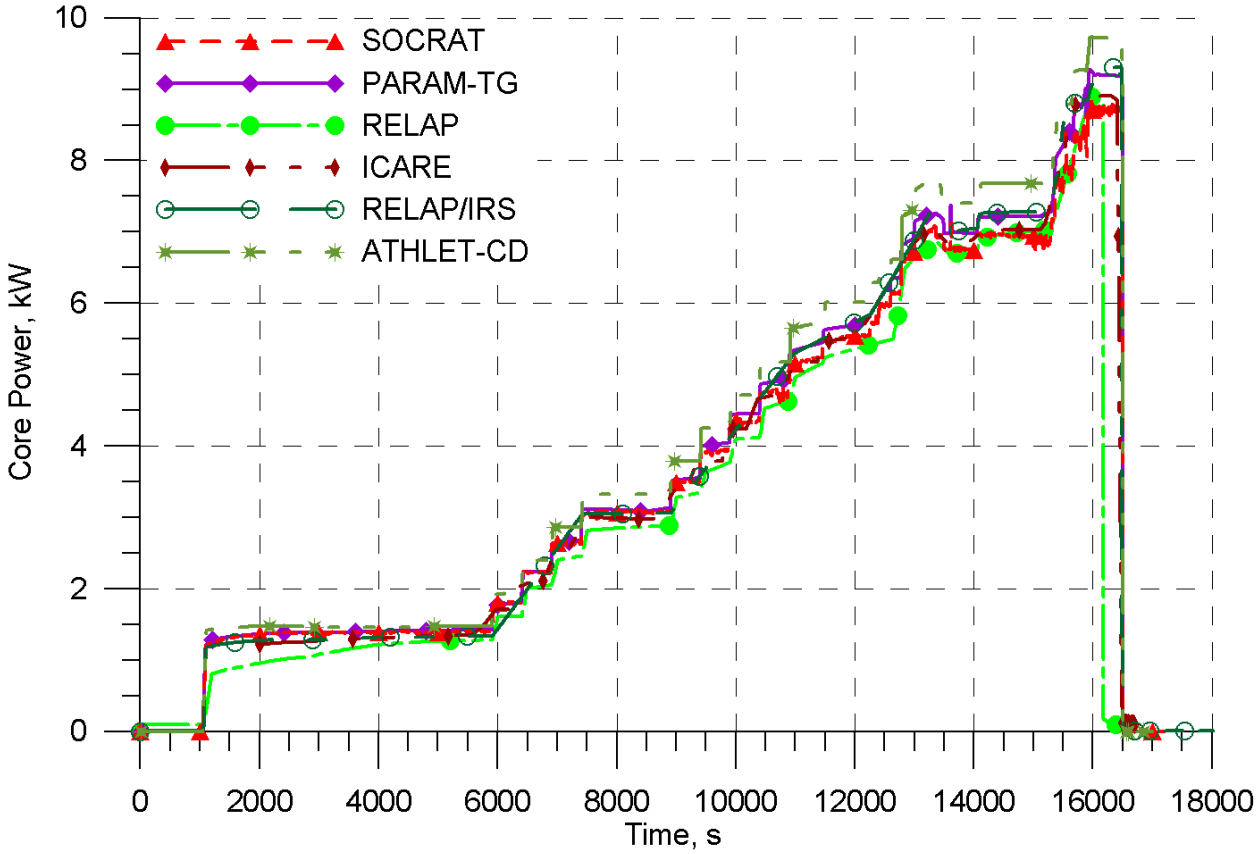

Figure 1.25. Joule heating power over the heated part. PARAMETER-SF2 experiment. Post-test calculations.

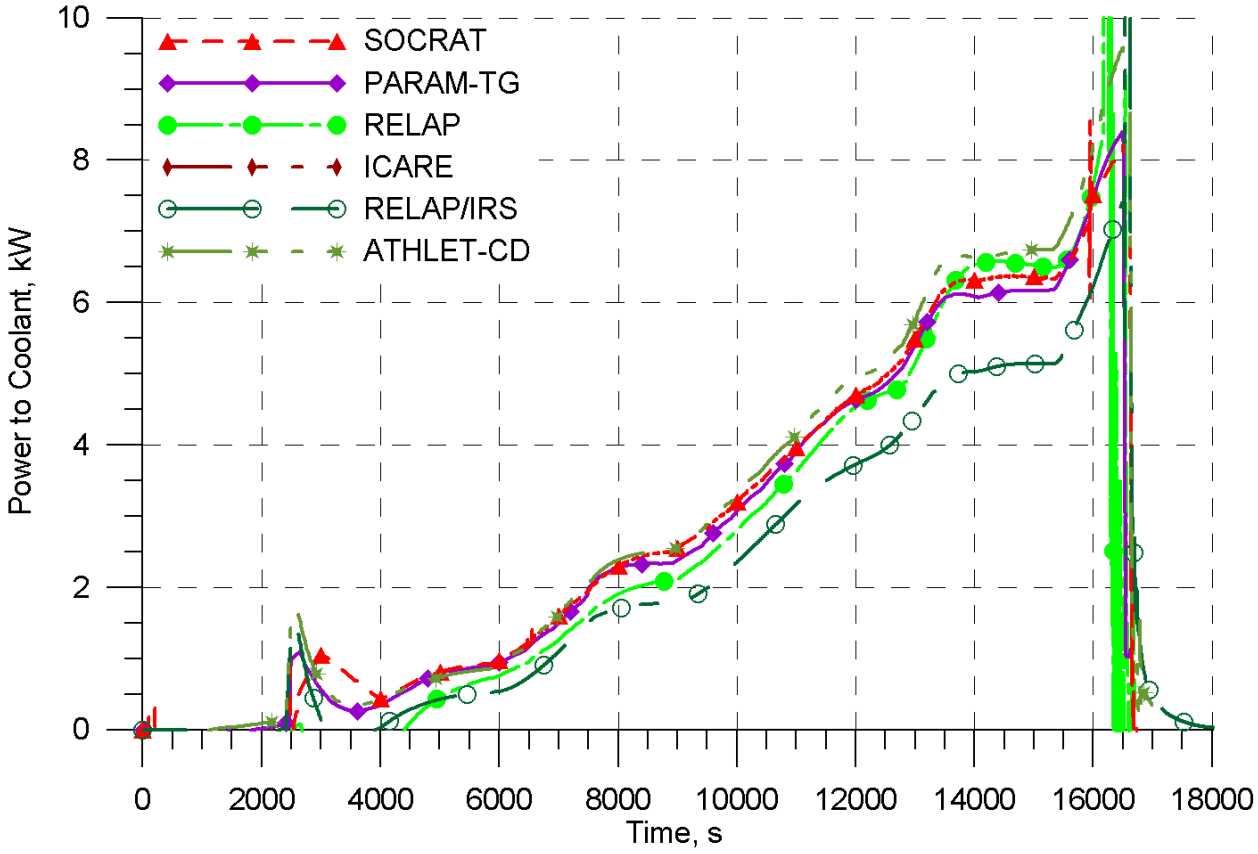

Figure 1.26. Power removed with coolant. PARAMETER-SF2 experiment. Post-test calculations.

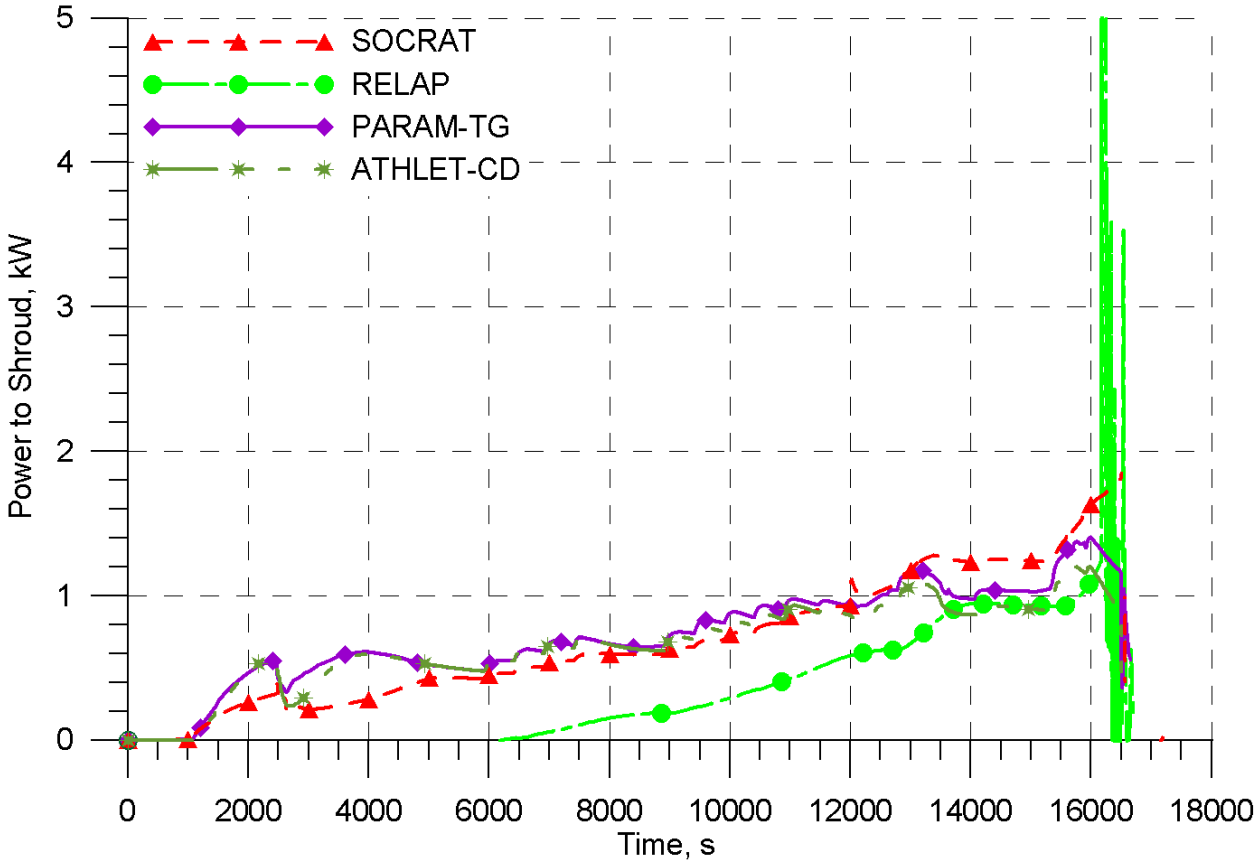

Figure 1.27. Radial heat loss through the shroud. PARAMETER-SF2 experiment. Post-test calculations.

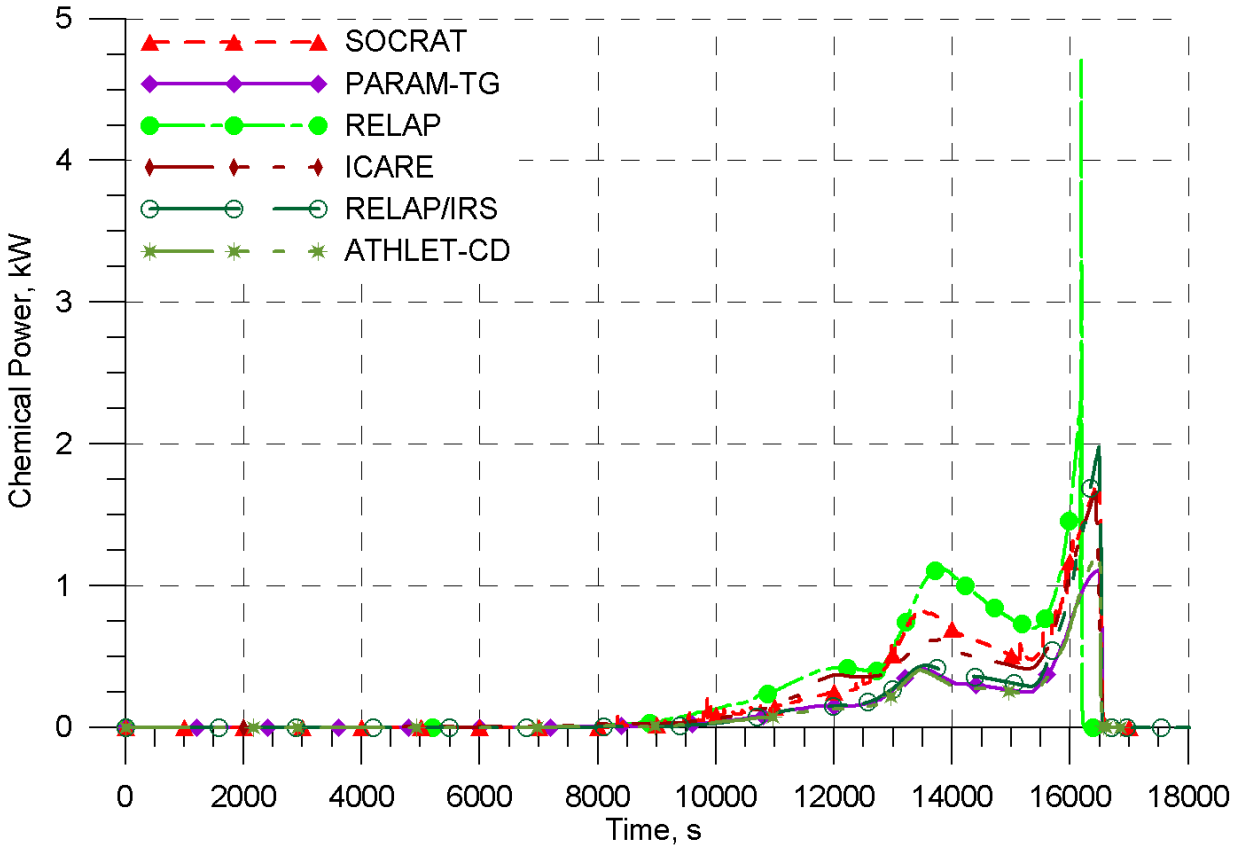

Figure 1.28. Power of oxidation reactions. PARAMETER-SF2 experiment. Post-test calculations.

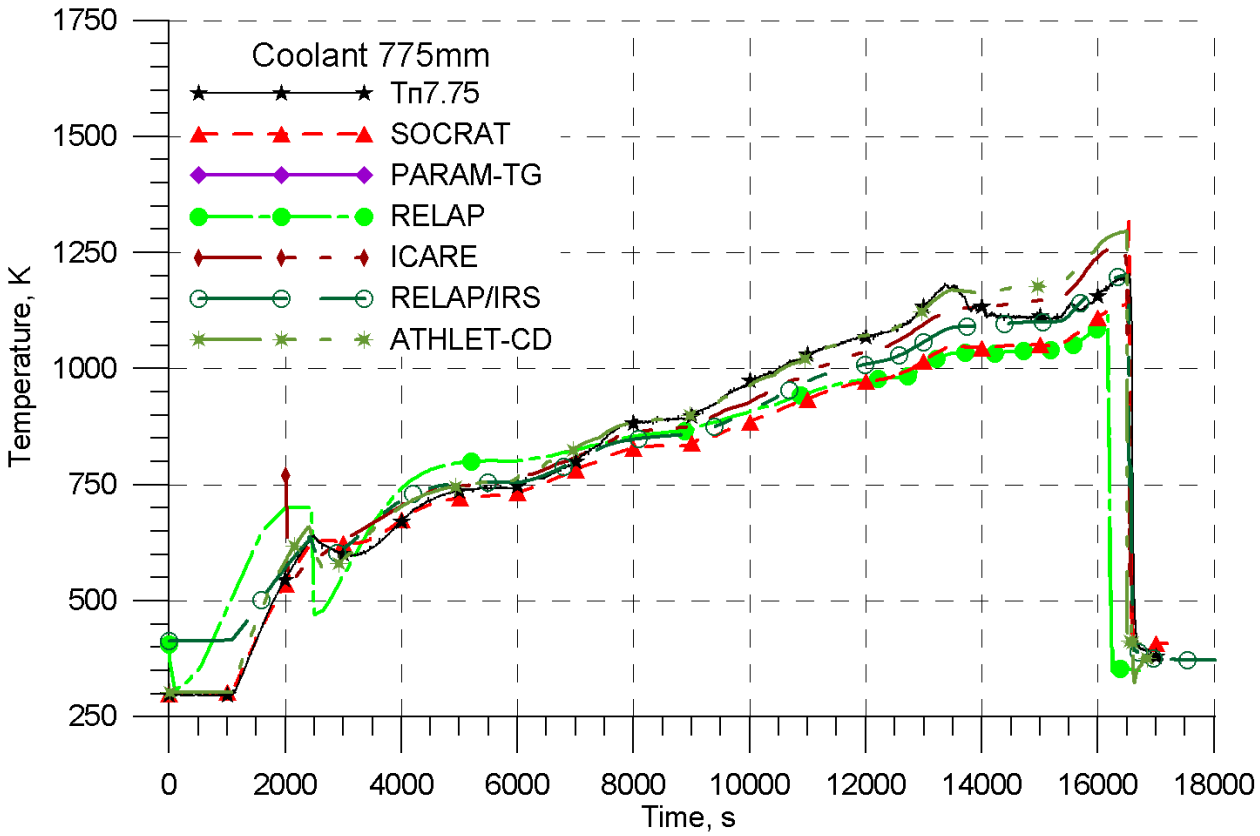

Figure 1.29. Coolant temperature at the elevation of 775 mm. PARAMETER-SF2 experiment. Post-test calculations.

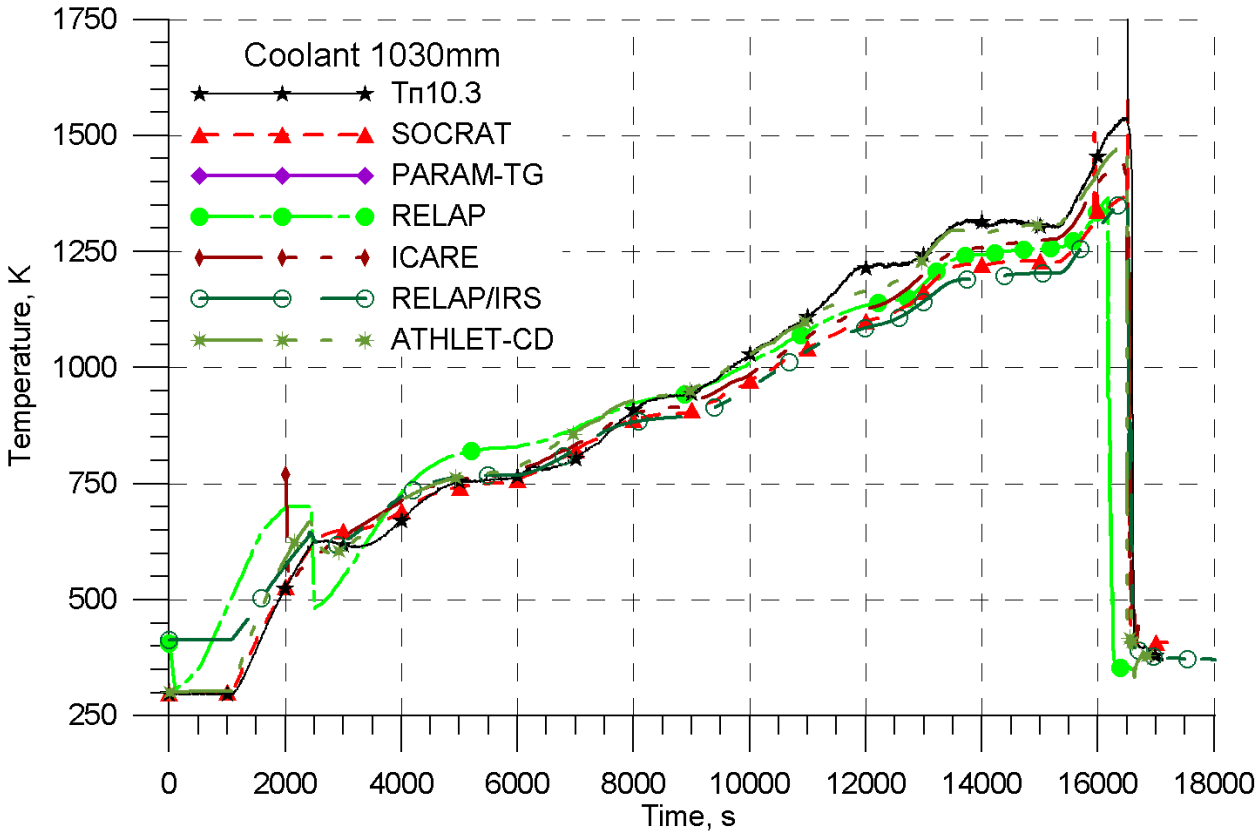

Figure 1.30. Coolant temperature at the elevation of 1030 mm. PARAMETER-SF2 experiment. Post-test calculations.

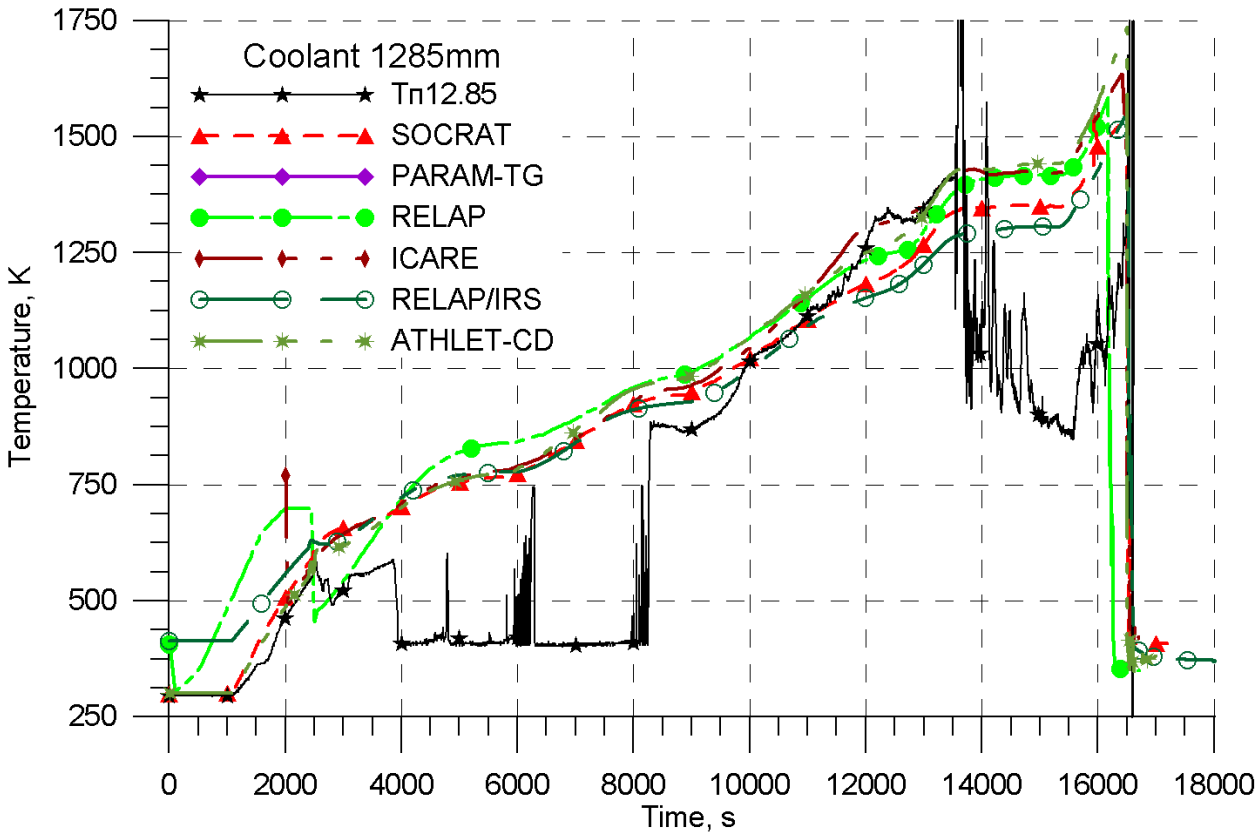

Figure 1.31. Coolant temperature at the elevation of 1285 mm. PARAMETER-SF2 experiment. Post-test calculations.

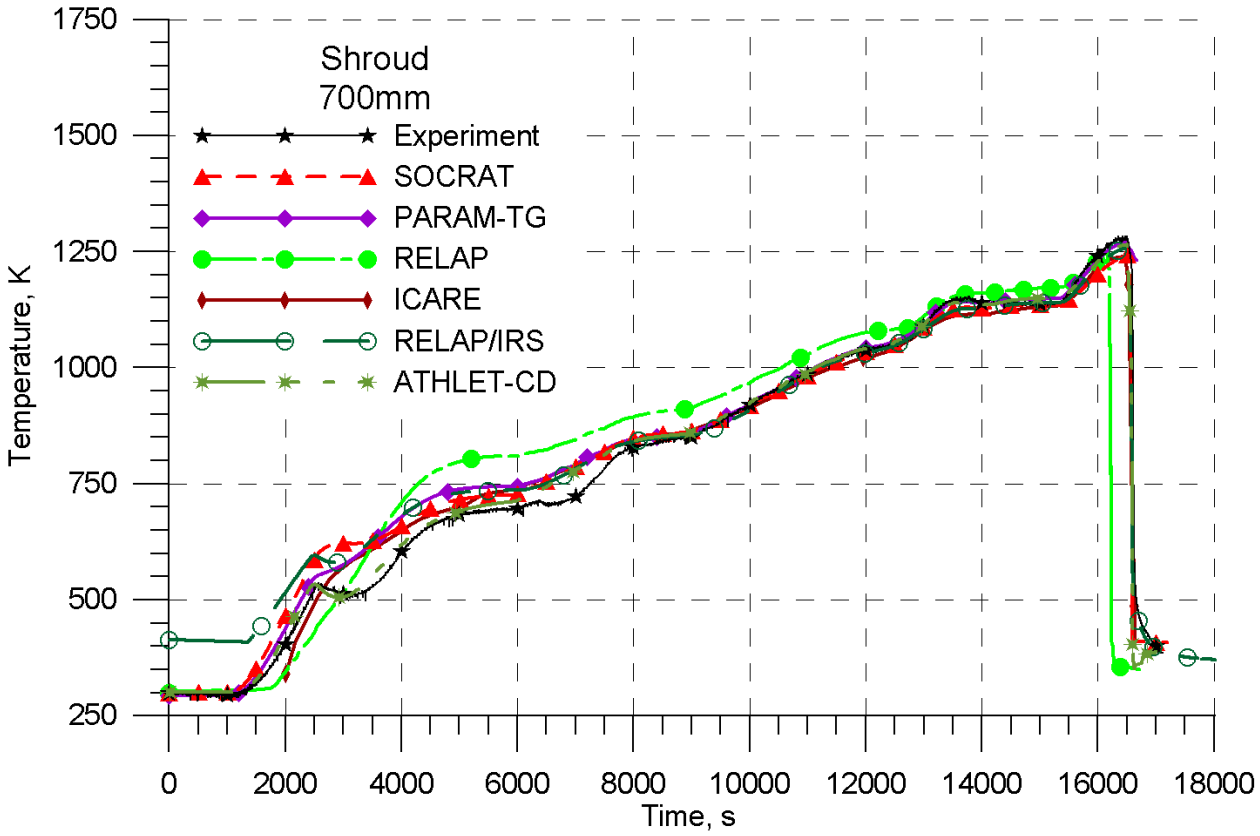

Figure 1.32. Shroud temperature at the elevation of 700 mm. PARAMETER-SF2 experiment. Post-test calculations.

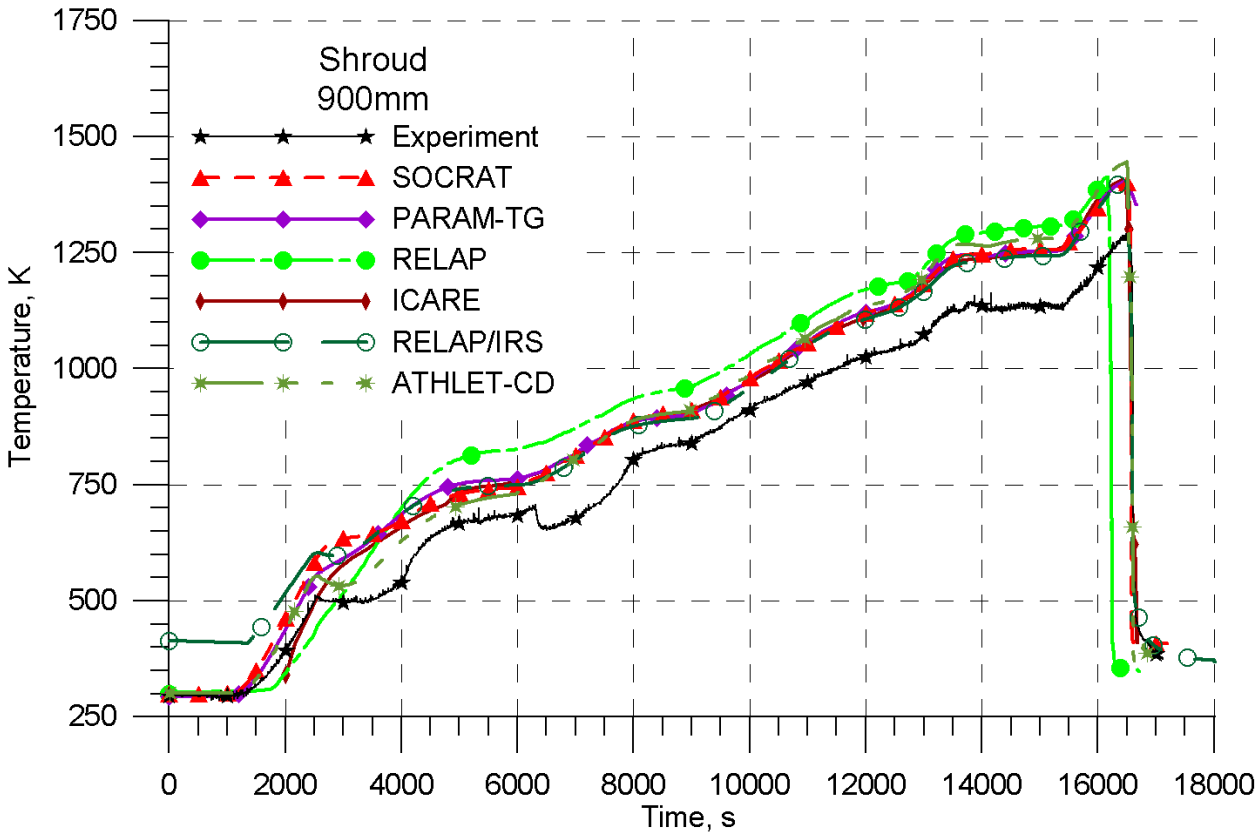

Figure 1.33. Shroud temperature at the elevation of 900 mm. PARAMETER-SF2 experiment. Post-test calculations.

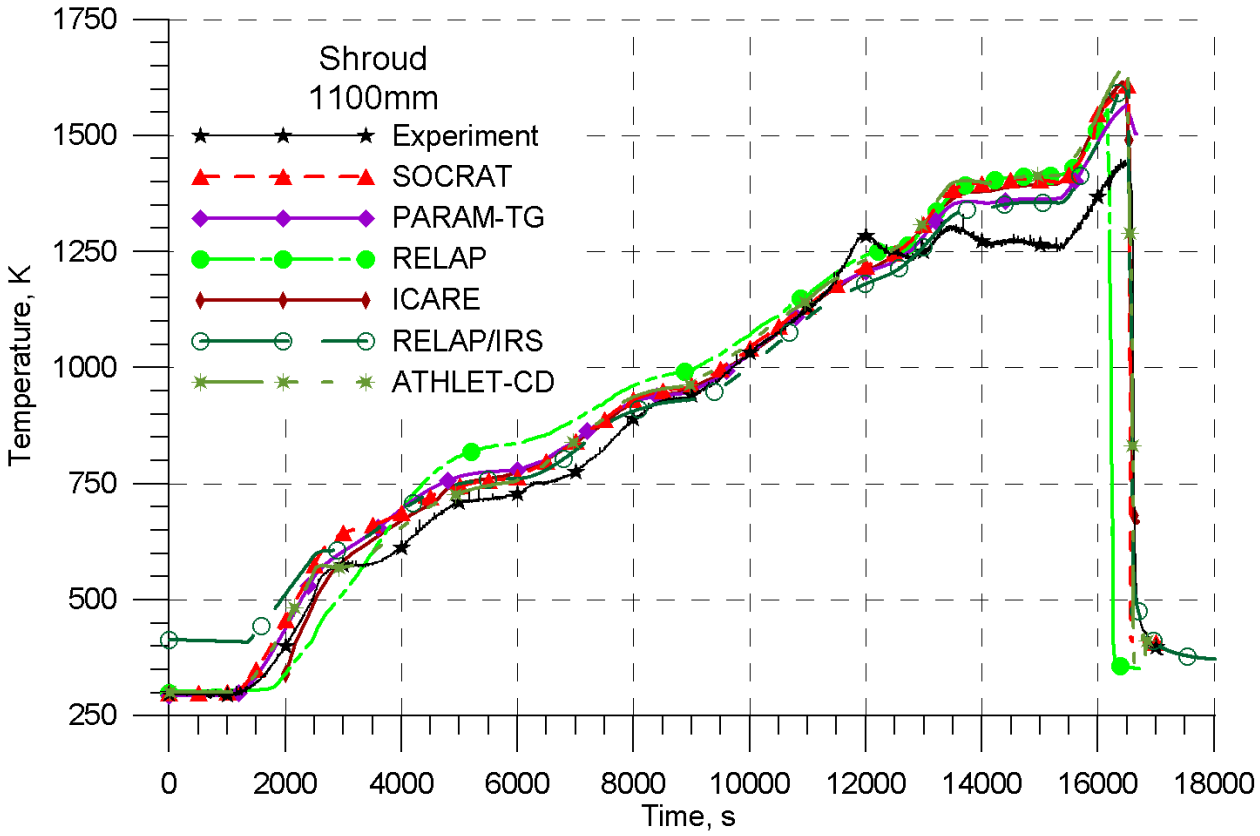

Figure 1.34. Shroud temperature at the elevation of 1100 mm. PARAMETER-SF2 experiment. Post-test calculations.

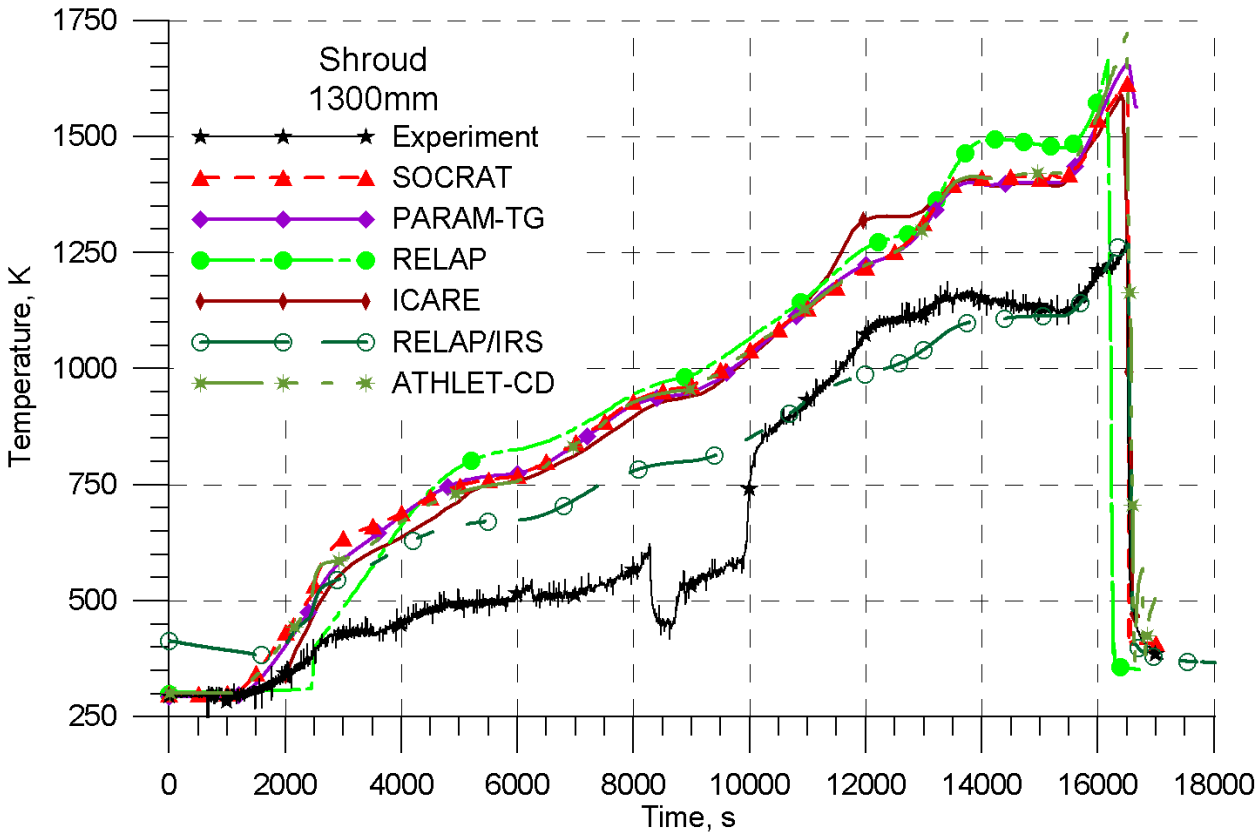

Figure 1.35. Shroud temperature at the elevation of 1300 mm. PARAMETER-SF2 experiment. Post-test calculations.

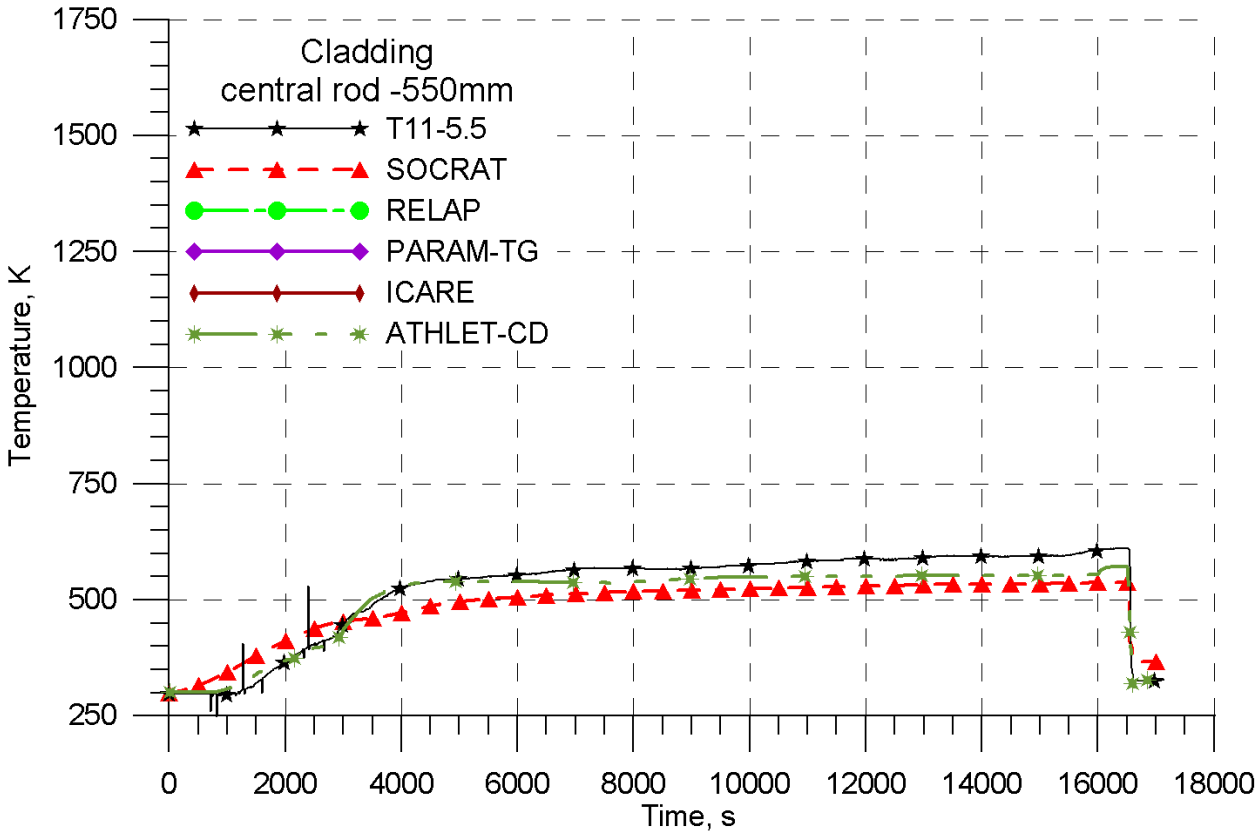

Figure 1.36. Temperature of central fuel rod cladding at the elevation of -550 mm. PARAMETER-SF2 experiment. Post-test calculations.

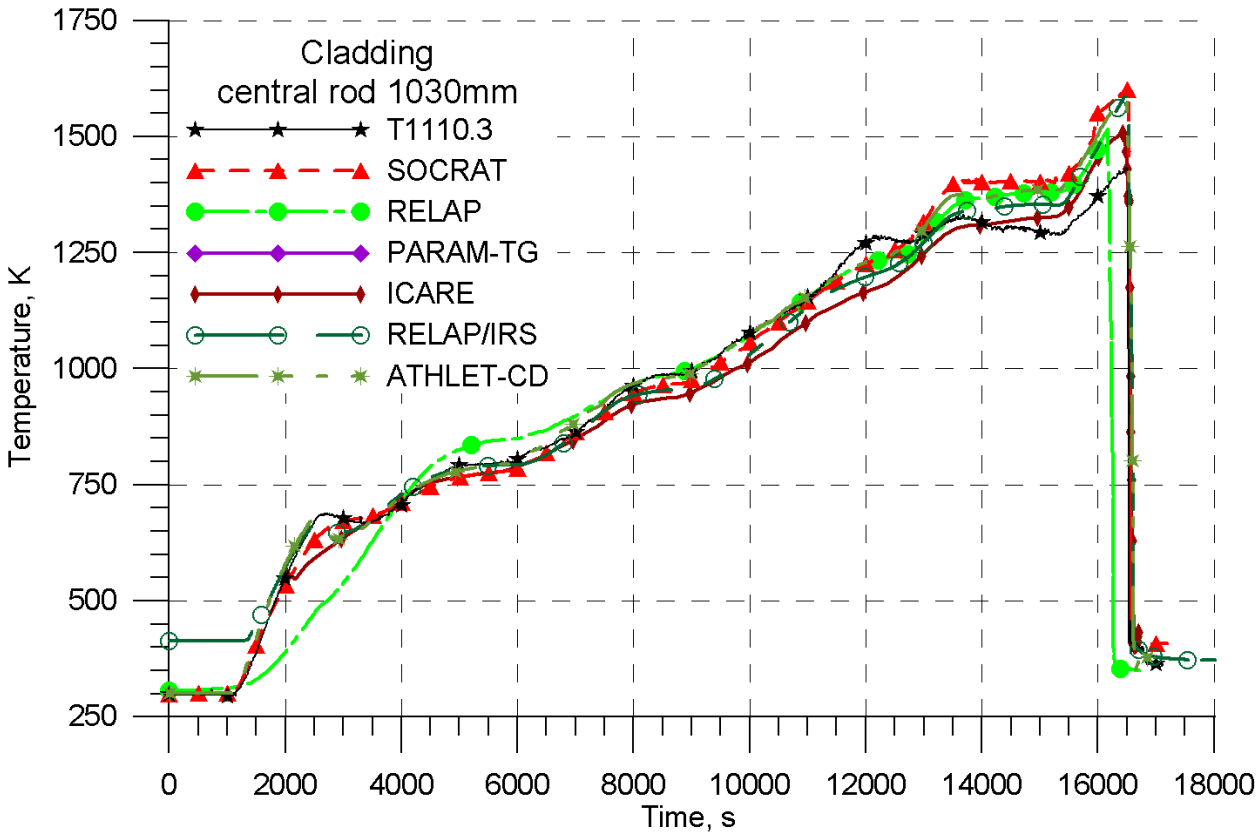

Figure 1.37. Temperature of central fuel rod cladding at the elevation of 1030 mm. PARAMETER-SF2 experiment. Post-test calculations.

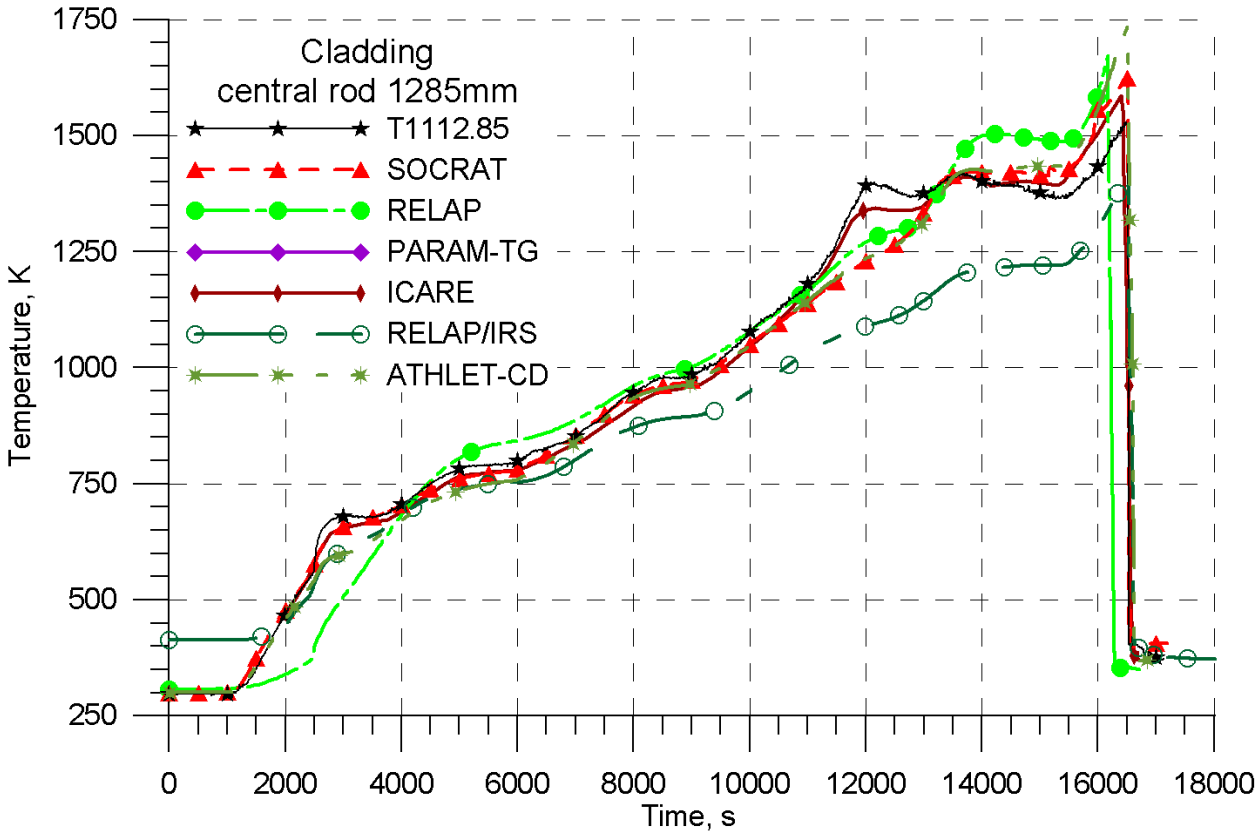

Figure 1.38. Temperature of central fuel rod cladding at the elevation of 1285 mm. PARAMETER-SF2 experiment. Post-test calculations.

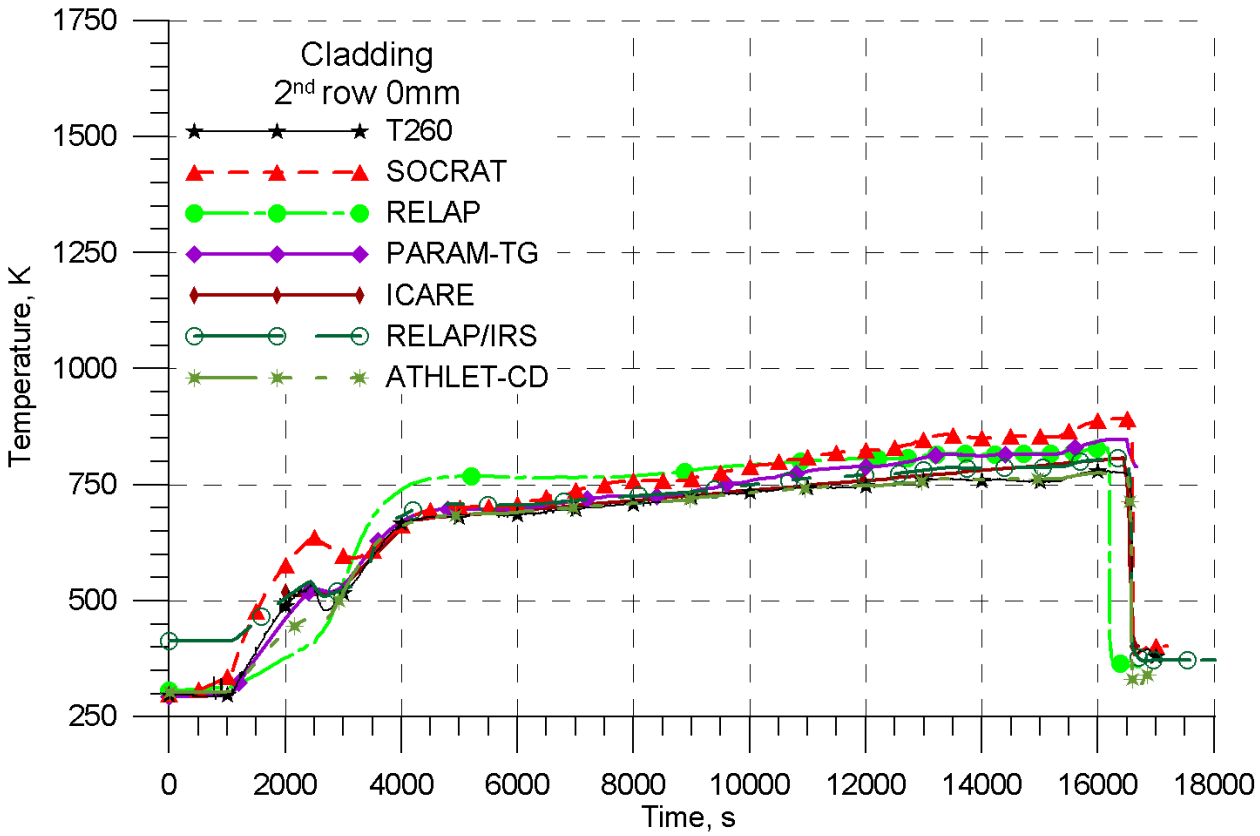

Figure 1.39. Cladding temperature of fuel rod in 2nd row at the elevation of 0 mm. PARAMETER-SF2 experiment. Post-test calculations.

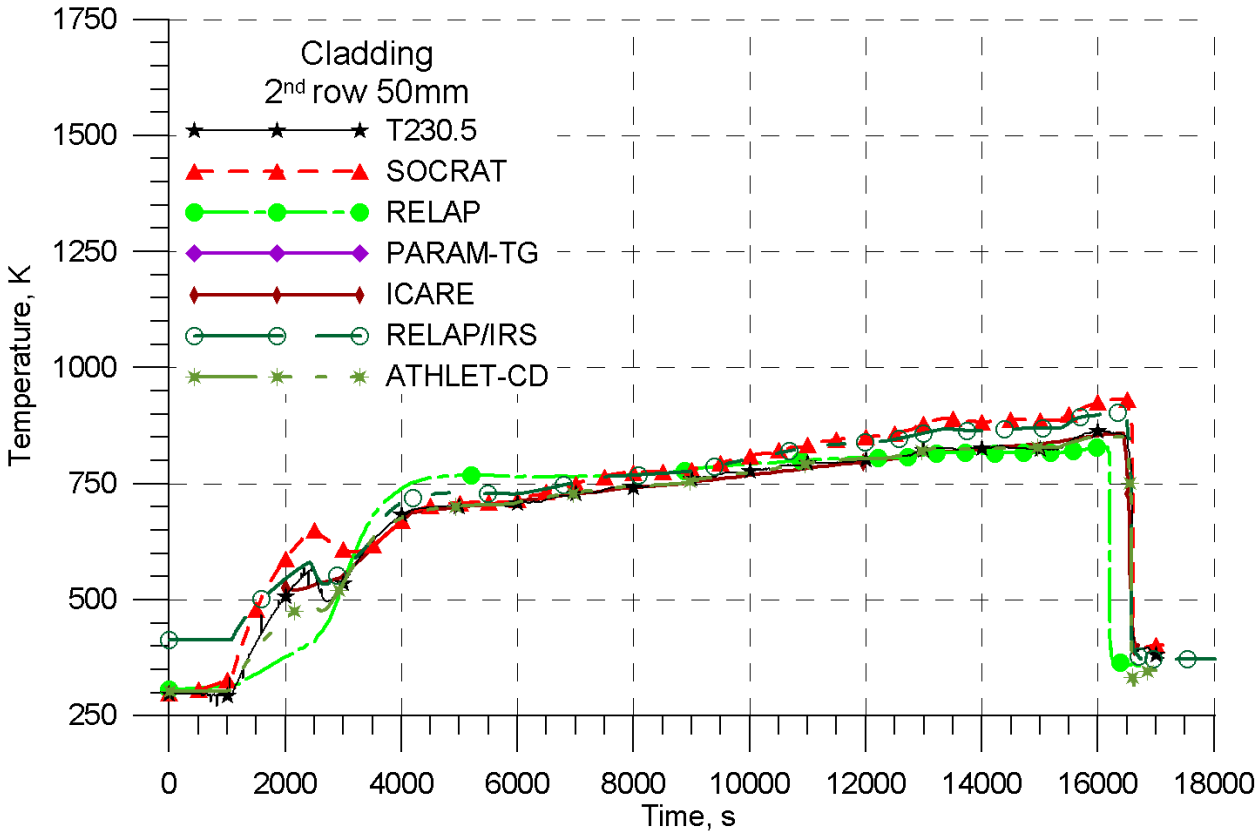

Figure 1.40. Cladding temperature of fuel rod in 2nd row at the elevation of 50 mm. PARAMETER-SF2 experiment. Post-test calculations.

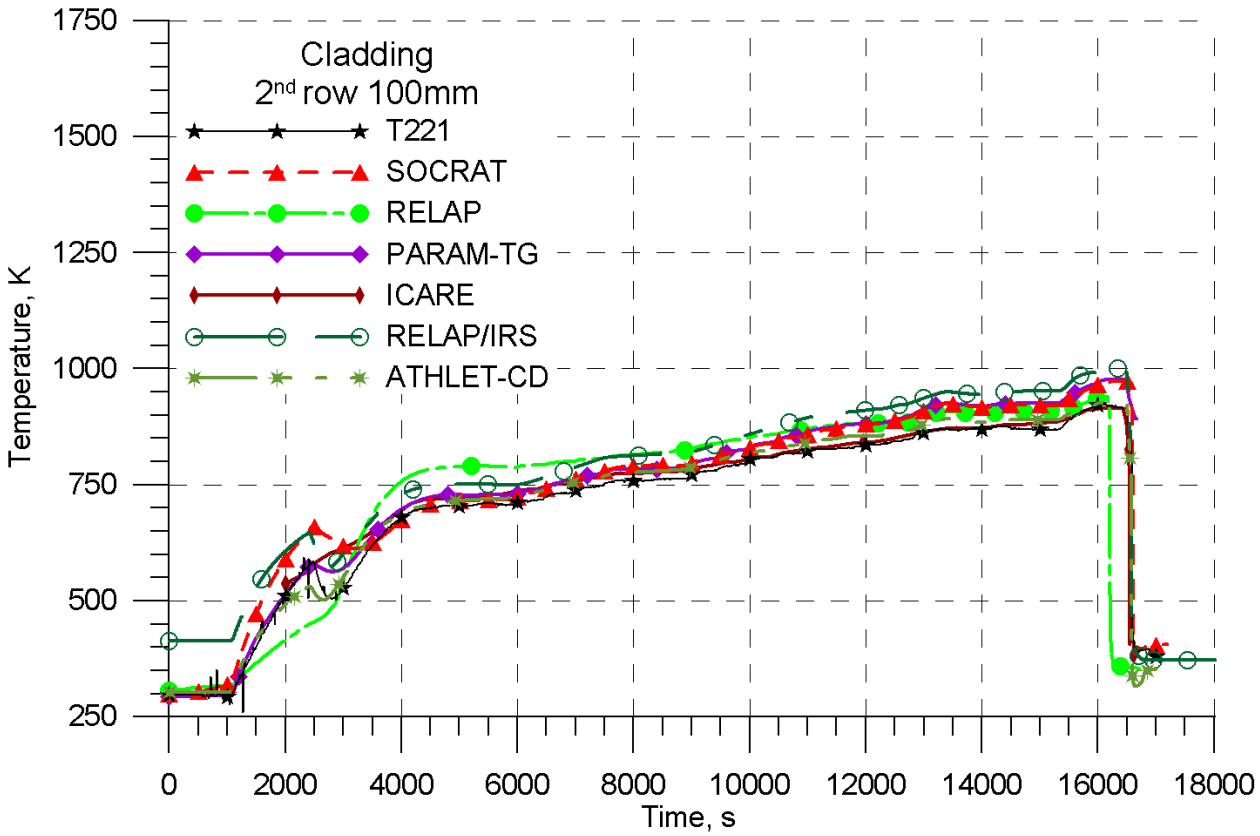

Figure 1.41. Cladding temperature of fuel rod in 2nd row at the elevation of 100 mm. PARAMETER-SF2 experiment. Post-test calculations.

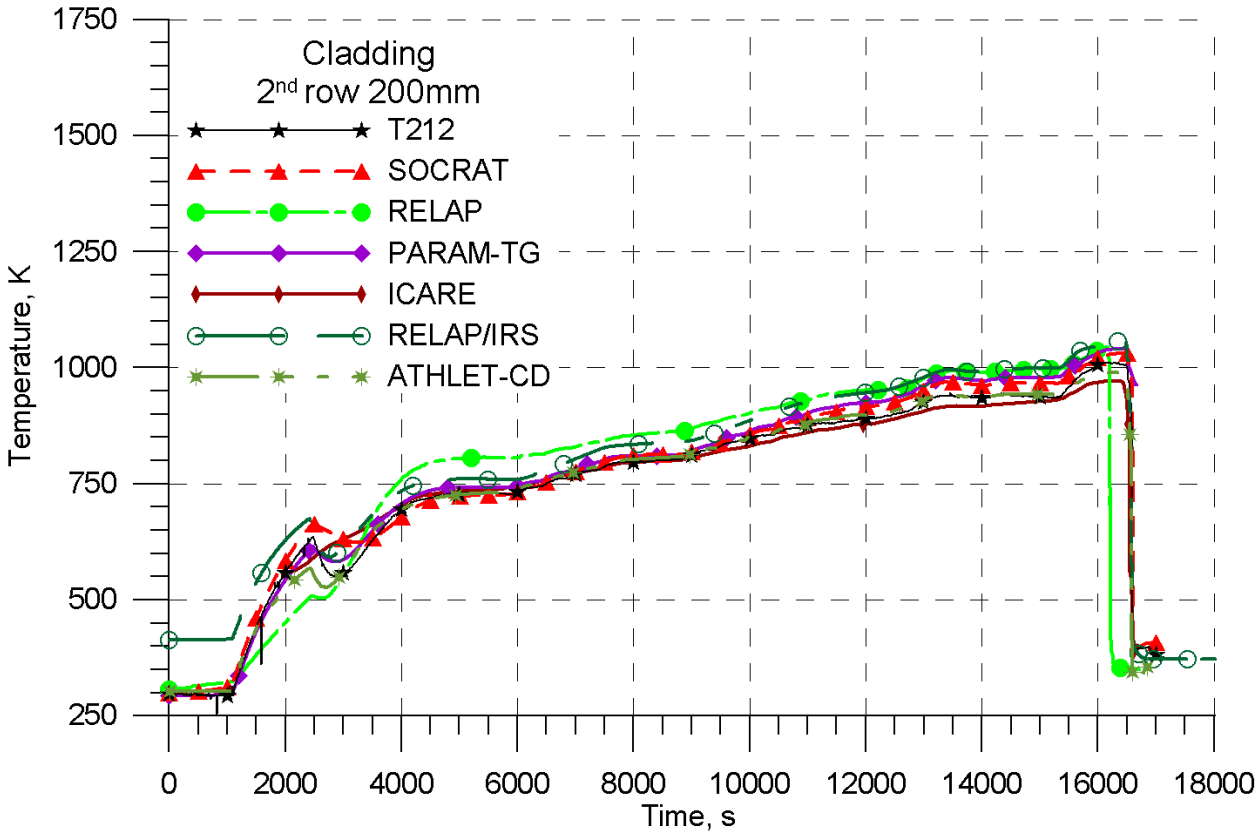

Figure 1.42. Cladding temperature of fuel rod in 2nd row at the elevation of 200 mm. PARAMETER-SF2 experiment. Post-test calculations.

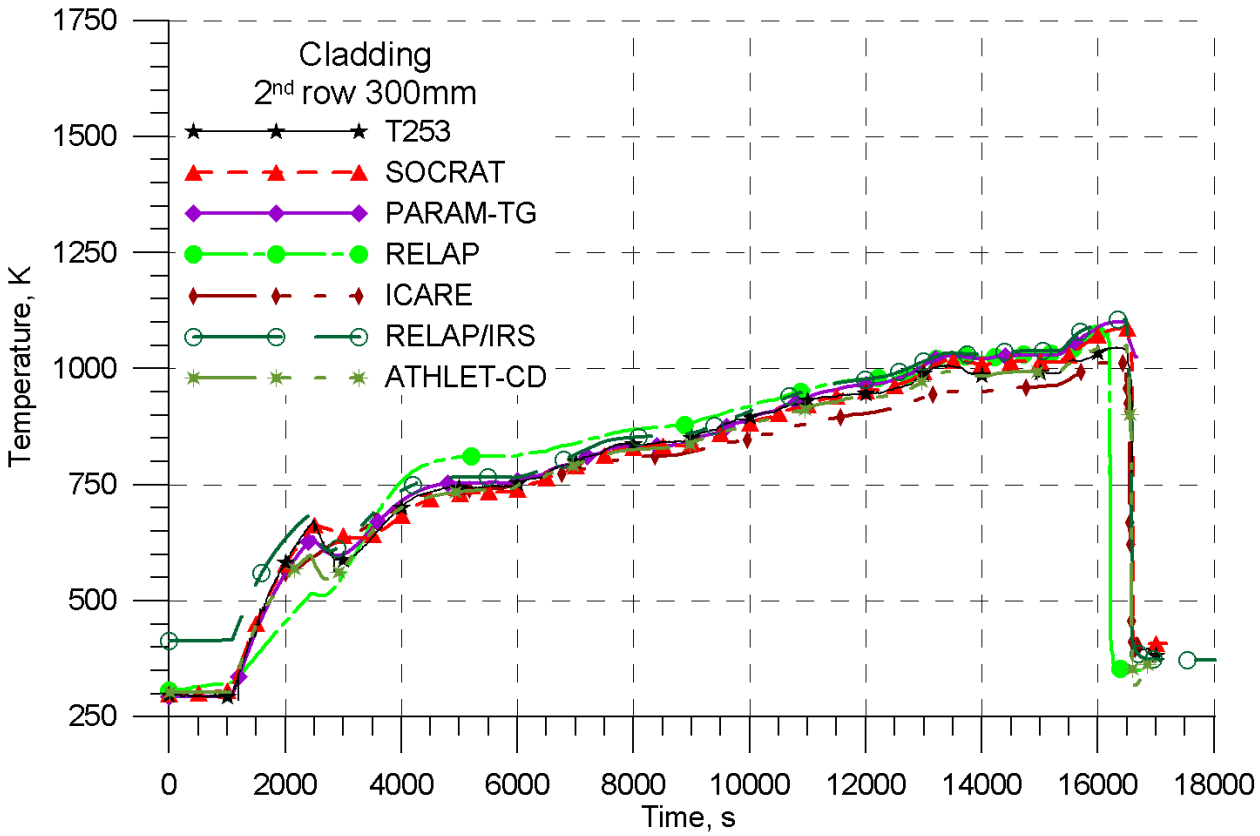

Figure 1.43. Cladding temperature of fuel rod in 2nd row at the elevation of 300 mm. PARAMETER-SF2 experiment. Post-test calculations.

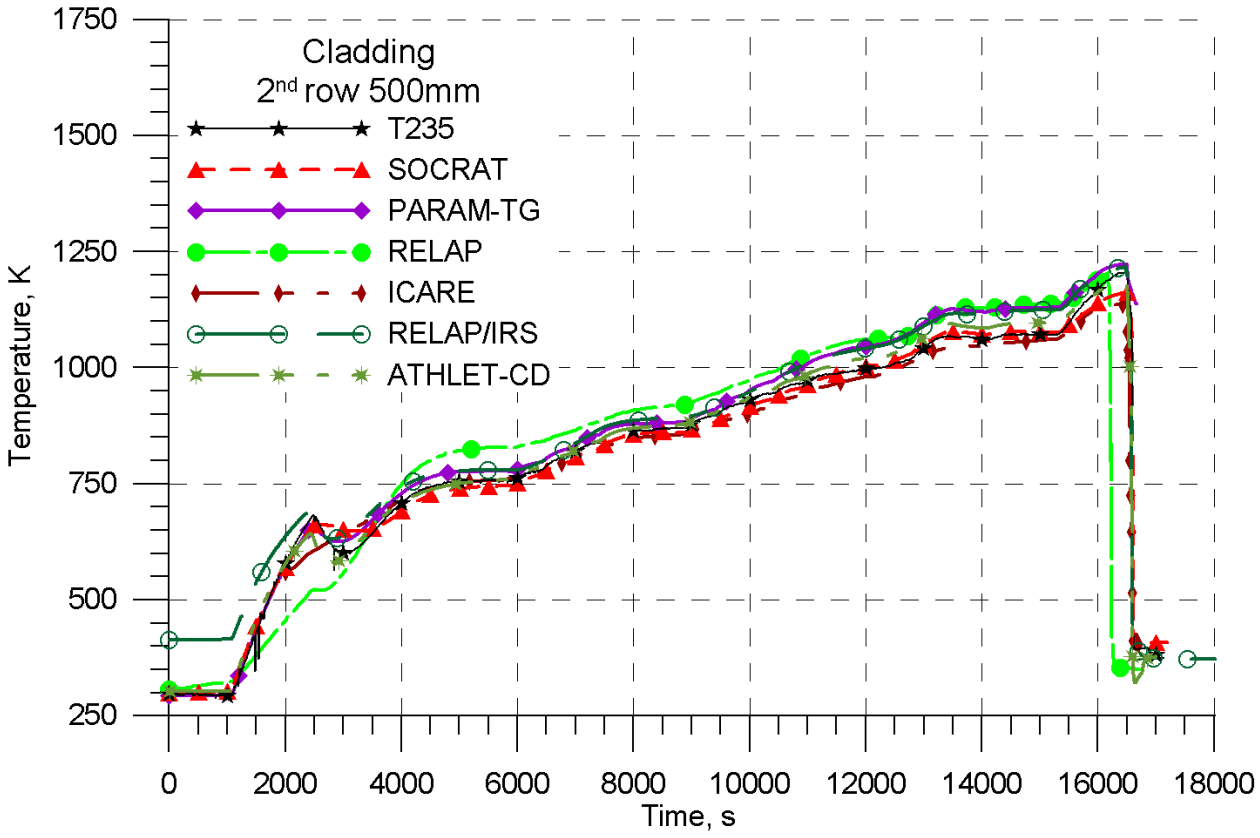

Figure 1.44. Cladding temperature of fuel rod in 2nd row at the elevation of 500 mm. PARAMETER-SF2 experiment. Post-test calculations.

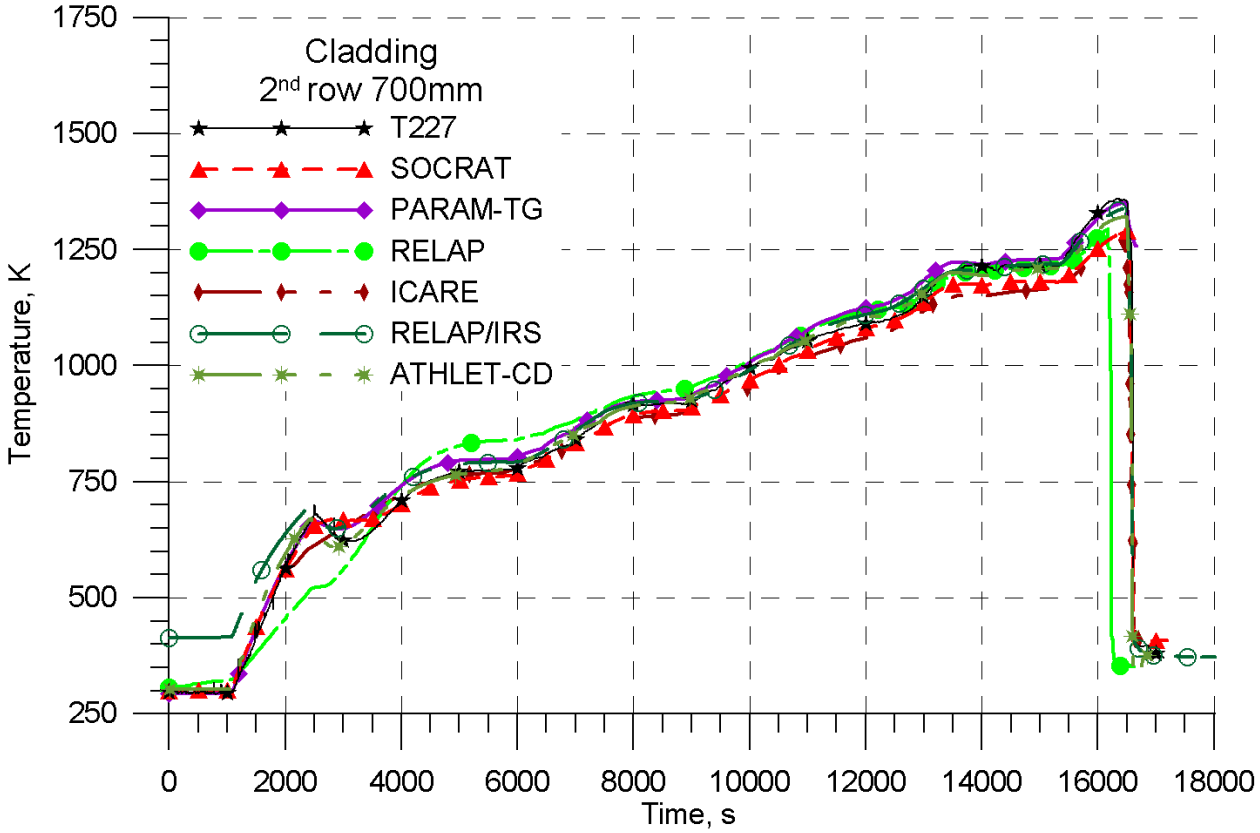

Figure 1.45. Cladding temperature of fuel rod in 2nd row at the elevation of 700 mm. PARAMETER-SF2 experiment. Post-test calculations.

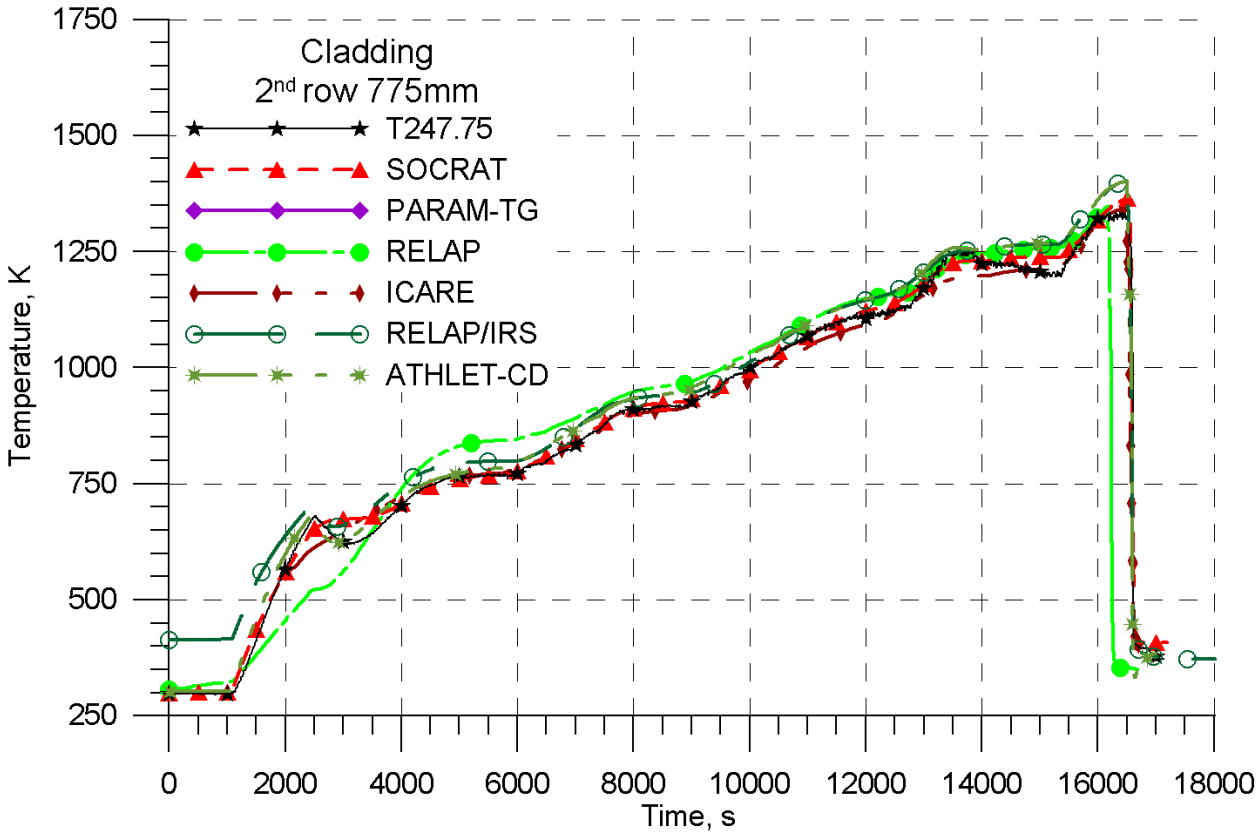

Figure 1.46. Cladding temperature of fuel rod in 2nd row at the elevation of 775 mm. PARAMETER-SF2 experiment. Post-test calculations.

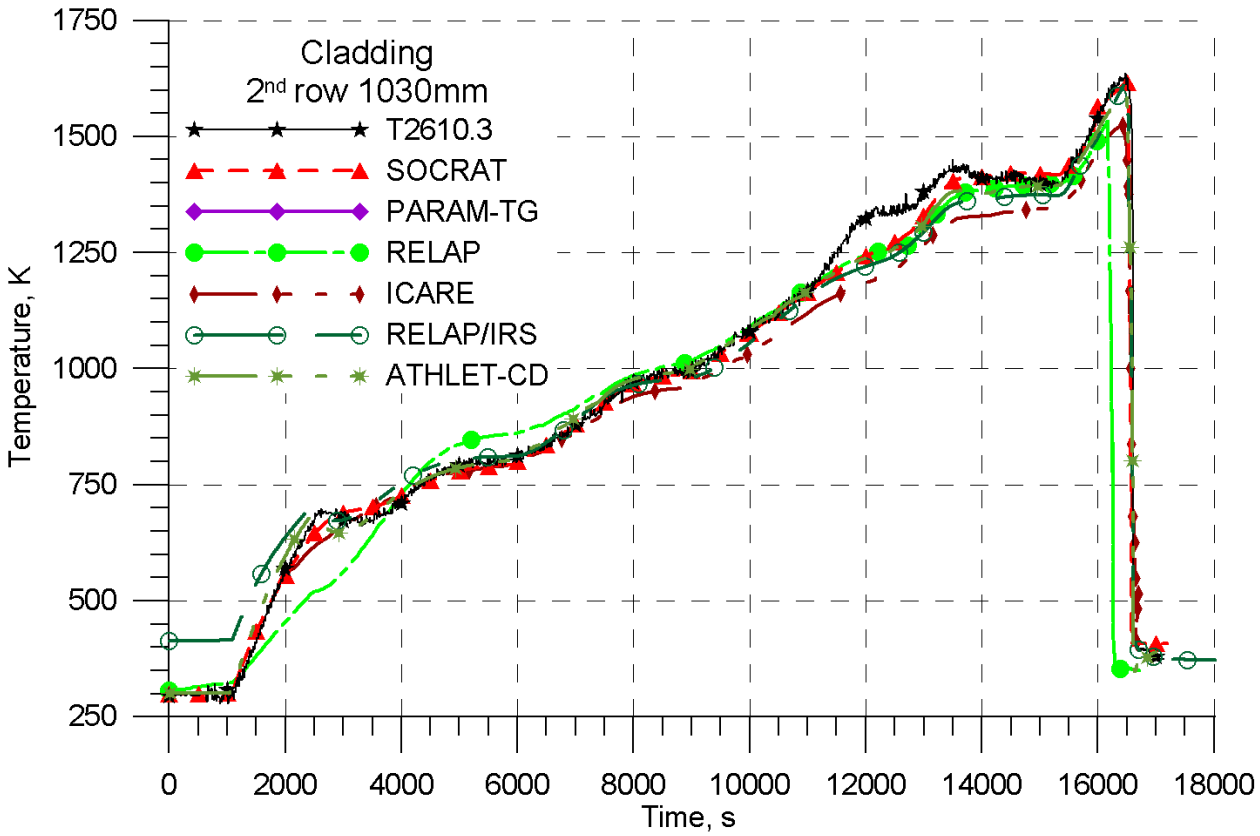

Figure 1.47. Cladding temperature of fuel rod in 2nd row at the elevation of 1030 mm. PARAMETER-SF2 experiment. Post-test calculations.

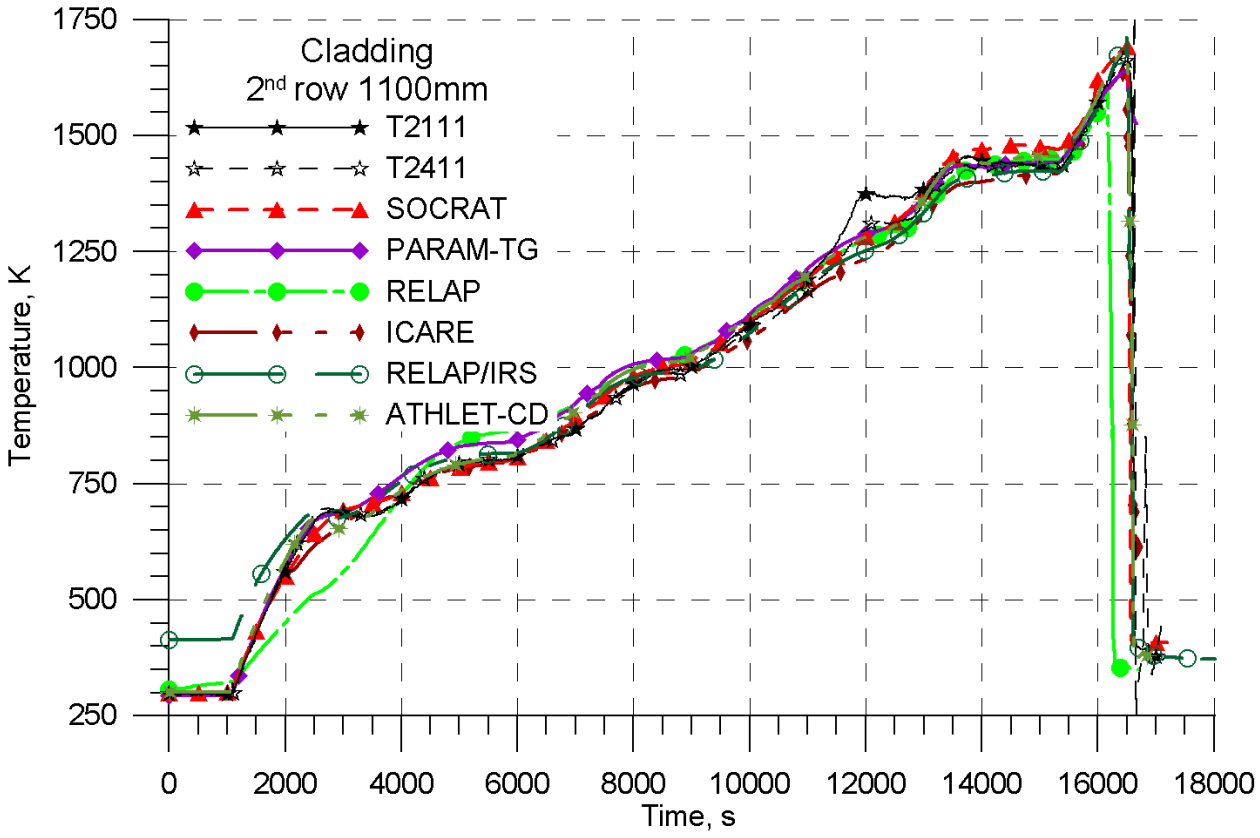

Figure 1.48. Cladding temperature of fuel rod in 2nd row at the elevation of 1100 mm. PARAMETER-SF2 experiment. Post-test calculations.

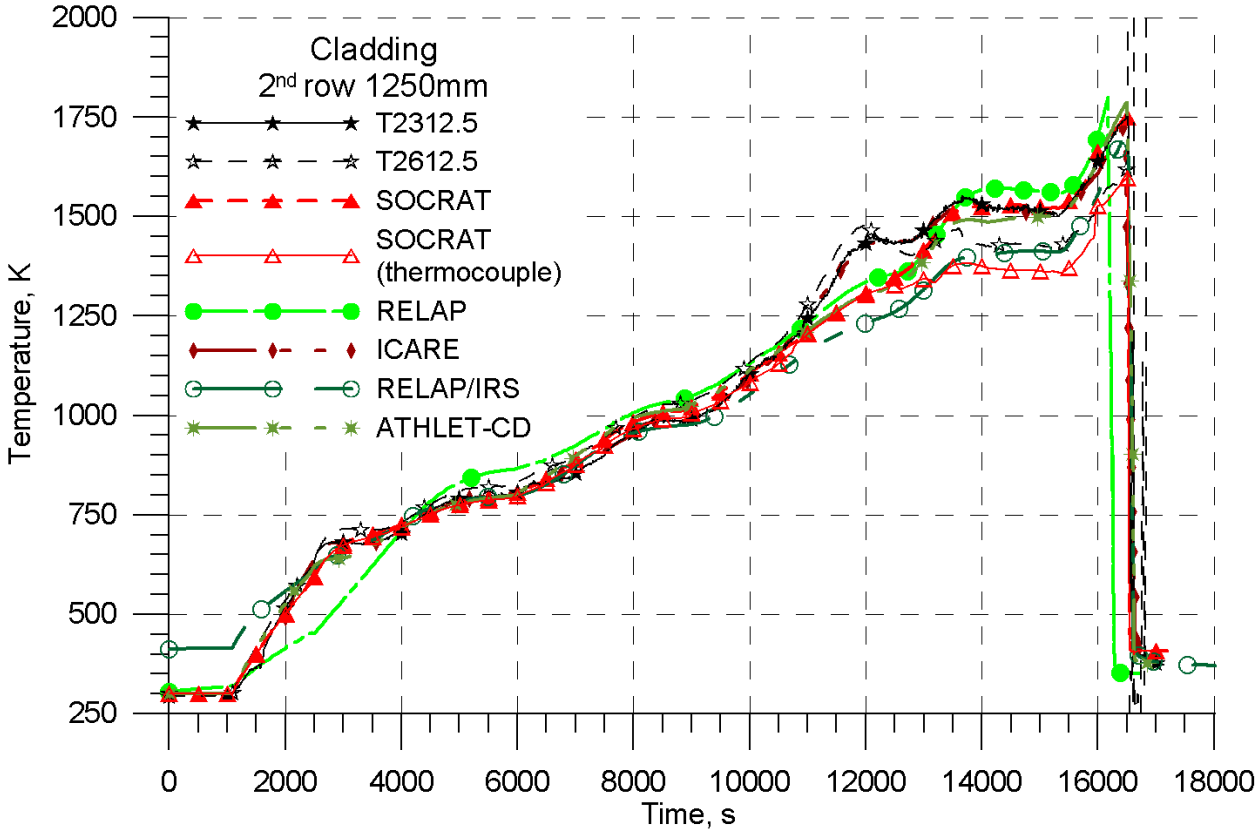

Figure 1.49. Cladding temperature of fuel rod in 2nd row at the elevation of 1250 mm. PARAMETER-SF2 experiment. Post-test calculations.

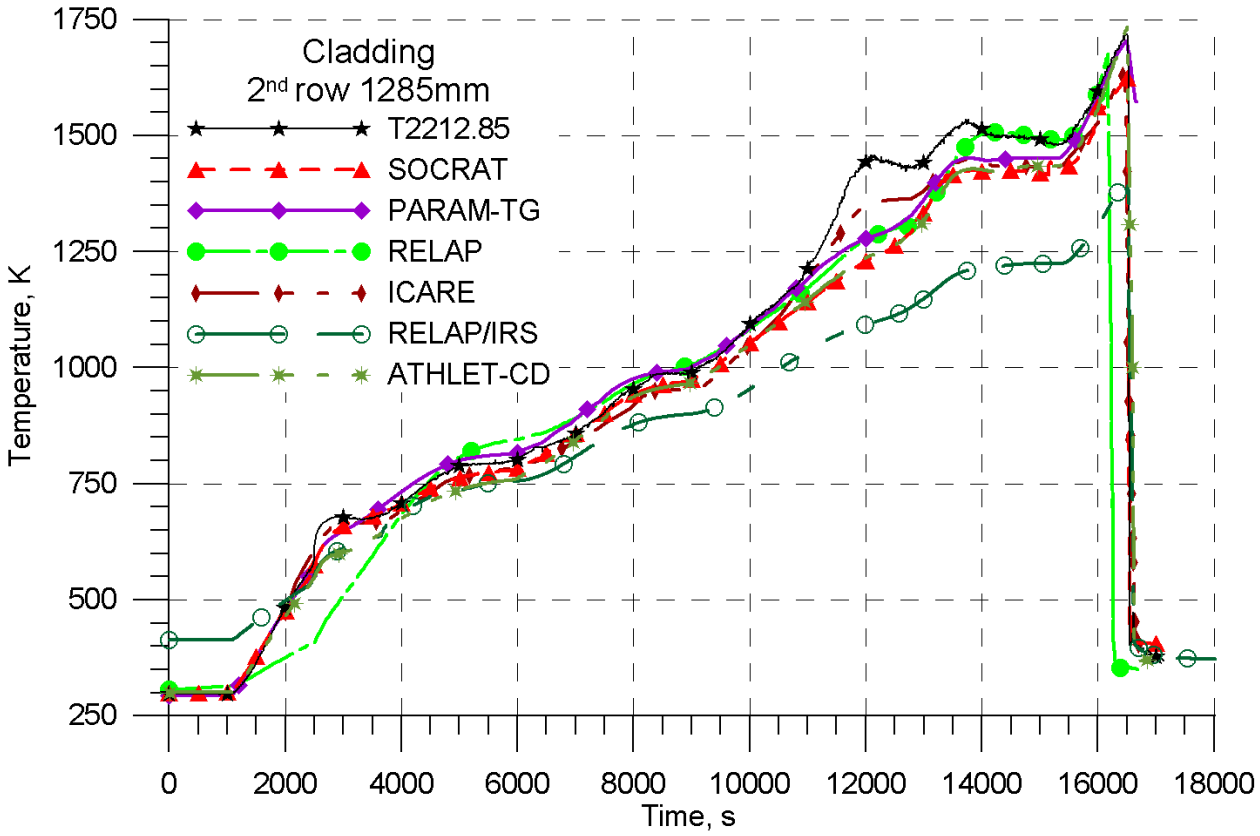

Figure 1.50. Cladding temperature of fuel rod in 2nd row at the elevation of 1285 mm. PARAMETER-SF2 experiment. Post-test calculations.

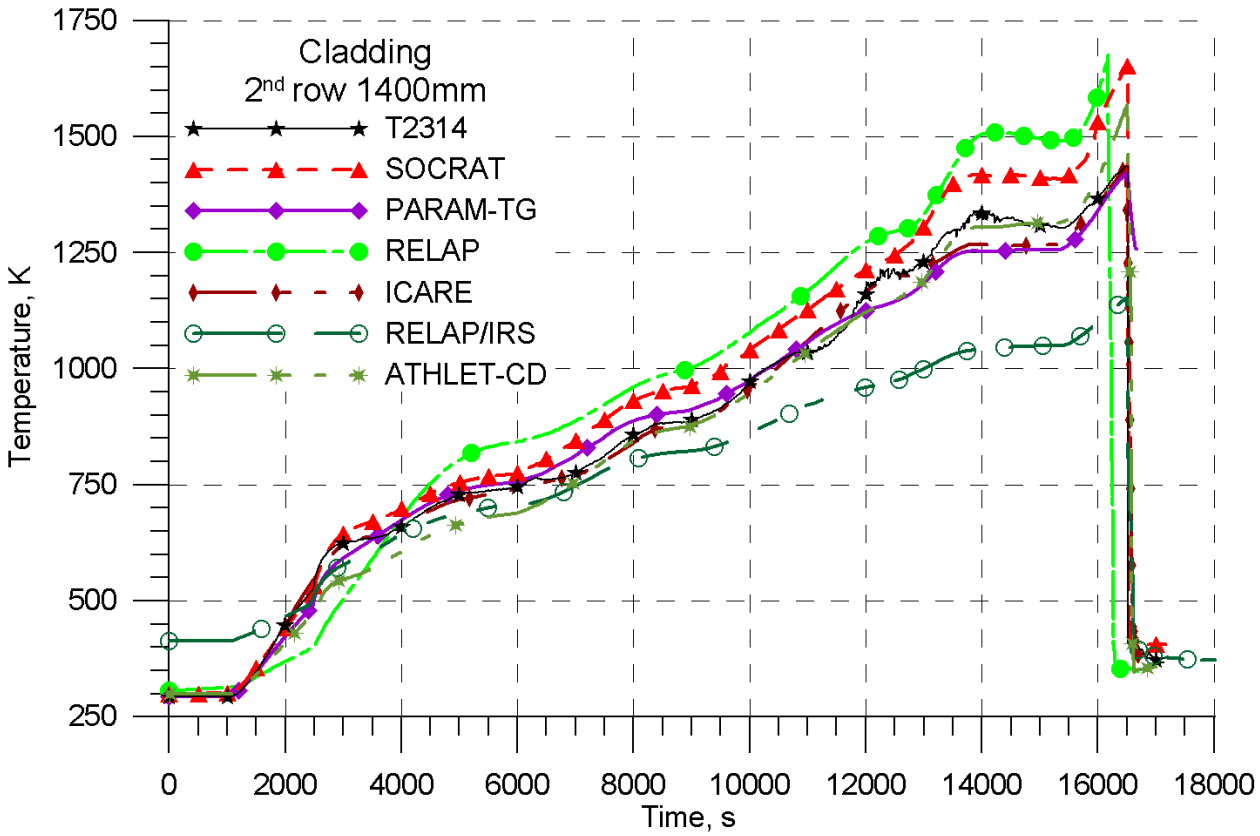

Figure 1.51. Cladding temperature of fuel rod in 2nd row at the elevation of 1400 mm. PARAMETER-SF2 experiment. Post-test calculations.

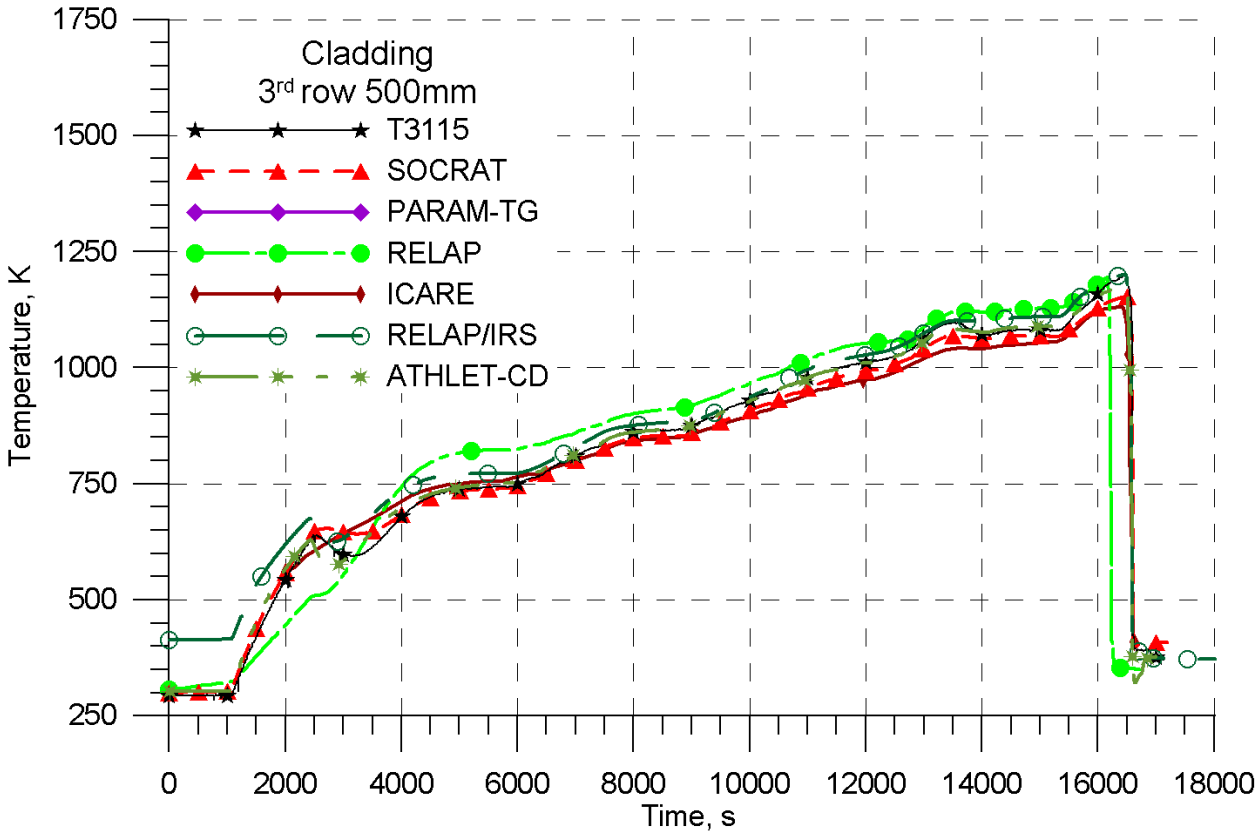

Figure 1.52. Cladding temperature of fuel rod in 3rd row at the elevation of 500 mm. PARAMETER-SF2 experiment. Post-test calculations.

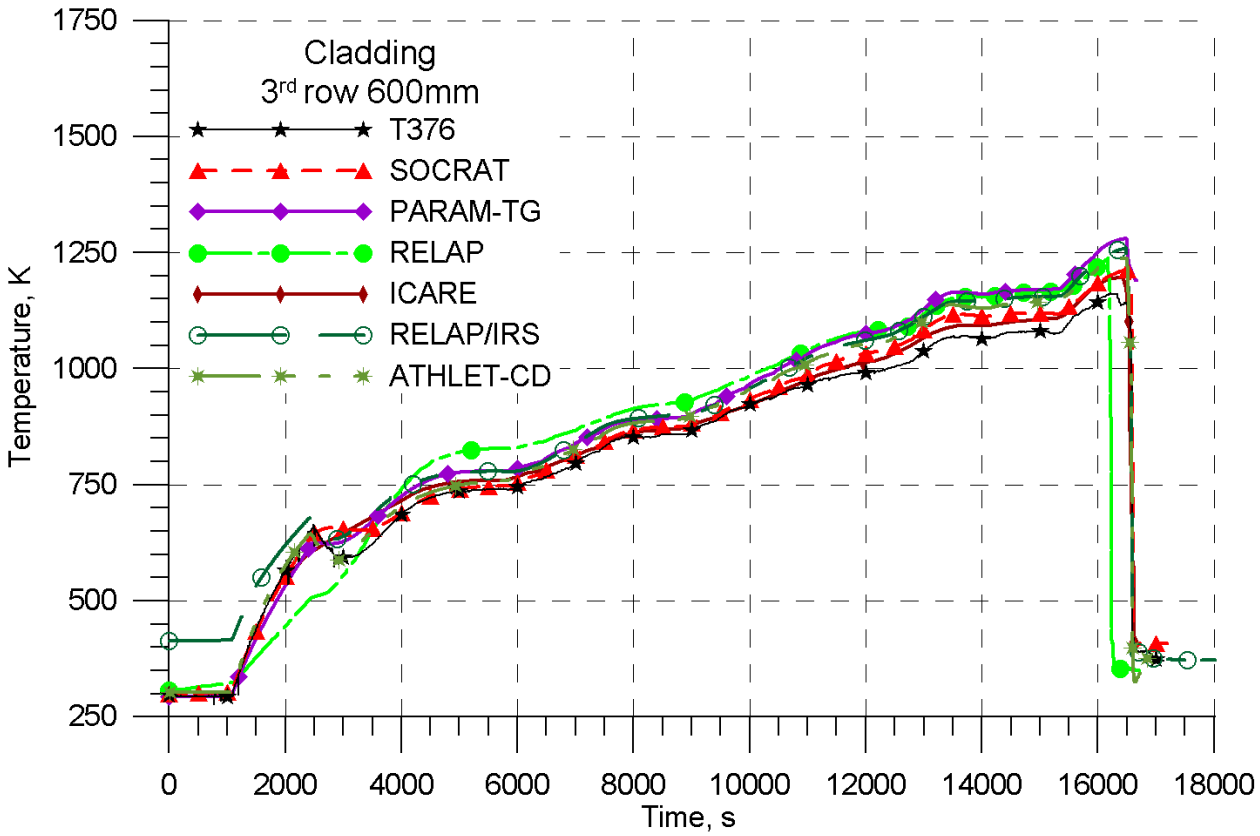

Figure 1.53. Cladding temperature of fuel rod in 3rd row at the elevation of 600 mm. PARAMETER-SF2 experiment. Post-test calculations.

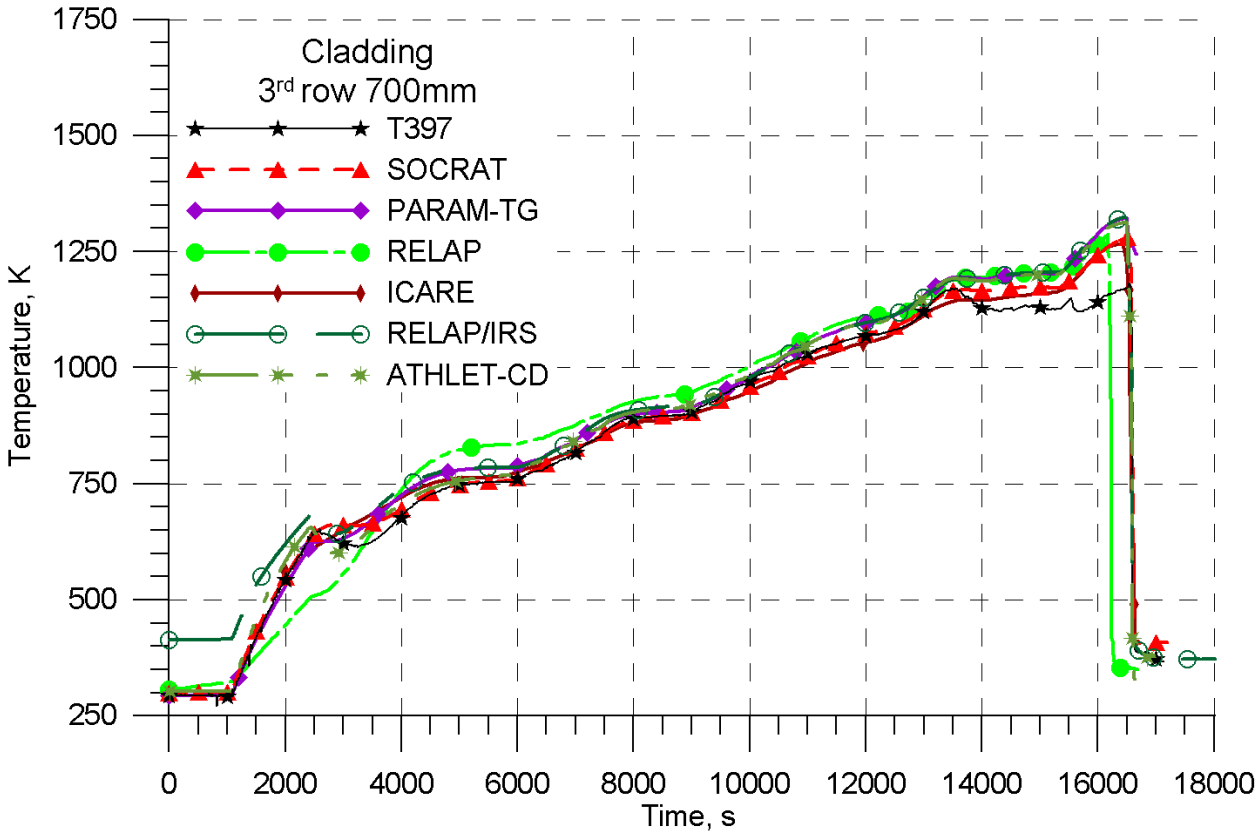

Figure 1.54. Cladding temperature of fuel rod in 3rd row at the elevation of 700 mm. PARAMETER-SF2 experiment. Post-test calculations.

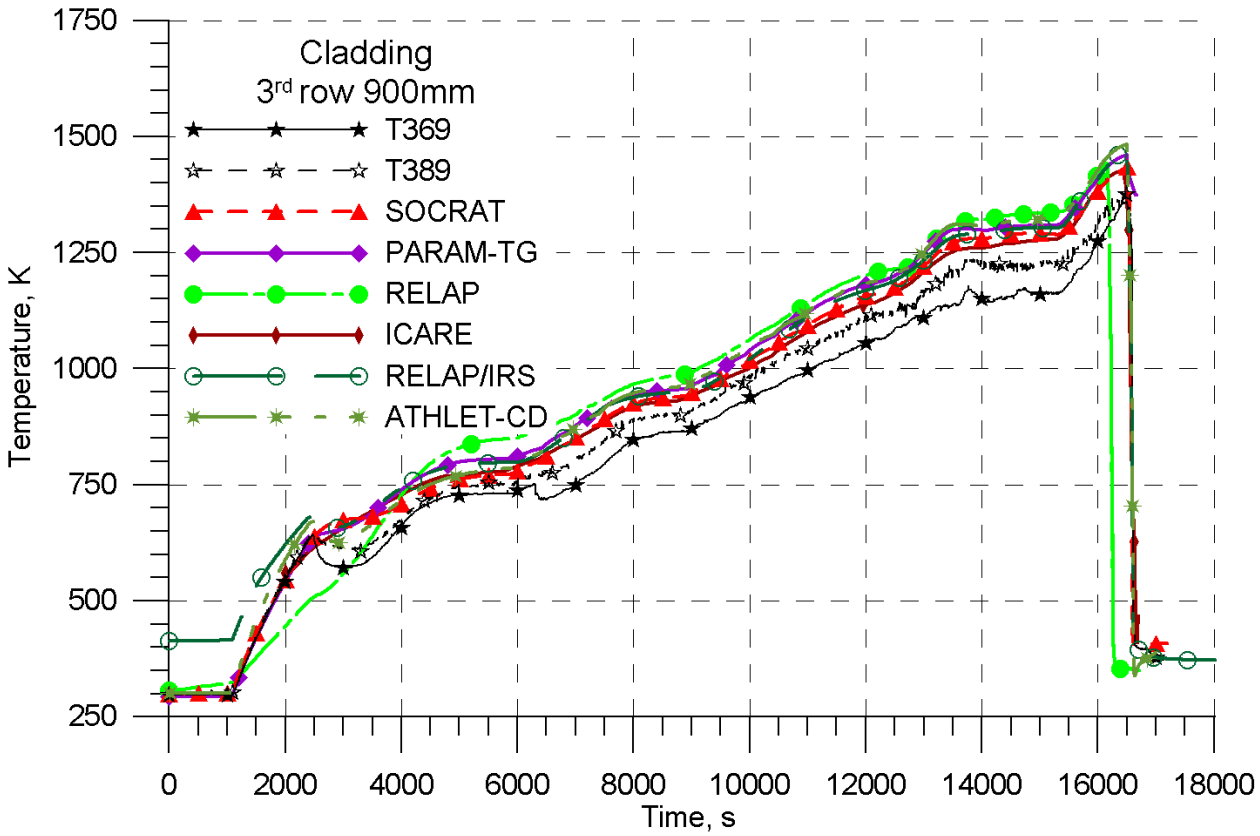

Figure 1.55. Cladding temperature of fuel rod in 3rd row at the elevation of 900 mm. PARAMETER-SF2 experiment. Post-test calculations.

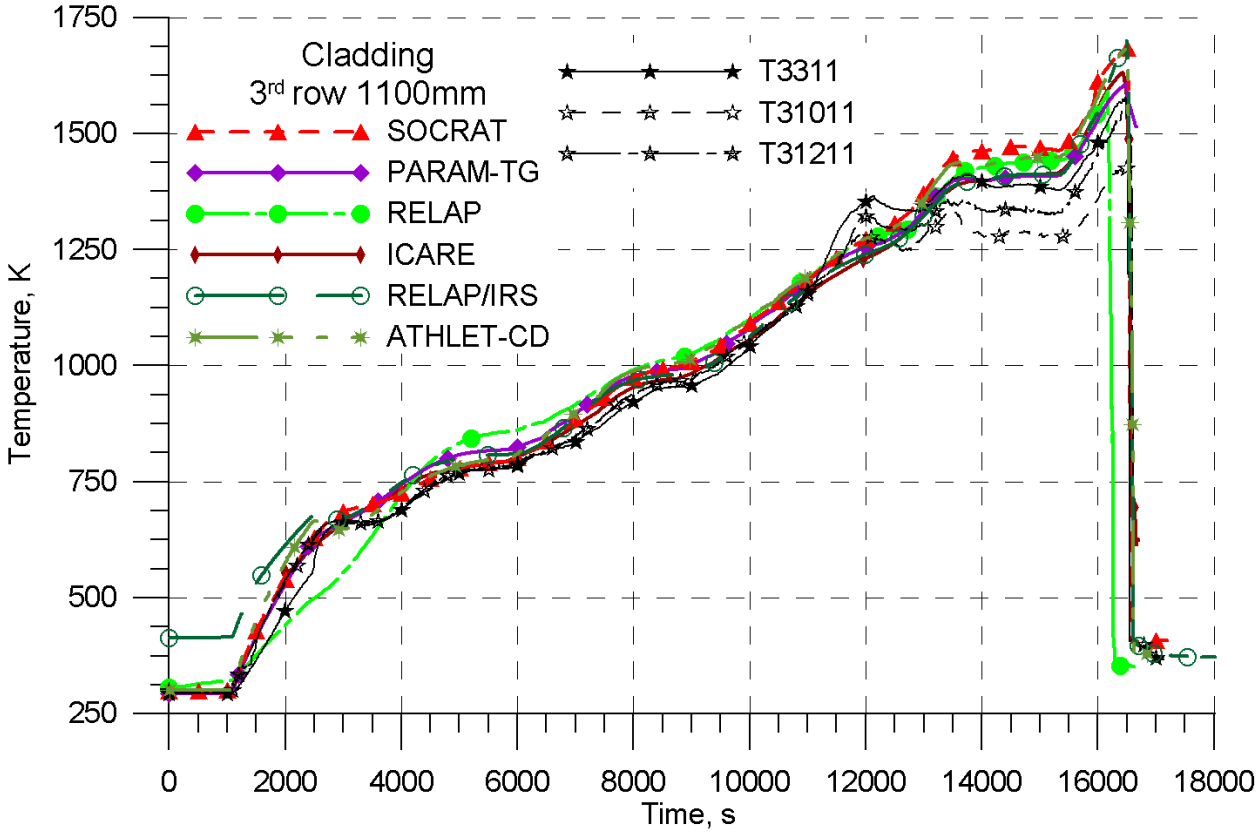

Figure 1.56. Cladding temperature of fuel rod in 3rd row at the elevation of 1100 mm. PARAMETER-SF2 experiment. Post-test calculations.

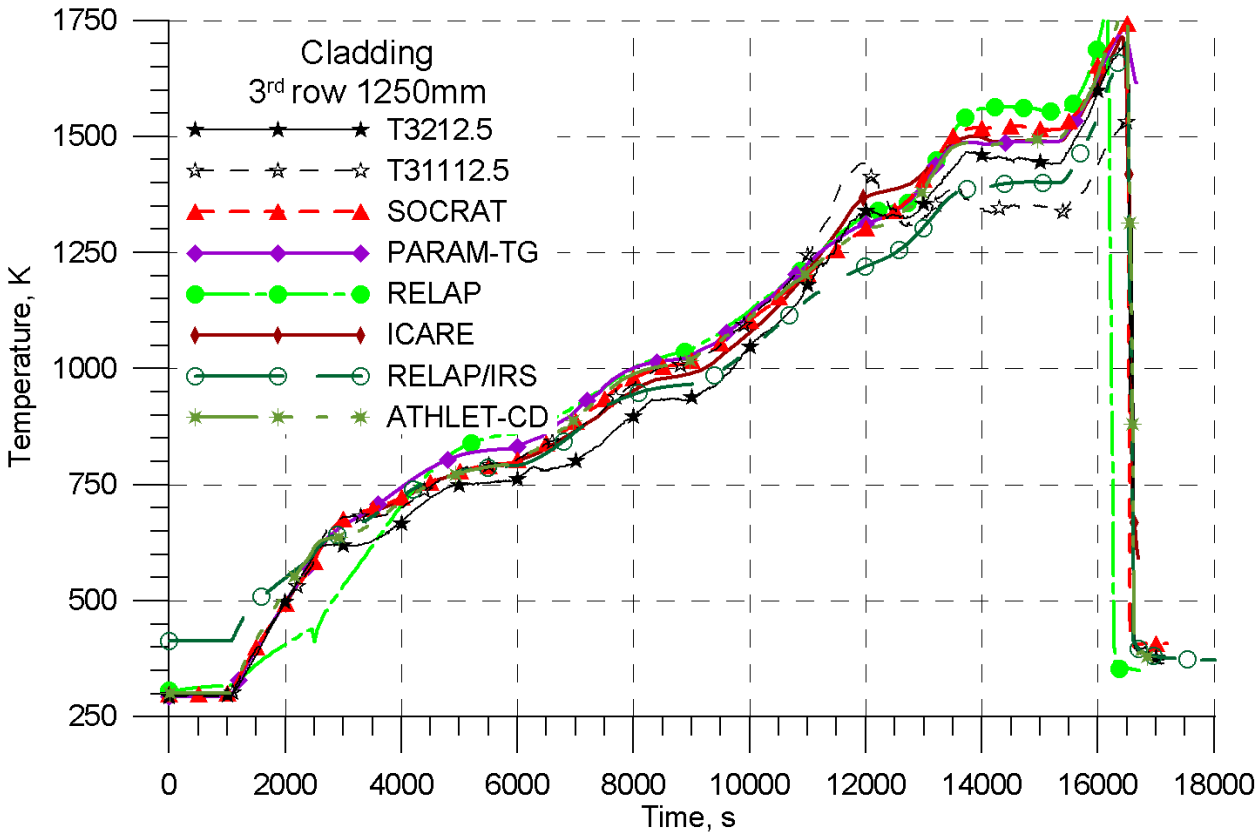

Figure 1.57. Cladding temperature of fuel rod in 3rd row at the elevation of 1250 mm. PARAMETER-SF2 experiment. Post-test calculations.

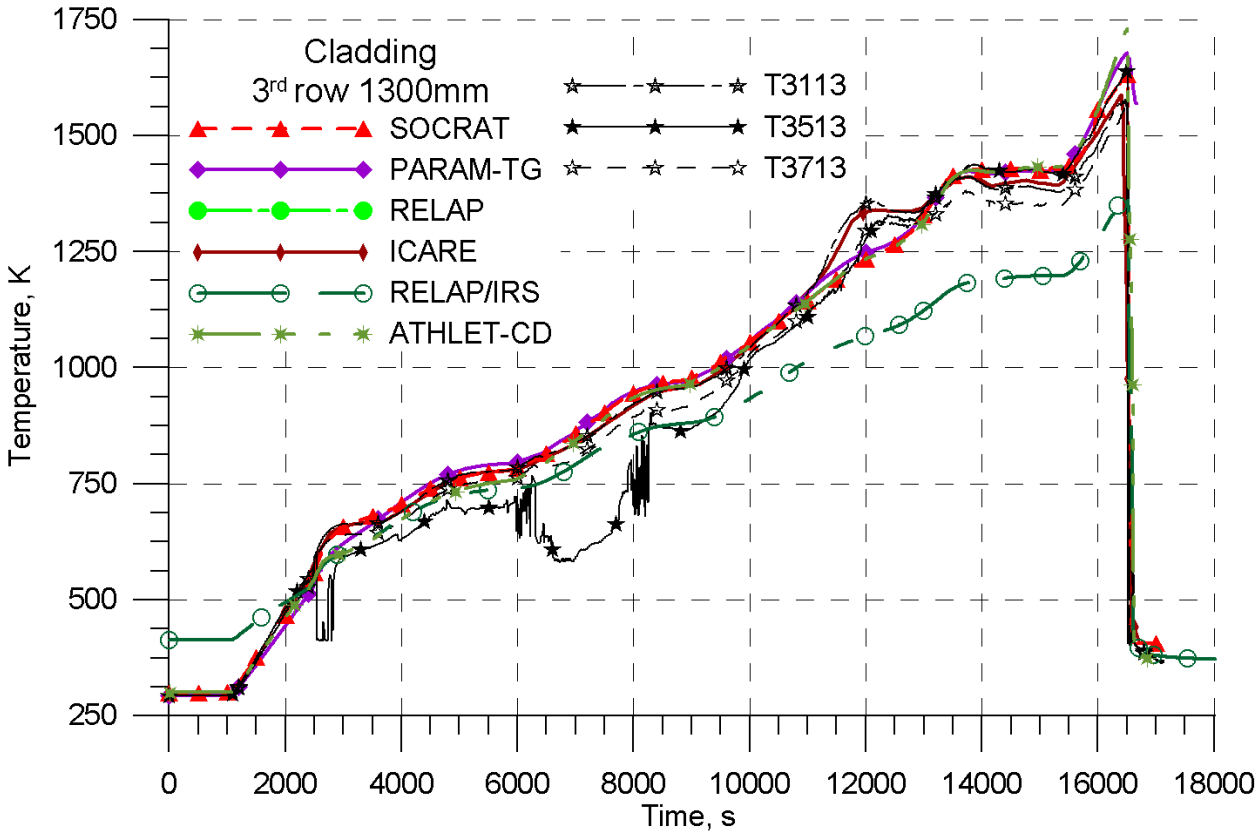

Figure 1.58. Cladding temperature of fuel rod in 3rd row at the elevation of 1300 mm. PARAMETER-SF2 experiment. Post-test calculations.

2 PRE-TEST CALCULATIONS OF PARAMETER-SF3 EXPERIMENT

In PARAMETER-SF3 experiment the initial stage of LB LOCA is simulated when the core dryout occurs, then it is heated up to ~1600°C and water top flooding is executed. The main purpose of the pre-test calculations was justification of experiment scenarios and elaboration of recommendations on performing the experiments.

2.1 THE COMPUTER CODES APPLIED FOR PRE-TEST ANALYSIS OF PARAMETER-SF3 EXPERIMENT

Numerical codes applied in the calculations can be conventionally divided into two groups:

– Engineering codes (I);

– Best estimate codes (D).

A brief comparison of numerical tools used by participants is presented in Table 2.1.

Table 2.1. Main characteristics of the codes applied in pre- and post-test calculations of SF3 experiment

Code	Code type	Organization	Thermo hydraulics	Simulation of oxidation	Oxidation correlations low/high temperatures
SOCRAT	D	IBRAE RAS	2p, 1D	Solution of diffusion equations	CP&LS/PC&LA
RELAP/SCDAPSIM	D	OKB «Gidropress»	2p, 1D+	Parabolic approximation	CP/UH
ICARE/ CATHARE	D	RRC «Kurchatov Institute»	2p, 1D	Parabolic approximation	based on CP&LS/PC
PARAM-TG	I	SRI SIA "LUCH"	2p, 1D+	Parabolic approximation	S
ATHLET-CD	D	GRS	2p, 1D	Parabolic approximation	L/PC
SCDAP/ RELAP/ FZK-PSI	D	PSI	2p, 1D+	Parabolic approximation	CP/UH

Thermohydraulics: p: phase; D: dimension; 1D: one-dimensional, 1D+:cross overflows.
Oxidation correlations: UH: Urbanic-Heidrick; L: Leistikov; PC: Prater/Courtright; LS: Leistikov-Schanz; LA: Leistikov-Aly, CP: Cathcart-Pawel, S: Sokolov.

2.1.1 Specific features of thermohydraulic simulation in codes

Main parameters of thermohydraulic simulation in different codes are briefly presented below:
Engineering codes:

- PARAM-TG – numerical engineering code developed especially for the analysis of PARAMETER facility, solves 3 conservation equations for gas phase (including steam and non-condensable gases). Temperature field in the test section is described: in separate bodies in unsteady two-dimensional approximation using the method of splitting into coordinates, liquid flowing in paths – in unsteady one-dimensional approximation.

Best estimate codes:

- In the system of best estimate codes SOCRAT the thermohyraulic part RATEG uses 7 equations – 6 equations for calculation of mass, momentum and energy for steam and water, as well as additional equation for a mixture of non-condensable gases.
- RELAP/SCDAPSIM code uses the system of 6 conservation equations for gas and water phases, and the mass balance equations for non-condensable gases available in steam phase and/or dissolved in liquid phase.

- ICARE/CATHARE is based on French thermohydraulic code CATHARE using 6 conservation equations for each of the phases and two equations of mass balance for two non-condensable gases.
- Best estimate code ATHLET-CD uses 5 equations for solution of 2-phase thermohydraulics. A single equation of motion is supplemented with the correlation of drift flux between phases.

2.1.2 Simulation of the test section

Main parameters of SF3 experiment simulation with different codes are presented below (Table 2.2).

Table 2.2. Main parameters of nodalizations used in pre- and post-test calculations of SF3 experiment

Code	Organization	Nodalization		Simulated length, m	Remarks
		Axial cells: total number/ within the core	Number of heat structures		External resistance, mΩ/rod
SOCRAT	IBRAE RAS	28/16	6	-0.41…1.9	5.5
RELAP/ SCDAPSIM	OKB «Gidropress»	37/16	5	-1.275…1.875	7
ICARE/ CATHARE	RRC «Kurchatov Institute»	28/22	6	-0.41…1.675	6.3
PARAM-TG	SRI SIA "LUCH"	179/67	37	-1.272…2.165	0
ATHLET-CD	GRS	21/14	7	-1.285…1.63	1
SCDAP/RELAP / FZK-PSI	PSI	29/14	5	-1.275…2.165	8.5

2.2 NODALIZATIONS

The given section presents the nodalizations of participants of pre-test calculations. The information is included here on the method of test section simulation for each code. The main simulation parameters (number of axial and radial groups, consideration of spacing grids and corner rods, etc.) are also presented in this section.

2.2.1 Nodalization for SOCRAT code

Nodalization for code SOCRAT is presented below (Figure 2.1). On the whole, the nodalization covers the range of axial elevations from -410 mm to 1900 mm where the elevation of the core bottom is assumed to be 0 mm (beginning of tantalum electrode). So the lower plenum and bottom part are not completely included into the nodalization that accelerates running speed considerably with the supposed absence of condensation.

For calculation of radiative heat transfer the position of each rod (x and y coordinates) are assigned in the corresponding section of the input file.

The fuel assembly channel was simulated with 28 hydrodynamic control elements: seven volumes between the lower plenum and zero elevation, 16 volumes along the length of 1,275 m and eight volumes above the elevation of 1.275 m:

Bundle_m3, Bundle_m2, Bundle_m1, Bundle_1÷ Bundle_4 – -0.41÷0.0 m;

Bundle_5÷ Bundle_20 –	0.0 ÷ 1.275 m;
Bundle_21÷ Bundle_28 – –	1.275÷ 1.9m.

The nozzles for coolant and water supply and discharge were simulated as well as lower plenum and upper plenum.

At the inlet of 1st hydrodynamic element, the boundary conditions were set for the coolant supply with the assigned mass flow rate.

At the assembly channel outlet, the boundary condition was set — coolant outlet with the assigned pressure simulating the test section body.

The core was simulated with 7 heat elements (Figure 2.1):

1. UNHEAT – unheated fuel rod simulator located in FA centre (1);
2. HEAT_2 – heated fuel rod simulators located in FA centre (6);
3. HEAT_3 – heated fuel rod simulators located in FA periphery (12);
4. HEAT_CORNER – corner rods (12);
5. SHROUD – shroud, insulation, steel cylinder;
6. SHROUDbyp – outer steel cylinder.

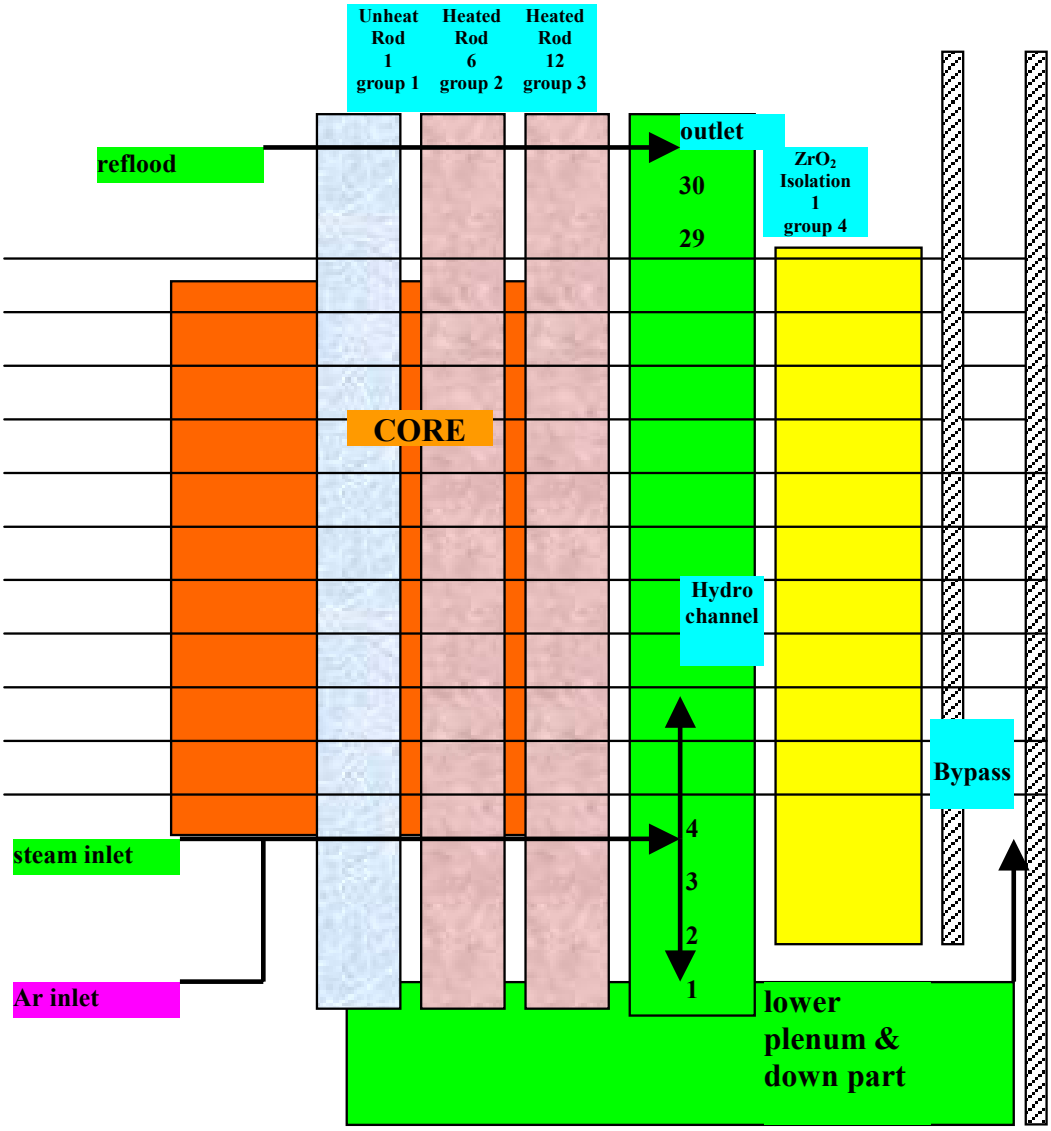

Figure 2.1. Nodalization for calculation with the use of code SOCRAT.

Between elements SHROUD and SHROUDbyp there is a channel of the cooling system (water jacket) as shown in Figures (Figure 2.1, Figure 2.3).

In the Figures (Figure 2.2, Figure 2.3) the radial material layers, located in FA and heat elements SHROUD and SHROUDbyp are shown schematically.

The calculations were performed with the options of automatic determination of radiation view factors and optical lengths at each step for a new geometry, as well as with new emissivities depending on material and its thickness.

Total number of axial cells in the nodalization of SOCRAT was 28. Among them 16 cells were related to FA heated zone (core), with this, all cells, except for the extreme upper cell were of the length of 80 mm. The length of the last cell was 75 mm.

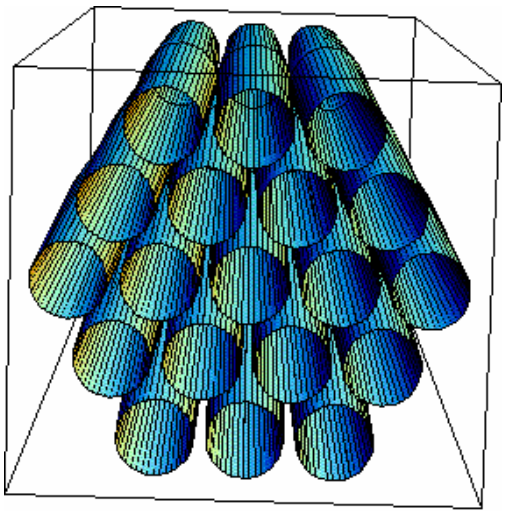

Figure 2.2. Central rod, internal and external row in FA of PARAMETER-SF3.

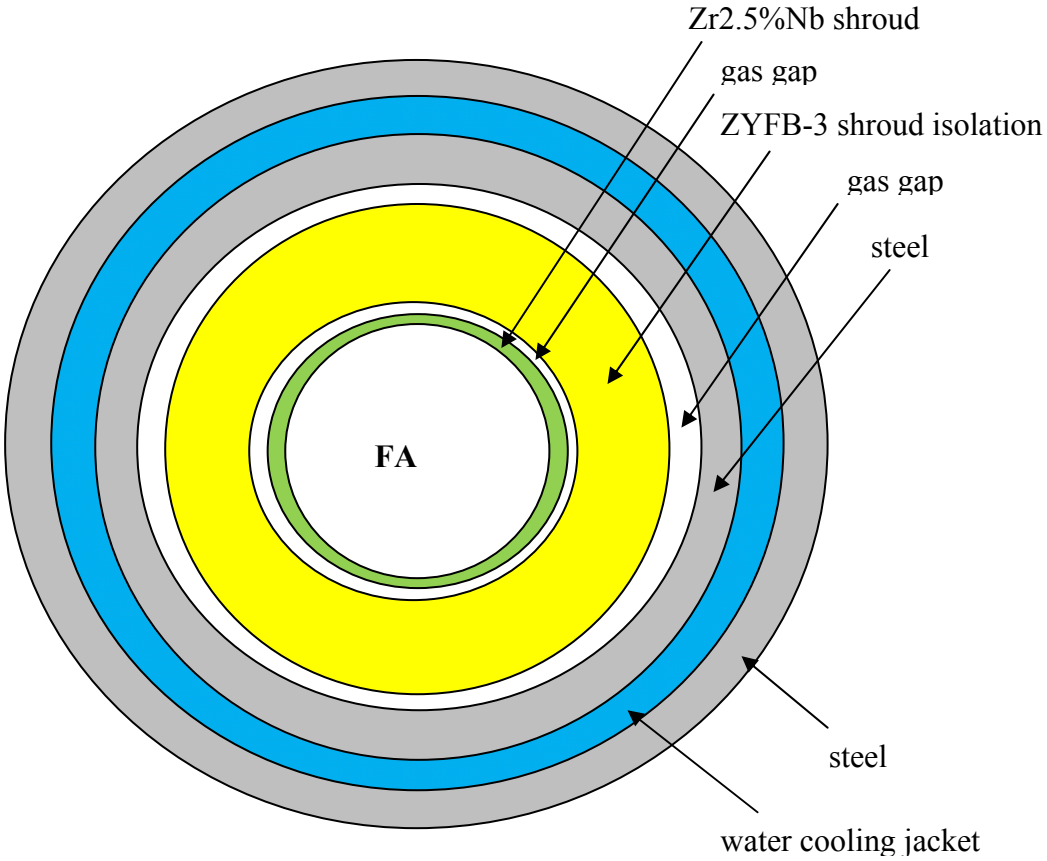

Figure 2.3. Schematic representation of radial material layers in heat elements surrounding the FA.

Simulation of the given experiment with SOCRAT code is made with the help of
– hydrodynamic channels - 48;
– quasi-channels -3;
– plenums - 2;
– boundary conditions of different types (rigid wall, coolant outflowing at the assigned pressure, inlet of coolant with the assigned flow rates and properties) - 11;
– table functions (material properties, energy release, external wall heat transfer coefficients, time dependencies of processes, etc.) - 59;
– libraries of material physical properties integrated into the package.

Thermal conductivity of isolating layer of porous zirconium dioxide is assigned according to the data presented by the Manufacturer (ZYFB-3 isolation, www.zircarzirconia.com).

2.2.2 Nodalization for ICARE/CATHARE code

For simulation in ICARE/CATHARE V1 code the detailed nodalization is used with fixing separate FA physical elements to the geometry of meshing into radial and vertical cells. In Figures 2.4 and 2.5 the scheme of FA test zone model is given in two cross-sections.

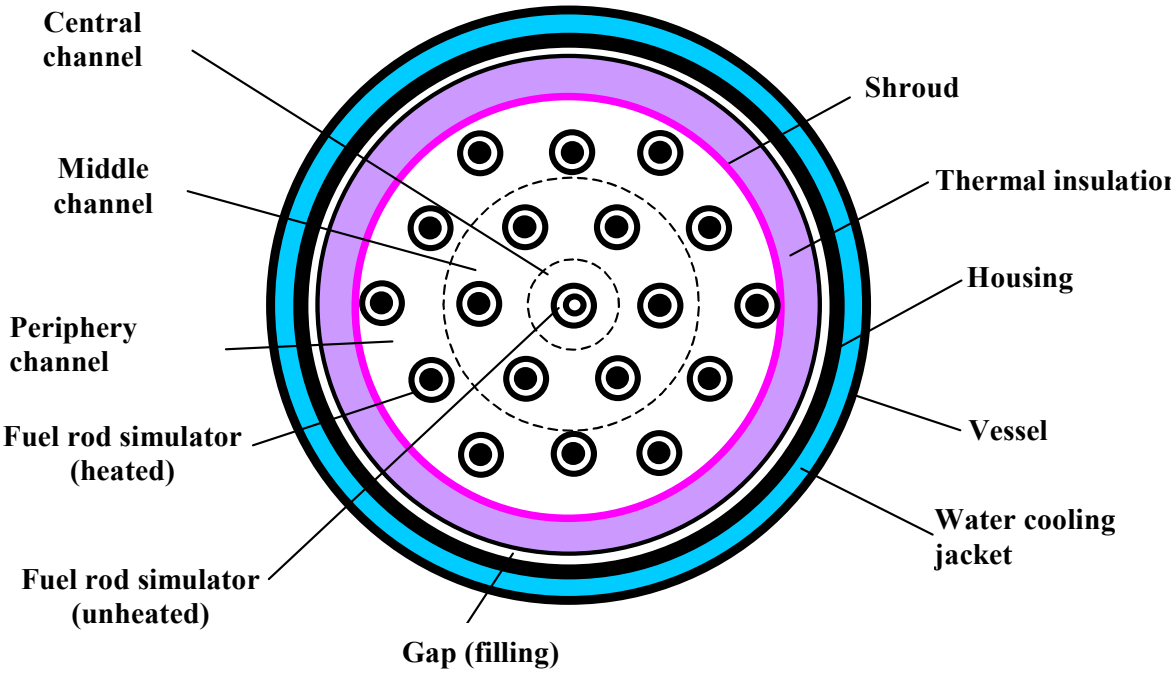

Figure 2.6. Scheme of model FA arrangement in radial section.

Figure 2.7 presents the radial meshing of FA hydraulic channel at PARAMETER facility into three parts (cells) embracing the central fuel rod simulator, six adjacent fuel rod simulators and 12 periphery ones, respectively. With this, among the periphery simulators two groups by six simulators are picked out with different distance to the centre for detailed consideration of radiative heat transfer.

The shroud and thermal insulation in the model (see Figure 2.8) are represented by conical rings. In all radial concentric structures the heat conduction transfer is simulated up to the water cooling jacket. Additionally, for the region of the gap with filling the model of radiative heat transfer is used.

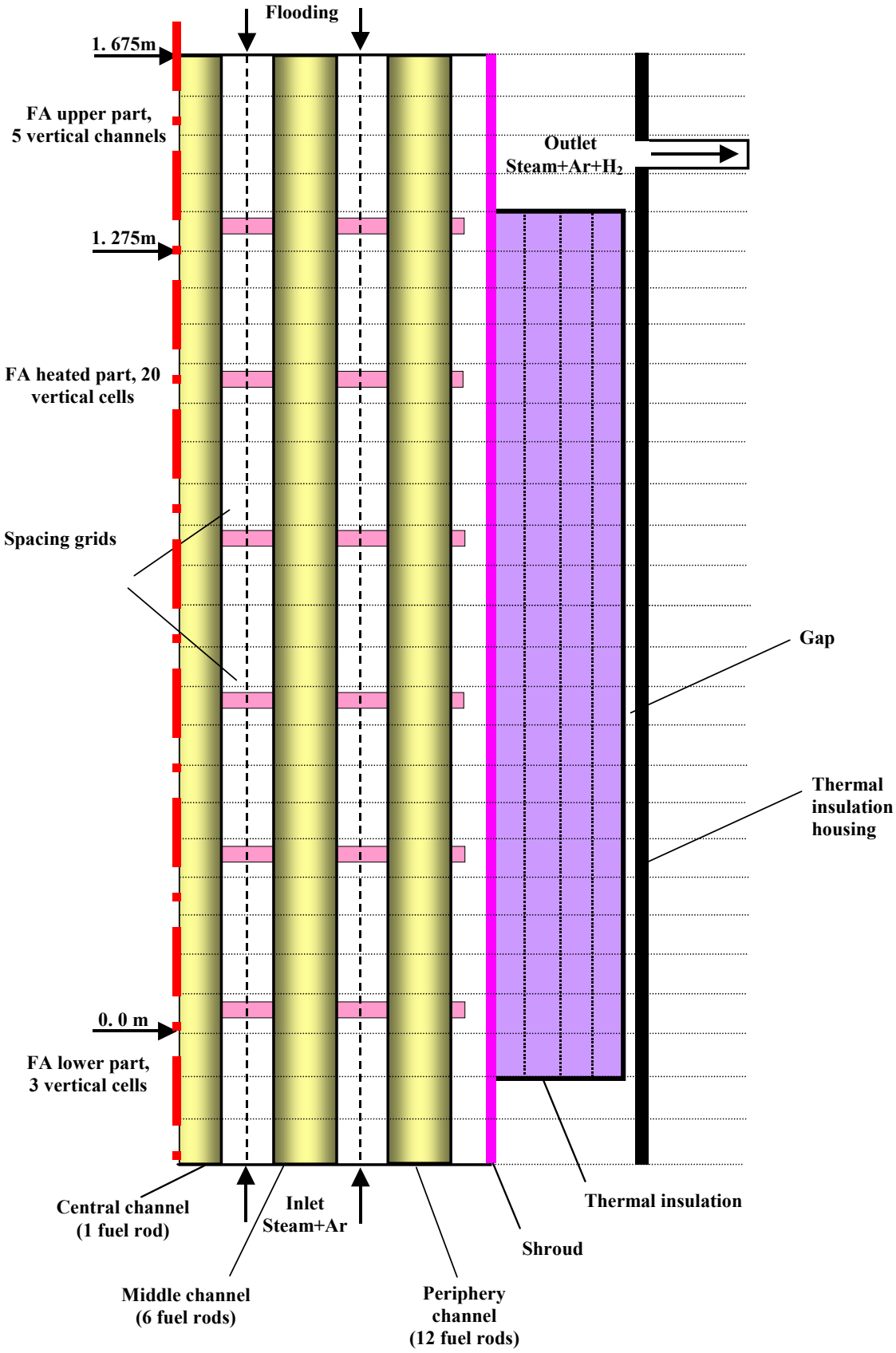

Figure 2.9. Scheme of model FA arrangement in vertical section (right side).

As shown in Figure 2.10, the FA hydraulic channel of PARAMETER facility is divided in vertical direction into 28 cells and there are three typical parts:

– lower part - upstream of the heated zone beginning;
– central part including the heated zone;
– upper part.

During simulation the nodalization is applied with small axial cell spacing (up to 6 cm in the heated zone). Proceeding from the previous calculations of experiments on reflood using ICARE/CATHARE V1 computer code, such meshing provides for satisfactory accuracy of the flooding front motion simulation.

2.2.3 Nodalization for SCDAP/RELAP/FZK-PSI code

Figure 2.11 presents nodalization [13] of the test section of PARAMETER facility with the use of SCDAP/RELAP/FZK-PSI code.

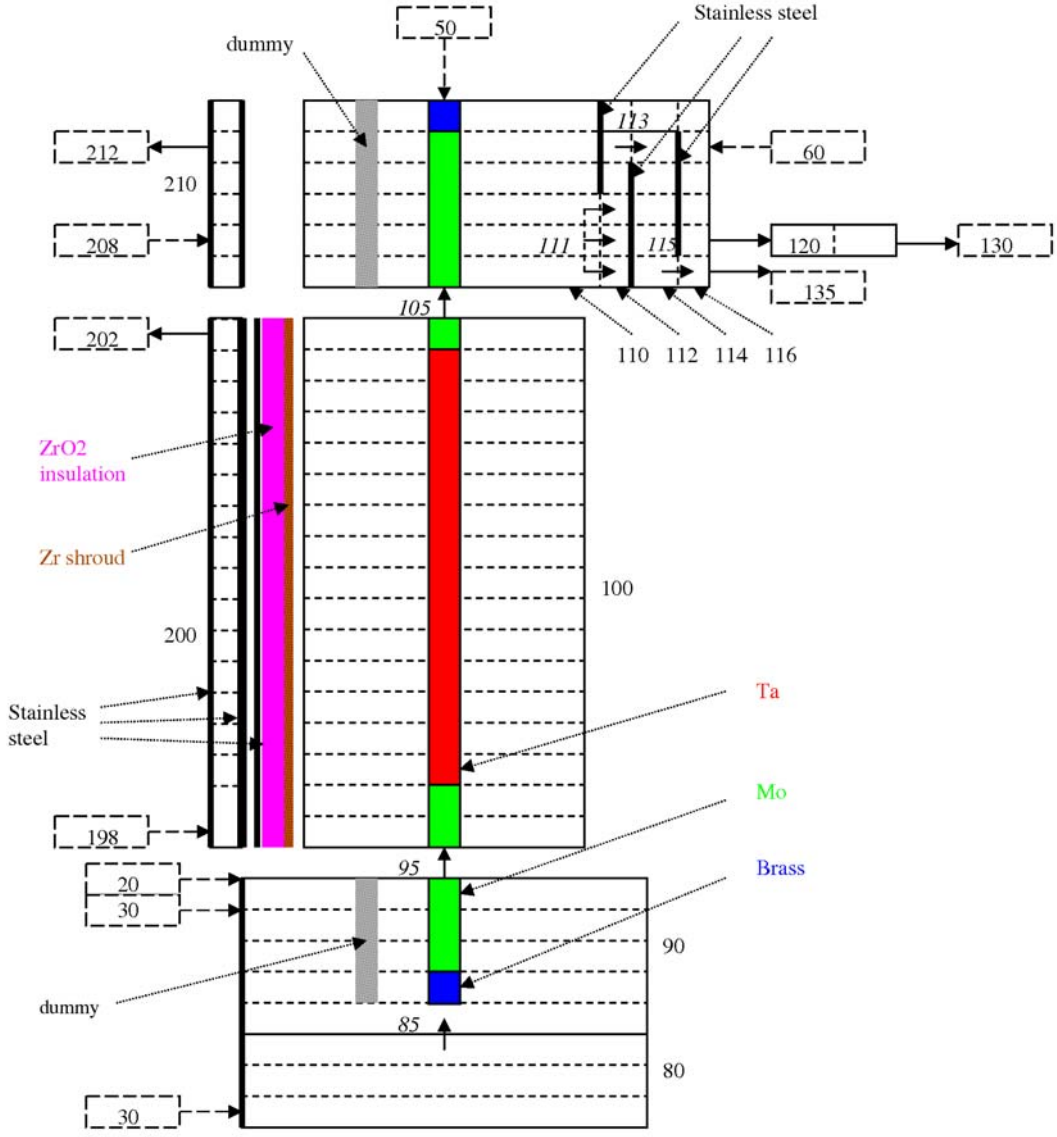

Figure 2.12. Nodalization used for simulation of PARAMETER-SF3 with the use of SCDAP/RELAP/FZK-PSI code.

Experimental boundary conditions:
– pressure, mass flow rates and temperatures of steam and argon at the inlet;
– power dynamics;
– conditions in the "cooling jacket";
– mass flow rate of coolant under flooding;
– some dummy components defined to suppress "unphysical" insulation.
Initial conditions:
– temperature is increased to 410 K to avoid instability under steam condensation;
– external resistance of 5 mΩ/rod;
– hydraulic diameter of 3.4 mm in the test section.

2.2.4 Nodalization for PARAM-TG code

Nodalization used in pre-test calculations of SF3 is the same as that described in section 1.2.4 and presented in Figures 1.8, 1.9. Some values of Table 1.3 are changed only. The changes are put down into Table 2.1 in bold italics.

Table 2.1. Main parameters of the test section in pre-test calculations of SF3

Inner radii of TS layers in the core region, mm, and their materials (in brackets – No. of a layer in Figure 1.9)		Value, material
Shroud (4)		***33.65***, Zr1%Nb
Gas gap (5)		***34.85***, argon
Thermal insulation (6)		*35,* ZYFB-3
Thermal insulation shroud (7)		58, steel
Gas gap (8)		59, argon
Test section body (9)		60.5; steel
Cooling path in cooling jacket (10)		66.5; water
External tube of cooling jacket (11)		68.5; steel
Gas atmosphere in room (12)		69.5; nitrogen
Room wall (13)		1000, steel
Some parameters along the length		
Coordinate of steam and argon supply from core beginning,mm		-372
Coordinate of steam and argon outlet from test section, mm		1425
Coordinates of modelled section beginning and end, mm		***-1222 : 2161***
Total number of heat structures (from…to) Solid Gaseous or liquid		 21 – ***49*** 37 – ***53***
Total number of cells along the length and within the core		***187 : 79***
Composition of the heater (from the test section bottom)		
Material	Length, mm	Diameter, mm
Brass *)	50	4.71
Copper **)	***340***	9.13
Brass	230	6
Copper cable	150	6
Brass	130	6
Copper	22	6
Molybdenum	300	6
Tantalum	1275	4
Molybdenum	***400***	6
Copper	20	6
Brass	***466***	6
In calculation all ***12*** displacers (corner rods), indicated in Figure 1.9, were considered.		
In calculation the evident consideration was made for ***14*** upper thermocouples located in paths ***2, 4, 6, 8, 10, 12, 14, 16, 18, 20,22,24,26,34*** (Figure 1.9)*:* ***T239, T269, T339, T2110, T3320, T3810, T3411, T3711, T2212.5, T3612.5, T31012.5, T2513, T3513, T1114***		
Coordinates of cooling path of the middle section and water flow rate: ***-44 mm, 1283 mm***, 50 g/s		
Coordinates of cooling path of the upper section and water flow rate: ***1335 mm, 1813 mm, 30 g/s***		
Water level in the test section bottom, mm		-550
Coordinates of insulation, mm	***-115***	***1335***

2.2.5 Nodalization for ATHLET-CD code

Figure 2.13 presents the nodalization used in pre-test and post-test calculations of PARAMETER-SF3 experiment with application of ATHLET-CD code. The same nodalization was used also for SF2 post-test calculations.

The main features of the simulation were presented in the work of [12]. Below are listed some parameters of the simulation:

Hydraulic channels:

– central test channel - 85.7 %;
– bypass - 14.3 %;
– «cooling jacket» - according to specification.

Heat structures:

– ROD1 (multiplicity 1);
– ROD2 (multiplicity 6);
– ROD3 (multiplicity 12);
– Spacing grids (in the number of 6);
– Shroud/insulation;
– Walls of "cooling jacket".

Detailed simulation:

– Additional elements below the inlet nozzles;
– Shape of the outlet channel corresponds to the geometry of steam-gas mixture flowing in the facility;
– Hydraulic diameter in the test section $3.8 \cdot 10^{-3}$ m;
– Separate inlet channels for argon and steam.

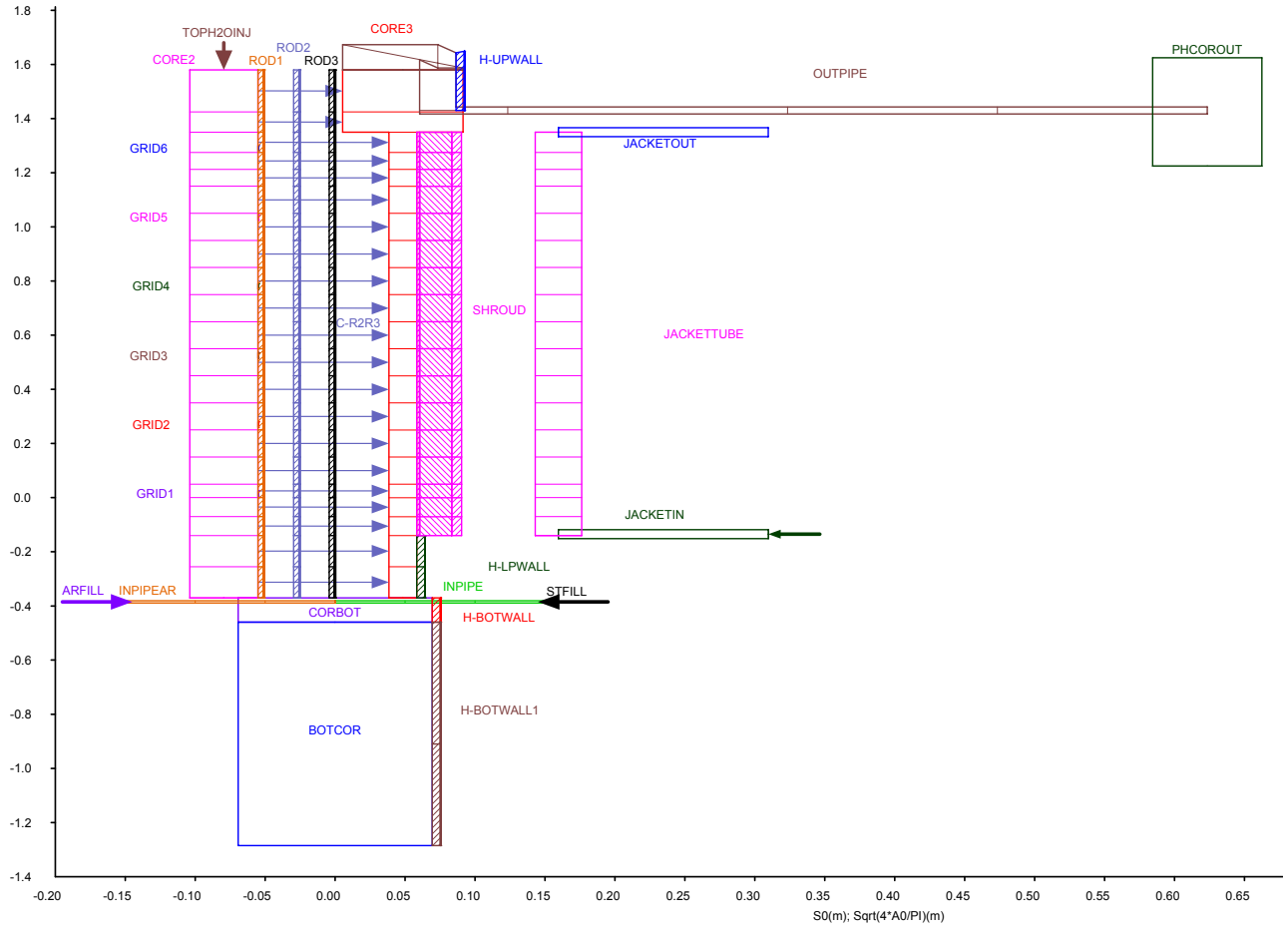

Figure 2.13. Nodalization for ATHLET-CD computer code. PARAMETER-SF3 experiment. Pre-test calculations.

Some model parameters of ATHLET-CD code for post-test calculations of PARAMETER-SF2 experiment and pre-test calculations of PARAMETER-SF3 experiment:

- Oxidation correlation of Leistikow/Prater-Courtright (IOXMOD = 19) was used instead of Sokolov's correlation recommended earlier (VVER: Zr1%Nb, IOXMOD = 18);
- The default values of inter-phase friction were used;
- External resistance was 1 mΩ/rod;
- Hydraulic diameter in the heated zone $D_H = 3.8 \cdot 10^{-3}$ m (= D_H at the elevation corresponding to the spacer grid).

2.2.6 Nodalization for RELAP/SCDAPSIM code

Nodalization (Figure2.14) is divided into three parts:

–lower part (1167 mm) from the level of current leads to the elevation –177 mm from the beginning of the heated part;

–central part wherein power release occurs, 1275 mm with tantalum electrodes, 158 mm above and 177 mm with molybdenum;

–upper part with the length of 600mm from the end of central part.

Central part of the test section nodalization includes heat elements for simulation of the central rod (element *fuel*), 6 heating fuel rod simulators of the internal row (element *cora*), 12 heating fuel rod simulators of the external row (element *cora*), of the shroud and external structures (element SHROUD), of spacing grids (6 pieces), located in the central part.

Inlet nozzles, a path upstream of hydrogen detector were not included into the test section nodalization.

Presence of spacing grids was considered both in hydraulic processes, and under oxidation. Presence of thermocouples and pressure measuring channels was not considered. Mixing of argon and steam was assumed ideal. Radiant heat transfer was simulated in radial direction only.

Due to limitation of the given version of the code it is not feasible to breakdown the elements *cora* for simulation of fuel rods over the height by more than 20 elements and to use more than 2 types of materials for heaters. Therefore outside the central section the presence of fuel rods was simulated only by their account in the channel flow area. The tantalum heater was simulated along the length of the assembly heated part 1275 mm and a part of current leads (along the length of 177 mm down of the tantalum heater and 158 mm above it. Power losses in non-simulated current leads, as well as in electric wires from the generator terminals to current leads were considered by introducing the additional electric resistance (7 mΩ per a simulator). In calculation of resistance of the simulated section the temperature dependence is considered.

The scheme of the shroud structure (element Shroud) is presented in Figure 2.15.

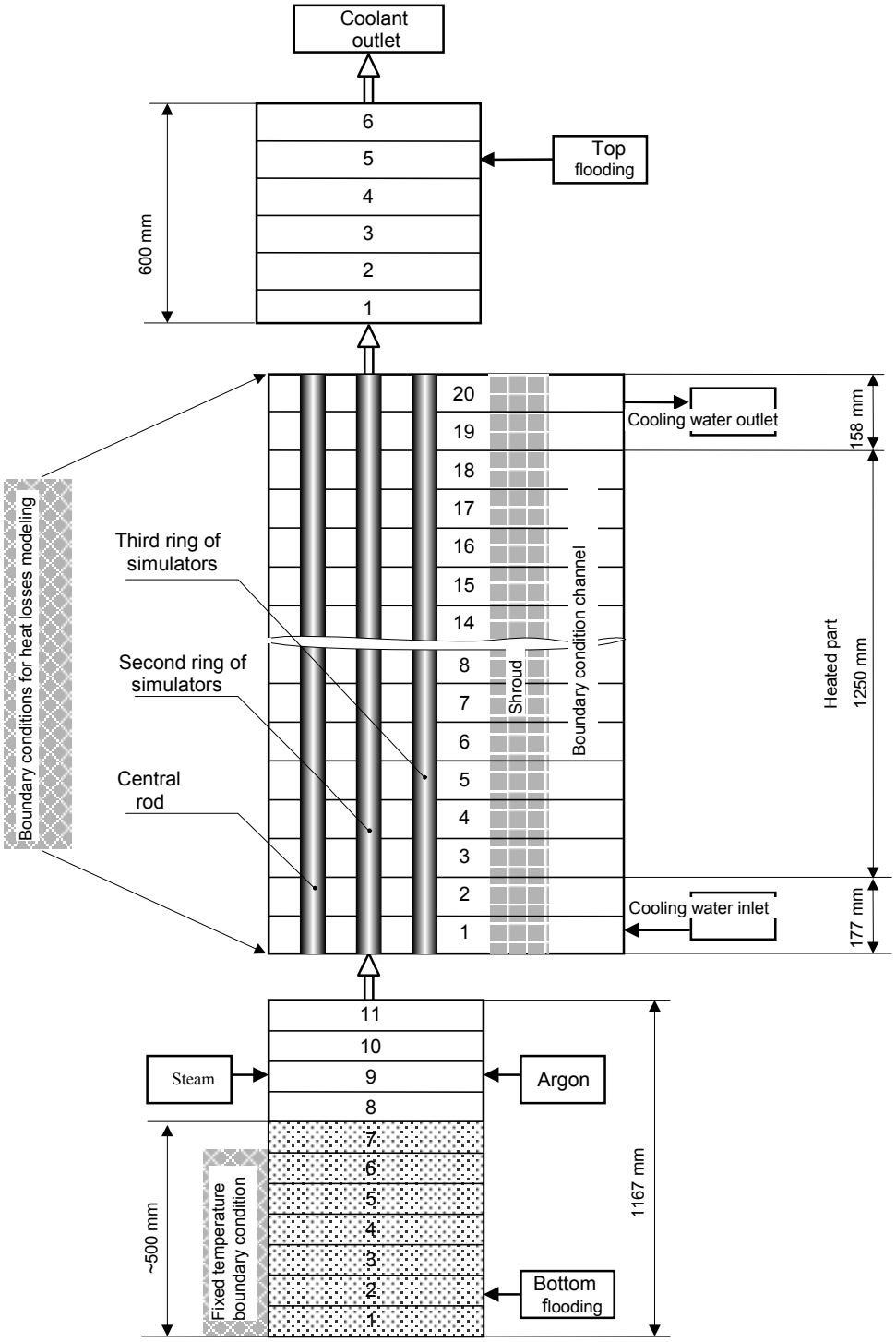

Figure 2.14. Nodalization of PARAMETER-SF facility for the code RELAP/SCDAPSIM.

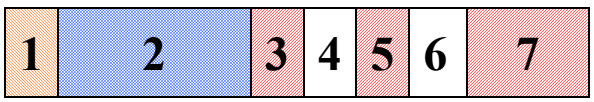

1 - shroud (zirconium);
2 - insulation;
3 - insulation housing;
4 - air gap;
5 - water cooling housing;
6 - air gap;
7 - steel vessel

Figure 2.15. Schematic representation of the assembly shroud.

2.2.6.1 Initial and boundary conditions

The supplied electric power, temperatures, flow rates of steam, argon, top flooding water corresponded exactly to the experiment plan.

For simulation of heat transfer between the vessel and air environment of the room the constant temperature was assigned as the boundary condition on the housing outer surface. With this aim the channel with high water flow rate was connected to its outer surface to maintain the constant temperature of the wall of about 70ºC.

In the assembly lower part from the lower current leads to the inlet nozzles the wall temperature and water level in this channel are maintained constant. During the time of calculation the level of water that cools the current leads decreases by less than 0.5%, and hence does not influence the behaviour of the heated part. As compared to thee calculations of SF2 experiment the model of axial heat run off at the boundaries of the assembly simulated part was added. The model is a tabulated assigned temperature at ends of the heated section (with the length of 1610 mm, see the above given explanations). For the pre-test calculations this temperature was taken on the basis of SF2 experiment.

2.2.6.2 Database on material properties

The following database on material properties is used: for the shroud materials – according to the data on experimental facility (specification SF1), for fuel, heaters and cladding – from the standard library RELAP/SCDAPSIM MATPRO.

2.3 OBJECTIVES OF PARAMETER-SF3 EXPERIMENT

The experiment SF3 was planned to study the behaviour of 19-rod model FA of VVER-1000 under simulated conditions of severe accident including the stage of low rate top flooding, and namely:

– Study of behaviour of structural components of 19-rod model FA of VVER-1000 (fuel pellets and claddings, shroud, spacer grids);
– Study of oxidation degree of structural components of 19-rod model FA of VVER-1000;
– Study of interaction and structural-phase changes in the materials of model FA of VVER-1000 (fuel pellets and claddings);
– Study of hydrogen release.

2.3.1 Development of SF3 scenario, analysis of physical-chemical processes, recommendations on performing the experiment

The main objective of pre-test calculations are:
– definition of the modes of electric power supply for correspondence with the temperature scenario agreed with the project collaborators;
– elaboration of recommendations on performing the experiment proceeding from the analysis of the set of processes in the assembly;
– comparative analysis of results by different codes applied for the pre-test calculations.

As a rule, the input sets for pre-test calculations of PARAMETER-SF3 experiment corresponded to the sets for post-test calculations of PARAMETER-SF2 experiment except for the initial and boundary conditions.

Temperature scenario of the experiment is formulated in a very general form for the hottest zone and includes four main stages (Figure 2.18):
– stage of the assembly heating-up to temperature of 1473 K;
– stage of the assembly pre-oxidation at temperature of 1473 K;
– the assembly heating-up to the temperature of 1873 K;
– stage of top flooding.

The experiment shall be performed in the flow of steam-argon mixture under all phases, except for the flooding phase. Steam flow rates is 3.5 g/s, argon flow rate is 2 g/s (Figure 2.18). Due

to structural features of the facility the given argon flow rate causes the constant pressure of 0.3 MPa throughout the whole experiment, except for the flooding stage.

For correspondence with the proposed scenario it was necessary to optimize the scheme of electric power supply.

As an example, let's consider the results of pre-test calculation of SF3 with the use of SOCRAT code. The below given Figure 2.16 shows temperature curves at the hottest zone of 1250 mm for three variants of calculation. Figure 2.17 presents the parameters of full electric power corresponding to these variants. The base value of power is represented with the red curve. Power variation for two other variants of calculation is ±10%. It is seen from the plots that with decrease in power the temperature curves are far from reaching the temperature value on "plateau". At the same time the power increase by 10% of the base value results in sharp temperature escalation and, finally, in leaving the permissible range.

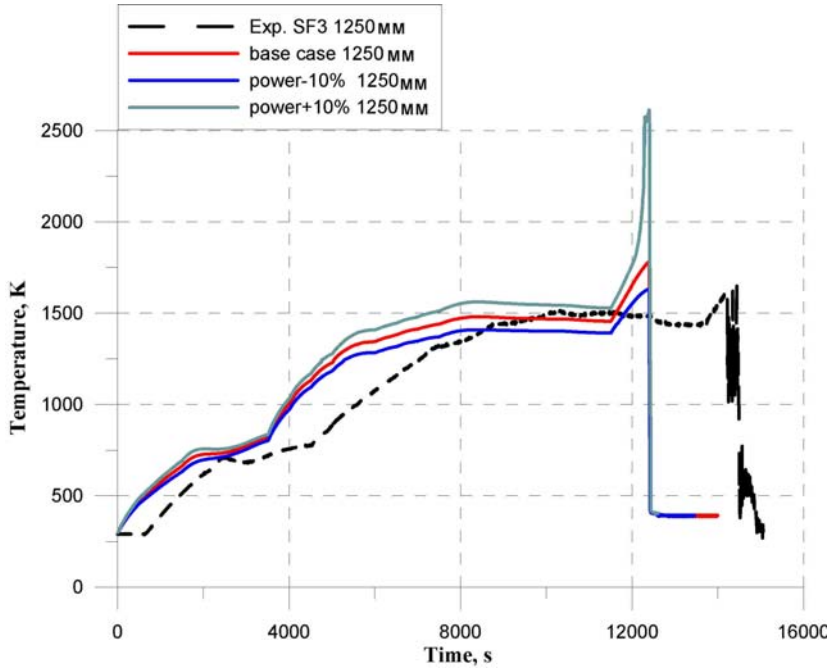

Figure 2.16. Time history of temperature in the hottest zone (elevation of 1250 mm) for three variants of calculation with the use of SOCRAT code.

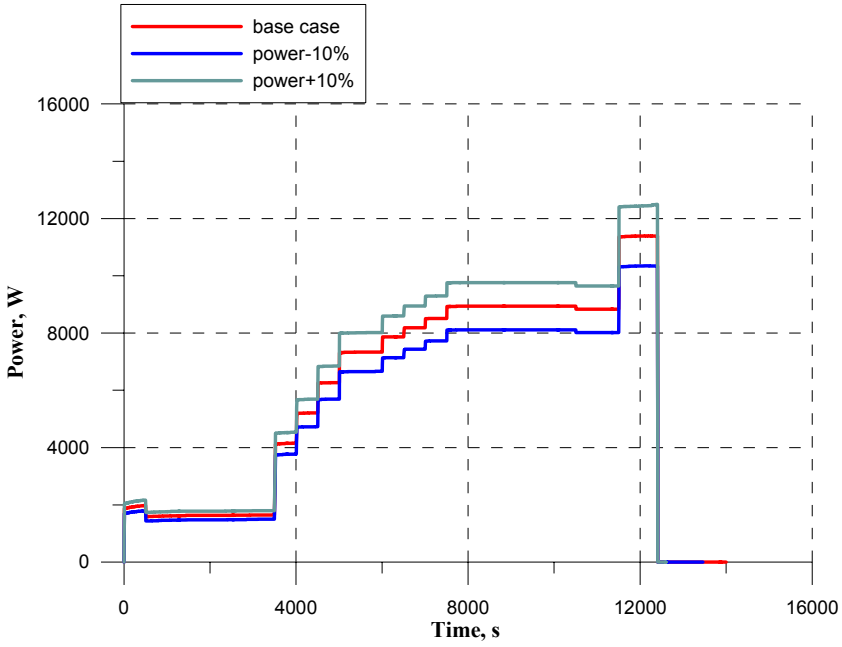

Figure 2.17. Full electric power for three variants of calculation with the use of SOCRAT code.

The electric power chosen for pre-test calculations is presented below (Figure 2.19). Using the given scheme of electric power supply and the parameters of steam-argon mixture as the boundary conditions the calculations were carried out with application of codes SOCRAT, ICARE/CATHARE, RELAP/SCDAPSIM, ATHLET-CD, SCDAP/RELAP/FZK-PSI, PARAM-TG. Results of calculations with the use of different codes are presented in Figures 2.26-2.99. By the results of the analysis of calculations the recommendations were given to experimentators on the procedure and correction of parameters in the "on-line" mode if the measured parameters will differ substantially from the predicted values.

Energy release as a result of chemical reactions, obtained by different codes, is presented below (Figure 2.20). It is seen that in heat balance the power of chemical reactions plays especially noticeable role at the transient stage before flooding onset.

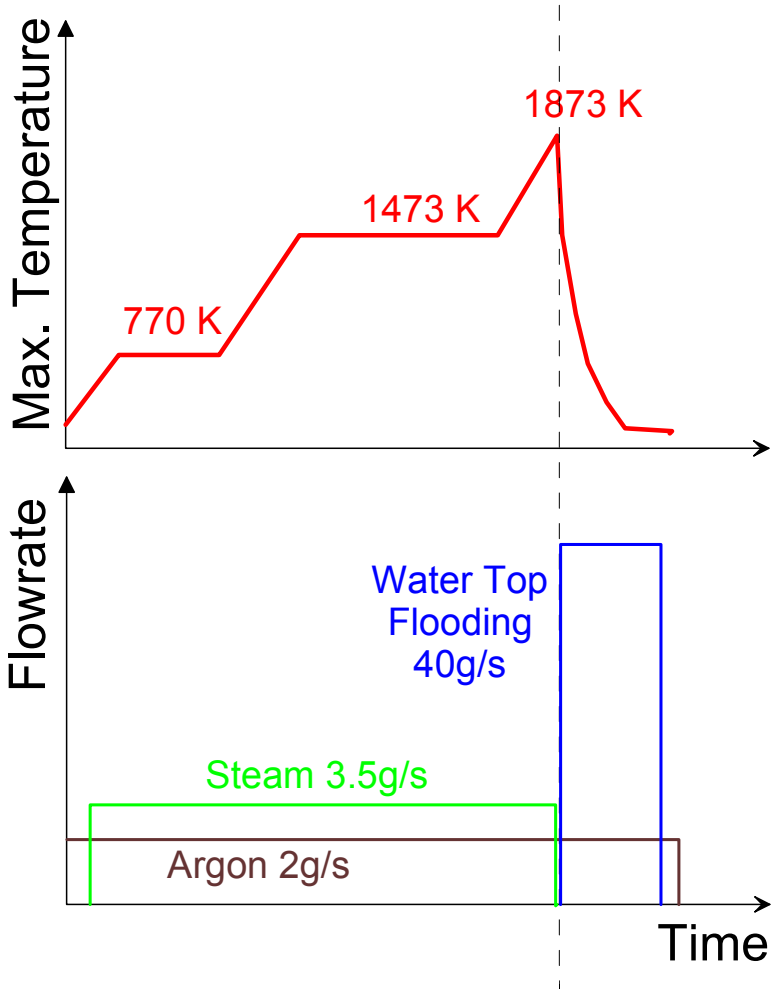

Figure 2.18. Scenario of SF3 experiment (scheme).

The method of the assembly heating, used in the given experiment, causes a sequential heating-up of fuel rods, shroud, thermal insulation. Each change of the electric power supplied brings about the assembly disbalance. In case of absence of the assembly oxidation the typical time of setting the heat balance can reach hundreds of seconds. This time is longer at low temperatures and shorter at high temperatures.

At temperatures up to 1000 K the main factors governing the time of setting the balance is gas heat conduction (rises with temperature) and the flow velocity (rises with temperature due to decrease in density). Due to insignificant contribution of chemical reaction within the temperature range lower than ~1000 K the facility can be heated by rather large surge of power with monitoring the rate of heating of the hottest zone. With this, one should achieve temperature equilibrium both in claddings, and in shroud and thermal insulation. Bringing the facility into the state of temperature equilibrium at **each** of the elevations needs time that is approximately in reverse proportion to the level of temperatures. Unsteady state in the facility lower part will necessarily influence the behaviour of the upper hottest part.

At higher temperatures (1000-1500 K) the local effects manifested regularly in some fuel rods. These effects in the form of “humps” arising at random can be seen on temperature curves of the experiments performed earlier. Such temperature jumps are caused probably by intensive local oxidation due to specific local conditions (loss of heat removal) and/or breakaway effect (separation of protective oxide scale). At the initial moment a sharp local temperature rise of separate fuel rod caused by chemical reaction will be observed. Then, with accumulating of oxide scale and prevailing of heat removal owing to convection and radiation, the temperature will decrease. This local temperature increase of one fuel rod will be reflected lately on temperature behaviour of adjacent fuel rods: “excessive” local energy is carried over by radiation to the nearest surfaces, therefore one should expect local temperature rise in the group of adjacent fuel rods at the given elevation and adjacent elevations. Transfer of this energy to fuel rods spacing from each other on more than one pitch is extremely small.

As a rule, in the mentioned temperature region such local effects do not influence the integral heat balance because, first, they embrace a small area of metal surface, second, the released energy is not sufficient for reaching the temperatures at which the self-sustaining reaction of oxidation is started leading to a swift temperature rise and extension of the site of origin of intensive oxidation to the adjacent regions. At higher temperatures such local effects may be hazardous. The local heating of the simulator due to steam-zirconium reaction will cause, with a delay of 5-30 s, the obligatory local decrease in electric power owing to rise in the heater resistance with rise in temperature. Rise in **local** temperature of a simulator (in reaching the pre-oxidation stage) above 1500 K at a rate exceeding 0.2 K/s is indicative of insufficient cooling and requires a smooth decrease in electric power (for example, in steps by 0.5 kW with the interval of 30 s) to the moment when temperature stops to rise. After that, it is necessary to return to the smooth increase in power avoiding the temperature decrease near a “hot spot” section averaged. Typical time of power return to the level close to that required for maintaining the achieved temperature level shall not exceed 100-150 s to prevent cooling of the facility lower part and its transition into the pulsing mode when temperature rise at one or another elevation does not correlate with the power input due to delayed heat transfer from the below sections.

At temperatures above 1500 K the radiative heat transfer makes a substantial influence. In this case the local effects become smoother more quickly. So, at the stage of the assembly bringing to the flooding phase no instable behaviour of temperatures in the assembly upper (the hottest) part is expected.

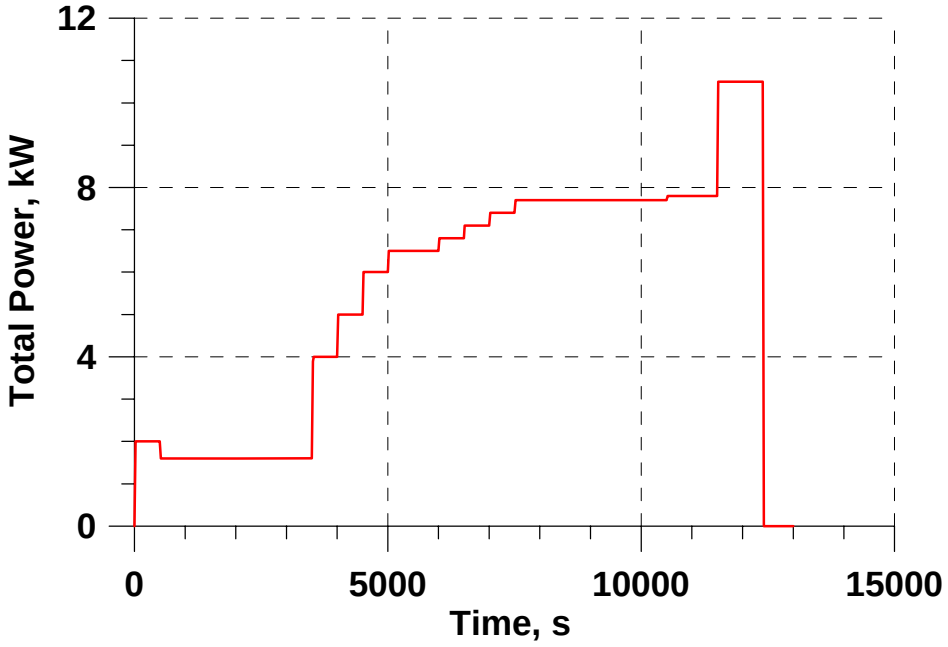

Figure 2.19. Proposed scheme of electric power supply.

Supply of the first 2 kW during 3500 s, together with supply of steam-argon mixture at temperature of 770 K, will make possible to heat-up the assembly uniformly (on the length of 0-1300 mm) to the temperature of 770 K and to provide the heat balance in thermal insulation (the

settled temperature gradient in thermal insulation). After that it is necessary to switch on the system of cooling the upper unit and make sure in the fact that temperatures in the test section did not change, i.e. there is no condensation in the upper unit.

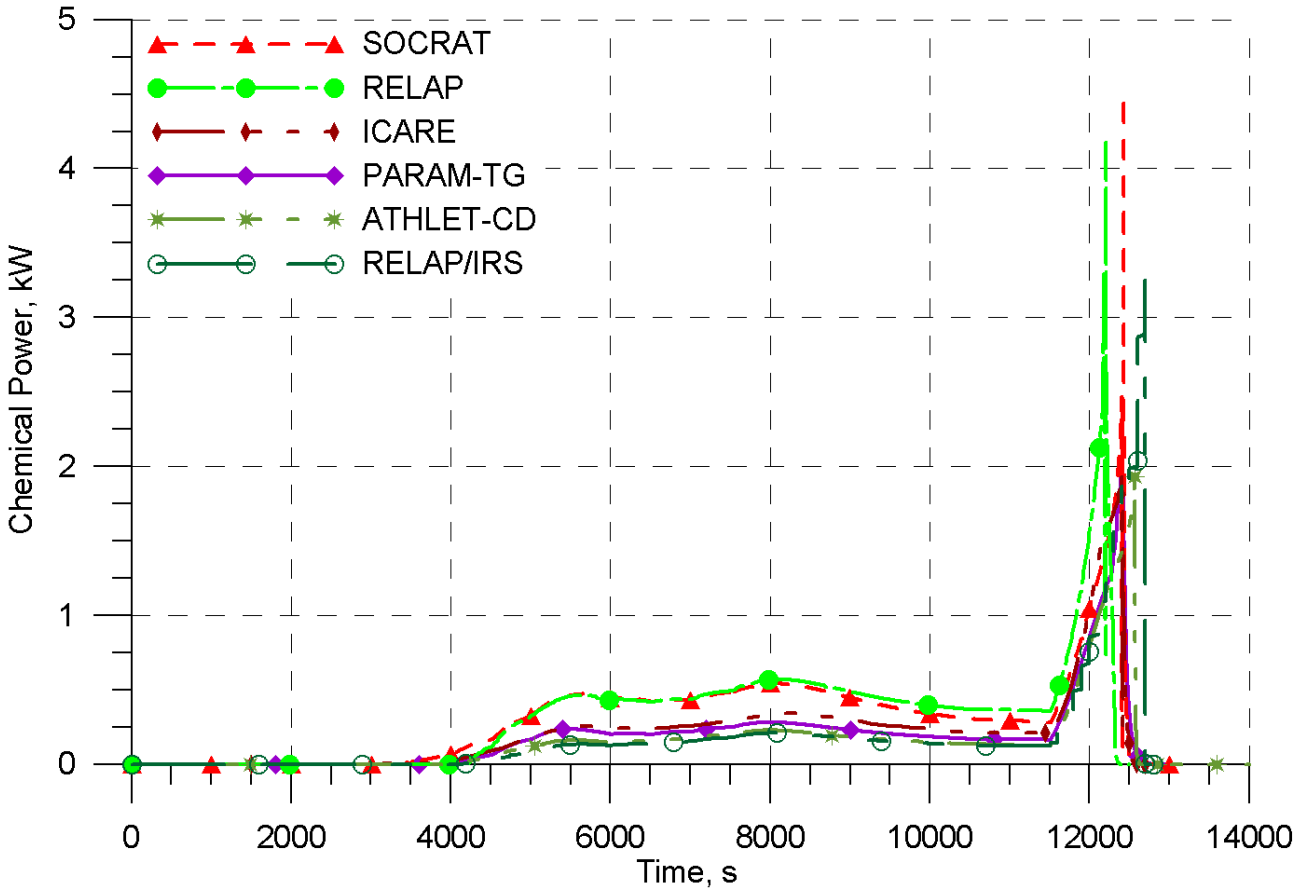

Figure 2.20. Power of steam-zirconium reaction.

Calculations with the use of SOCRAT code show that supply of the first 2 kW during 3500 s, together with supply of steam-argon mixture at temperature of 770 K, will make possible to heat-up the assembly uniformly (on the length of 0-1300 mm) to the temperature of 770 K and to provide heat balance in thermal insulation (the settled temperature gradient in thermal insulation).

The assembly heating-up to maximum temperature is supposed to make by jumpwise change in electric power from 7.8 to 10.5 kW. The predicted rate of temperature rise at the beginning of this stage corresponds to 0.4 K/s, and before flooding the rate increases and can reach 1-2 K/s owing to intensification of oxidation at temperature above ~1800 K.

The stage of flooding is started from the moment when the assembly temperature reaches 1873 K. In the specification for PARAMETER-SF3 experiment, containing sequence of process procedures at the flooding stage, the electric power switching off is stipulated when temperature reaches the value of 1873 K. In 5 s the switching off is started for the steam supply systems and switching over of the systems of argon supply into the assembly. Total duration of the procedures is 10 s. By the moment of opening the valve for water supply into the test section the calculated temperature of fuel rod claddings will not exceed 1893 K.

It is predicted that in ~150 s after the beginning of water supply the simulators will be cooled to the temperature of ~400 K.

By the results of generalization of calculated parameters the following conclusions can be made:

– Results of pre-test calculations made by the participants (Figures 2.26 – 2.99) with the use of different codes show, on the whole, a good agreement for temperature behaviour of the assembly, though there is a definite scatter in temperatures (to 200 K maximum) at some elevations.

– Parameters of oxide scale thickness and of hydrogen production time history are not in so good agreement. These differences are governed, on the main, by difference in temperatures obtained by participants of the pre-test calculations. Another reason of the observed differences can be caused by difference in the oxidation models applied in the presented codes (Table 2.1).

The evident causes of differences in temperature time history obtained by different participants of the pre-test studies are:

- Different models for description of thermohydraulics (Table 2.1);
- Using of different parameter "hydraulic diameter" (see also sections 2.4.1 and 2.4.2);
- Radiative heat transfer in the facility is simulated differently (1-, 2-, 3-dimensional simulation, taking into account of radiation emission and absorption by the surrounding steam-gas mixture, etc.);
- Different extent of details in simulation of the test section (Table 2.2);
- Parameter of the additional electric resistance was also assumed different (Table 2.2).

2.4 CALCULATIONAL ANALYSIS

The calculational analysis shows that the assembly state is rather simple described by the codes if the state is quasi-equilibrium (temperature gradient on the radius of the assembly, shroud, thermal insulation) and changes accordingly. Otherwise the front of thermal wave in thermal insulation shall be considered while thermal-and-physical properties of thermal insulation are determined not rather exactly. At least due to method of its cutting and placing into the circular gap.

Let's give examples when there is no equilibrium in the assembly. Figure 2.21 presents the experimental temperature behaviour of simulator claddings (Tcl), housing (Tsh) and thermal insulation (Tth) at the elevation of 700 mm at the initial stage of SF2 experiment.

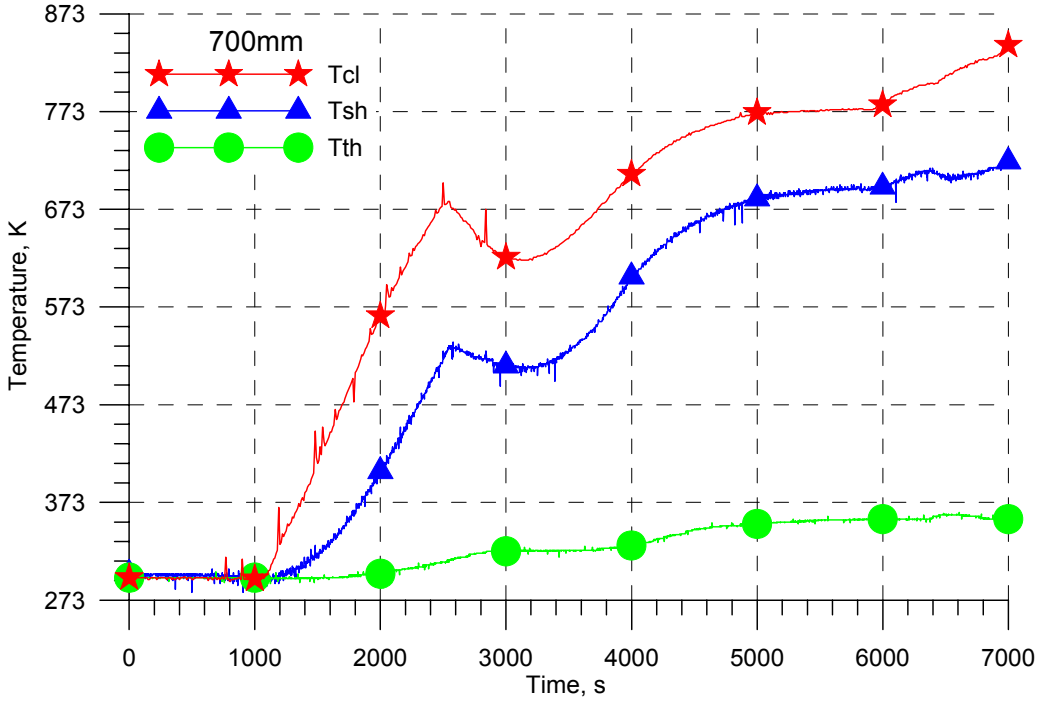

Figure 2.21. Temperature behaviour at the elevation of 700 mm in SF2 experiment.

It is seen in the plots that the largest delay on stabilization of the temperature radial profile is observed within the following time intervals:

- 1000-1500 s, when the shroud is not heated practically on the background of high rise of cladding temperatures;
- 3000-4000 s – thermal insulation is not heated completely: on the background the shroud temperature rise the temperature of the insulation outer surface does not change practically;

- 5000-6000 s, when the rise of the shroud temperature occurs on the background of the simulators stabilized temperature, and consequently, the temperature of steam-argon mixture, entering the above part of the facility, changes also.

The cause of disturbance of heat equilibrium in the assembly can be not only the "internal" (changes in electric power supplied), but also the "external" – changes of outside cooling conditions, as well as displacement of the insulation itself due to thermal expansion. The indicated changes lead to change in heat flux through the thermal insulation that, in its turn, influences the cladding temperatures. Accordingly, the cooling conditions (cooling water temperatures) shall be controlled by the operator for taking the precautionary actions (Figure 2.13, ~6500 s).

Further assembly heating-up to the temperature of 1473 K is recommended to perform in jumpwise manner by several steps. Duration of the assembly holding at each step (~500 s) is governed by the time of settling the quasi-steady state in the assembly. Slowing down the rate of temperature rise in fuel rods, shroud and thermal insulation with a tendency of approaching the constant local temperature is indicative of the fact that the assembly is reaching the quasi-steady state. After each power surge the operator shall control the temperature response of fuel rods, shroud and thermal insulation to the electric power supplied.

A step of power surge in PARAMETER-SF3 experiment in bringing the assembly to the pre-oxidation phase (from 770 to 1473 K) depends on temperature in the assembly: first 2.4 kW is proposed (this is corresponded by the rate of fuel rod temperature rise 0.25 K/s), with increase in temperature the step is decreased (Figure 2.19). With reaching the temperature of 1373 K the heat released in the course of steam-zirconium reaction shall be considered in the assembly heat balance, therefore it is recommended to obtain the assembly steady state (to hold the assembly for 1000 s), and to decrease the step of electric power surge to 0.3 kW. Low rate of cladding temperature rise of 0.1 K/s will make possible to reach the pre-oxidation temperatures smoothly.

Maximum temperatures in the assembly at the phase of the assembly heating-up to temperature of 1870 K are predicted at the elevation of 1200-1250 mm on claddings of the fuel rods of the second row. In performing the experiment one should follow indications of the corresponding thermocouples.

Temperatures predicted by the codes at the elevation of 1250 mm with the value of electric power of 7.7 kW are within the range of 1400-1520 K (see Figure 2.22). It is seen that a scatter for the most codes is ~100 K. Only in the calculation with the use of SCDAP/RELAP/FZK-PSI code a considerable underestimation of temperature is observed. Therefore the proposed value of electric power should be corrected in the course of the experiment. With this, it should be noted that in this region of temperatures the facility is very sensitive even to small power variations (due to steam-zirconium reaction). As, for instance, just at the value of 8 kW (see Figure 2.22) the minimum calculated temperatures increase to 1500 K.

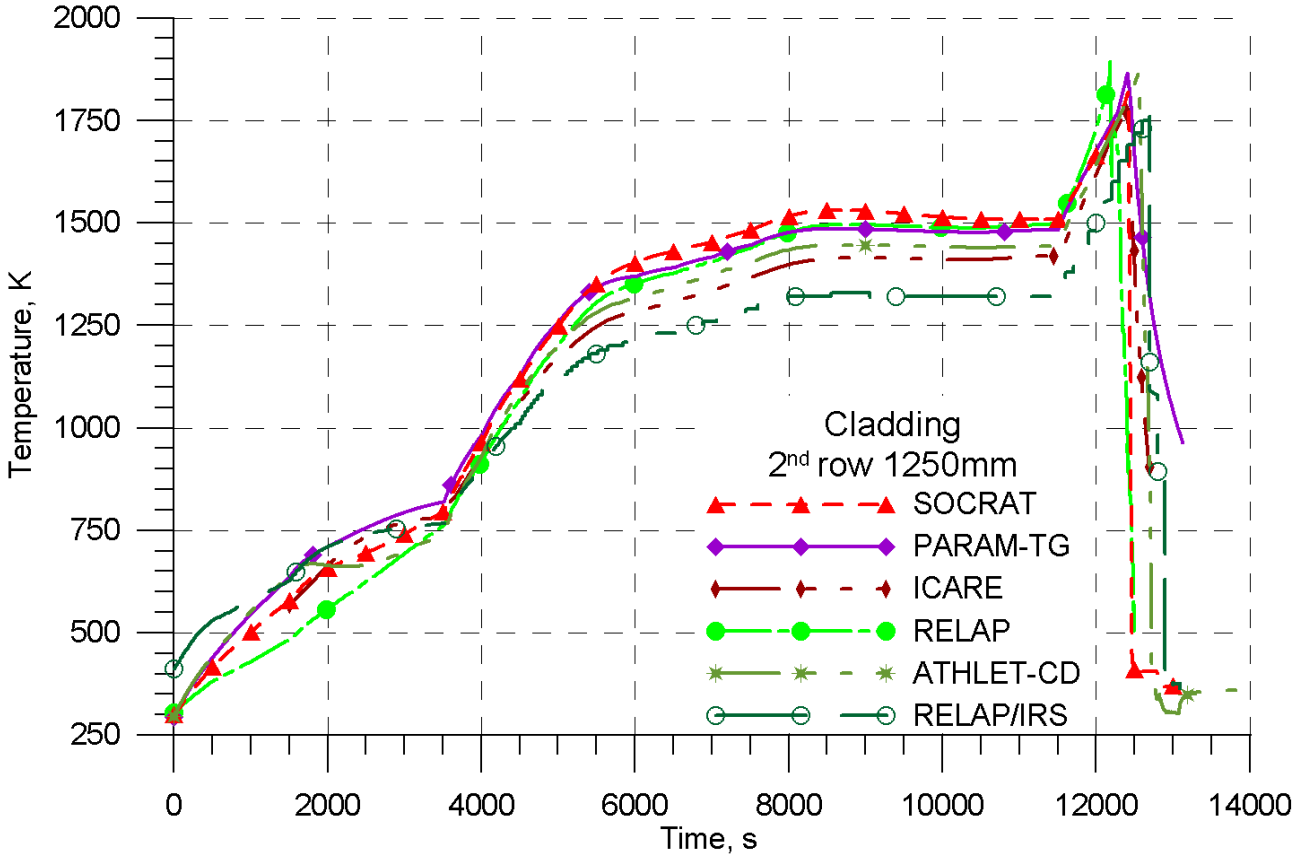

Figure 2.22. Predicted temperatures of claddings of fuel rods of 2nd row at elevation 1250 mm.

With the rise in zirconium dioxide on surfaces of claddings and shroud its protective function is enhanced, therefore the intensity of steam-zirconium reaction becomes weaker with the time. To compensate decrease in heat release from chemical reaction it is recommended to increase the electric power by the end of pre-oxidation phase.

The calculated duration of the pre-oxidation phase (by duration of "plateau" in the power supplied) corresponds to ~4000 s (7500s – 11500 s in Figure 2.19). The calculations show that the assembly pre-oxidation at temperature of 1440-1520 K (see the calculations with the use of SOCRAT, ATHLET-CD codes, Figures 2.95 and 2.96) will make possible to create the protective layer of zirconium dioxide with thickness of 200-300 μm on surfaces of fuel rod claddings in the hottest section to reduce the contribution of heat release from chemical reaction at the subsequent phase of the assembly heating-up to maximum temperature, especially at high temperatures (1773-1873 K). In oxidation at lower temperatures ~1400 K a breakaway effect can be manifested that is characterized by formation of the layered zirconium dioxide. Such oxide does not fulfil a protective function. The assembly behaviour considering the breakaway effect is not analyzed in the given work because such models are not available in the codes applied. Considering the fact that the used thermocouples within this range could give underestimation of temperature to 30 K [15], it is recommended to make pre-oxidation of the assembly at possibly higher temperatures but not exceeding the upper limit of the calculated temperature range. The calculations with the use of SOCRAT code show that in case of the assembly pre-oxidation at temperature of 1510 K (at the beginning of the phase) the contribution of heat from steam-zirconium reaction is small (not more than 0.5 kW at the beginning of the phase, then the power drops – Figure 2.33), no temperature escalation is predicted.

2.4.1 Evaluation of the transition section length

In flowing of steam-gas mixture through the working channel the velocity profile is settled not at once but some distance after entering the channel from the plenum. Similarly, if some elements are placed in the working channel that change the channel geometry, for instance, rings, diaphragms, grids, etc., then after passing them also some distance is required to pass to restore the

profile flow velocity. Typical dimension on which the thermohydraulic parameters are determined coincides in both cases as to the order of value. Let's determine the typical length of this transition section. The given parameter, in case of coolant entering from the plenum into the tube, is called as the length of hydrodynamic initial section.

Further on, we'll use for short the term "length of transition section" – LTS. By the analogy with the hydrodynamic LTS, the thermal length of transition section is meant to be a distance along the channel wherein the temperature profile is settled. As a rule, the hydrodynamic and thermal LTS are the values of one order.

Let's study the main thermohydraulic characteristics of coolant in the experiment of PARAMETER series using thermohydraulic characteristics of PARAMETER-SF3 for evaluations.

Mass A_i and mole B_i flow rates of steam and argon entering the test section in the course of PARAMETR-SF3 experiment present the following values (subscripts 1 and 2 are marks for steam H_2O and argon Ar, respectively):

$$A_1 = 3.5\frac{g}{s},\ A_2 = 2\frac{g}{s},\ B_1 = A_1 / M_1 = 0.194\frac{mole}{s},\ B_2 = A_2 / M_2 = 0.050\frac{mole}{s},$$

here $M_1 = 18$ g/mole and $M_2 = 40$ g/mole – molecular masses of steam and argon.

Hence the mole fractions of components are

$\alpha_1 = B_1 / (B_1 + B_2) = 0.795$, $\alpha_2 = B_2 / (B_1 + B_2) = 0.205$.

Full pressure of the mixture in the experiments of series is:

$$p = p_1 + p_2 \approx 3.0 \cdot 10^5 \frac{N}{m^2}, \tag{2.1}$$

here p – operating pressure in the channel, p_1 and p_2 - partial pressures of steam and argon, respectively. Assuming behaviour of components as of ideal gases we can write:

$$p_1 = \frac{\rho_1}{M_1} RT,\ p_2 = \frac{\rho_2}{M_2} RT, \tag{2.2}$$

here ρ_1 and ρ_2 - densities of steam and argon in mixture, $R \approx 8.31\frac{J}{moleK}$ - universal gas constant, T – temperature of mixture.

As

$$\frac{\rho_2 / M_2}{\rho_1 / M_1} = \frac{\alpha_2}{1-\alpha_2}, \tag{2.3}$$

we can obtain partial pressures:

$$p_1 = p(1-\alpha_2),\ p_2 = p\alpha_2, \tag{2.4}$$

and the following relationships will be true for densities of components:

$$\rho_1 = p(1-\alpha_2)\frac{M_1}{RT},\ \rho_2 = p\frac{\alpha_2 M_2}{RT}. \tag{2.5}$$

Density of mixture will be equal to

$$\rho = \rho_1 + \rho_2 = \frac{p}{RT}\left[(1-\alpha_2)M_1 + \alpha_2 M_2\right]. \tag{2.6}$$

Under conditions p = 3 10^5 Pa, T = 700K the mixture density $\rho \approx 1.16\frac{kg}{m^3}$.

With this, densities of components will be:

$$\rho_1 \approx 0.74\frac{kg}{m^3},\ \rho_2 \approx 0.42\frac{kg}{m^3}. \tag{2.7}$$

Argon differs greatly from steam by its thermophysical characteristics. At atmospheric pressure and typical temperature of 700 K the specific heat of steam and argon are equal approximately to the following values:

$$c_{p1} \approx 2 \cdot 10^3 \frac{J}{kgK},\ c_{p2} \approx 0.52 \cdot 10^3 \frac{J}{kgK}. \tag{2.8}$$

Difference in heat conduction of these gases under the same conditions is not so significant:

$$k_1 \approx 4\cdot 10^{-2}\,\frac{Bm}{мК},\quad k_2 \approx 3\cdot 10^{-2}\,\frac{Bm}{мК}. \tag{2.9}$$

There is a difference also in dynamic viscosity:

$$\mu_1 \approx 2.1\cdot 10^{-5}\,Па\cdot с,\ \mu_2 \approx 3.8\cdot 10^{-5}\,Па\cdot с. \tag{2.10}$$

For calculation of viscosity of steam-argon mixture we use the calculation procedure proposed by Wilk [16]:

$$\mu = \frac{\mu_1}{1+\frac{\alpha_2}{\alpha_1}\Phi_{1,2}} + \frac{\mu_2}{1+\frac{\alpha_1}{\alpha_2}\Phi_{2,1}}, \tag{2.11}$$

here α_i - mole fractions of components ($\sum \alpha_i = 1$), viscosity functions $\Phi_{i,k}$ are:

$$\Phi_{2,1} = \frac{\mu_2 M_1}{\mu_1 M_2}\Phi_{1,2} = \frac{\left[1+\left(\mu_2/\mu_1\right)^{1/2}\left(M_1/M_2\right)^{1/4}\right]^2}{2\sqrt{2}\left(1+M_2/M_1\right)^{1/2}}, \tag{2.12}$$

here M_i - molecular masses of components.

Mixture viscosity at the given parameters according to (2.11) will be $\mu \approx 2.5\cdot 10^{-5}$ Pa·s.

Let's make evaluations of the main thermohydraulic parameters of PARAMETR-SF3 experiment. The flow area for coolant is equal to the flow area of the round housing S_0 with diameter $d_{shr} = 6.7\cdot 10^{-2}$ m minus the sum of cross-section area of the simulators of fuel rods and corner rods, i.e.:

$$S = S_0 - 19\frac{\pi\cdot d_{rod}^2}{4} - 12\frac{\pi\cdot d_{corner}^2}{4} \approx 2.13\cdot 10^{-3}\,\text{m}^2,$$

here $d_{rod} = 9.13\cdot 10^{-3}$ m – diameter of fuel rod simulator, $d_{corner} = 4.0\cdot 10^{-3}$ m – diameter of corner rod, $S_0 = \pi\cdot d_{shr}^2/4 = 3.53\cdot 10^{-3}\,\text{m}^2$.

Wetted perimeter P is determined as a sum of perimeters of all rods and housing:

$$P = \pi\left(21 d_{rod} + 12 d_{corner} + d_{shr}\right) \approx 0.964\ \text{m}.$$

Then the hydraulic diameter will be

$$D_{hydr} = \frac{4S}{P} \approx 8.84\cdot 10^{-3}\ \text{m}. \tag{2.13}$$

The velocity of mixture at flowing parameters is

$$V = \frac{A}{\rho S} \approx 2.2\ \text{m/s},$$

here $A = A_1 + A_2$ - total flow rate of steam-argon mixture.

Reynolds number of this case is

$$\text{Re} = \frac{V D_{hydr}\rho}{\mu} \approx 902.$$

Using for evaluation the relationship $l_{transition,hydr} \approx 0.065 D_{hydr}\,\text{Re}$ from [17] for LTS (on length of transition section the velocity in the central section differs from the settled value by not more than 1%), valid for round tubes, we'll obtain:

$$l_{transition,hydr} \approx 59 D_{hydr} \approx 0{,}52\ \text{m}.$$

So, the length of transition section becomes rather large for the given parameters (approximately 7÷8 "gauges", namely the channel diameters). However it should be kept in mind that along this length the flow parameters are settled just with high accuracy (1%). Actually the profile of velocity and temperature profiles differ substantially from the initial profiles just at considerably less distances, probably by several "gauges".

The length of thermal transition section according to [18] is $l_{transition,therm} \approx 0.055 \cdot Pe \cdot D_{hydr} \approx 0{,}50$ m,

here $Pe = \mathrm{Re} \cdot \mathrm{Pr}$ - Peclet number, $\mathrm{Pr} = \frac{\mu c_p}{\kappa}$ - Prandtl number.

In [19] the following factors are proposed for calculation of heat transfer in FA:
$Nu = A\,\mathrm{Re}^{0.8}\,\mathrm{Pr}^{0.4}$, $A = 0{,}0165 + 0{,}02\left(1 - 0{,}91 s^2\right) s^{0{,}15}$, s=1,33023; A=0,003761

In [20] we can find one more dependence for Nusselt number in the grid of rods:

$$Nu_{пучок} / Nu_{труба} = 1 + 0.91\,\mathrm{Re}^{-0.1}\,\mathrm{Pr}^{0.4}\left[1 - 2\exp\left(-B\right)\right],\ B = \frac{2\sqrt{3}}{\pi} s^2 - 1$$

The last formula is recommended to use within the range of parameters $3 \cdot 10^3 < \mathrm{Re} < 10^6$, $0{,}66 < \mathrm{Pr} < 5{,}0$, $1{,}02 < s < 2{,}5$.

Dependence of local Nusselt number on the distance is of the following form:

$$Nu = 1.31\left[\frac{x}{Pe \cdot d}\right]^{-1/3},\ \frac{x}{Pe \cdot d} \le 0.001,$$

$$Nu = 4.36 + 1.31\left[\frac{x}{Pe \cdot d}\right]^{-1/3} \exp\left[-13\sqrt{\frac{x}{Pe \cdot d}}\right],\qquad \frac{x}{Pe \cdot d} > 0.001. \tag{2.14}$$

The following value from [21] is assumed to be the hydraulic diameter at the settled flow:

$$d_{эфф} = \frac{2\varepsilon}{(1-\varepsilon)^2}\left(\frac{\varepsilon}{2} - \frac{3}{2} - \frac{\ln\varepsilon}{1-\varepsilon}\right) d_{экв},\ d_{экв} = \left(\sqrt{\frac{2\sqrt{3}}{\pi}} s - 1\right) d_{ст}. \tag{2.15}$$

In the above-mentioned formula (2.15) ε - the grid density equal to the ratio of the cross-section area occupied with rods, to the full cross-section area, $d_{экв}$ - equivalent diameter of the bundle, $s = b / d_{ст}$ - relative grid spacing.

In the light of the above-mentioned during calculations with the use of SOCRAT code the hydraulic diameter in the input file was taken not constant but depending on the elevation.

2.4.2 Sensitivity analysis

Input parameter “hydraulic diameter”, presenting in all numerical codes applied, can have a substantial effect on calculated temperature behaviour of FA.

For evaluation of the degree of its effect a comparison was made for two variants of SF3 pre-test calculation with application of SOCRAT code:

– variant 1 (var1) – base variant with change in hydraulic diameter or Nusselt number by relationship (2.14);

– variant 2 (var2) - hydraulic diameter is constant and determined according to the settled value (2.13).

So, in the input file of base variant of the calculation not constant values of hydraulic diameter were used in calculated cells, but depending on axial level according to formula (2.14). Nusselt number (Figure 2.23) for the given dependence is given below.

Figure 2.24 shows the corresponding hydraulic diameter.

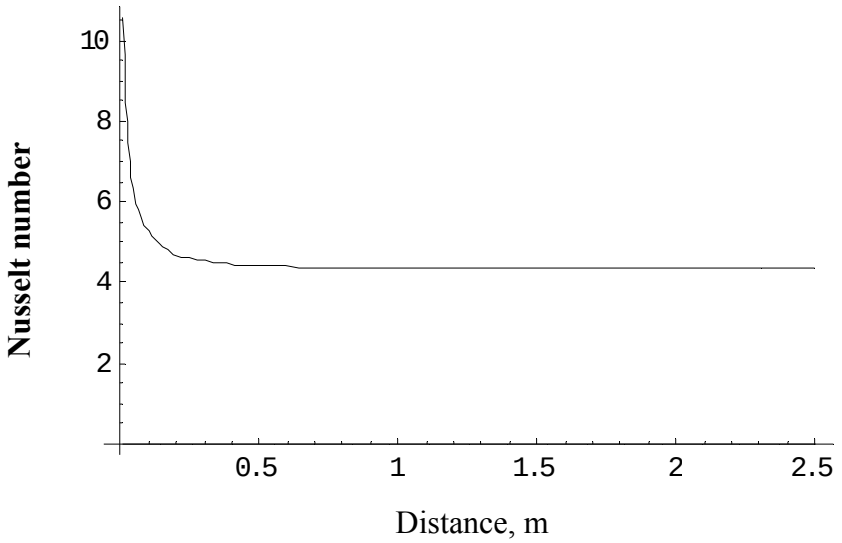

Figure 2.23. Local Nusselt number depending on the distance along the channel.

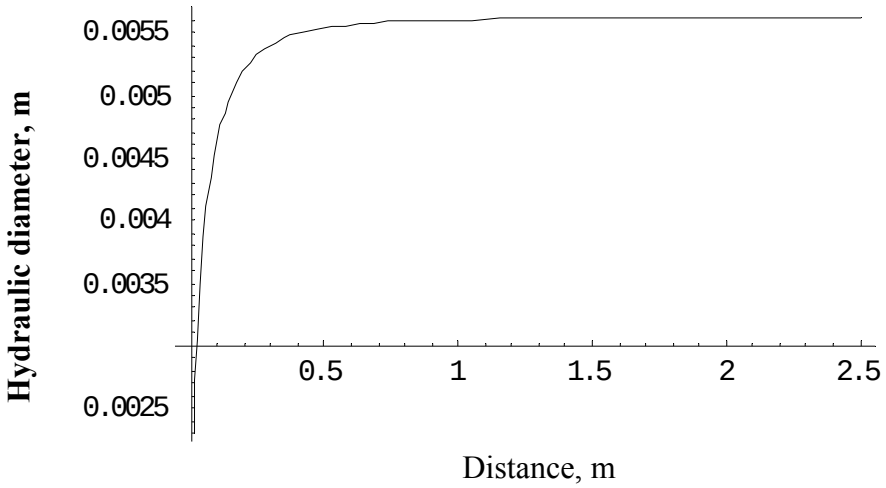

Figure 2.24. Effective hydraulic diameter depending on the distance along the channel.

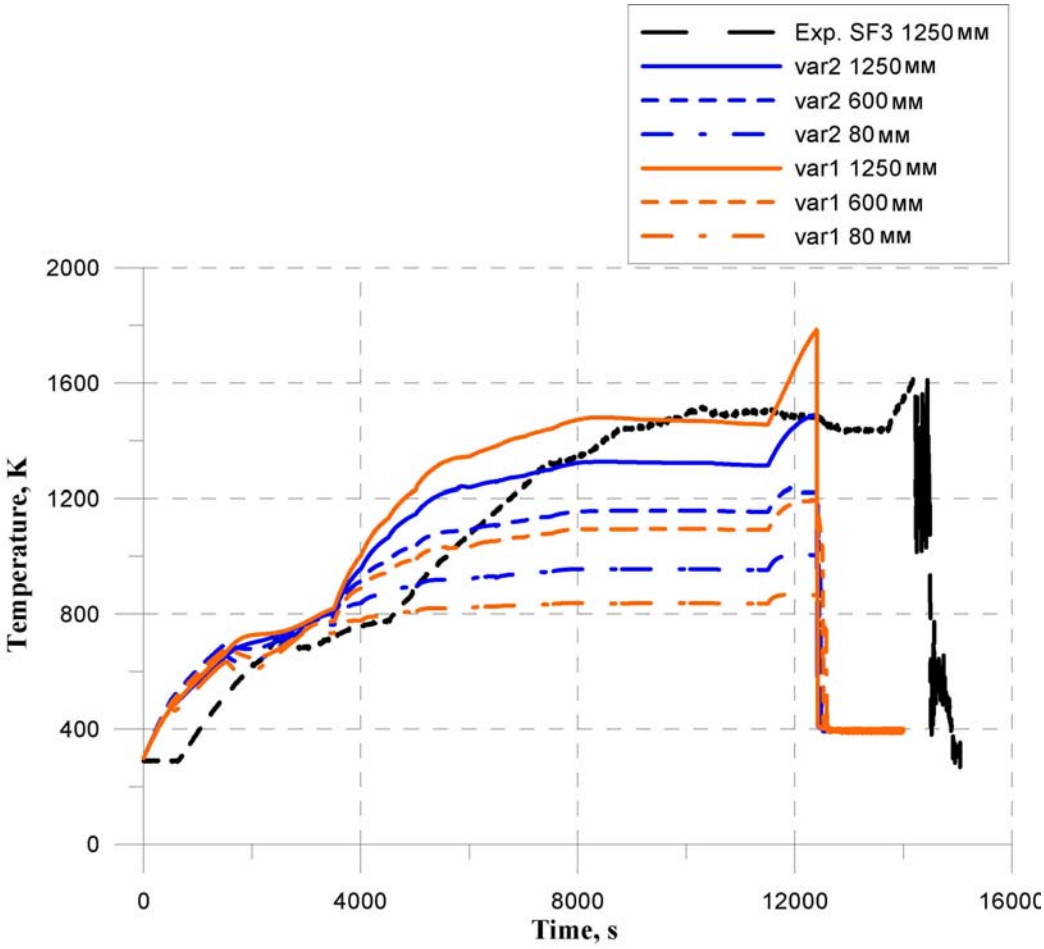

Figure 2.25. Comparison of temperatures at the upper, middle and low elevations for two variants of the calculation.

It is seen from a comparison of temperatures (Figure 2.25) that with the use of constant value of hydraulic diameter over the total height of the assembly we obtain the underestimated values of temperatures in the assembly upper part and overestimated values in the assembly lower part as compared to the base variant. Actually in the assembly lower part the heat transfer rod-coolant is high (Figure 2.23). This is explained by the fact that in this case (variant 2) the heat transfer between rods and coolant is underestimated at lower elevations. Accordingly, the calculated temperature of fuel rod heater is higher. At constant hydraulic diameter (Nusselt number) the linear power of electric heating is also found out to be overestimated in the facility lower part. At constant hydraulic diameter this circumstance can not be considered and the code gives the distorted temperature profile.

2.4.3 Brief description of results of the participants' calculations

2.4.3.1 SOCRAT

At the pre-oxidation phase the full electric power in the system is about 8 kW, as in post-test calculations of SF2 with the coolant mass flow rate was close by its value (about 3.5 g/s of steam and 2 g/s of argon).

On the whole, the results of pre-test calculations, obtained with the use of SOCRAT code, are in agreement with the results obtained by other participants. Integral hydrogen production by SOCRAT code was about 26 g (against 23 g in post-test analysis of SF2).

The FA thermohydraulic behaviour under flooding is of special interest. The code SOCRAT gives a prediction on the stable motion of the flooding front and the guaranteed cooling down of the assembly within the time of the order of 150 s. The time history of temperatures at different elevations under flooding is shown in Figure 2.26.

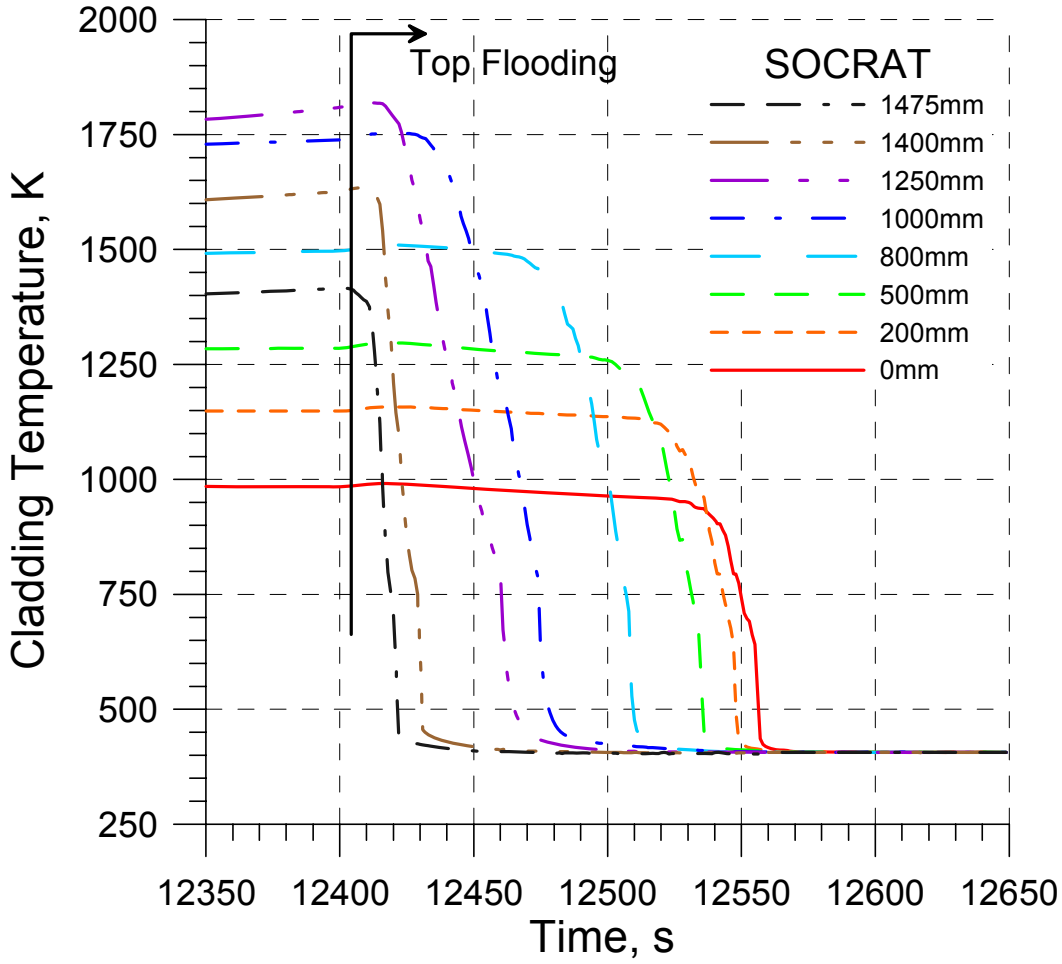

Figure 2.26. PARAMETER-SF3 experiment. Pre-test calculations.

2.4.3.2 RELAP/SCDAPSIM

Losses on electrodes are simulated by assigning the contact resistance. As the input data the full power supplied to the assembly is assigned. By assigning the contact resistance the losses in current leads are simulated. Dependence of these losses on temperature is considered automatically.

The main purpose in constructing the nodalization was obtaining the most exact model in the temperature range of 1000-2000 K. As compared to the calculation of SF2 experiment it was managed to achieve the considerable improvement in temperature behaviour at the stage of the assembly heating-up from indoor temperature. However the disagreement with the calculations applying other codes as to heat removal through the shroud and with coolant remains till the moment of the assembly heating to 900 K.

On the whole, the temperature field is in agreement with those calculated with the use of other codes. Owing to simulation of axial heat conduction, the temperature field in the assembly upper part became in better agreement with other codes. Accordingly, the simulation of oxide scale thickness versus height became better. Maximum temperature at the pre-oxidation stage is 1495 K, maximum temperature is 1900 K, the hottest zone is located at the elevation of 1250 mm. Maximum thickness of oxide scale is 386 μm.

Upgrading of the assembly model by means of consideration of heat losses in axial direction allowed to make more exact simulation of temperature of the central unheated rod in the lower part and temperature distribution in the assembly upper part. Temperatures inside the shroud became lower that makes possible to expect (based on SF2 results) less oxidation of the shroud. By the results of calculations the shroud oxidation gives 6 g of hydrogen, that is, a quarter less than in SF2.

2.4.3.3 ATHLET-CD

Temperature behaviour

– Maximum temperature of 1600°C was reached at the time moment t=12567 s at the elevation of 1250 mm;

– After starting of the top flooding the calculated temperature drops at all elevations;

Unlike the calculation and experiment results of PARAMETER-SF2 owing to top flooding only in PARAMETER-SF3 the calculations showed that the pre-cooling at upper elevations is more than in the lower elevations.

Hydrogen production

Full mass of the released hydrogen is 26.1 g (18,7 g in the test section) with the use of Leistikow/Prater-Courtright correlation of oxidation, the result corresponds to the calculated hydrogen production in PARAMETER-SF2.

Thickness of zirconium dioxide scales

– At the phase of pre-oxidation the oxide scale thickness was 200 μm (according to the assignment);

– Maximum thickness of oxide scale of 427 μm was achieved at the end of calculation (elevation of 1250 mm).

Change in time interval of switching off the steam supply before the flooding stage did not influence much the results due to quick process of FA cooling down at all elevations under flooding.

2.4.4 Results of numerical calculations

2.4.4.1 Initial and boundary conditions

The initial conditions of PARAMETER-SF3 experiment include the values of temperatures in the assembly, shroud, insulation, vessel at the beginning of the experiment (t=0), corresponding to indoor conditions, axial and, generally speaking, angle (if absence of axial symmetry is considered) dependences (profiles) of these temperatures. The same time moments (t=0) is accepted as the beginning of simulation with the use of codes. In the simulation the presence of axial symmetry was assumed.

The boundary conditions of SF-3 experiment include the wider list of not only temperature but also of thermohydraulic parameters. It includes temperatures and conditions of heat transfer on the test section boundaries, as well as flow rate and temperature of steam and argon entering the test section, pressure at the test section outlet, with this, all parameters are assigned for the whole time interval from t=0 to $t=t_{end}$, corresponding to performing the experiment. The list of boundary parameters also includes the temperature and flow rate of water supplied into the assembly under flooding.

Figures 2.27 and 2.28 present mass flow rates of steam and argon at test section inlet.

Figure 2.31 presents the full electric power in PARAMETER-SF2 experiment.

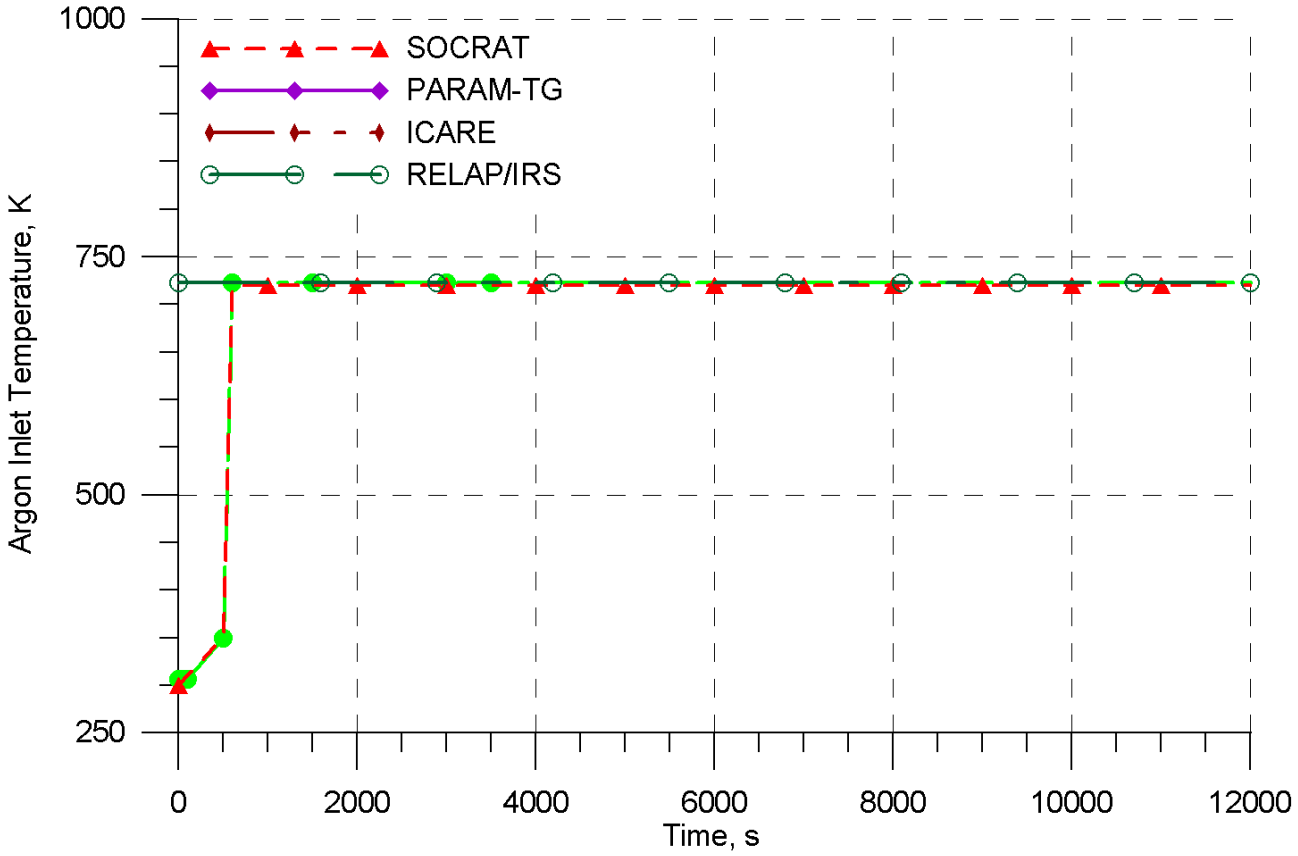

Figure 2.27. Argon temperature at the facility inlet. PARAMETER-SF3 experiment. Pre-test calculations.

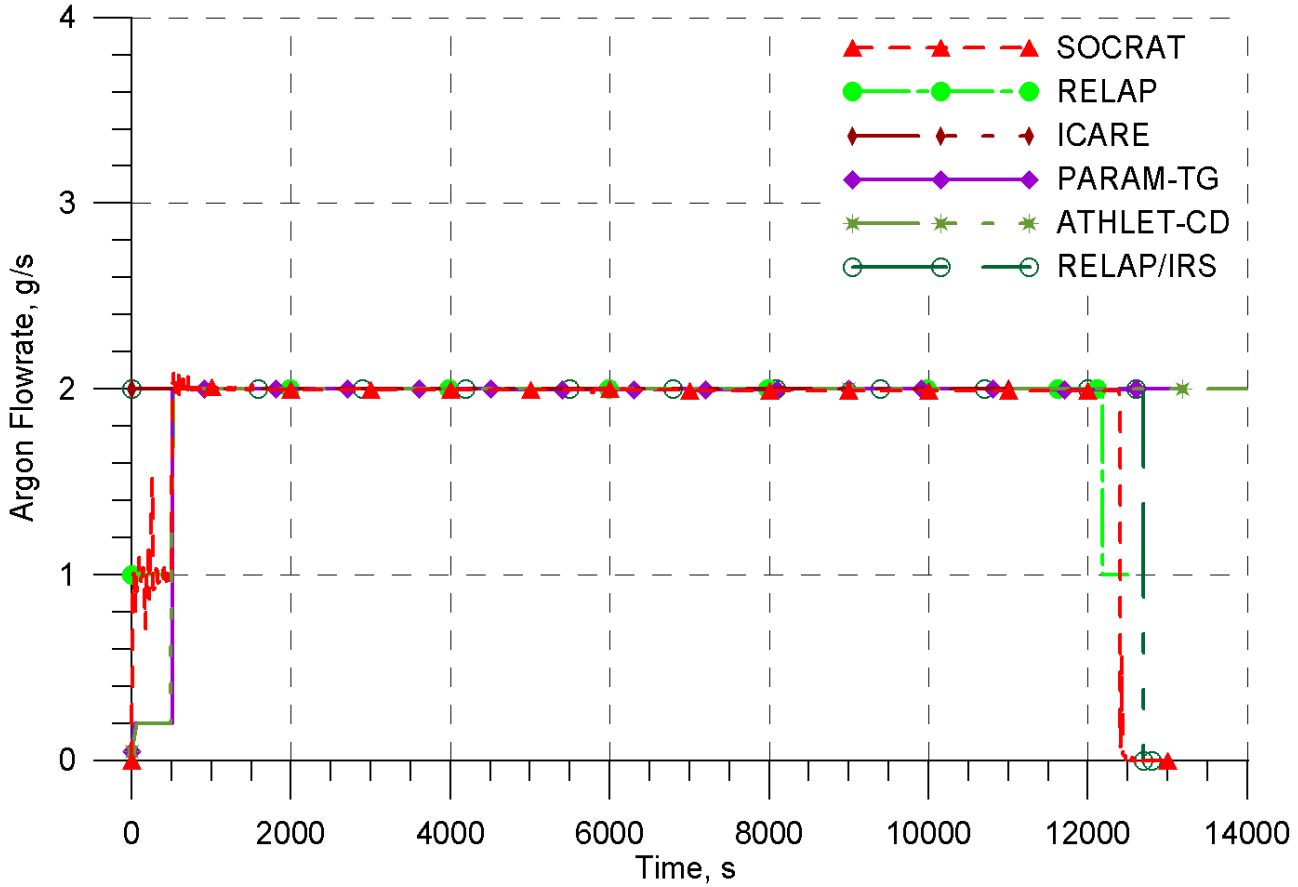

Figure 2.28. Argon flow rate at the facility inlet. PARAMETER-SF3 experiment. Pre-test calculations.

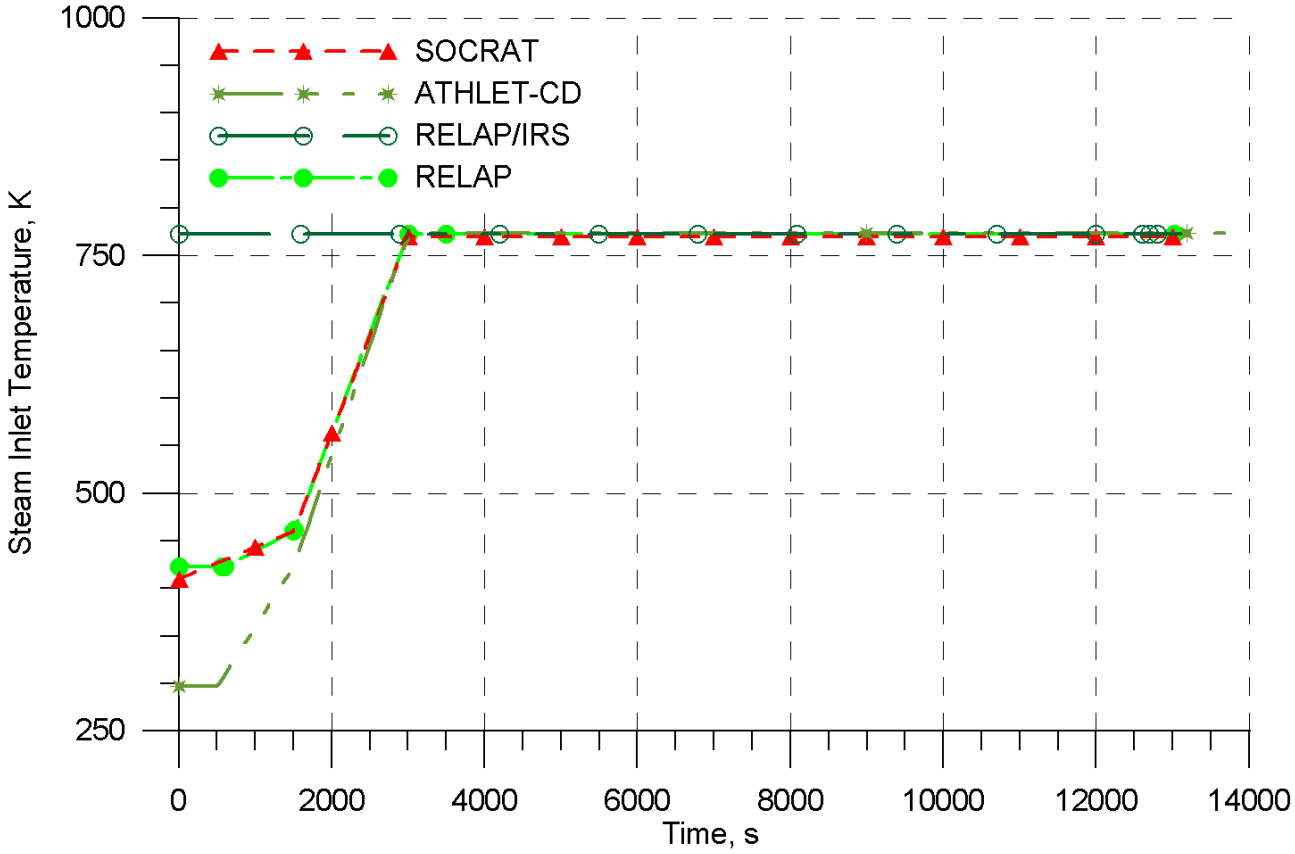

Figure 2.29. Steam temperature at the test section inlet. PARAMETER-SF3 experiment. Pre-test calculations.

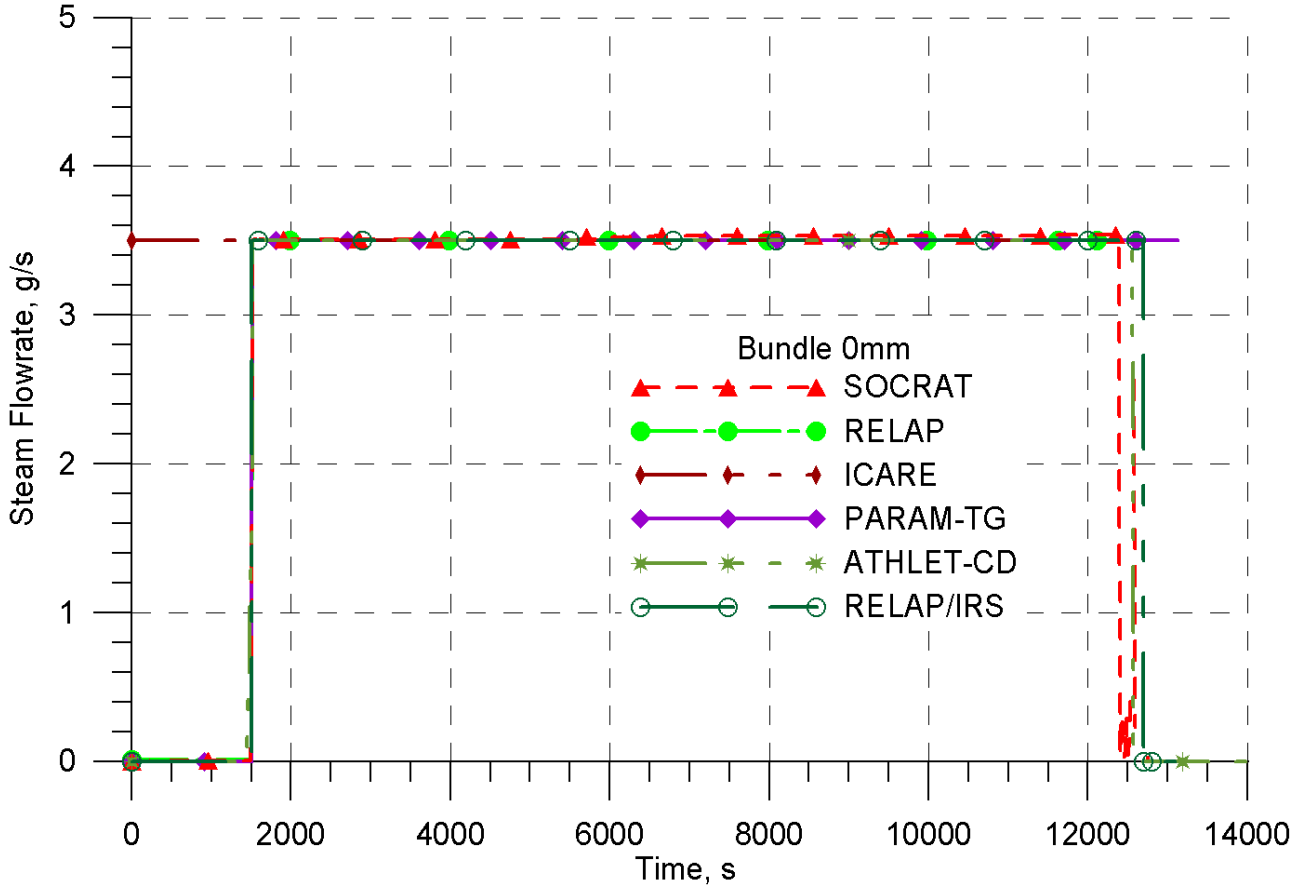

Figure 2.30. Steam flow rate at the facility inlet. PARAMETER-SF3 experiment. Pre-test calculations.

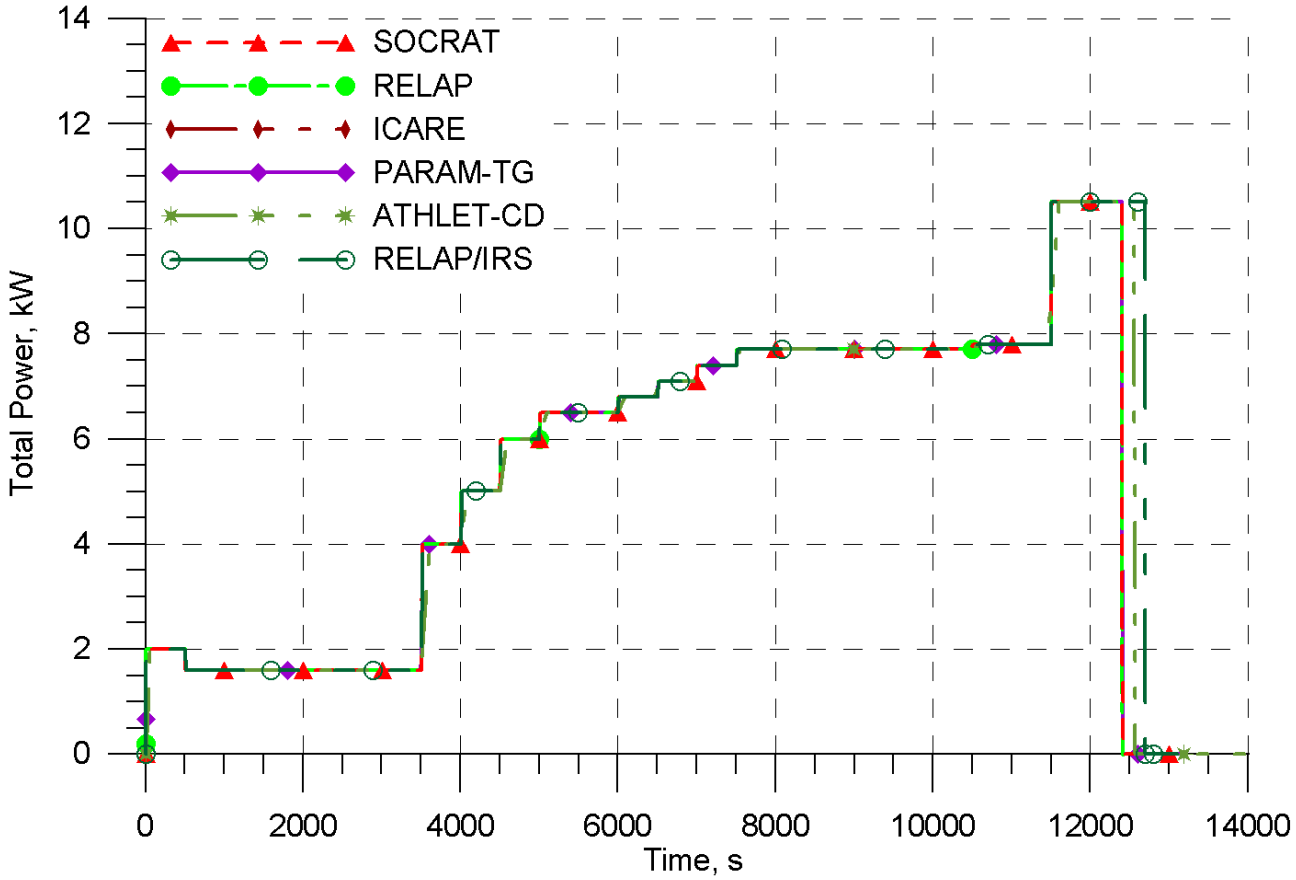

Figure 2.31. Full electric power. PARAMETER-SF3 experiment. Pre-test calculations.

2.4.4.2 Heat balance in the facility

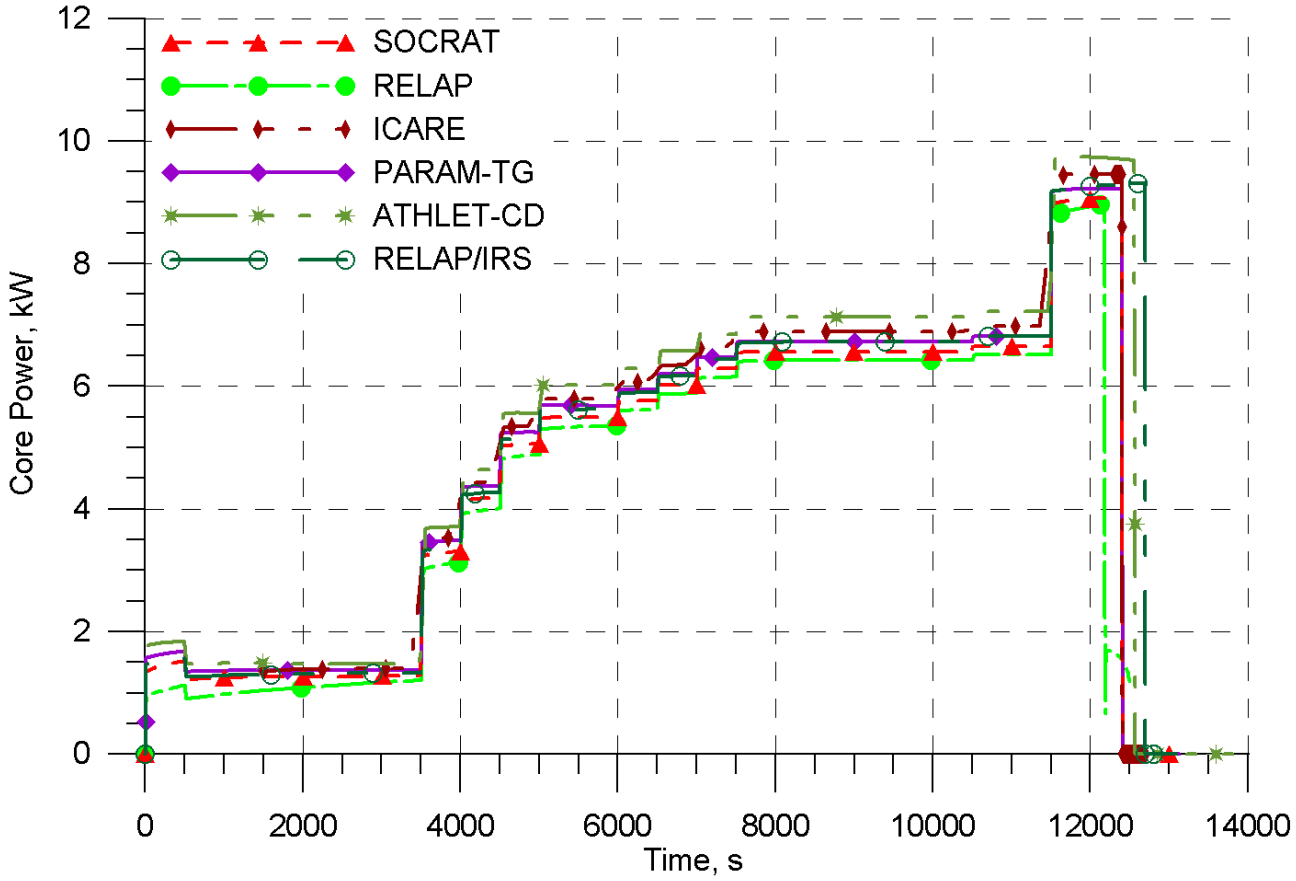

Figure 2.32. Electric power released in the assembly heated part. PARAMETER-SF3 experiment. Pre-test calculations.

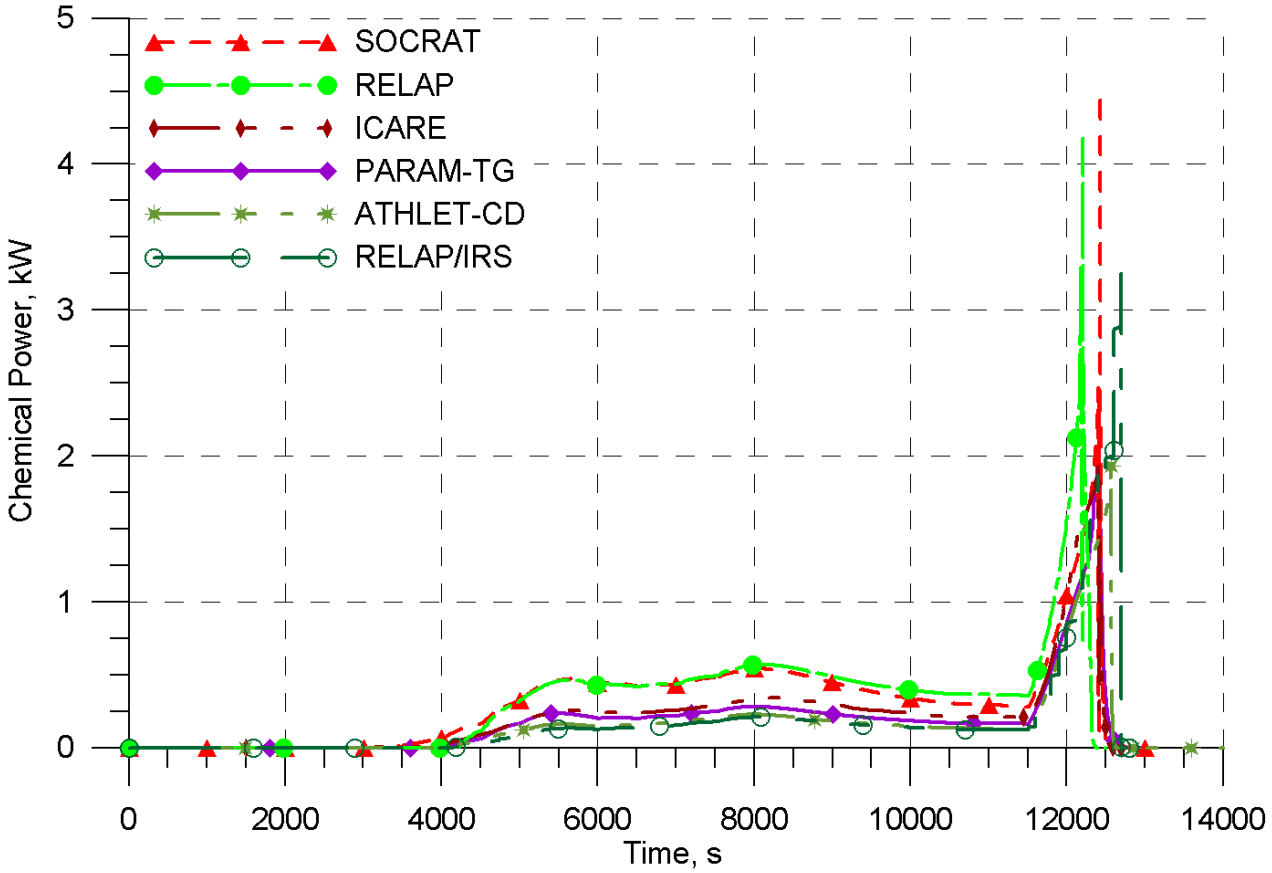

Figure 2.33. Power of chemical reactions. PARAMETER-SF3 experiment. Pre-test calculations.

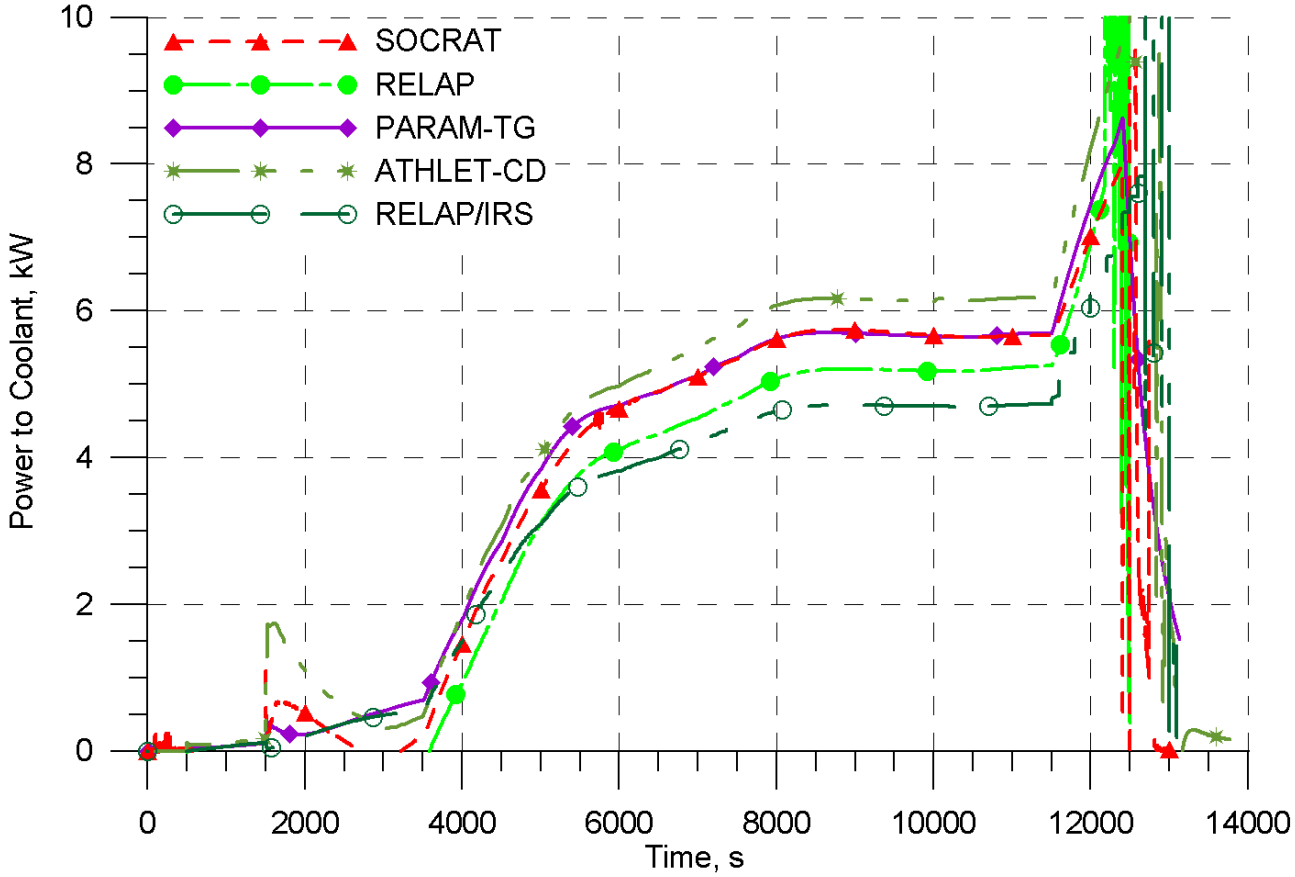

Figure 2.34. Power removed by coolant. PARAMETER-SF3 experiment. Pre-test calculations.

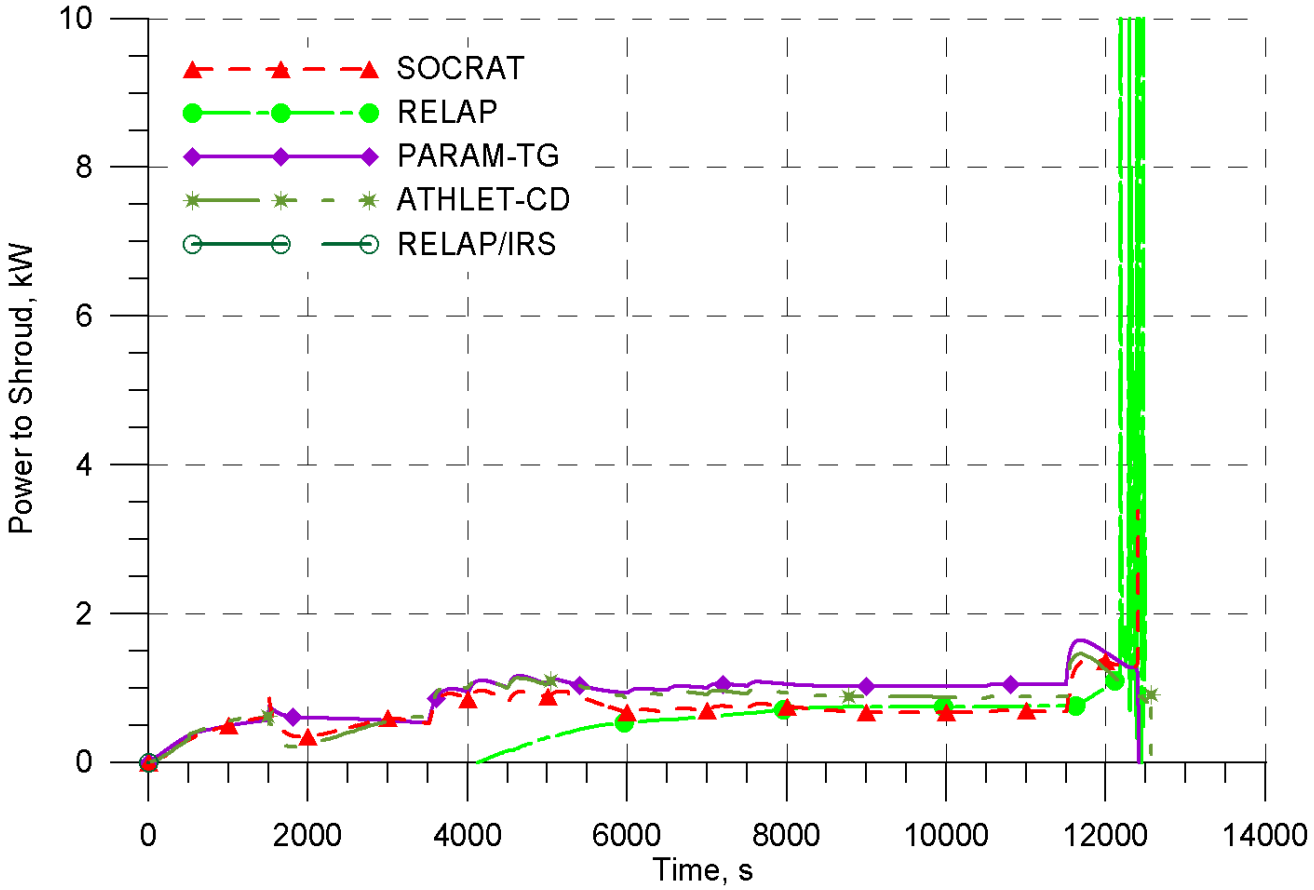

Figure 2.35. Power of heat losses through the shroud. PARAMETER-SF3 experiment. Pre-test calculations.

2.4.4.3 Temperature of simulator claddings

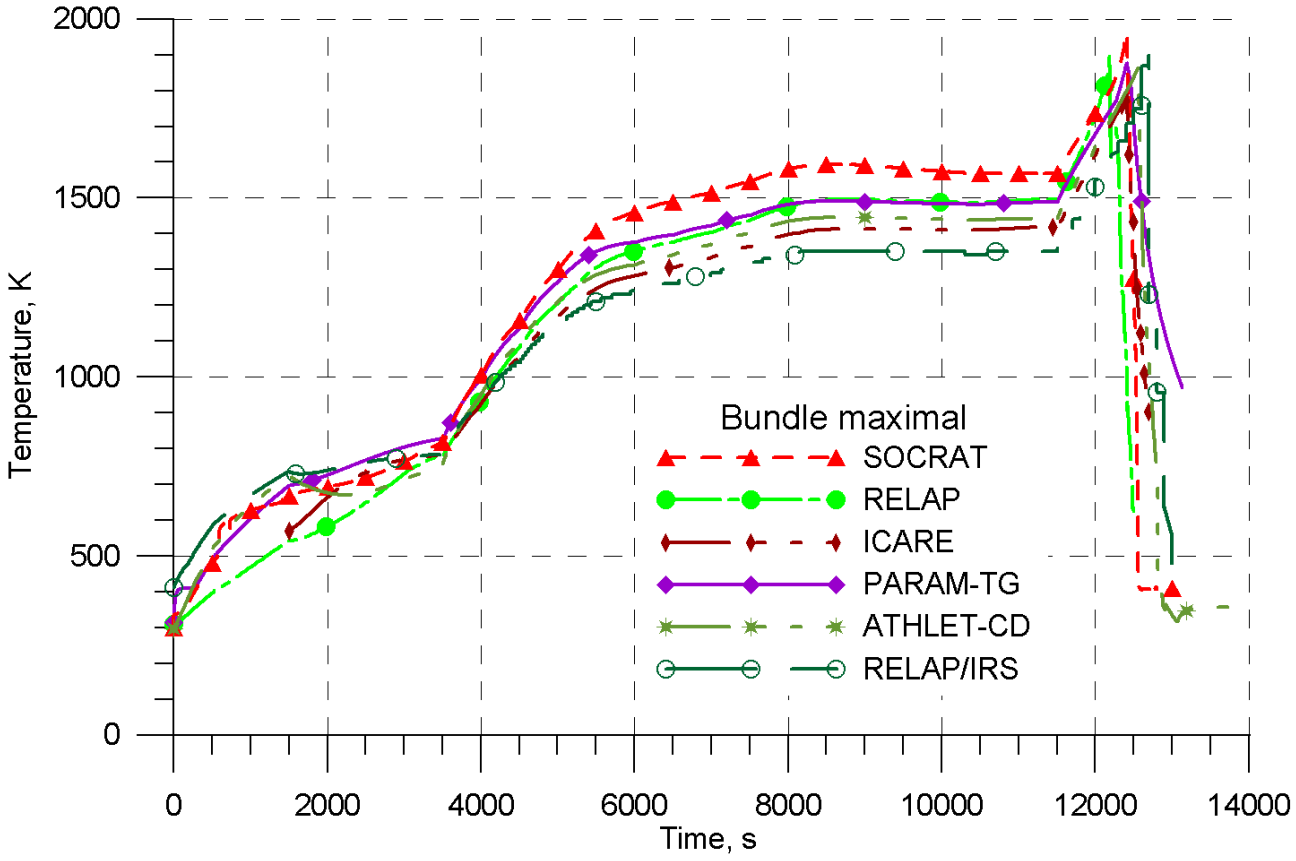

Figure 2.36. Maximum temperature of simulator claddings. PARAMETER-SF3 experiment. Pre-test calculations.

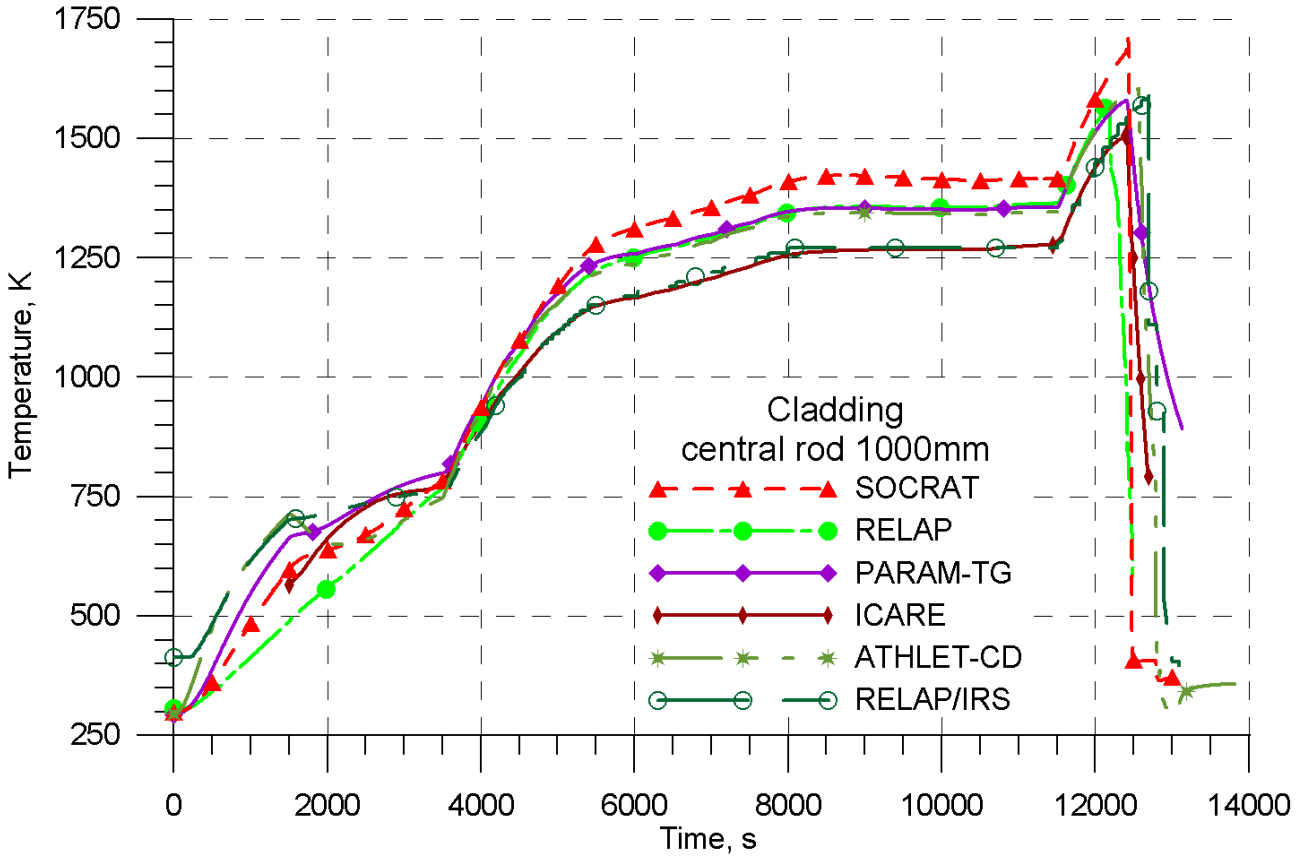

Figure 2.37. Temperature of central fuel rod cladding at the elevation of 1000 mm. PARAMETER-SF3 experiment. Pre-test calculations.

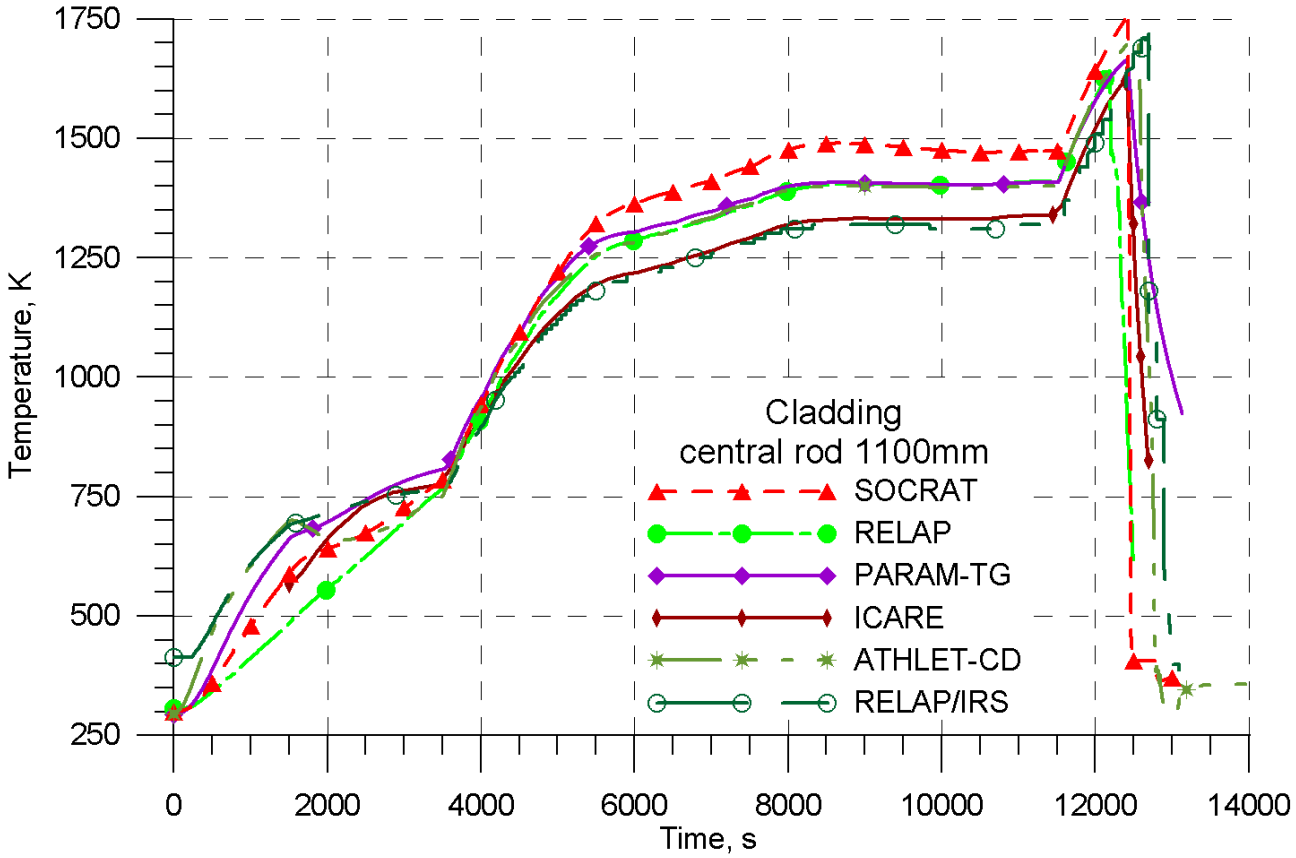

Figure 2.38. Temperature of central fuel rod cladding at the elevation of 1100 mm. PARAMETER-SF3 experiment. Pre-test calculations.

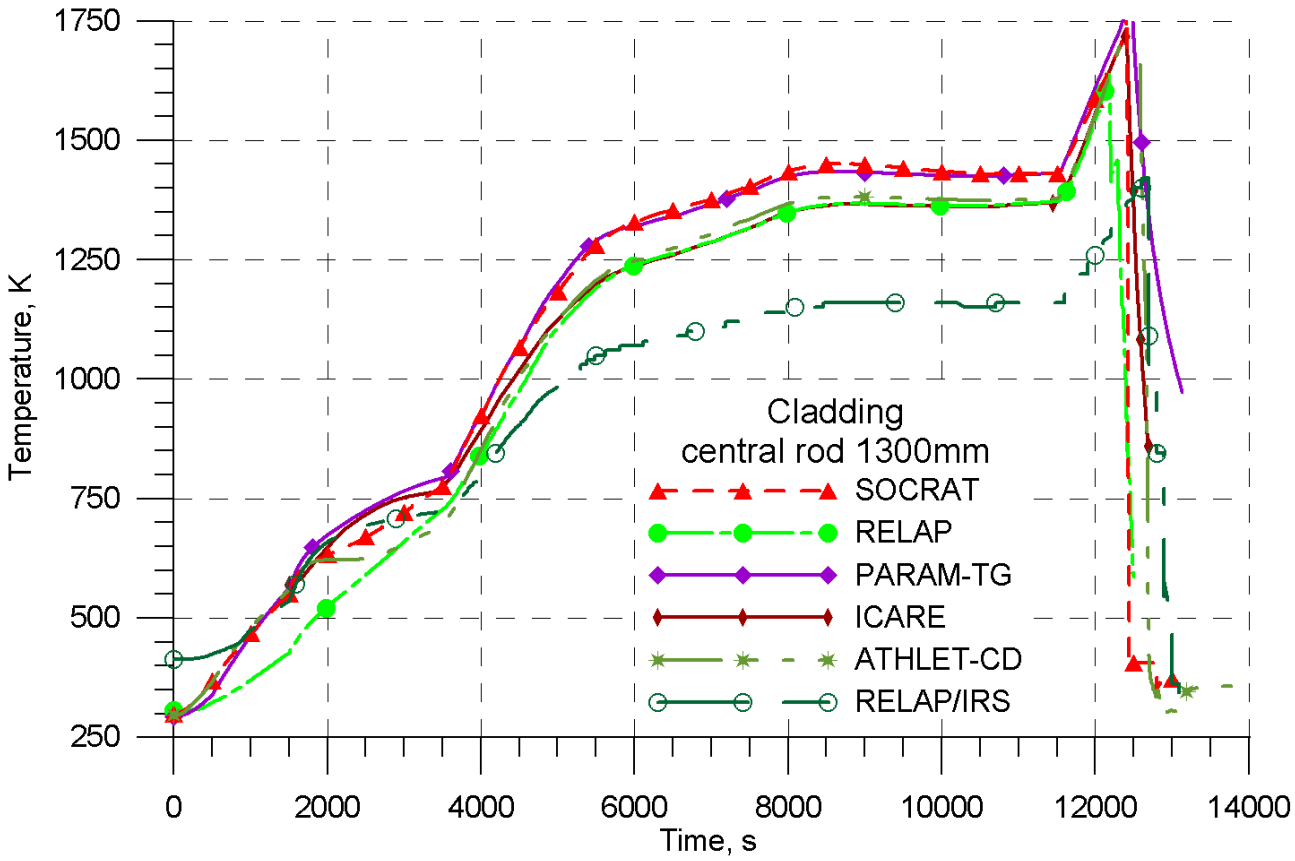

Figure 2.39. Temperature of central fuel rod cladding at the elevation of 1300 mm. PARAMETER-SF3 experiment. Pre-test calculations.

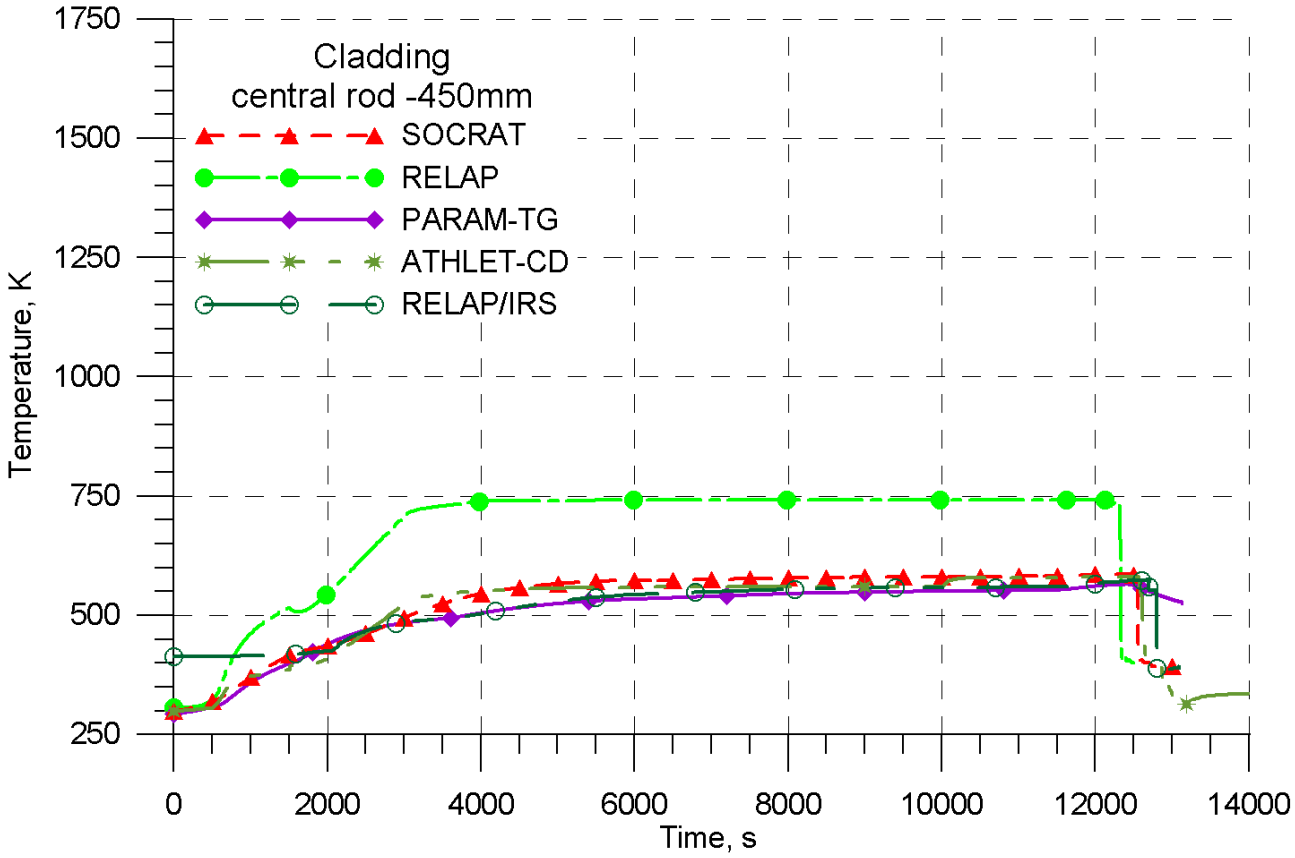

Figure 2.40. Temperature of central fuel rod cladding at the elevation of -450 mm. PARAMETER-SF3 experiment. Pre-test calculations.

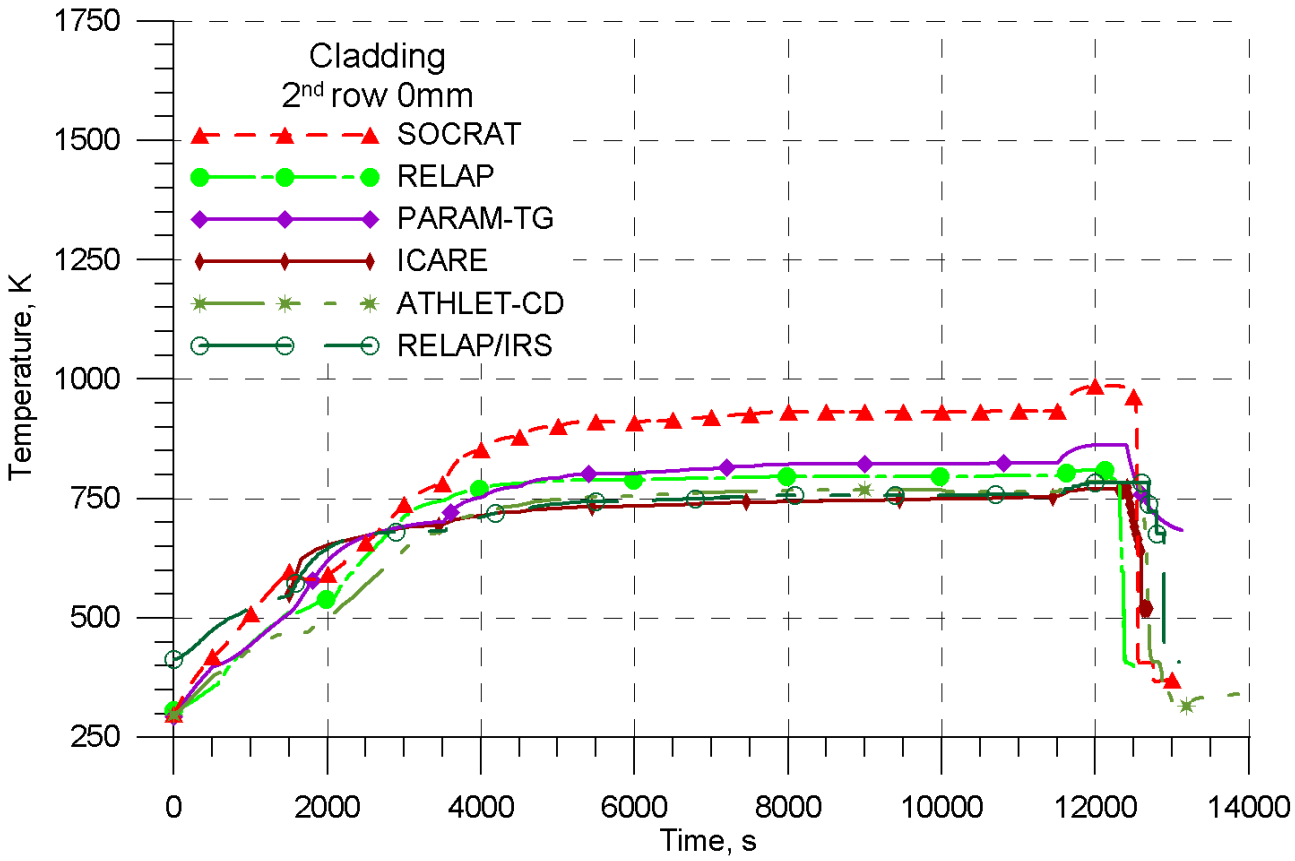

Figure 2.41. Cladding temperature of fuel rod in the second row at the elevation of 0 mm. PARAMETER-SF3 experiment. Pre-test calculations.

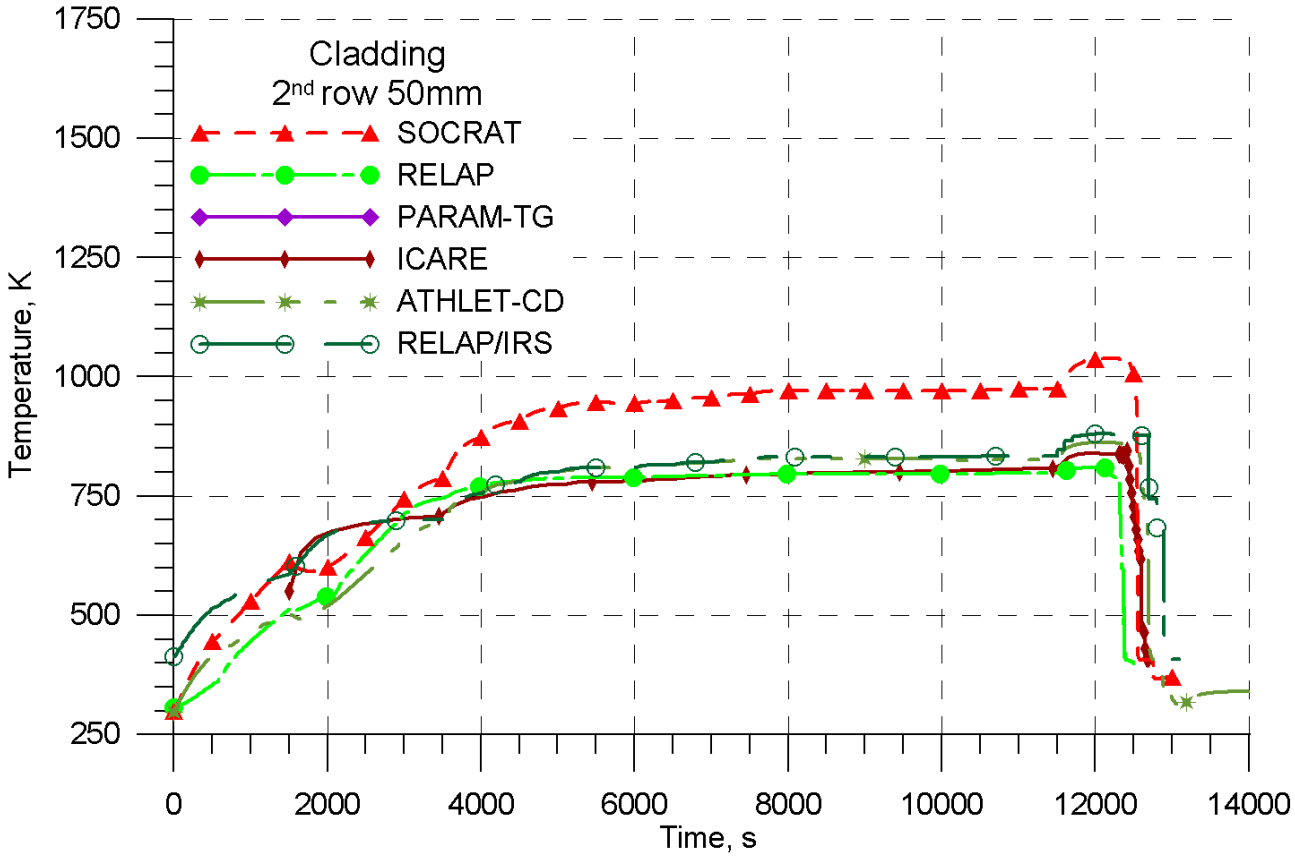

Figure 2.42. Cladding temperature of fuel rod in the second row at the elevation of 50 mm. PARAMETER-SF3 experiment. Pre-test calculations.

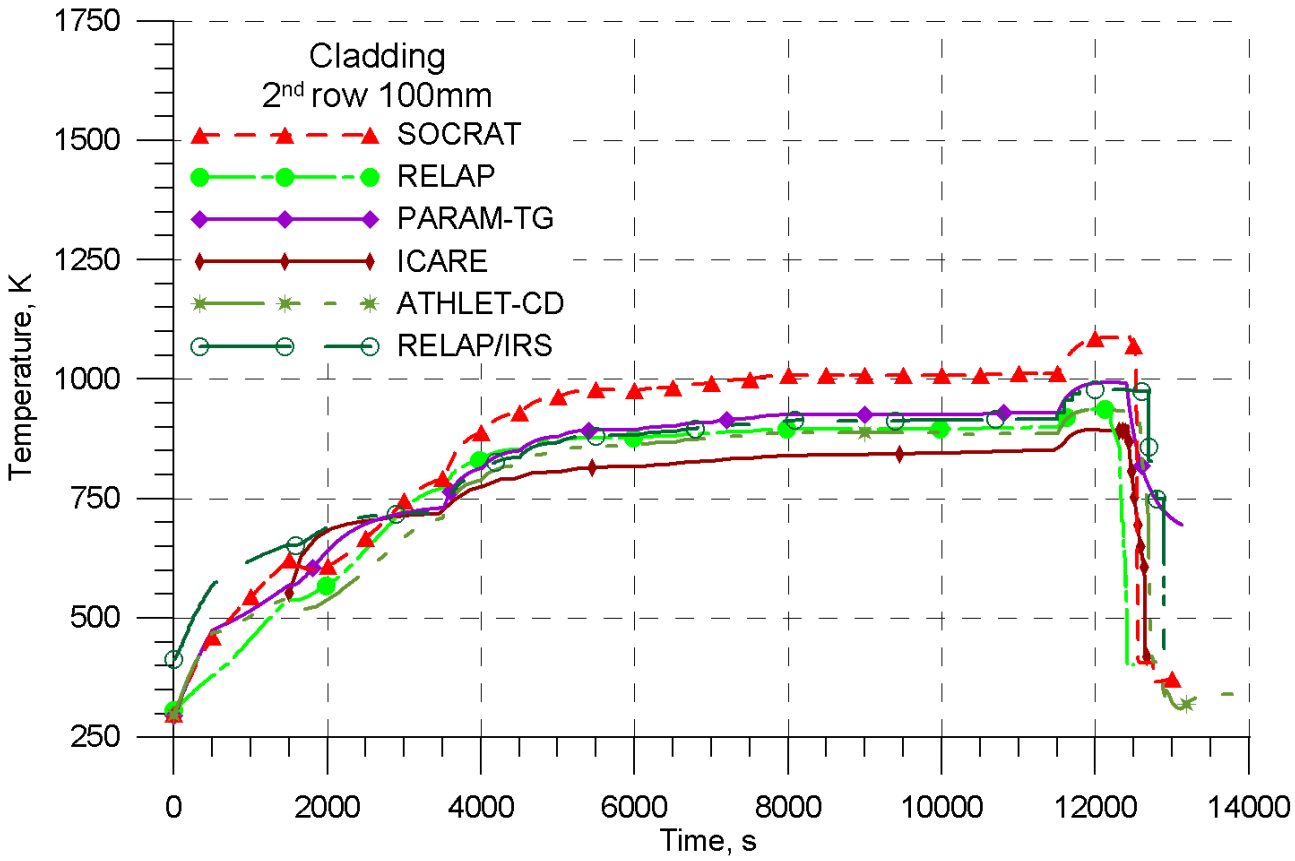

Figure 2.43. Cladding temperature of fuel rod in the second row at the elevation of 100 mm. PARAMETER-SF3 experiment. Pre-test calculations.

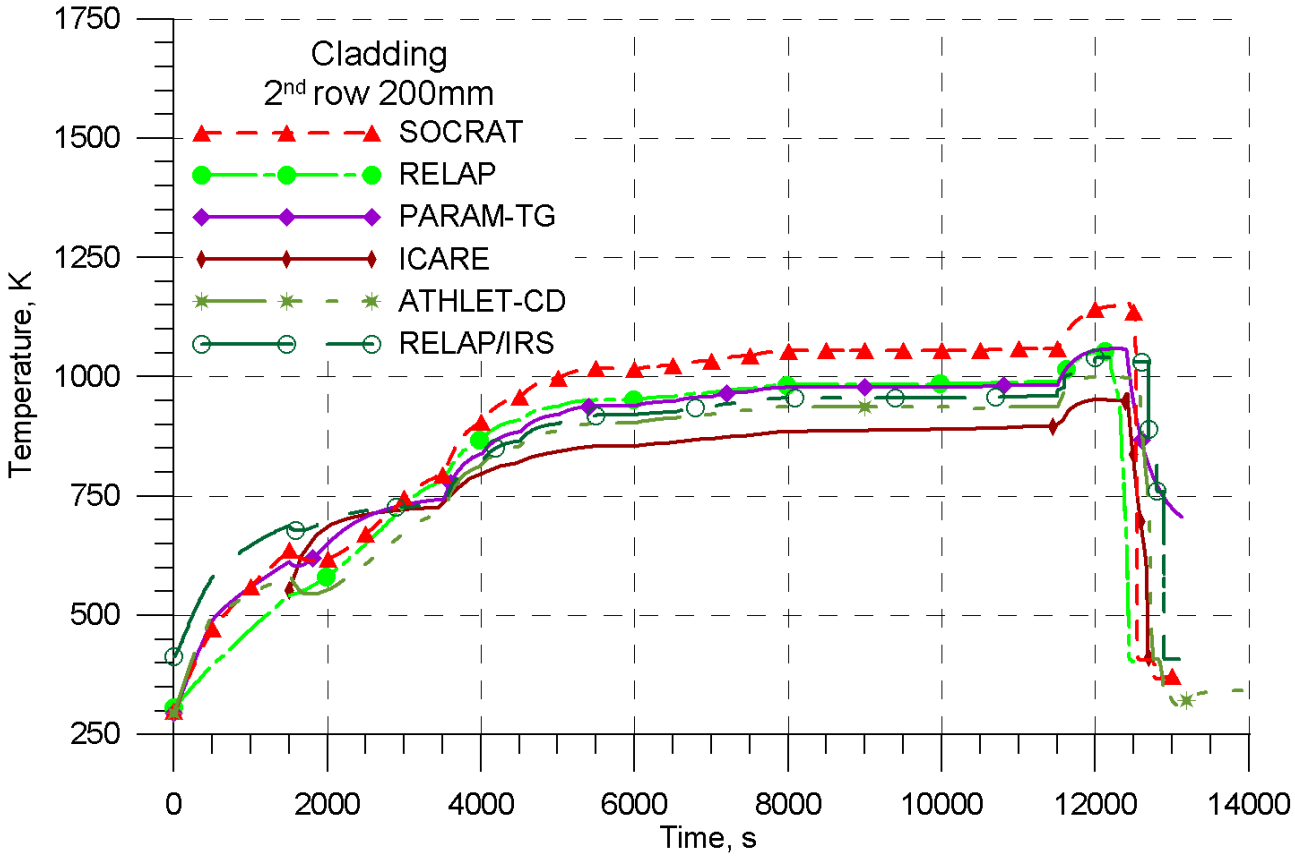

Figure 2.44. Cladding temperature of fuel rod in the second row at the elevation of 200 mm. PARAMETER-SF3 experiment. Pre-test calculations.

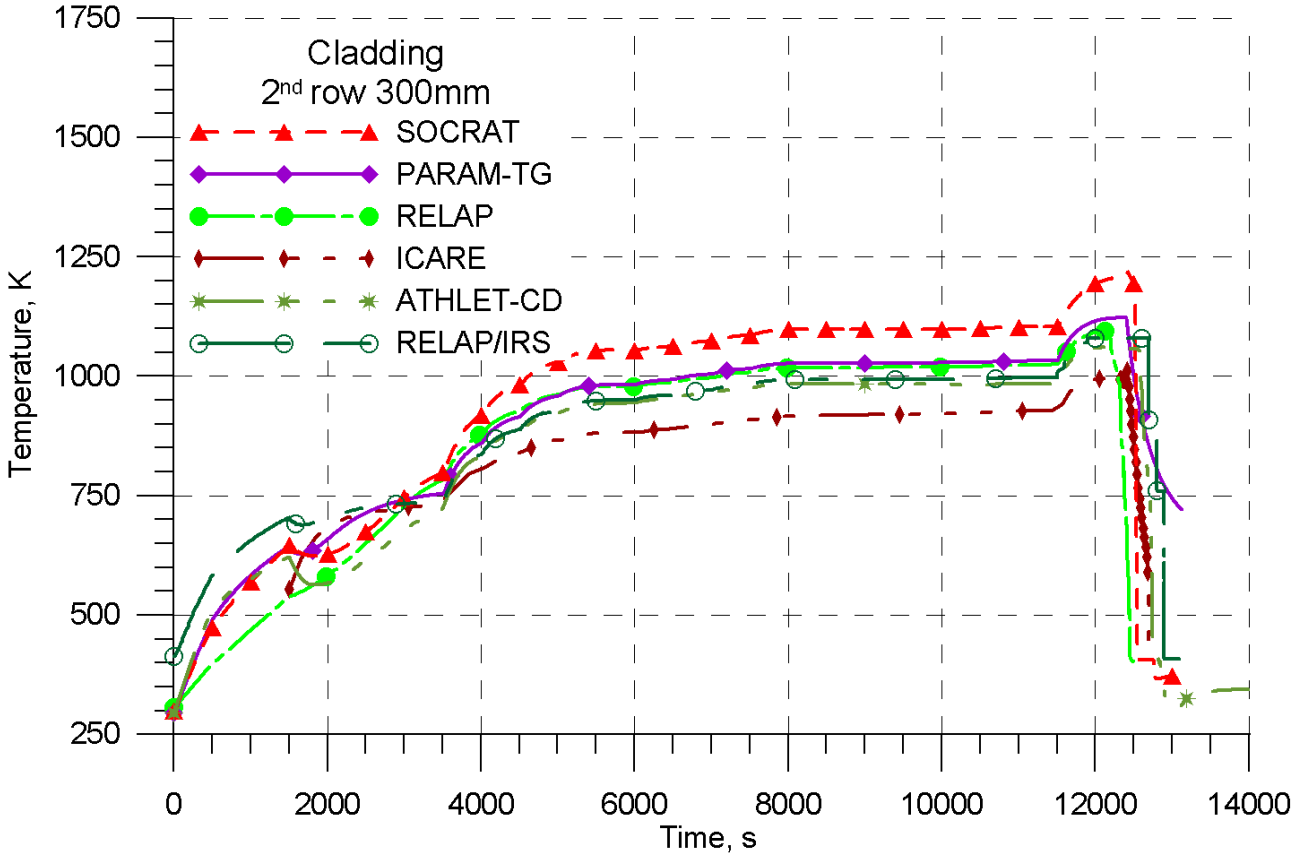

Figure 2.45. Cladding temperature of fuel rod in the second row at the elevation of 300 mm. PARAMETER-SF3 experiment. Pre-test calculations.

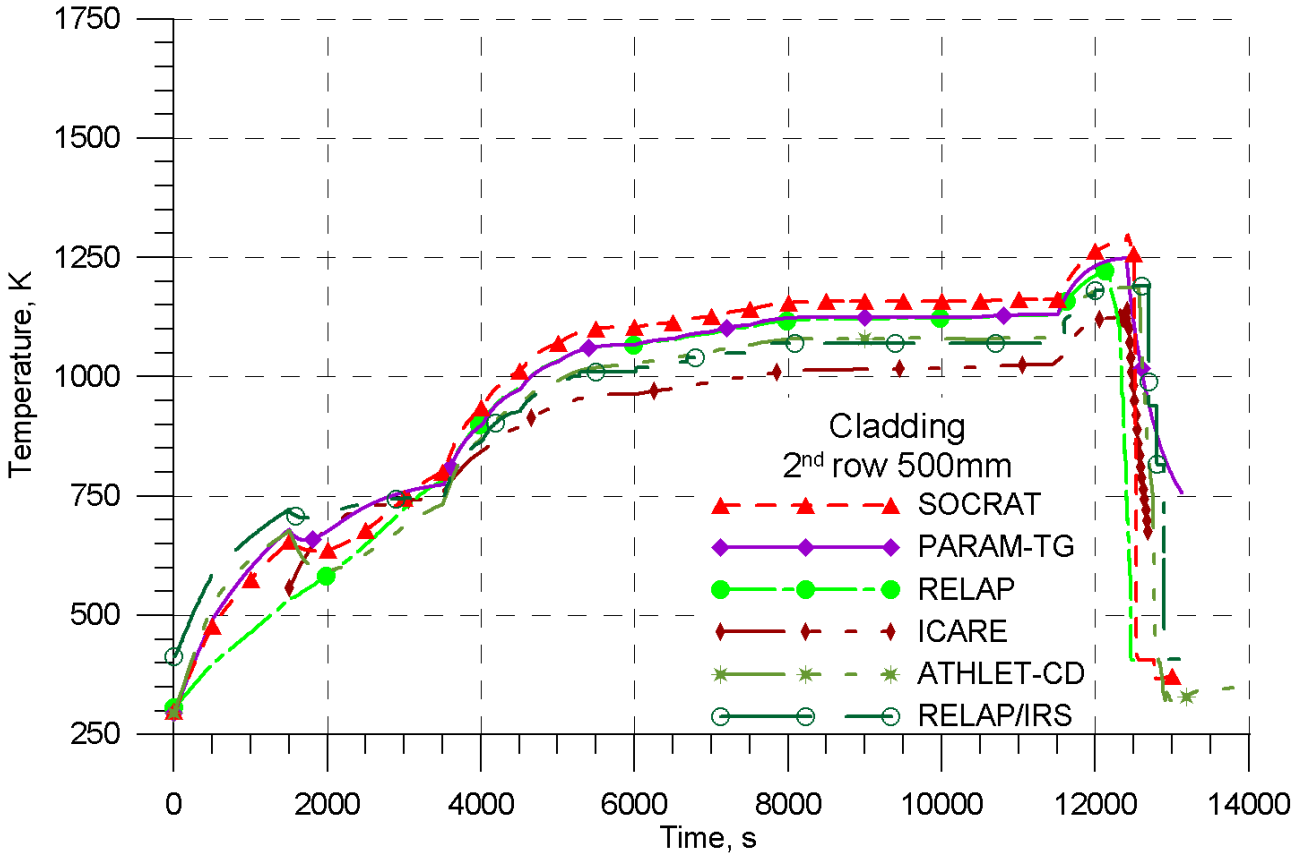

Figure 2.46. Cladding temperature of fuel rod in the second row at the elevation of 500 mm. PARAMETER-SF3 experiment. Pre-test calculations.

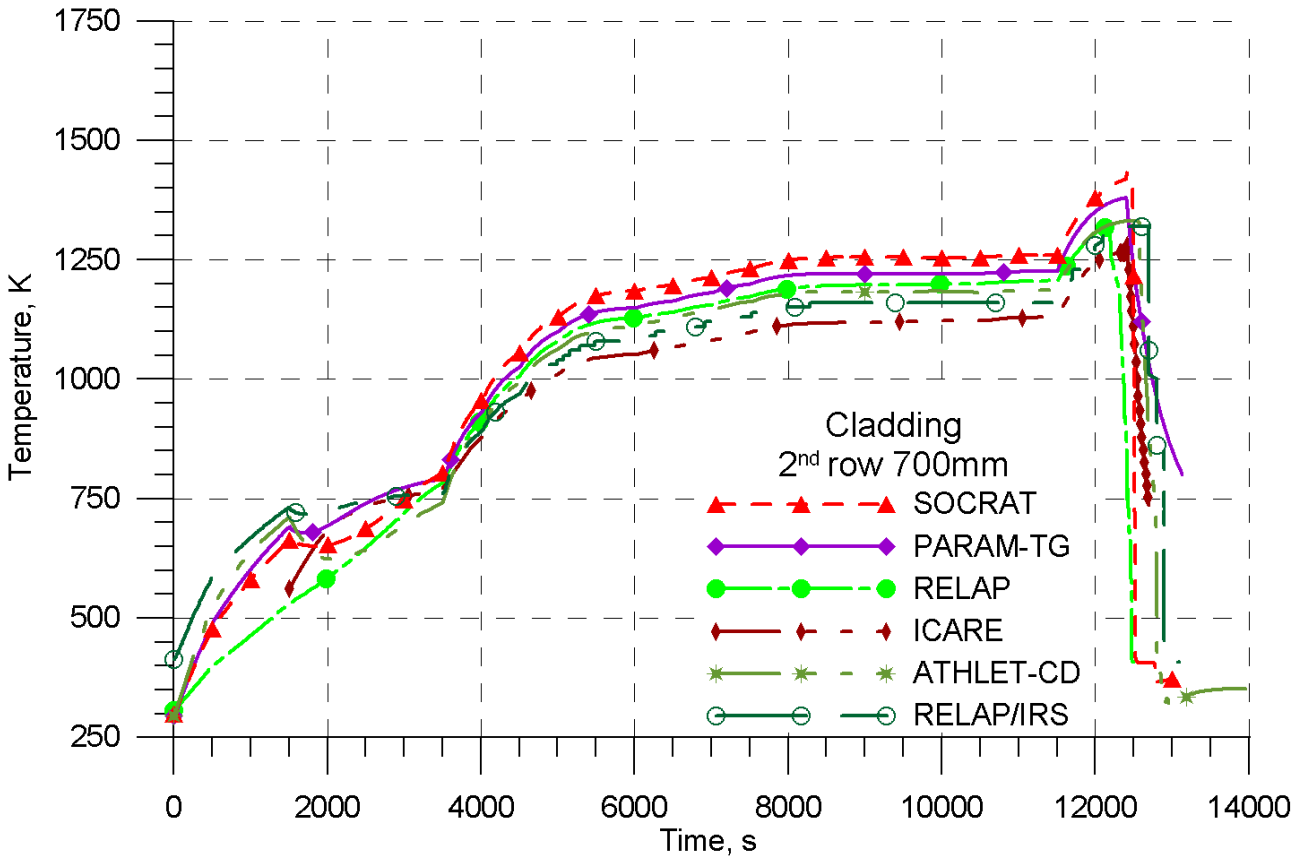

Figure 2.47. Cladding temperature of fuel rod in the second row at the elevation of 700 mm. PARAMETER-SF3 experiment. Pre-test calculations.

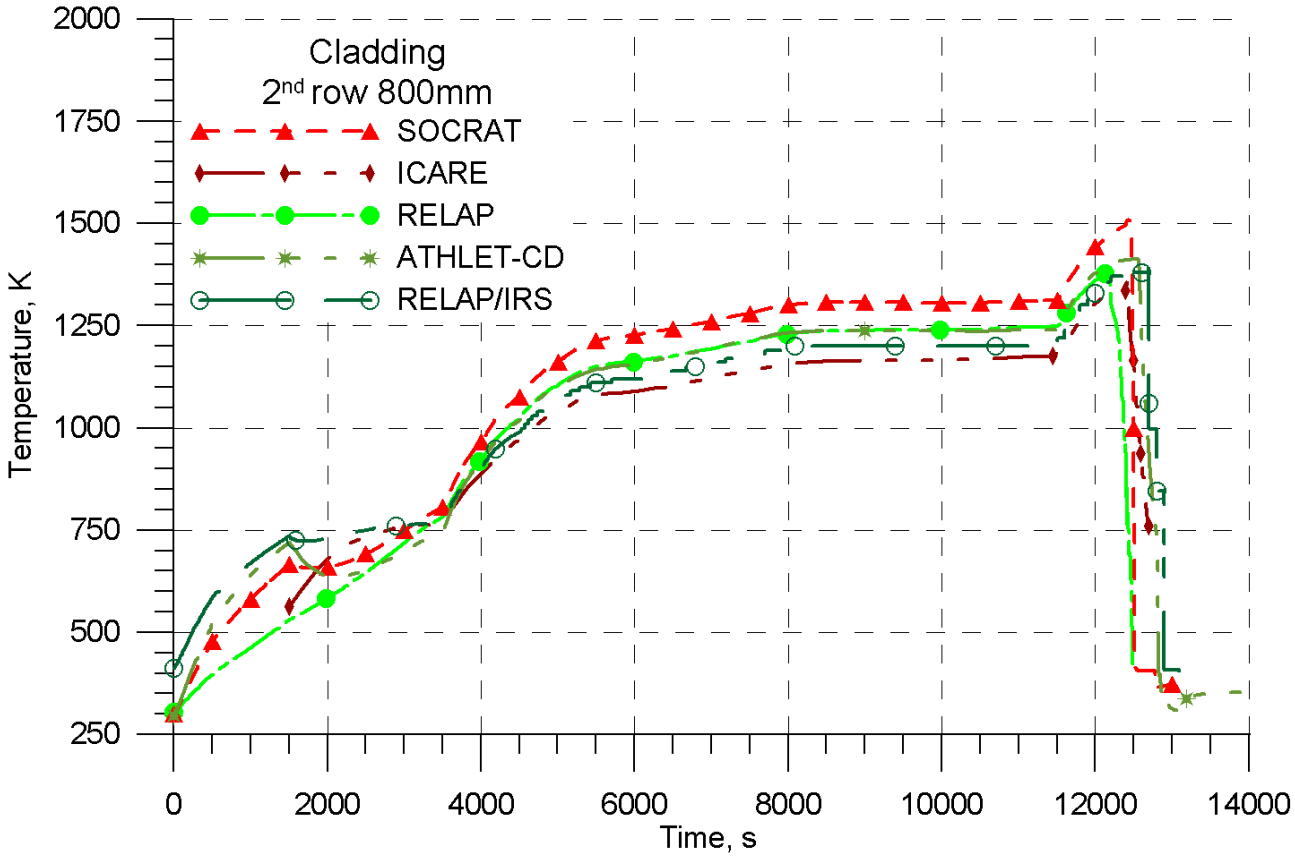

Figure 2.48. Cladding temperature of fuel rod in the second row at the elevation of 800 mm. PARAMETER-SF3 experiment. Pre-test calculations.

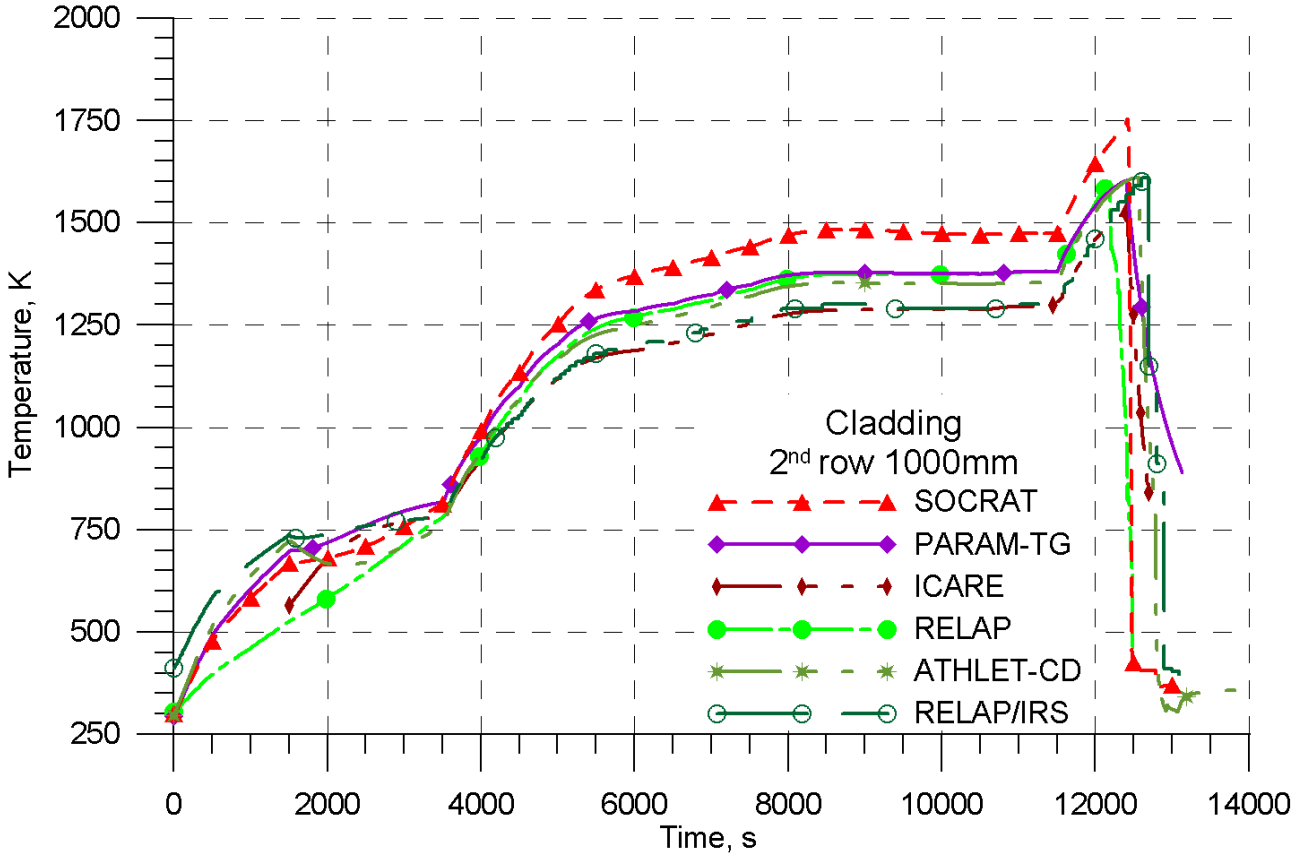

Figure 2.49. Cladding temperature of fuel rod in the second row at the elevation of 1000 mm. PARAMETER-SF3 experiment. Pre-test calculations.

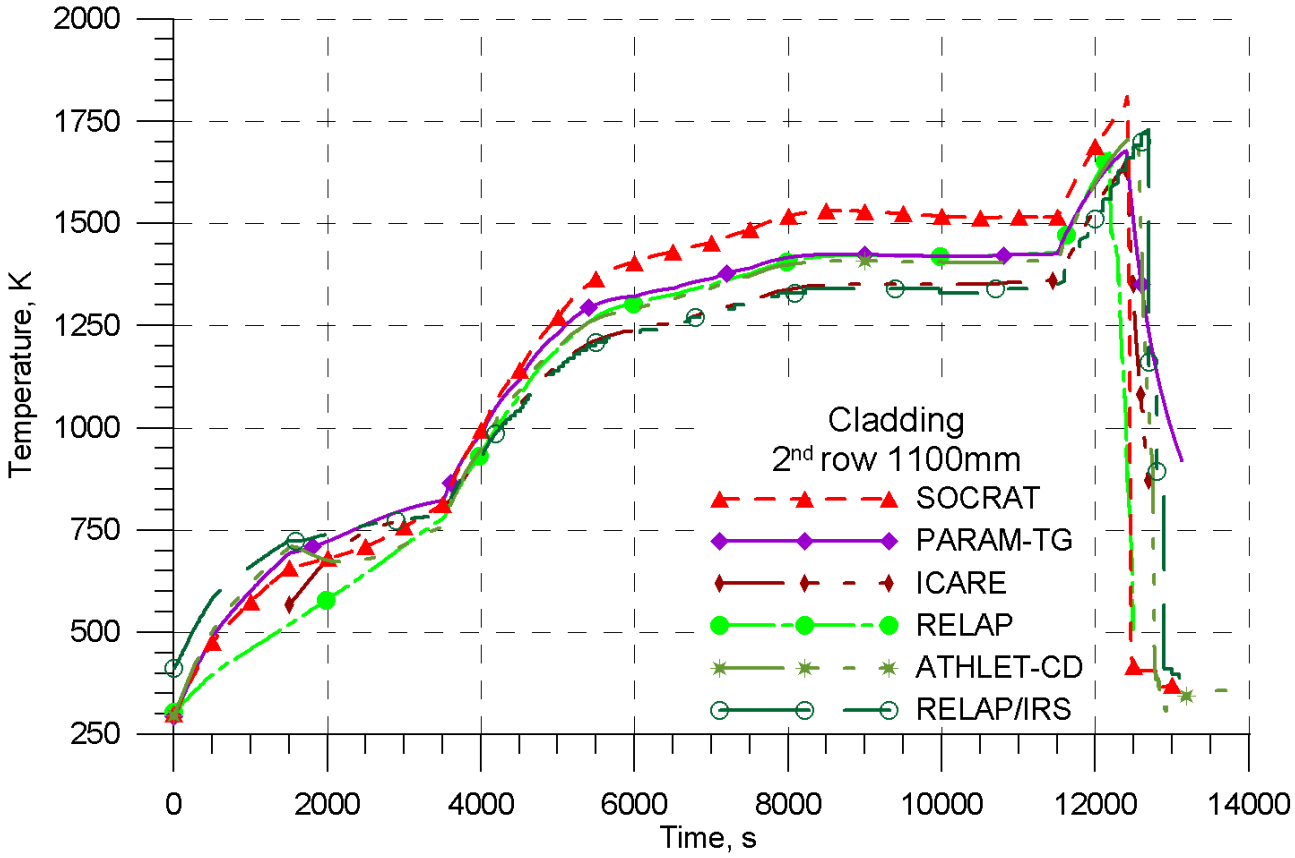

Figure 2.50. Cladding temperature of fuel rod in the second row at the elevation of 1100 mm. PARAMETER-SF3 experiment. Pre-test calculations.

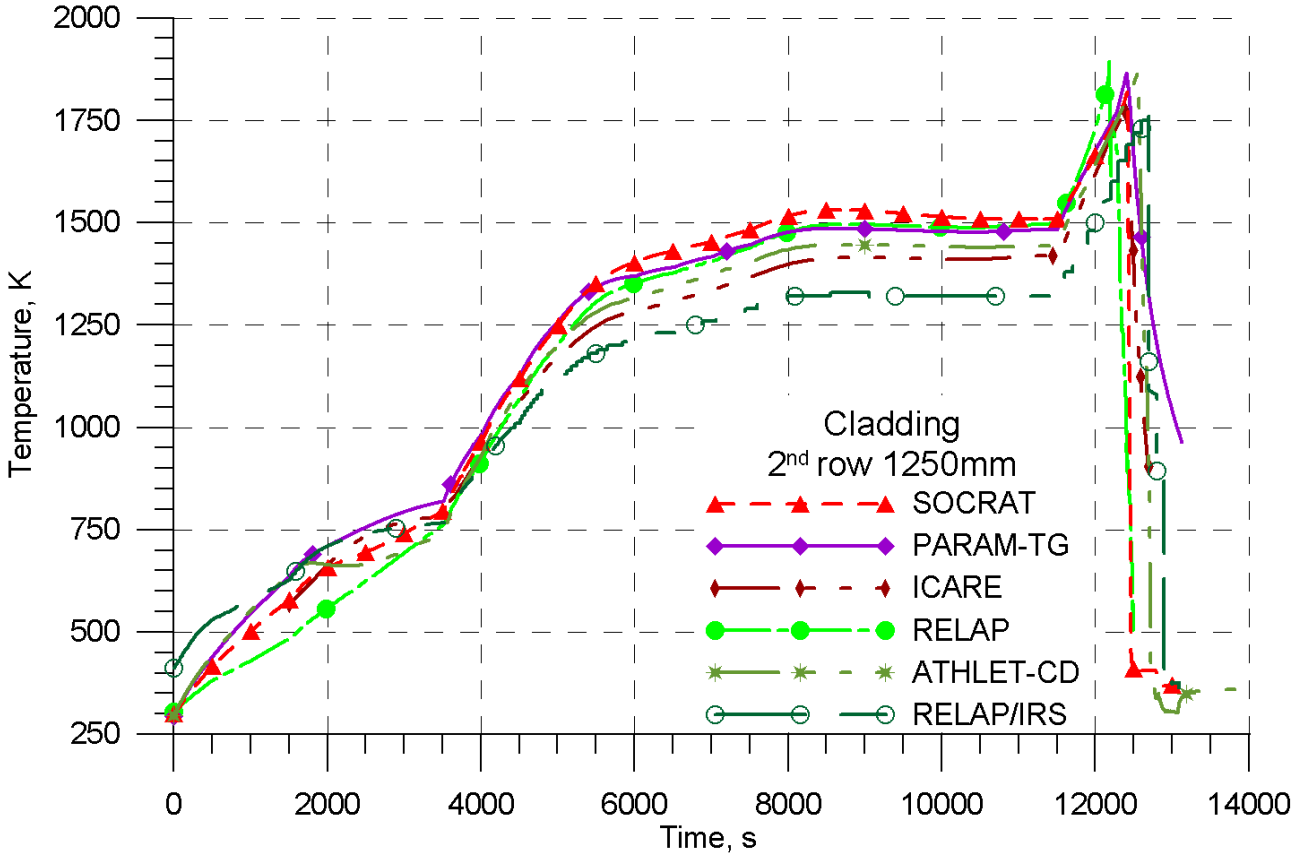

Figure 2.51. Cladding temperature of fuel rod in the second row at the elevation of 1250 mm. PARAMETER-SF3 experiment. Pre-test calculations.

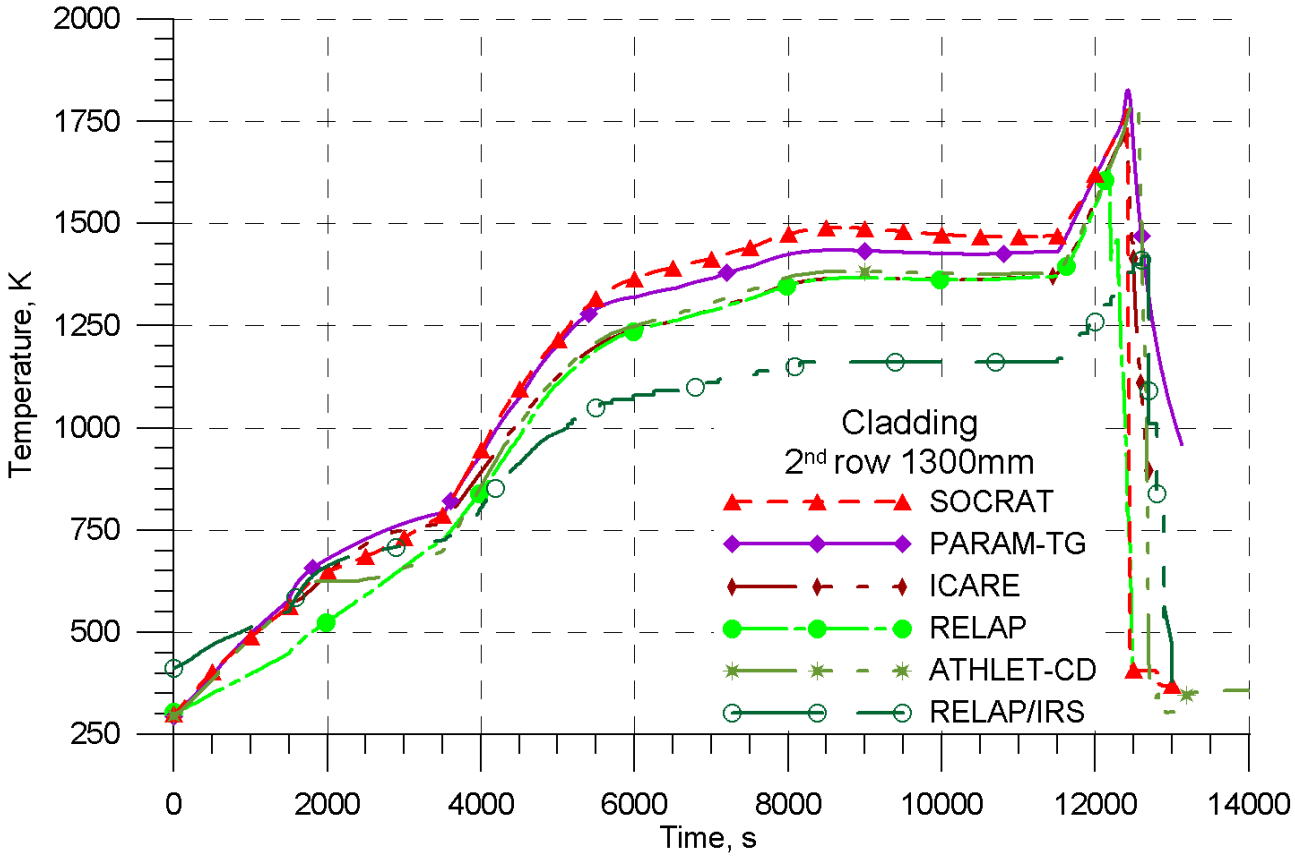

Figure 2.52. Cladding temperature of fuel rod in the second row at the elevation of 1300 mm. PARAMETER-SF3 experiment. Pre-test calculations.

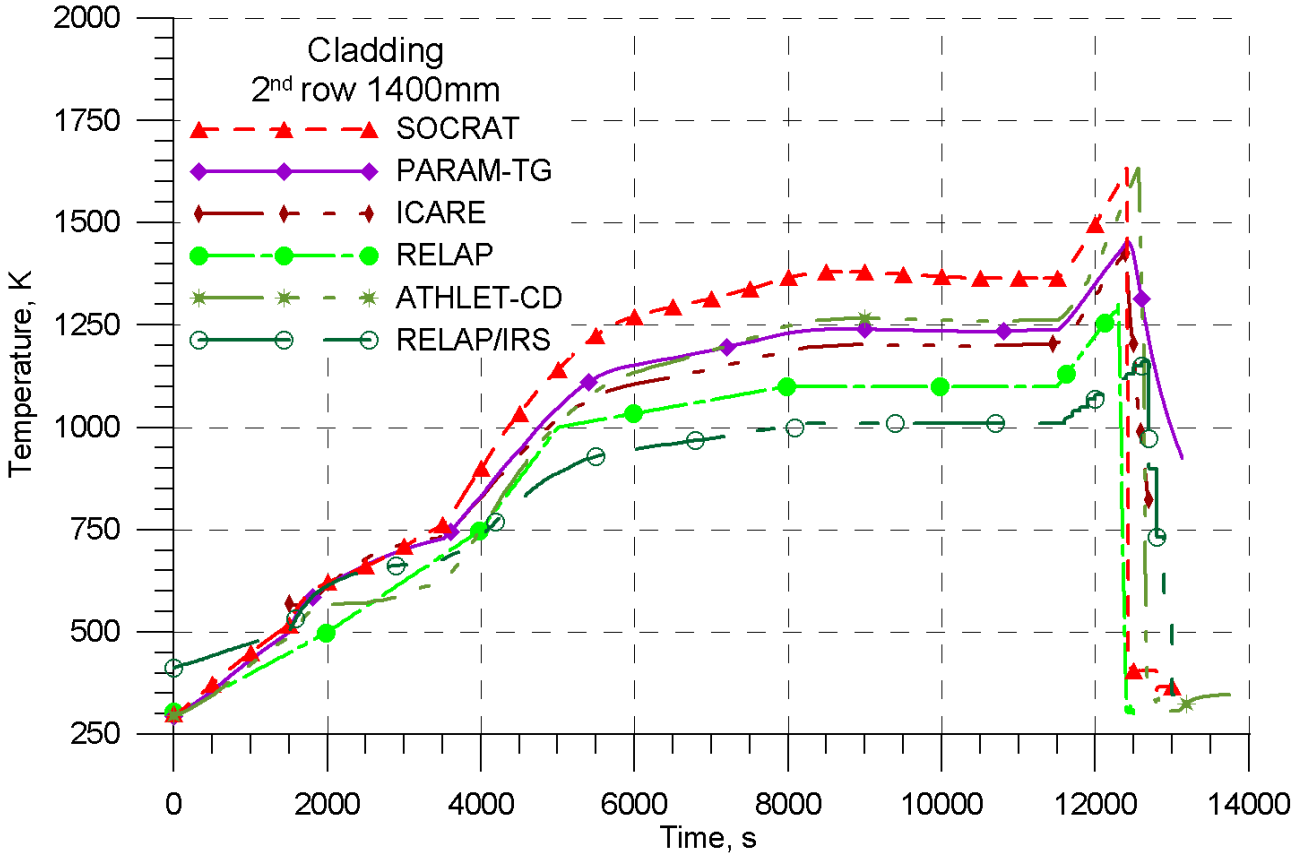

Figure 2.53. Cladding temperature of fuel rod in the second row at the elevation of 1400 mm. PARAMETER-SF3 experiment. Pre-test calculations.

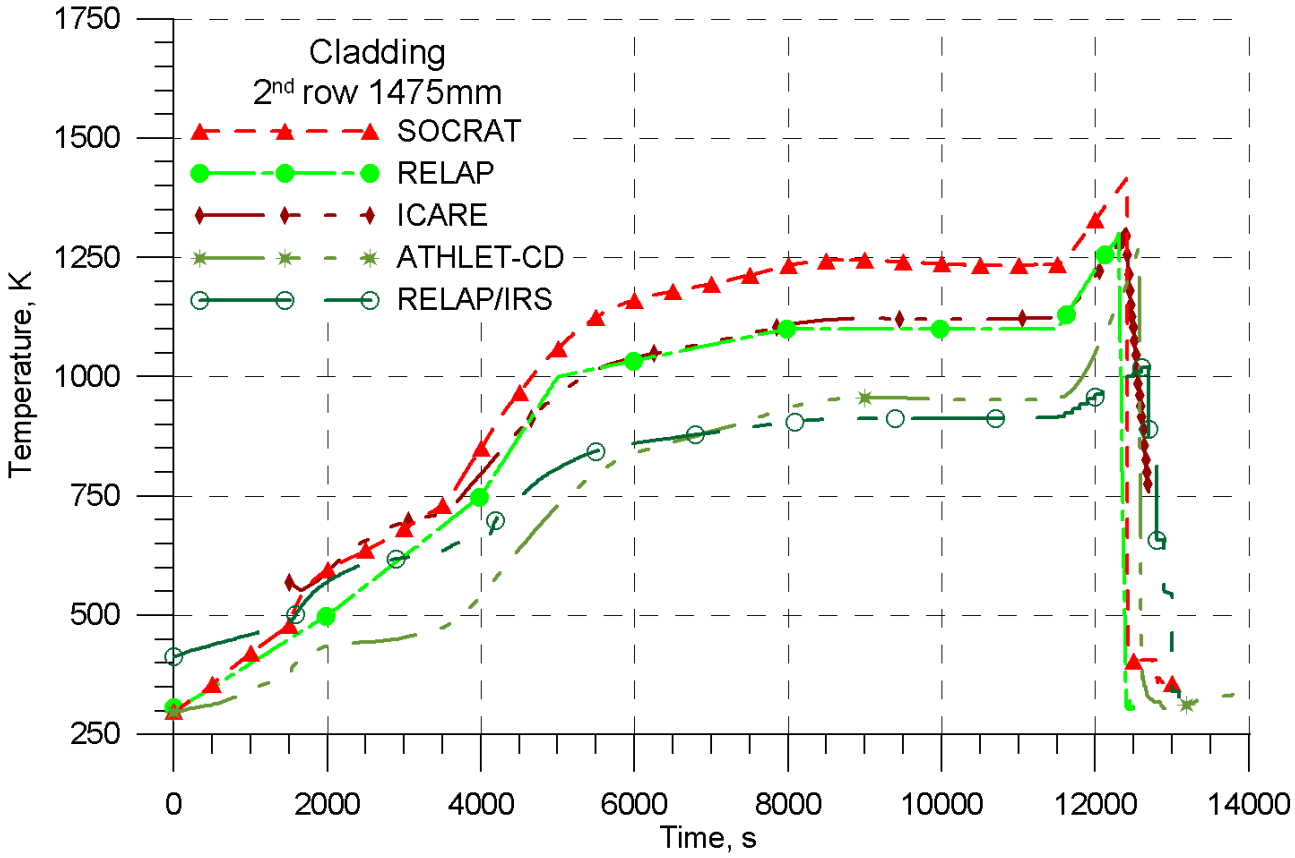

Figure 2.54. Cladding temperature of fuel rod in the second row at the elevation of 1475 mm. PARAMETER-SF3 experiment. Pre-test calculations.

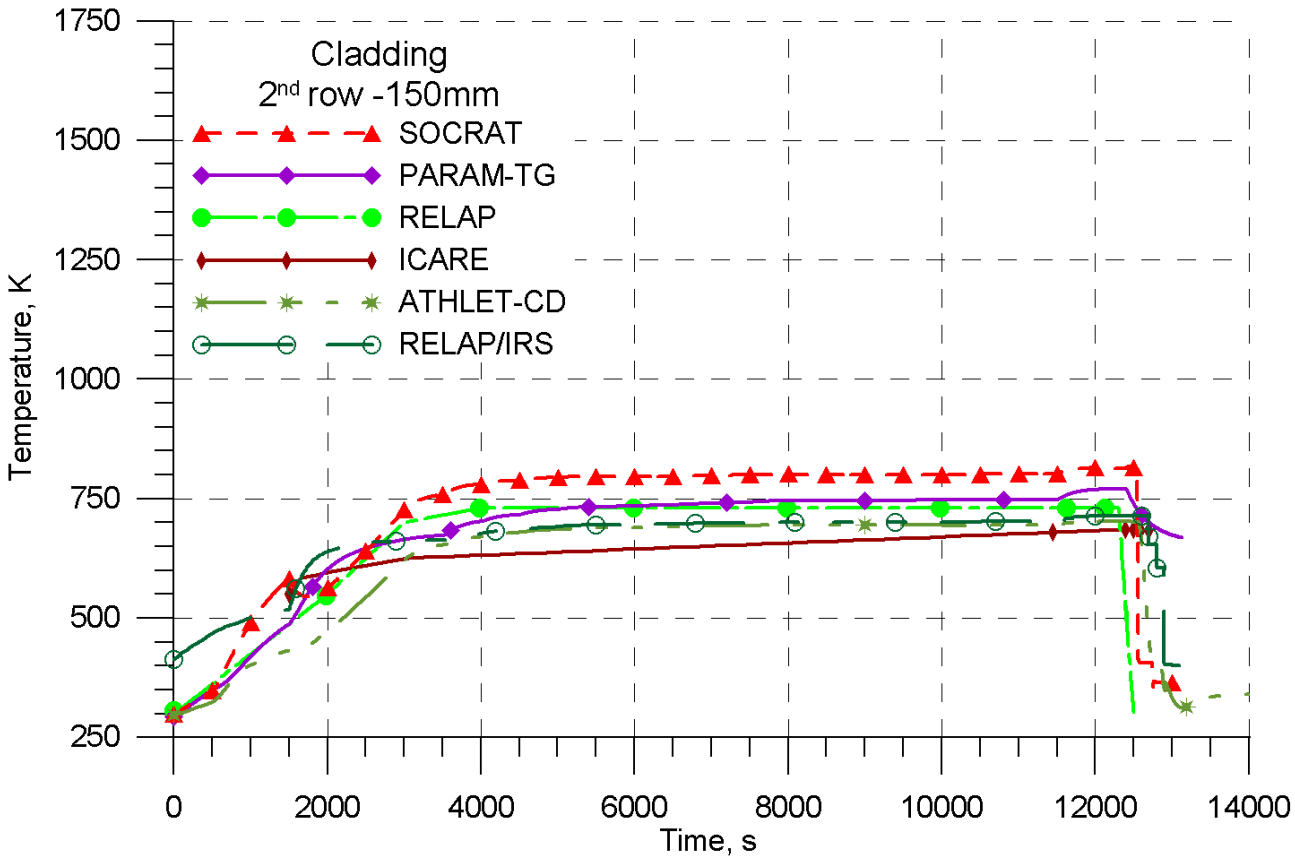

Figure 2.55. Cladding temperature of fuel rod in the second row at the elevation of -150 mm. PARAMETER-SF3 experiment. Pre-test calculations.

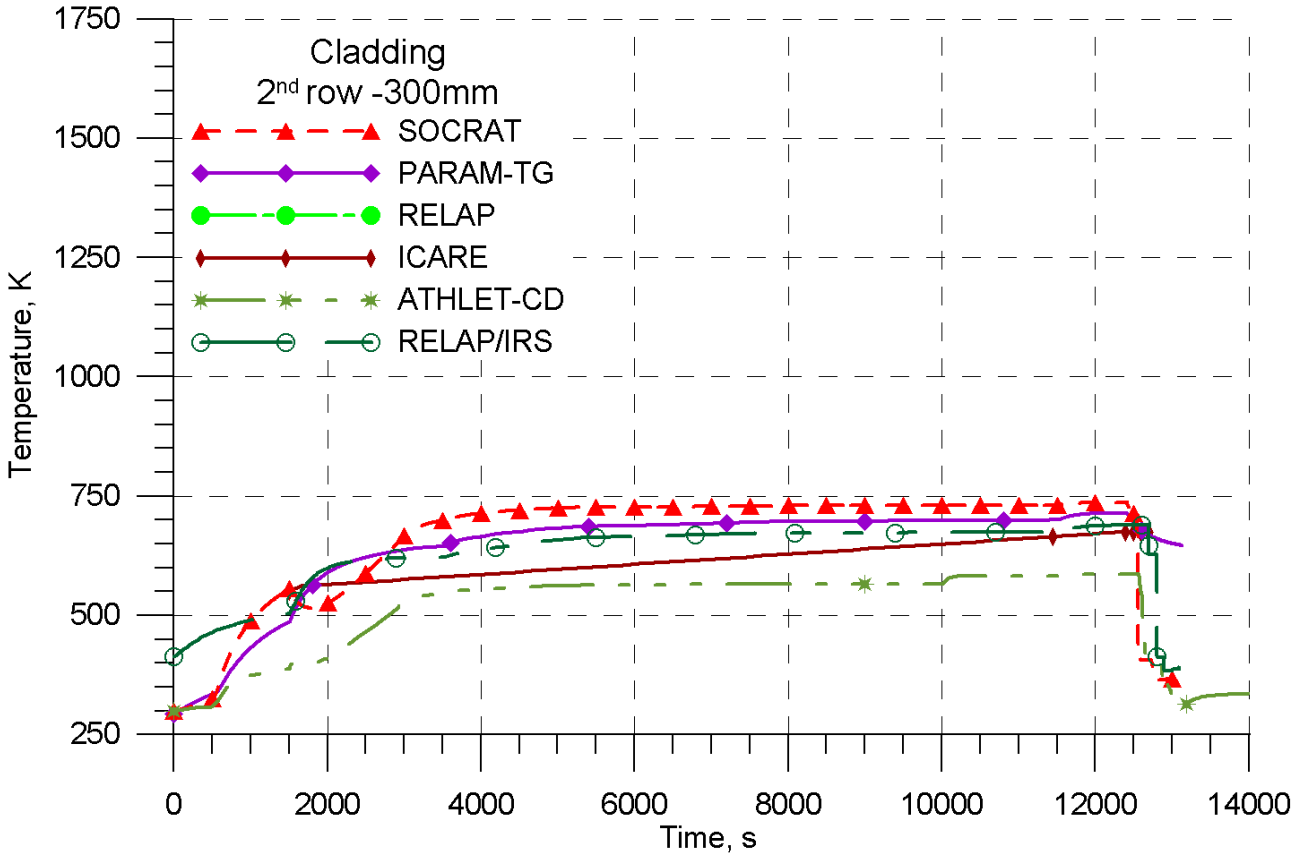

Figure 2.56. Cladding temperature of fuel rod in the second row at the elevation of -300 mm. PARAMETER-SF3 experiment. Pre-test calculations.

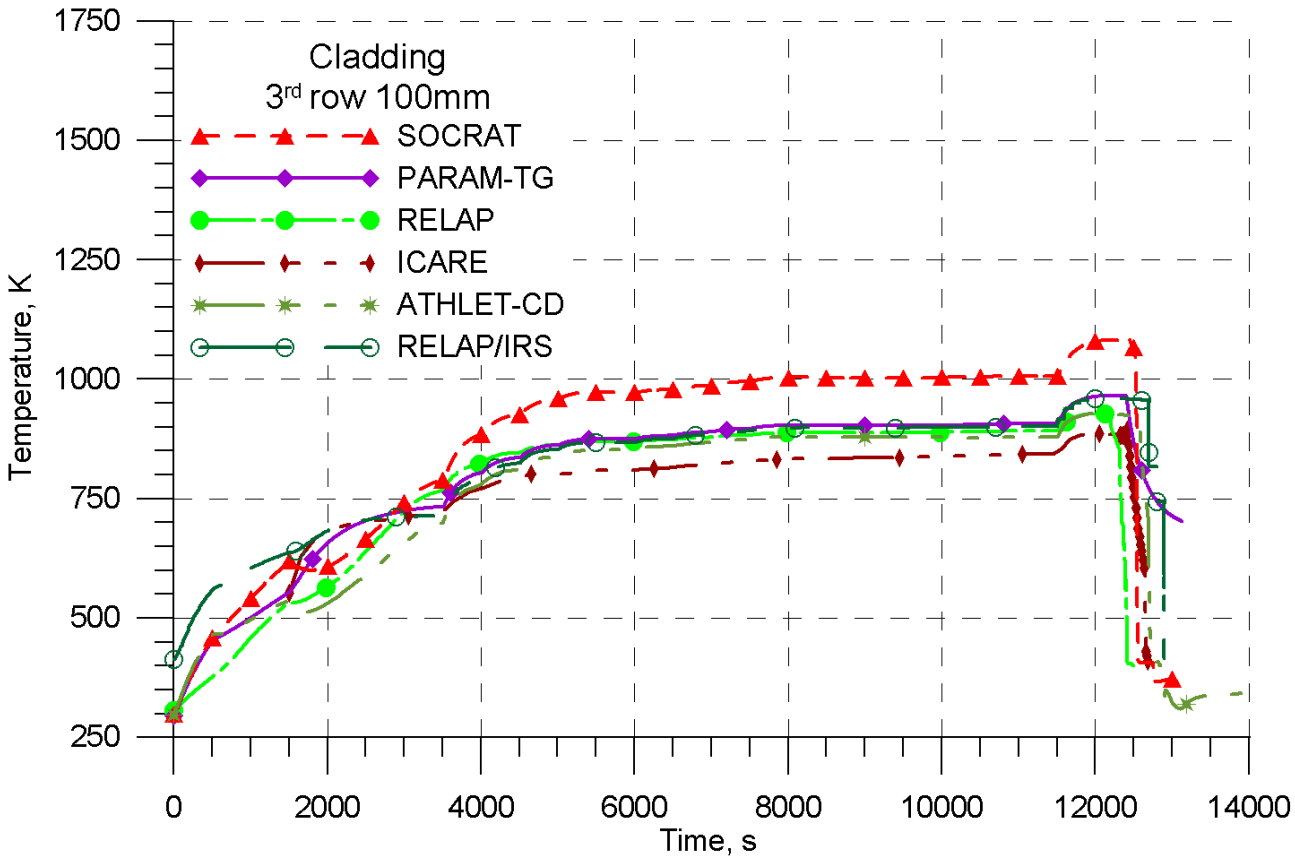

Figure 2.57. Cladding temperature of fuel rod in the third row at the elevation of 100 mm. PARAMETER-SF3 experiment. Pre-test calculations.

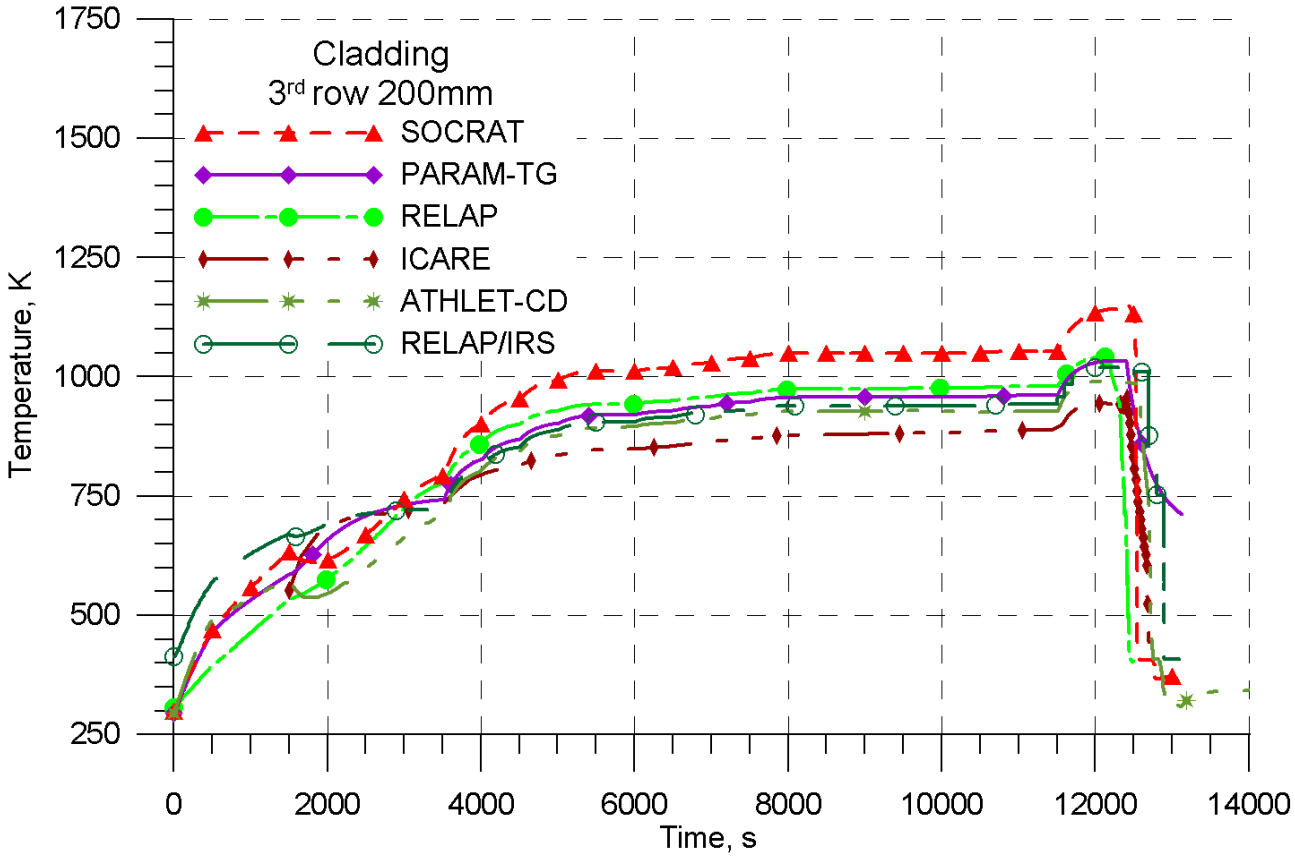

Figure 2.58. Cladding temperature of fuel rod in the third row at the elevation of 200 mm. PARAMETER-SF3 experiment. Pre-test calculations.

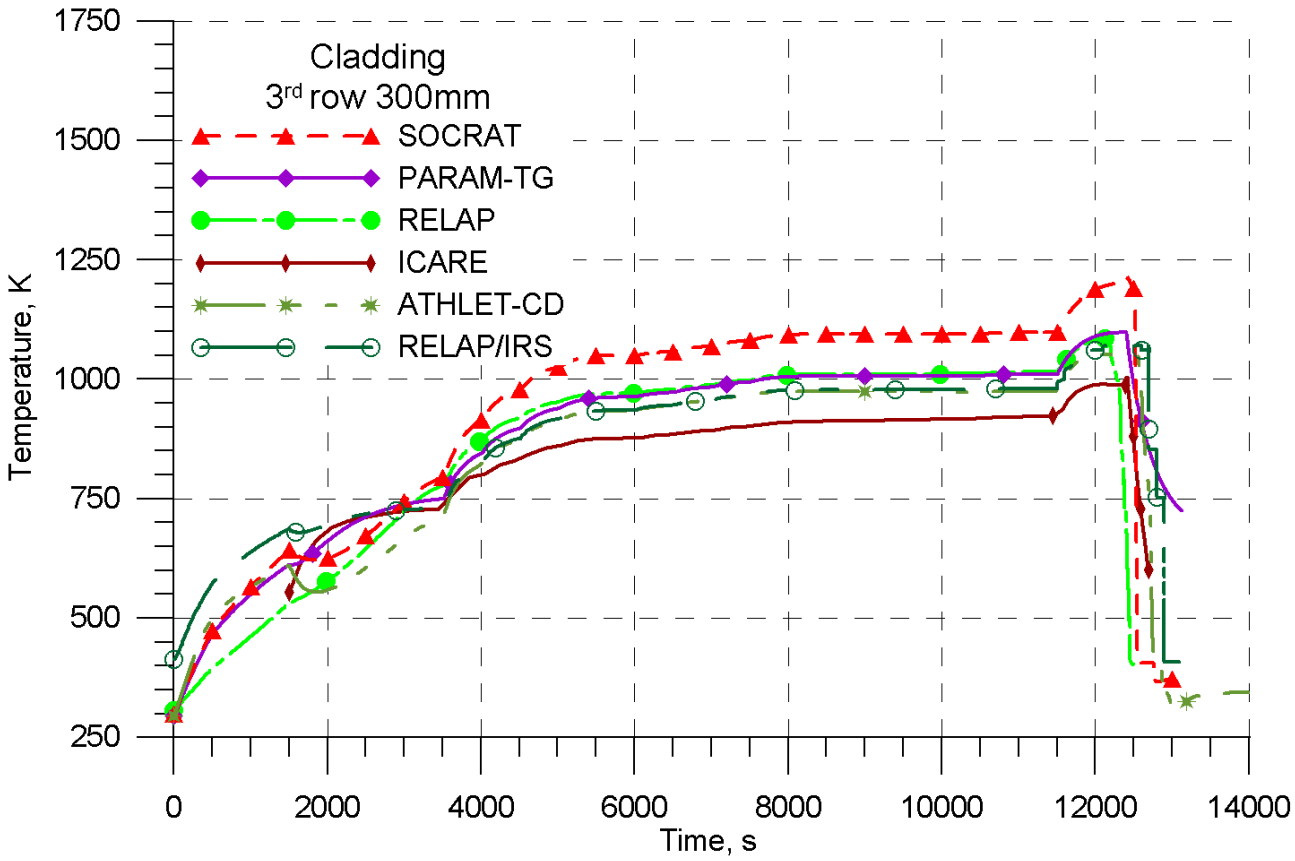

Figure 2.59. Cladding temperature of fuel rod in the third row at the elevation of 300 mm. PARAMETER-SF3 experiment. Pre-test calculations.

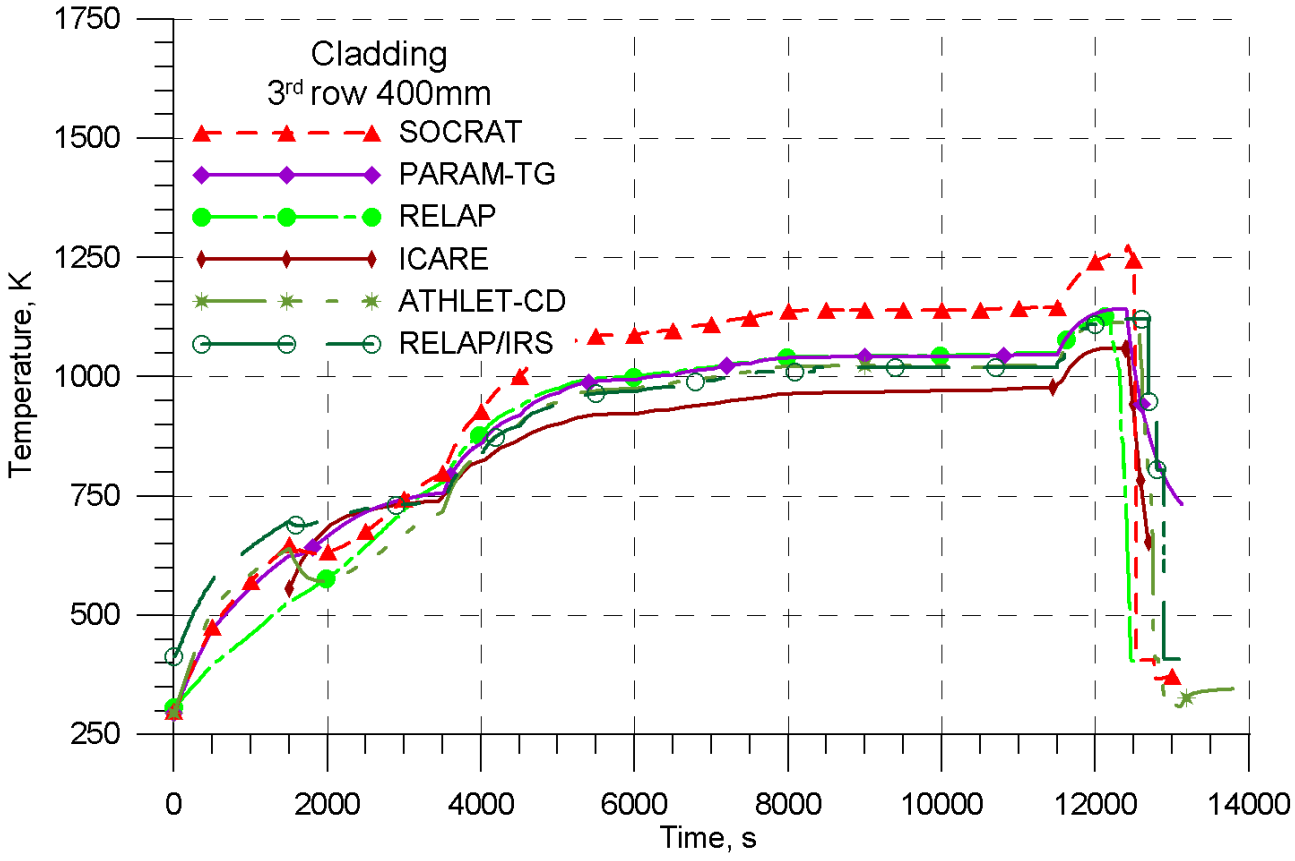

Figure 2.60. Cladding temperature of fuel rod in the third row at the elevation of 400 mm. PARAMETER-SF3 experiment. Pre-test calculations.

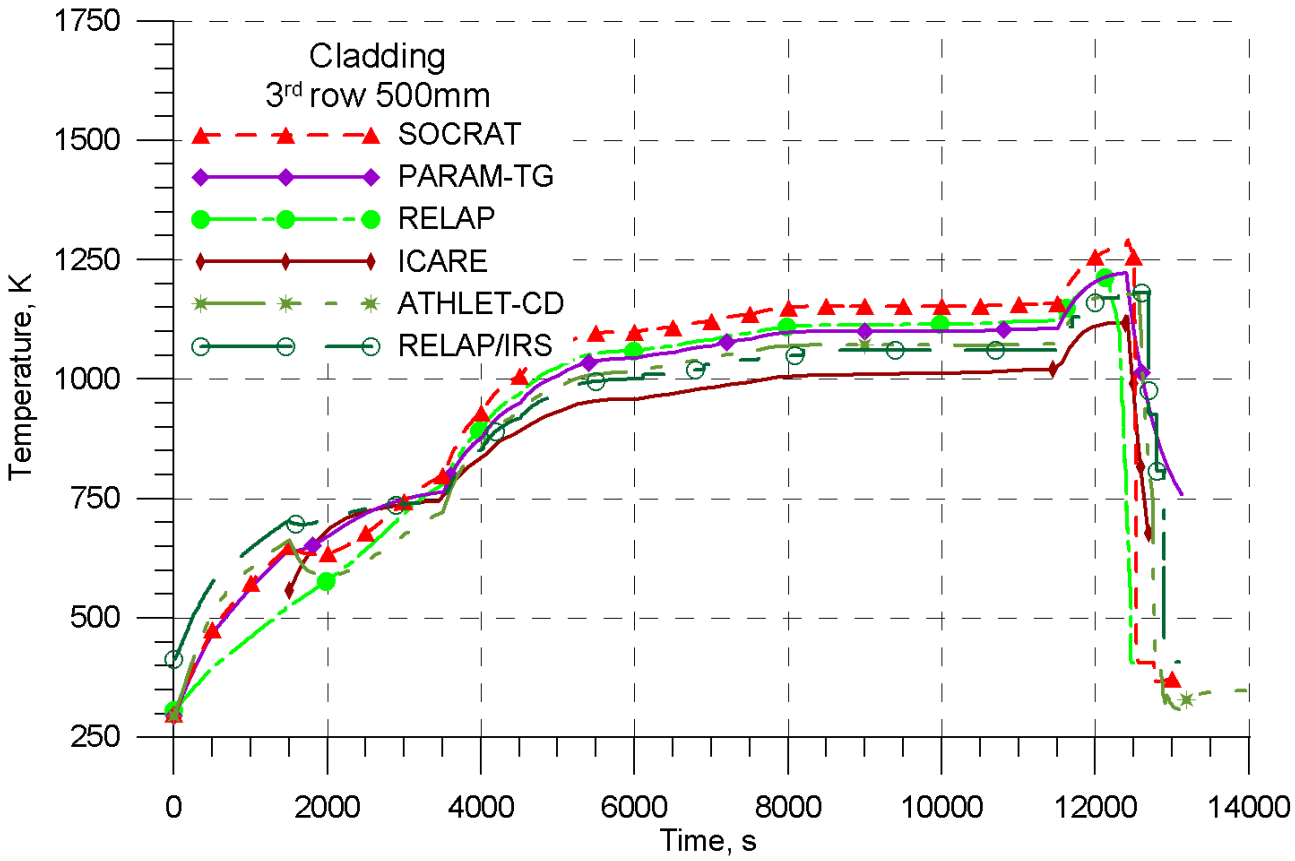

Figure 2.61. Cladding temperature of fuel rod in the third row at the elevation of 500 mm. PARAMETER-SF3 experiment. Pre-test calculations.

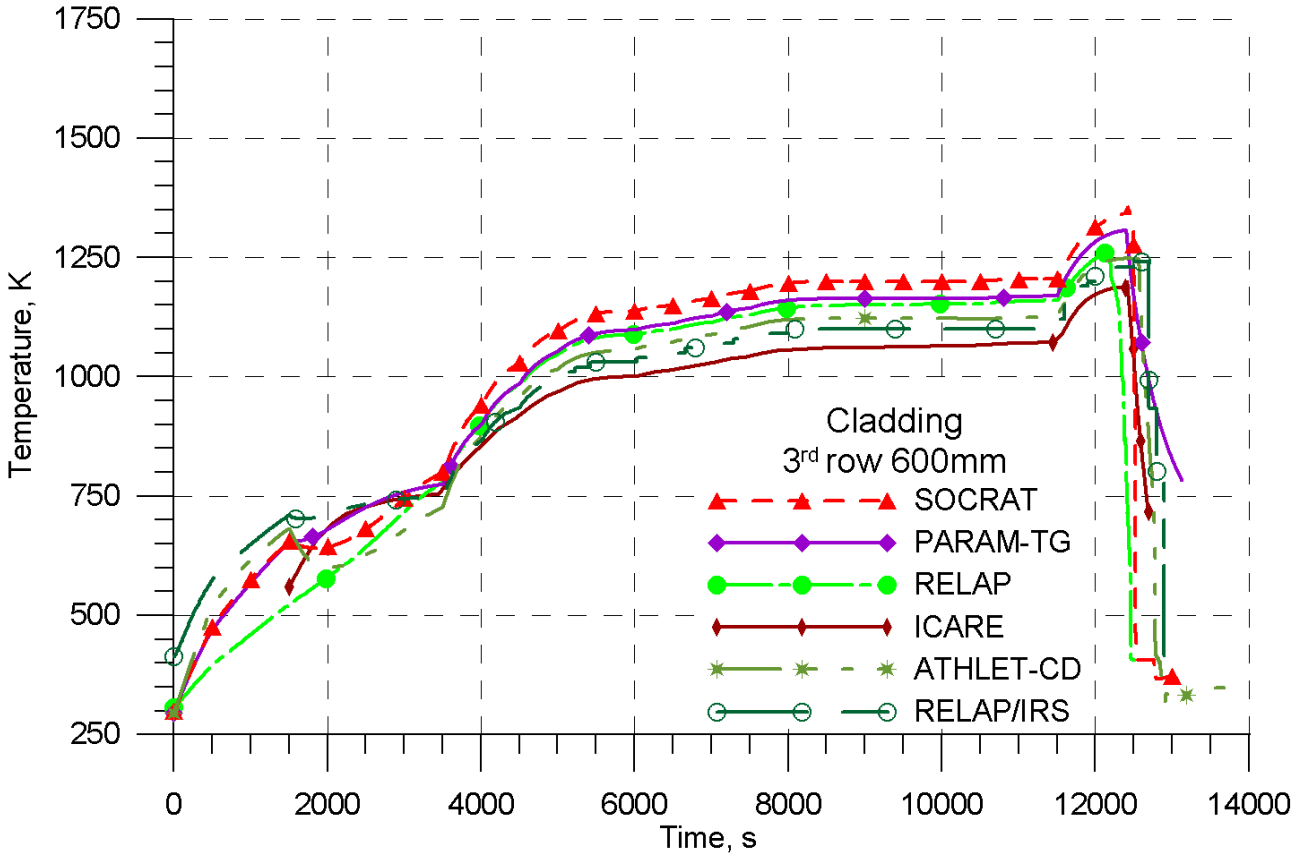

Figure 2.62. Cladding temperature of fuel rod in the third row at the elevation of 600 mm. PARAMETER-SF3 experiment. Pre-test calculations.

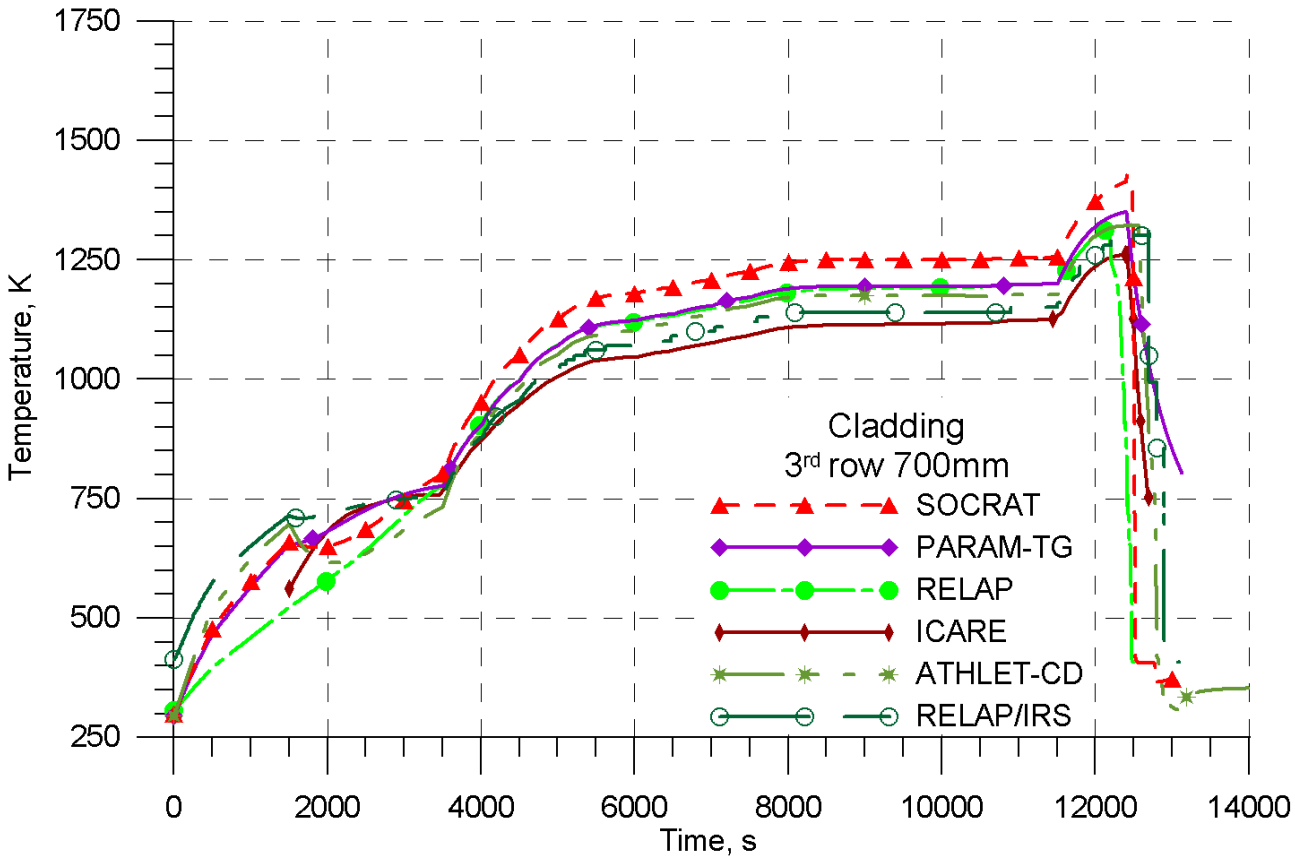

Figure 2.63. Cladding temperature of fuel rod in the third row at the elevation of 700 mm. PARAMETER-SF3 experiment. Pre-test calculations.

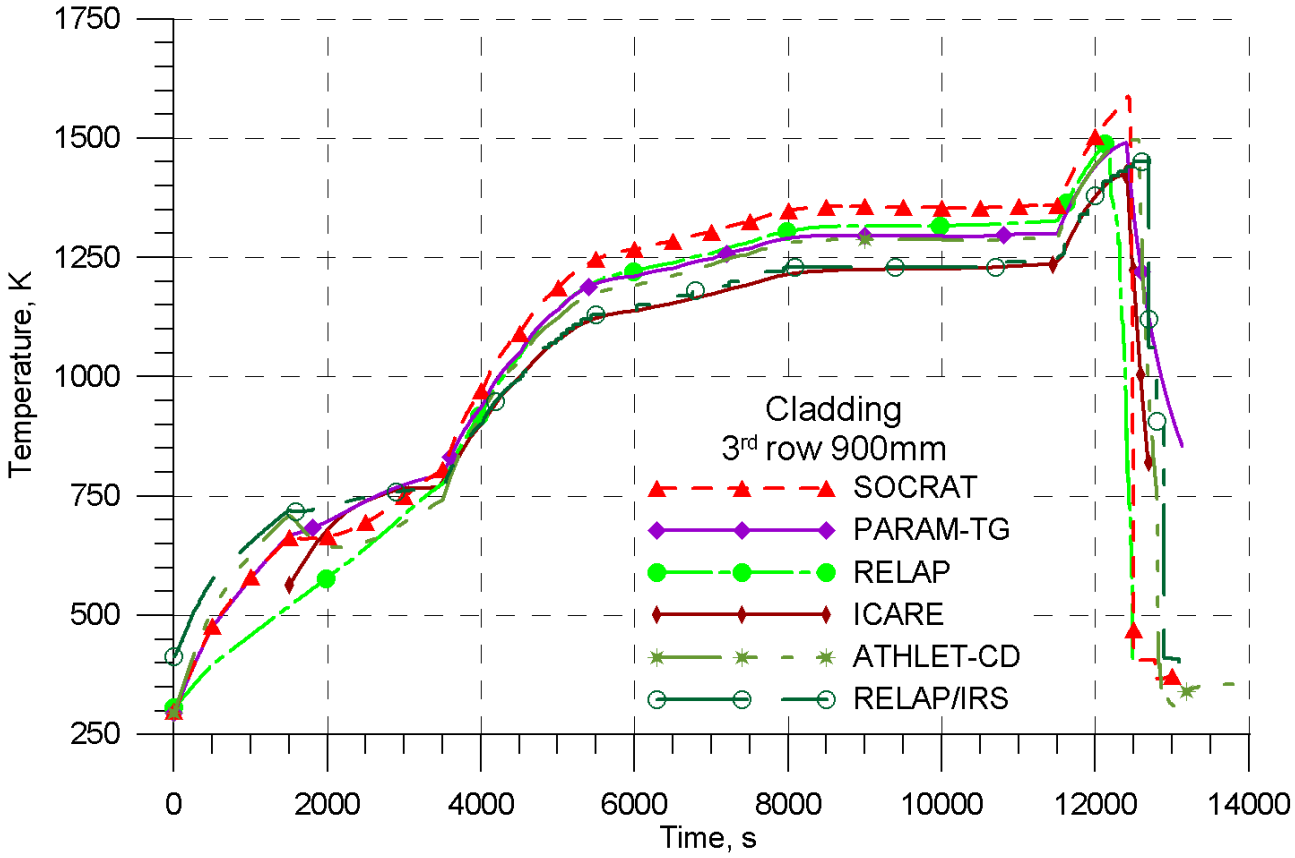

Figure 2.64. Cladding temperature of fuel rod in the third row at the elevation of 900 mm. PARAMETER-SF3 experiment. Pre-test calculations.

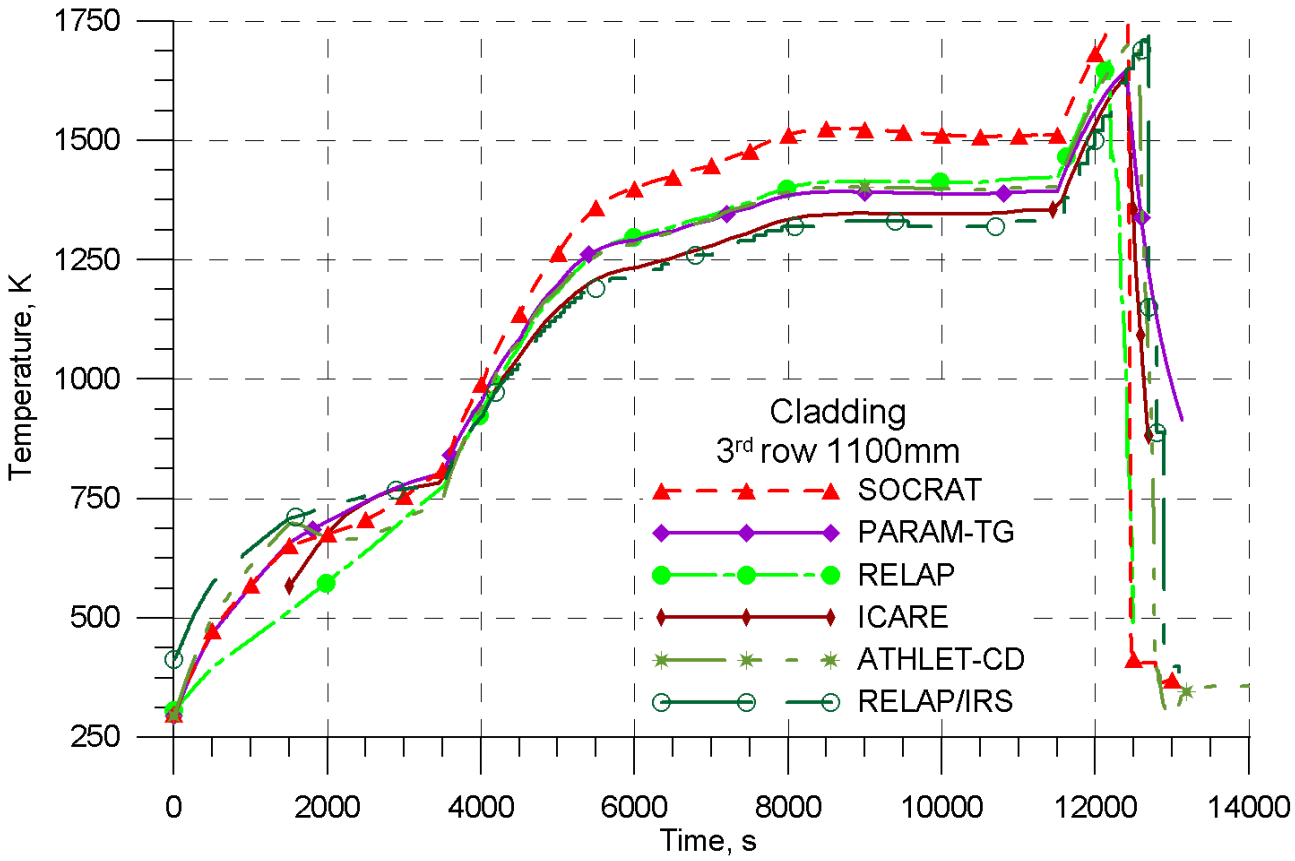

Figure 2.65. Cladding temperature of fuel rod in the third row at the elevation of 1100 mm. PARAMETER-SF3 experiment. Pre-test calculations.

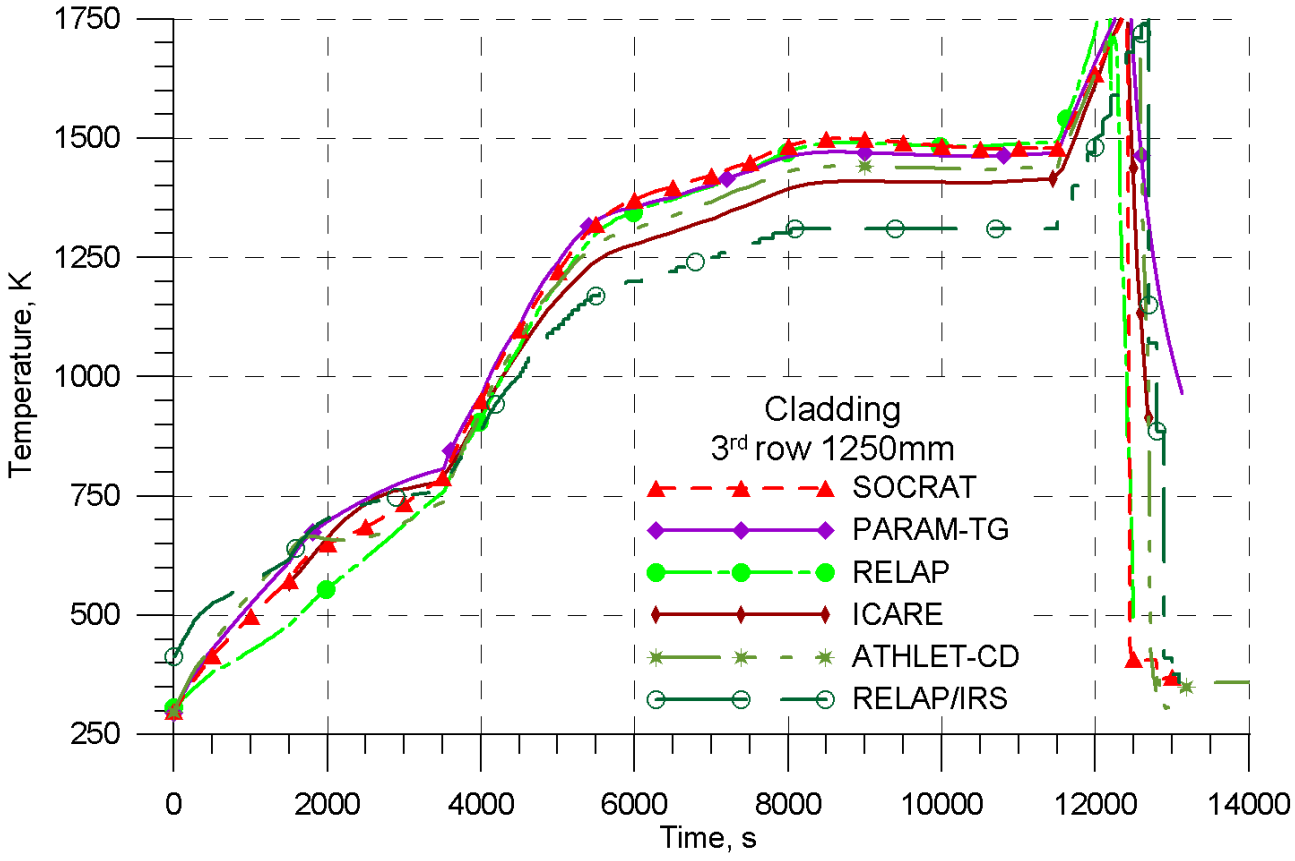

Figure 2.66. Cladding temperature of fuel rod in the third row at the elevation of 1250 mm. PARAMETER-SF3 experiment. Pre-test calculations.

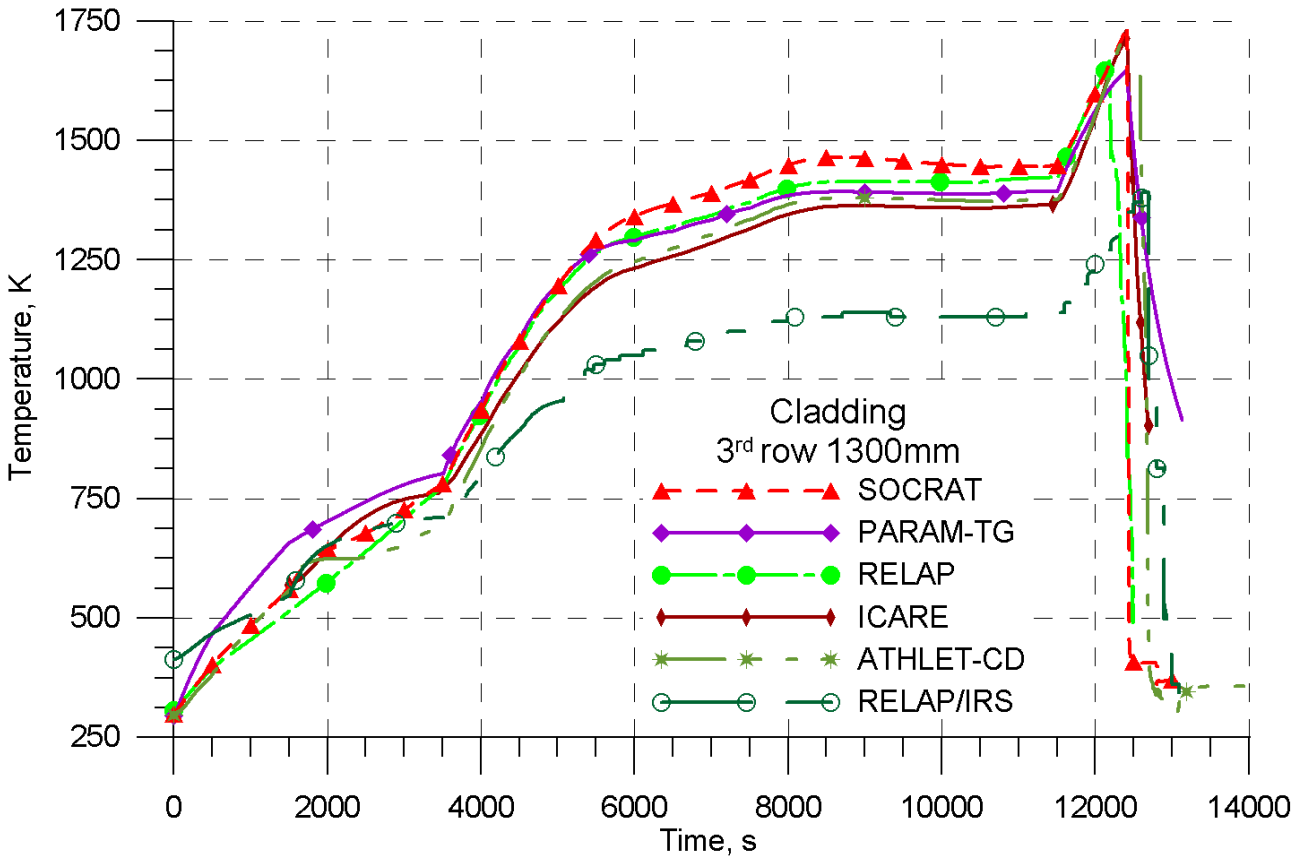

Figure 2.67. Cladding temperature of fuel rod in the third row at the elevation of 1300 mm. PARAMETER-SF3 experiment. Pre-test calculations.

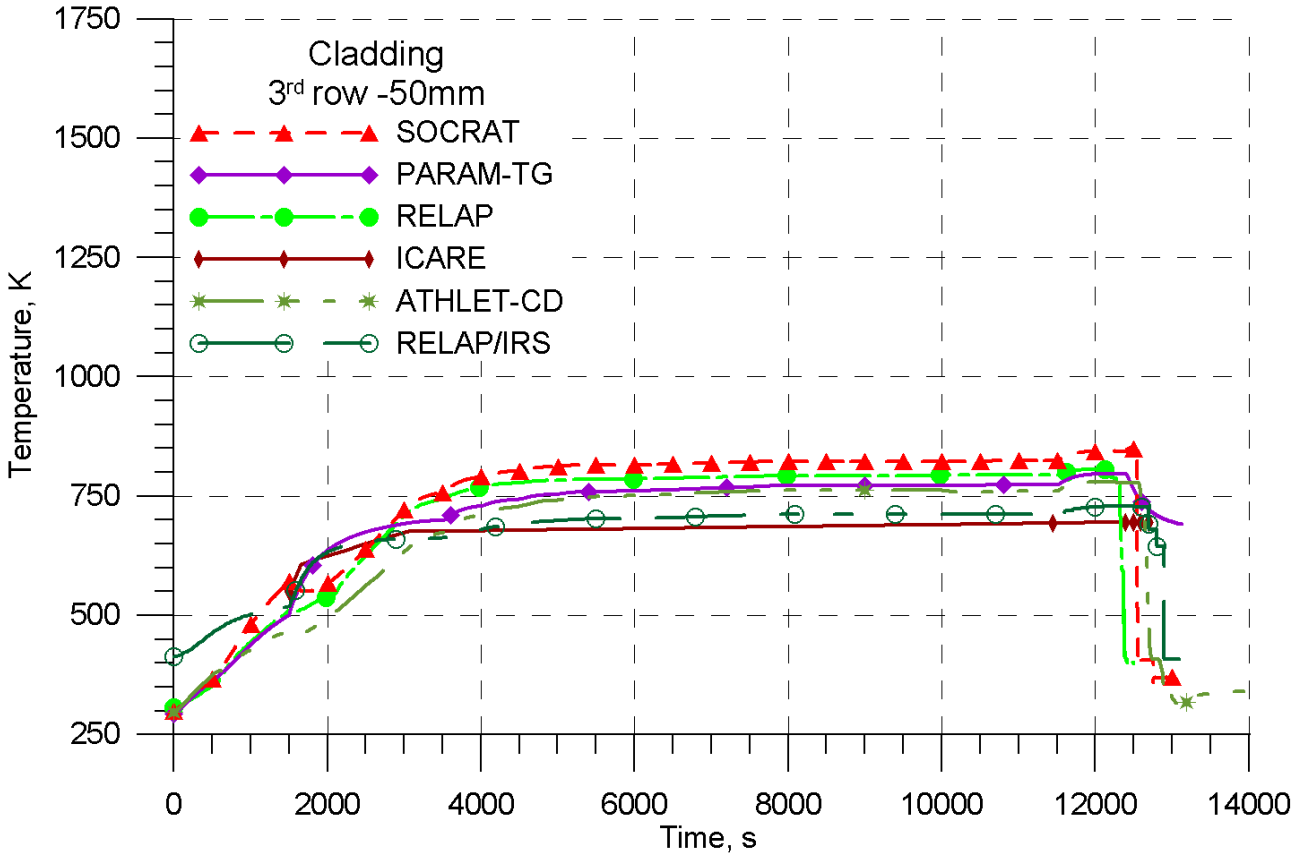

Figure 2.68. Cladding temperature of fuel rod in the third row at the elevation of -50 mm. PARAMETER-SF3 experiment. Pre-test calculations.

2.4.4.4 Coolant temperature in the test section

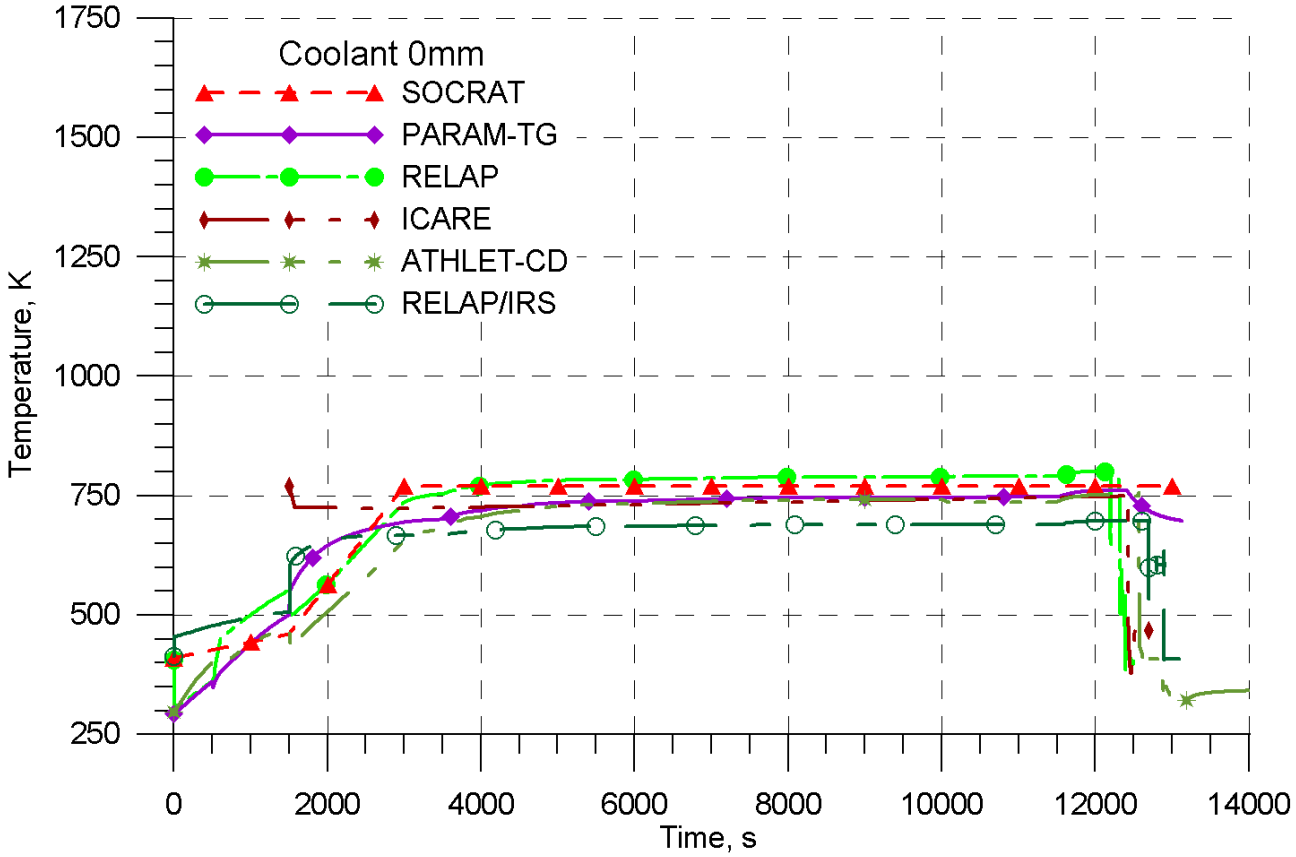

Figure 2.69. Coolant temperature at the elevation of 0 mm. PARAMETER-SF3 experiment. Pre-test calculations.

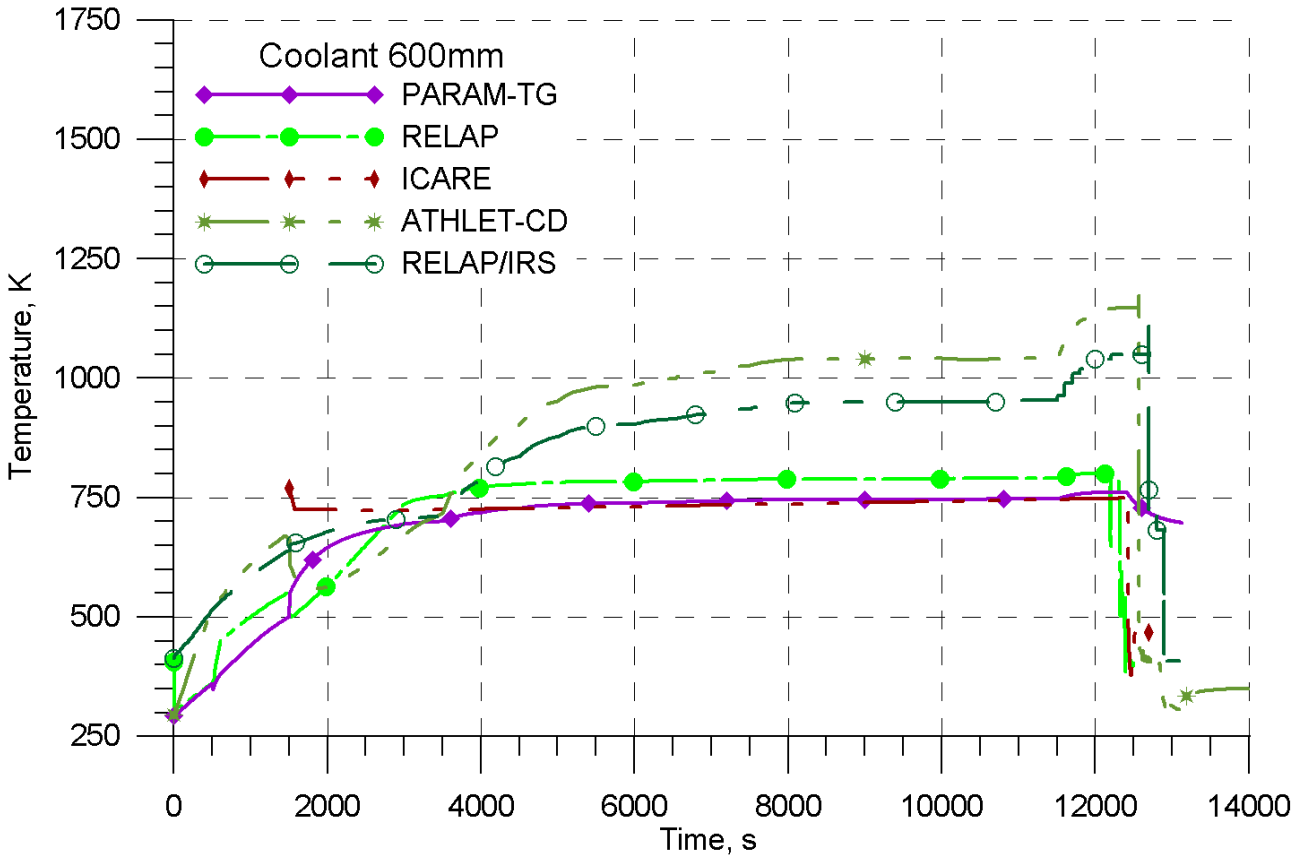

Figure 2.70. Coolant temperature at the elevation of 600 mm. PARAMETER-SF3 experiment. Pre-test calculations.

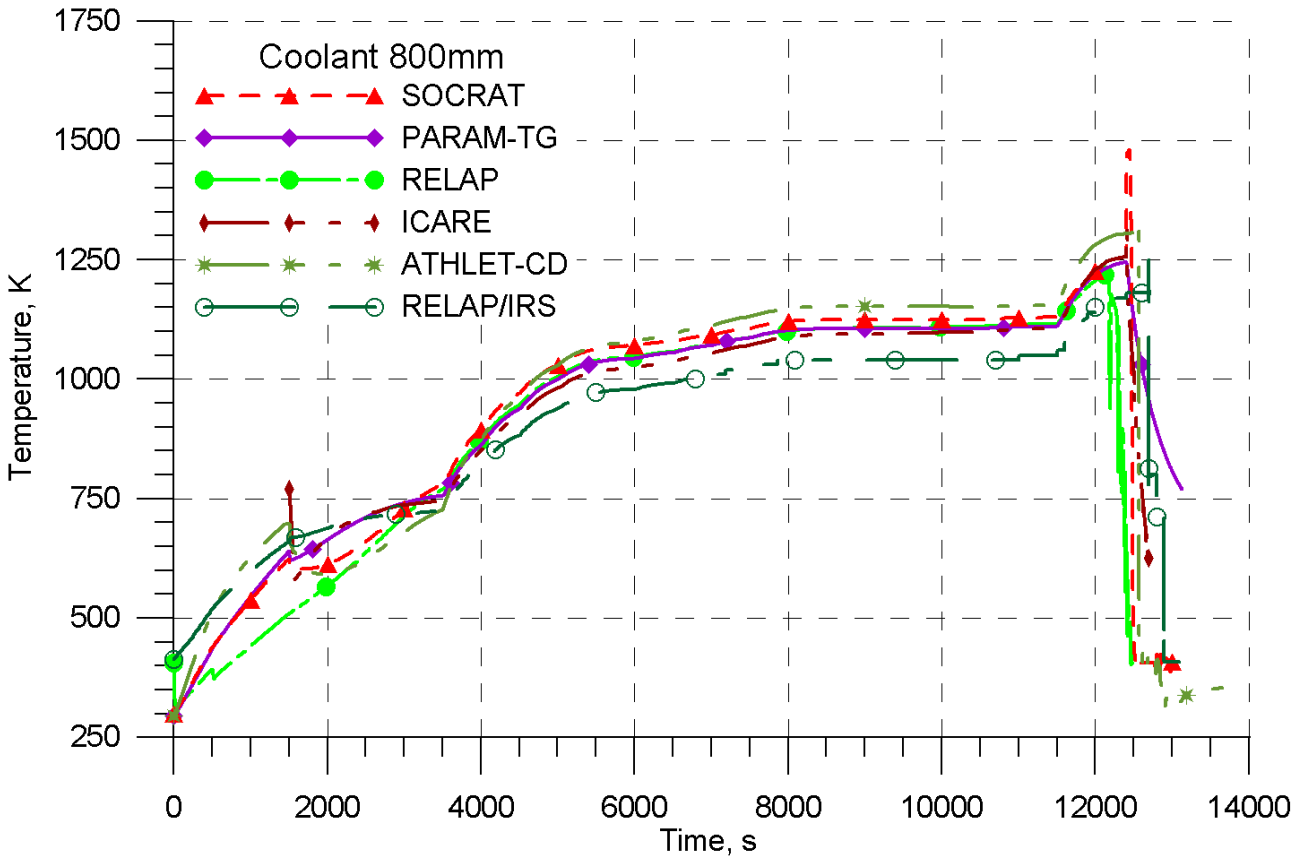

Figure 2.71. Coolant temperature at the elevation of 800 mm. PARAMETER-SF3 experiment. Pre-test calculations.

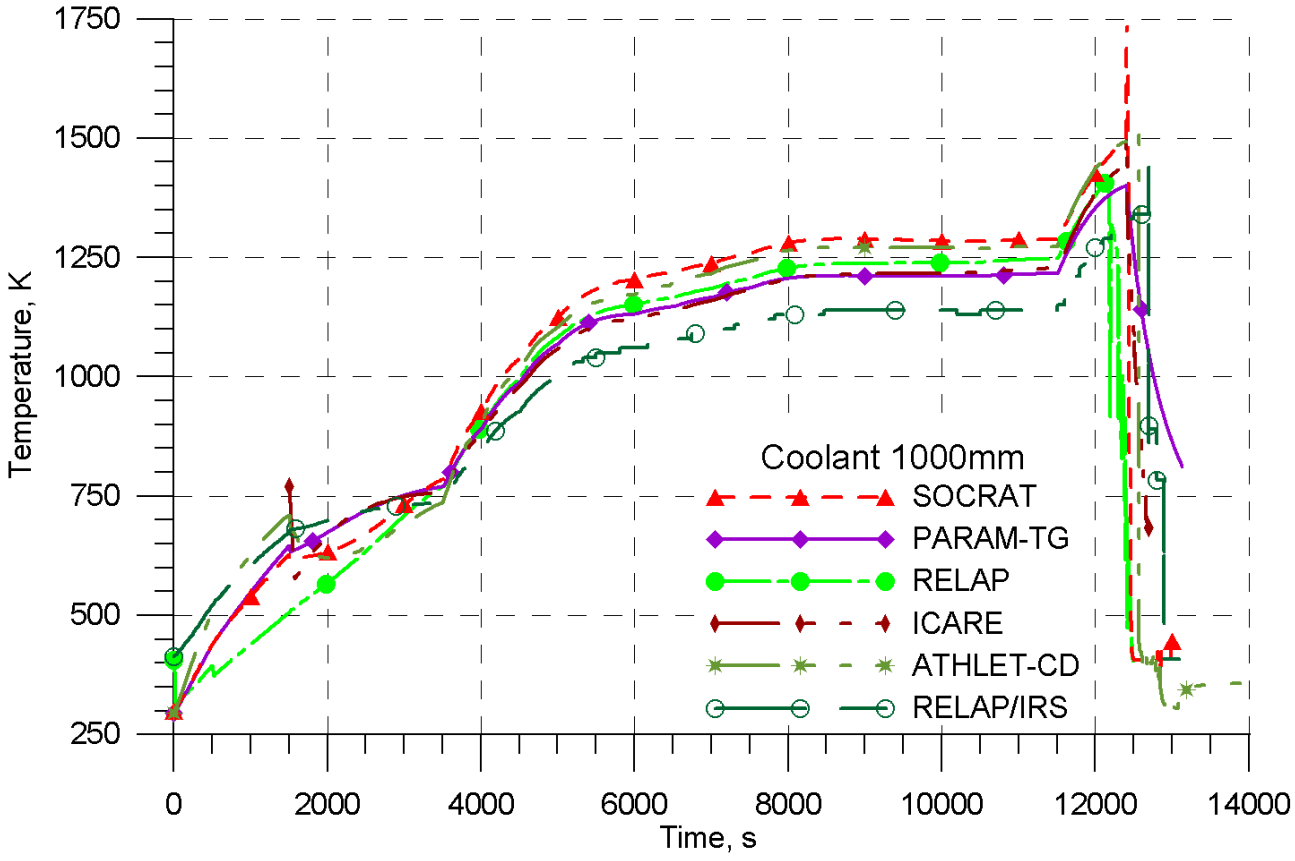

Figure 2.72. Coolant temperature at the elevation of 1000 mm. PARAMETER-SF3 experiment. Pre-test calculations.

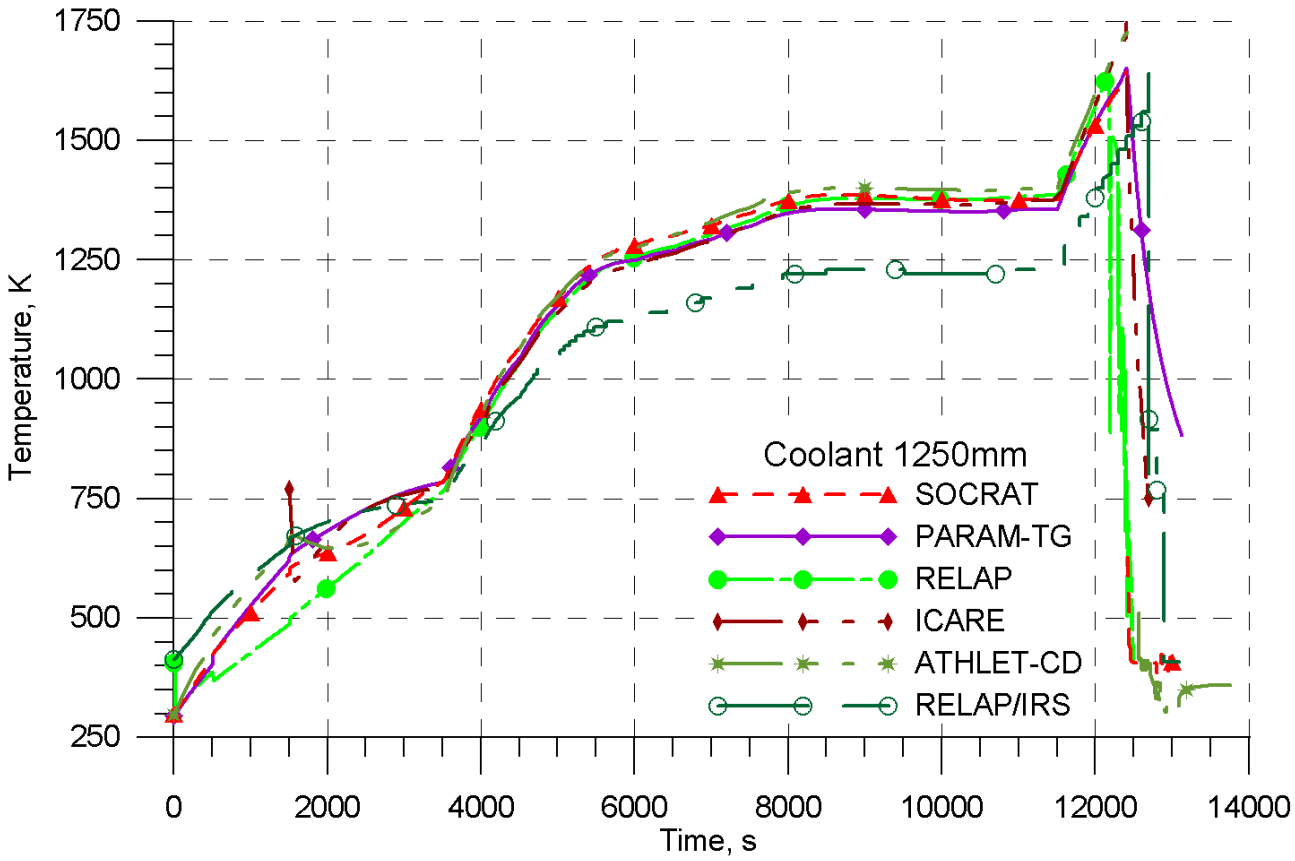

Figure 2.73. Coolant temperature at the elevation of 1250 mm. PARAMETER-SF3 experiment. Pre-test calculations.

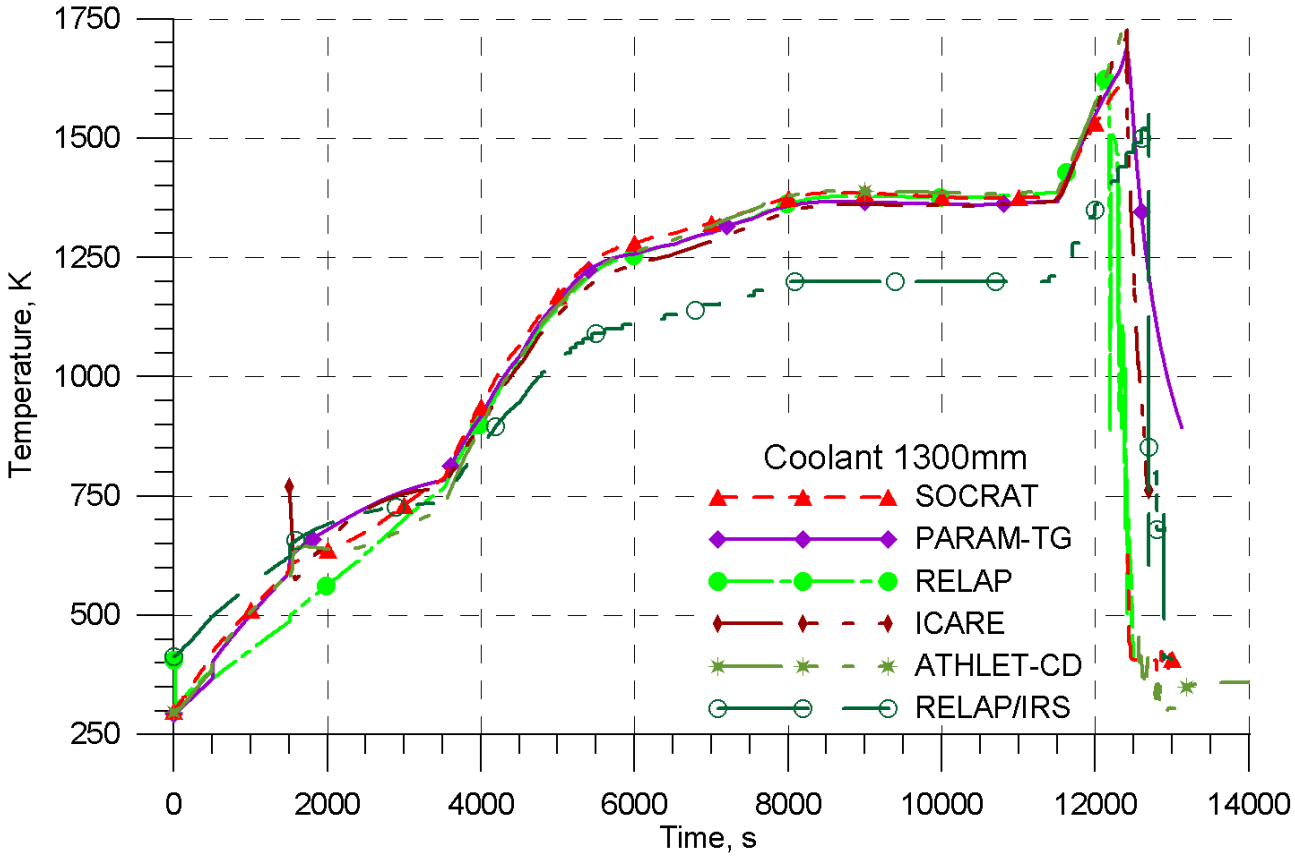

Figure 2.74. Coolant temperature at the elevation of 1300 mm. PARAMETER-SF3 experiment. Pre-test calculations.

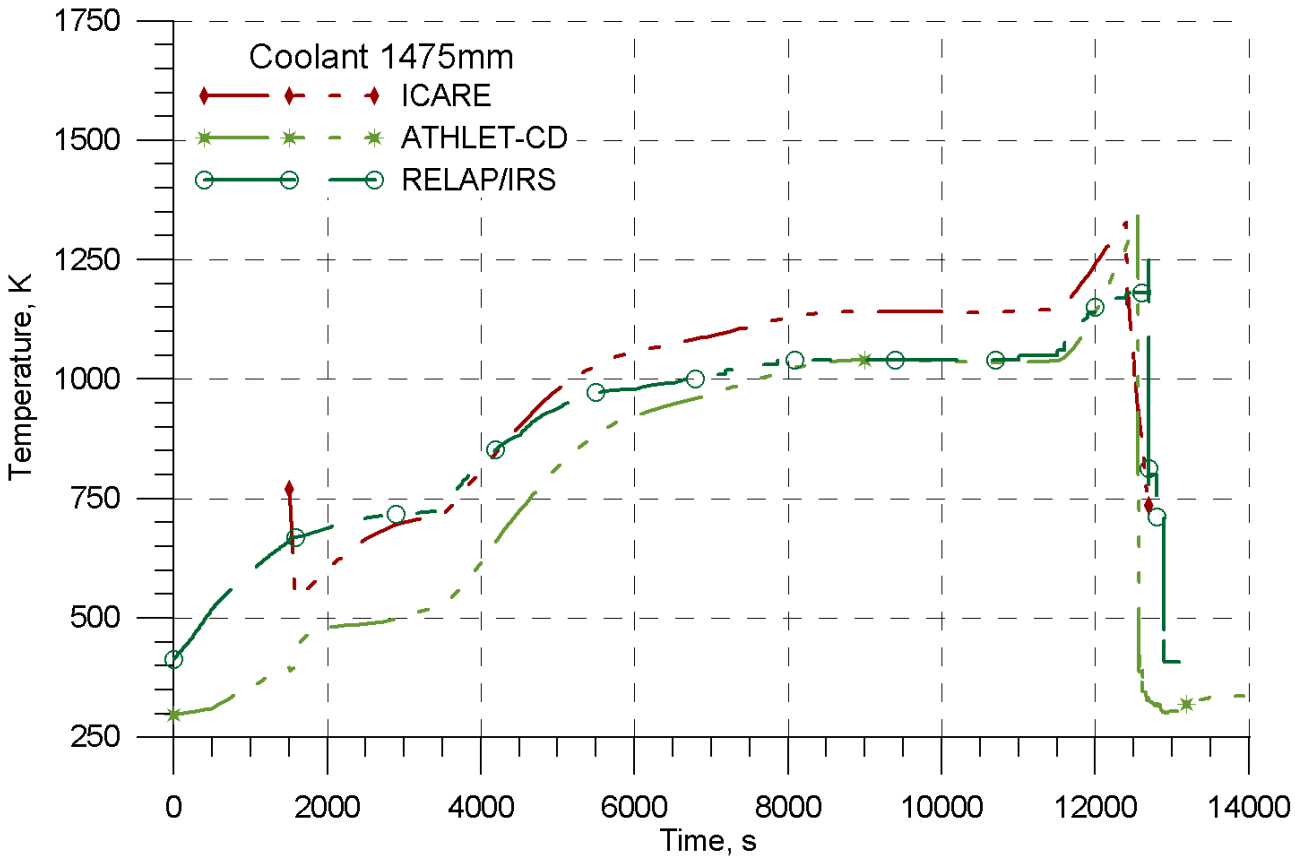

Figure 2.75. Coolant temperature at the elevation of 1475 mm. PARAMETER-SF3 experiment. Pre-test calculations.

2.4.4.5 Temperature of shroud and thermoinsulation

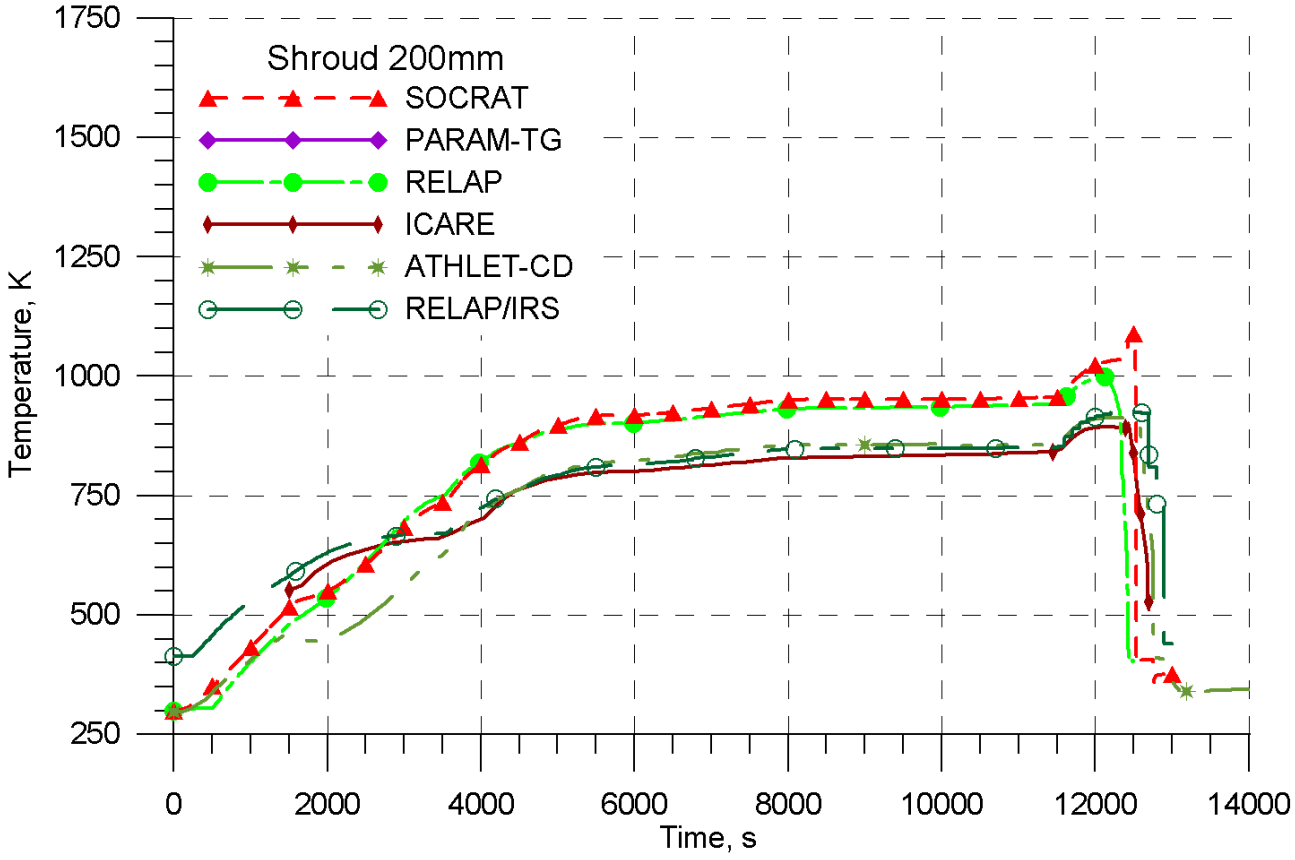

Figure 2.76. Temperature of shroud at the elevation of 200 mm. PARAMETER-SF3 experiment. Pre-test calculations.

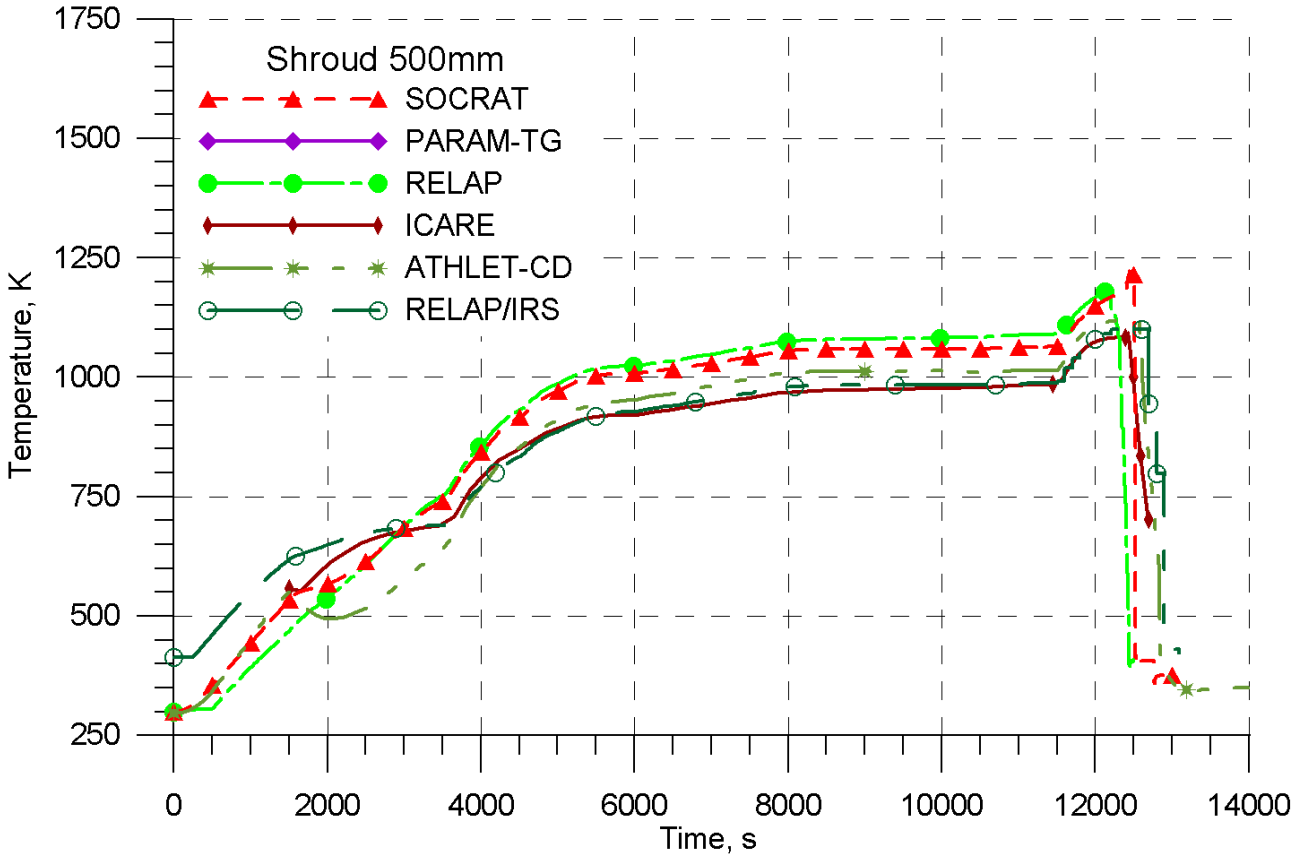

Figure 2.77. Temperature of shroud at the elevation of 500 mm. PARAMETER-SF3 experiment. Pre-test calculations.

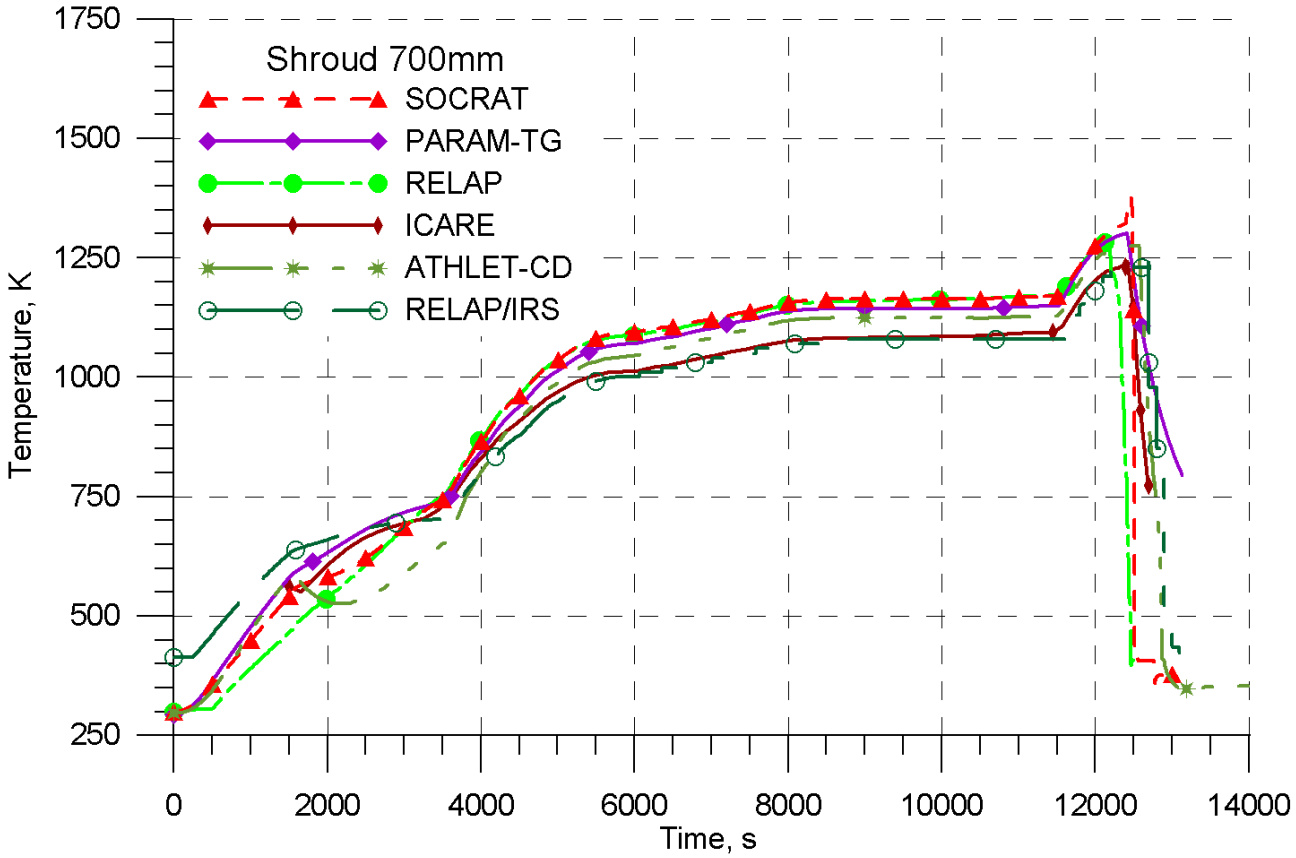

Figure 2.78. Temperature of shroud at the elevation of 700 mm. PARAMETER-SF3 experiment. Pre-test calculations.

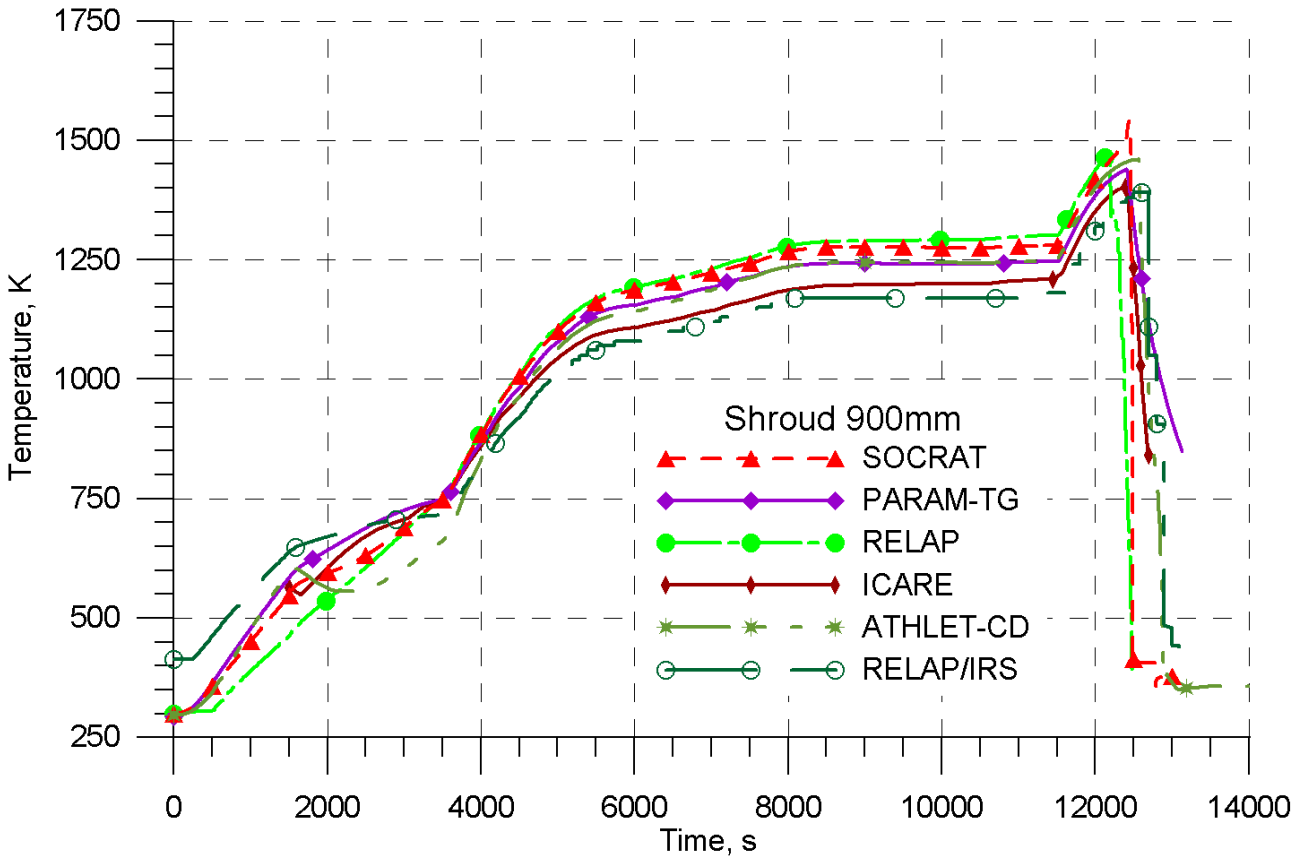

Figure 2.79. Temperature of shroud at the elevation of 900 mm. PARAMETER-SF3 experiment. Pre-test calculations.

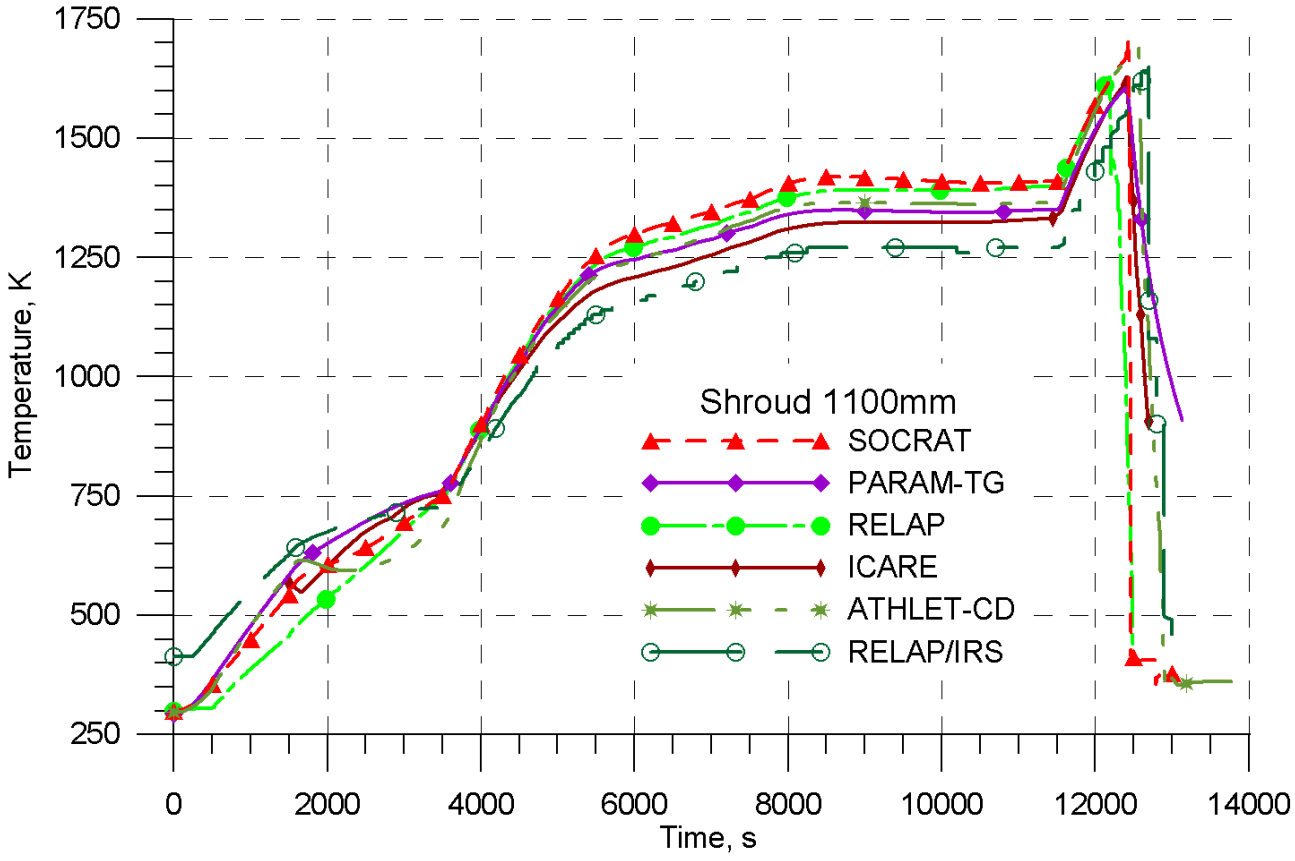

Figure 2.80. Temperature of shroud at the elevation of 1100 mm. PARAMETER-SF3 experiment. Pre-test calculations.

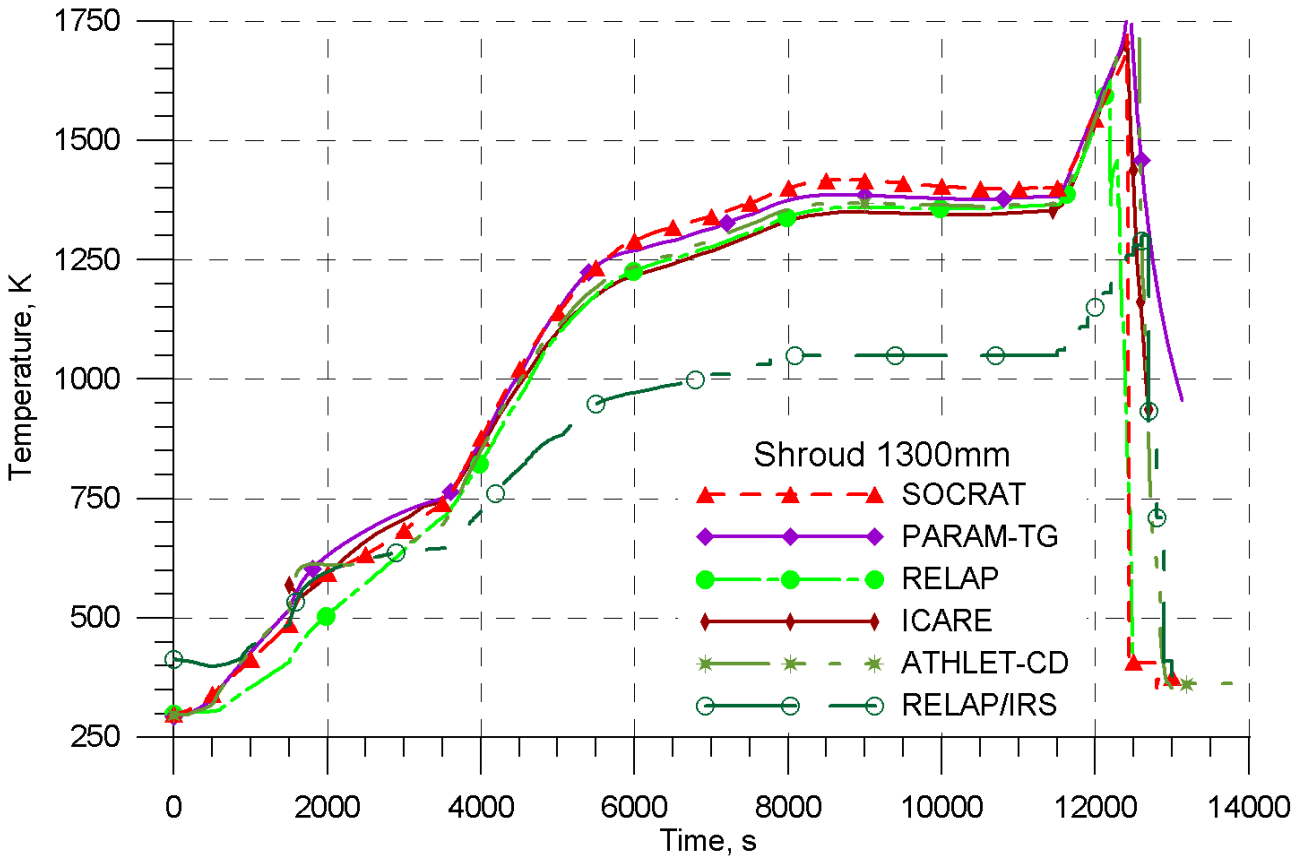

Figure 2.81. Temperature of shroud at the elevation of 1300 mm. PARAMETER-SF3 experiment. Pre-test calculations.

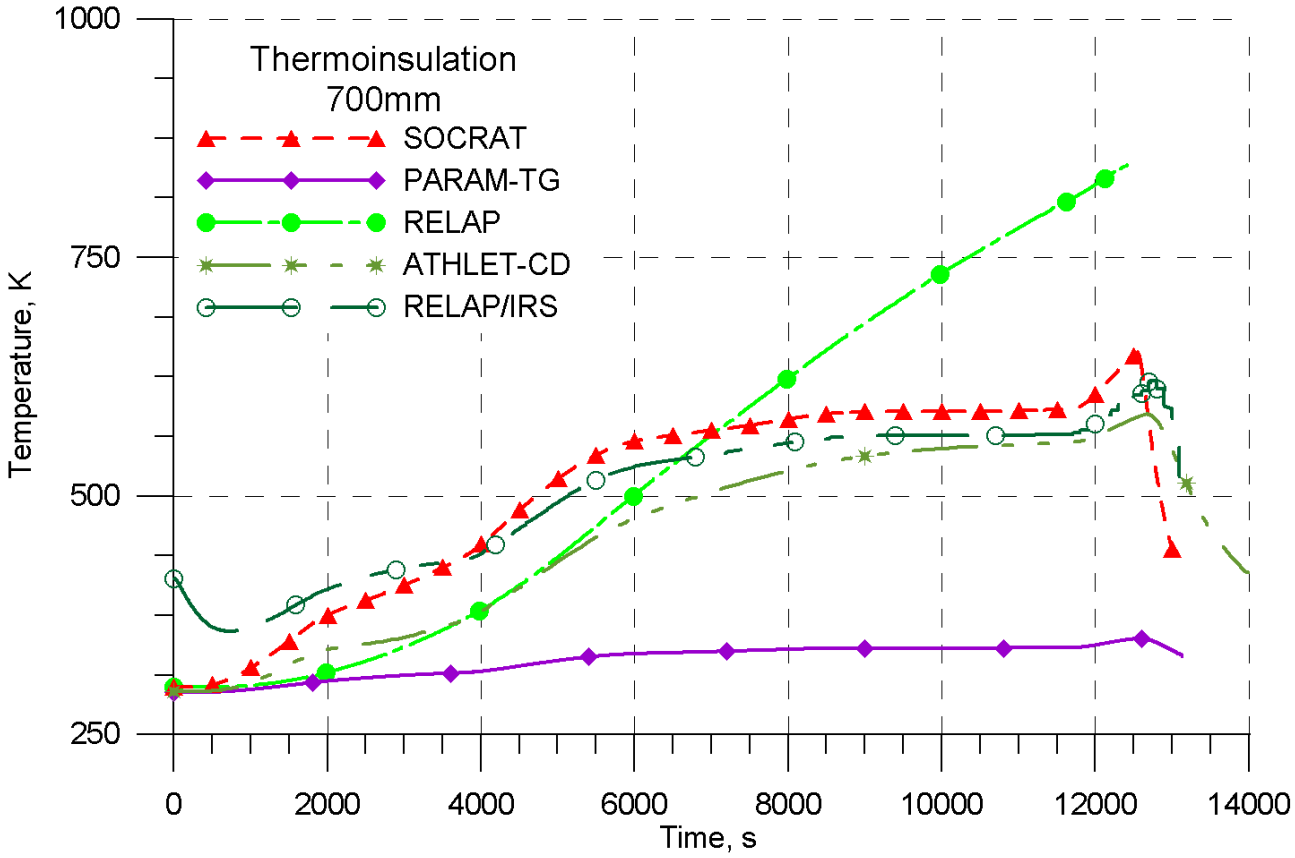

Figure 2.82. Temperature of thermoinsulation at the elevation of 700 mm. PARAMETER-SF3 experiment. Pre-test calculations.

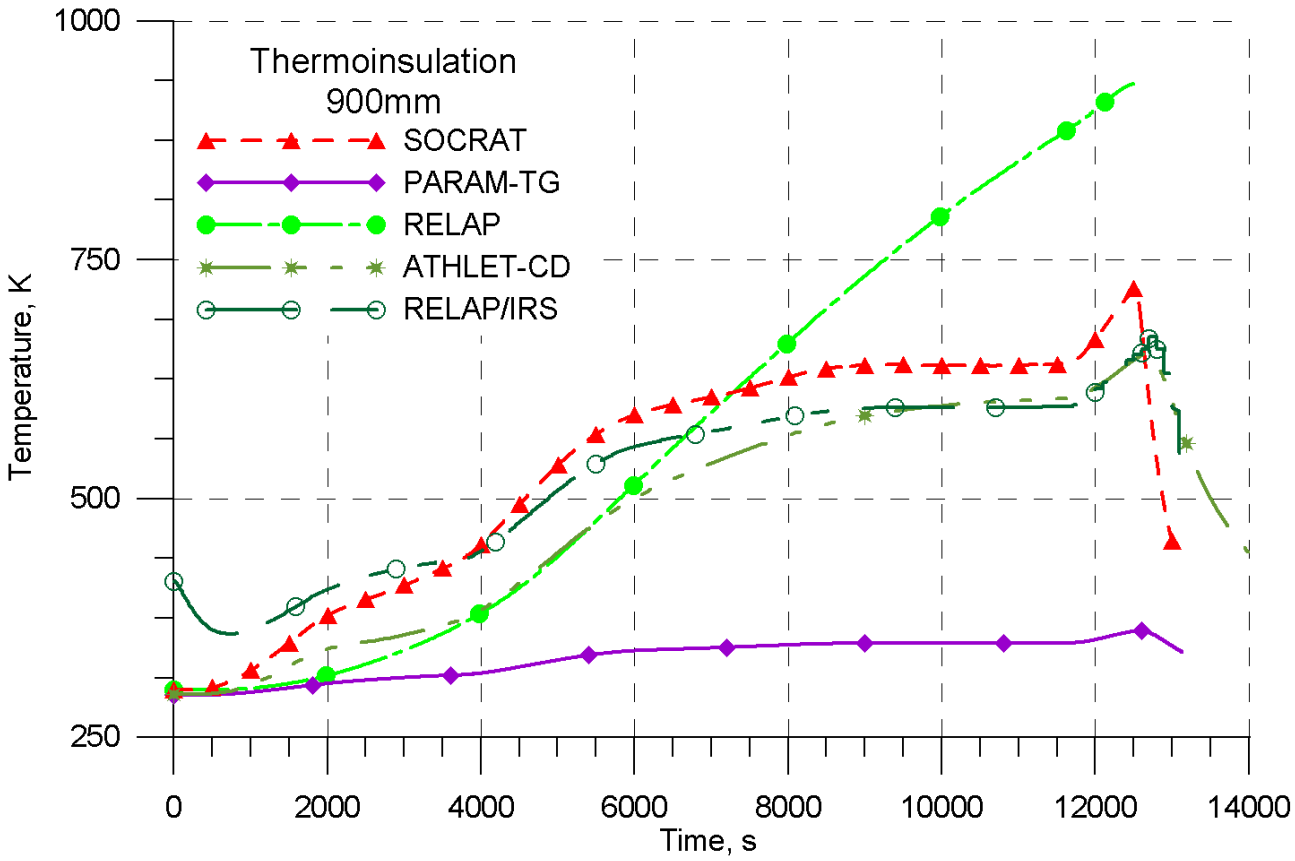

Figure 2.83. Temperature of thermoinsulation at the elevation of 900 mm. PARAMETER-SF3 experiment. Pre-test calculations.

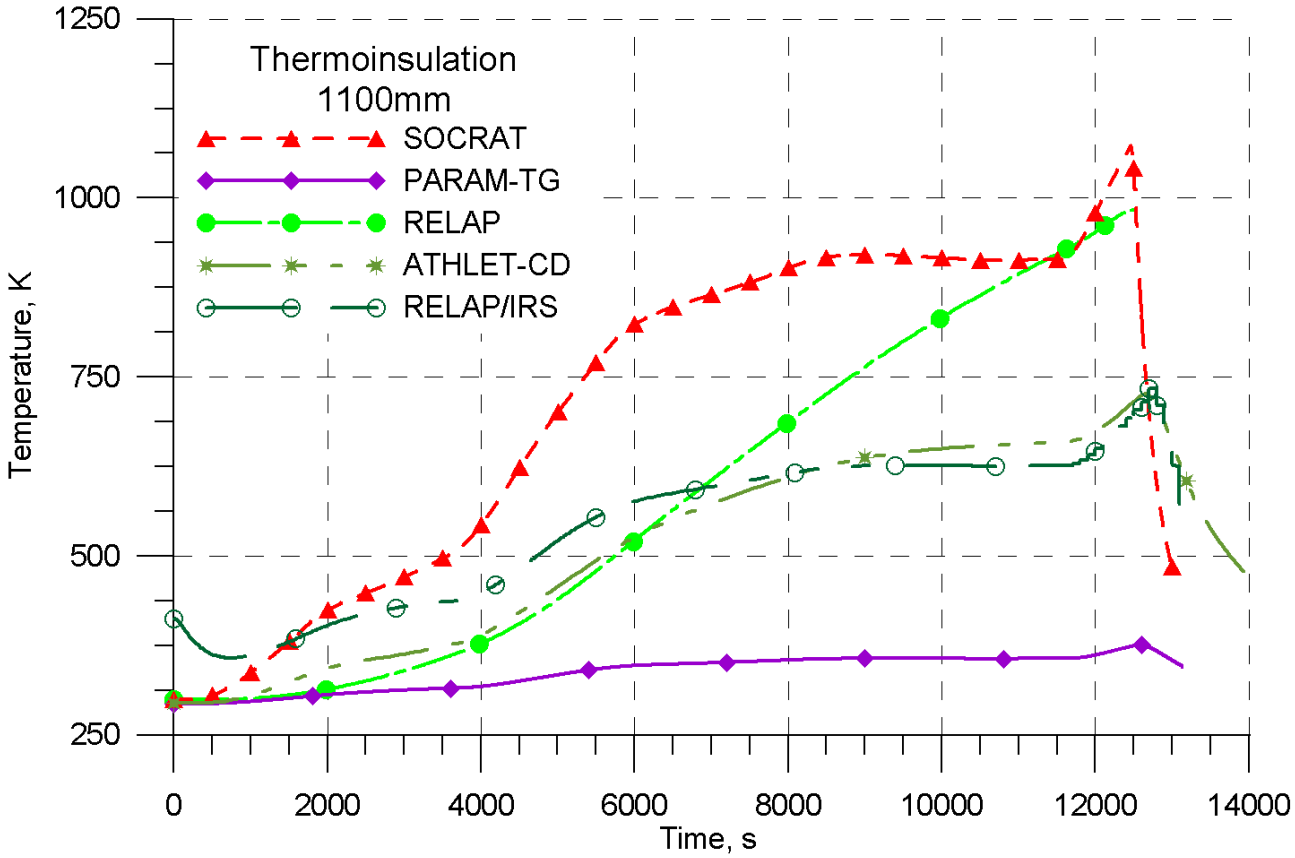

Figure 2.84. Temperature of thermoinsulation at the elevation of 1100 mm. PARAMETER-SF3 experiment. Pre-test calculations.

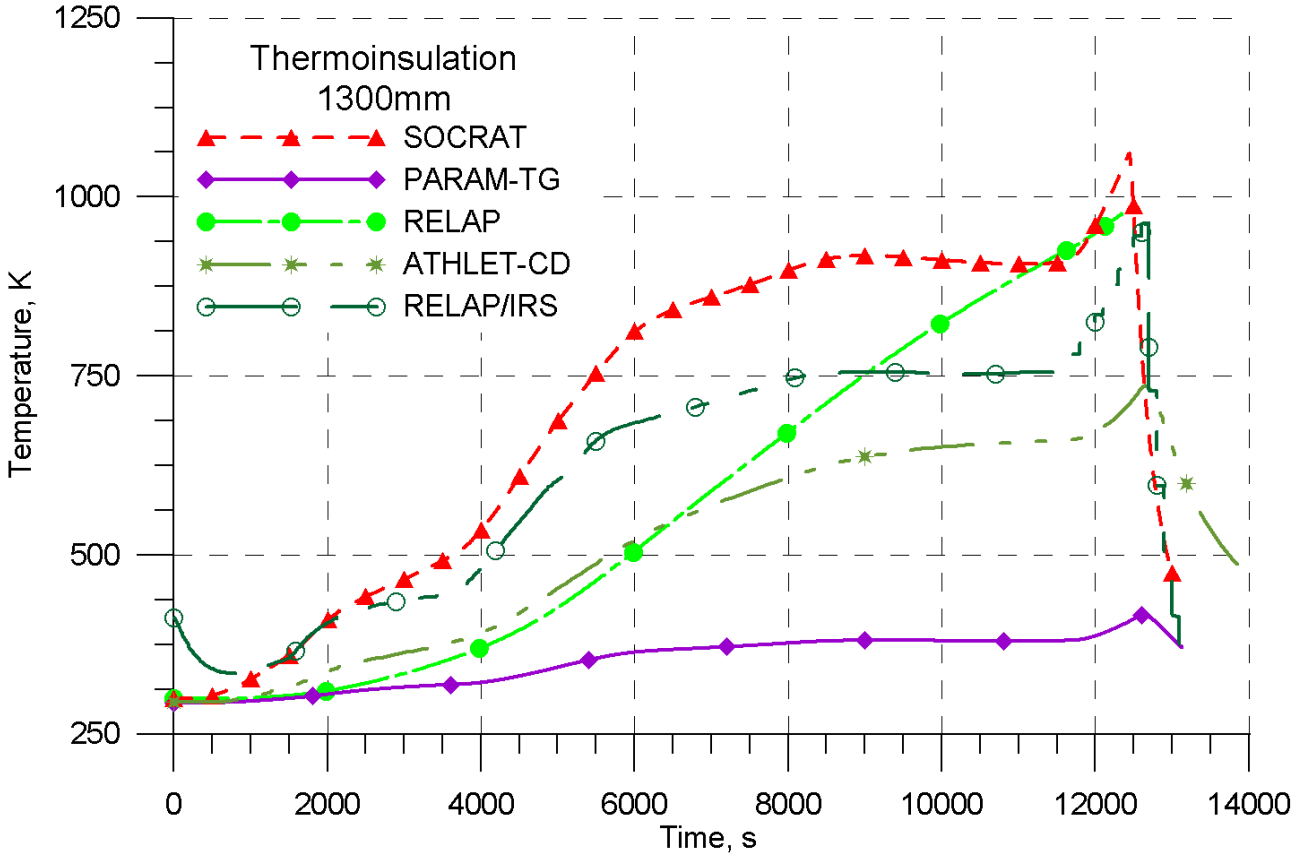

Figure 2.85. Temperature of thermoinsulation at the elevation of 1300 mm. PARAMETER-SF3 experiment. Pre-test calculations.

2.4.4.6 Oxidation and hydrogen production

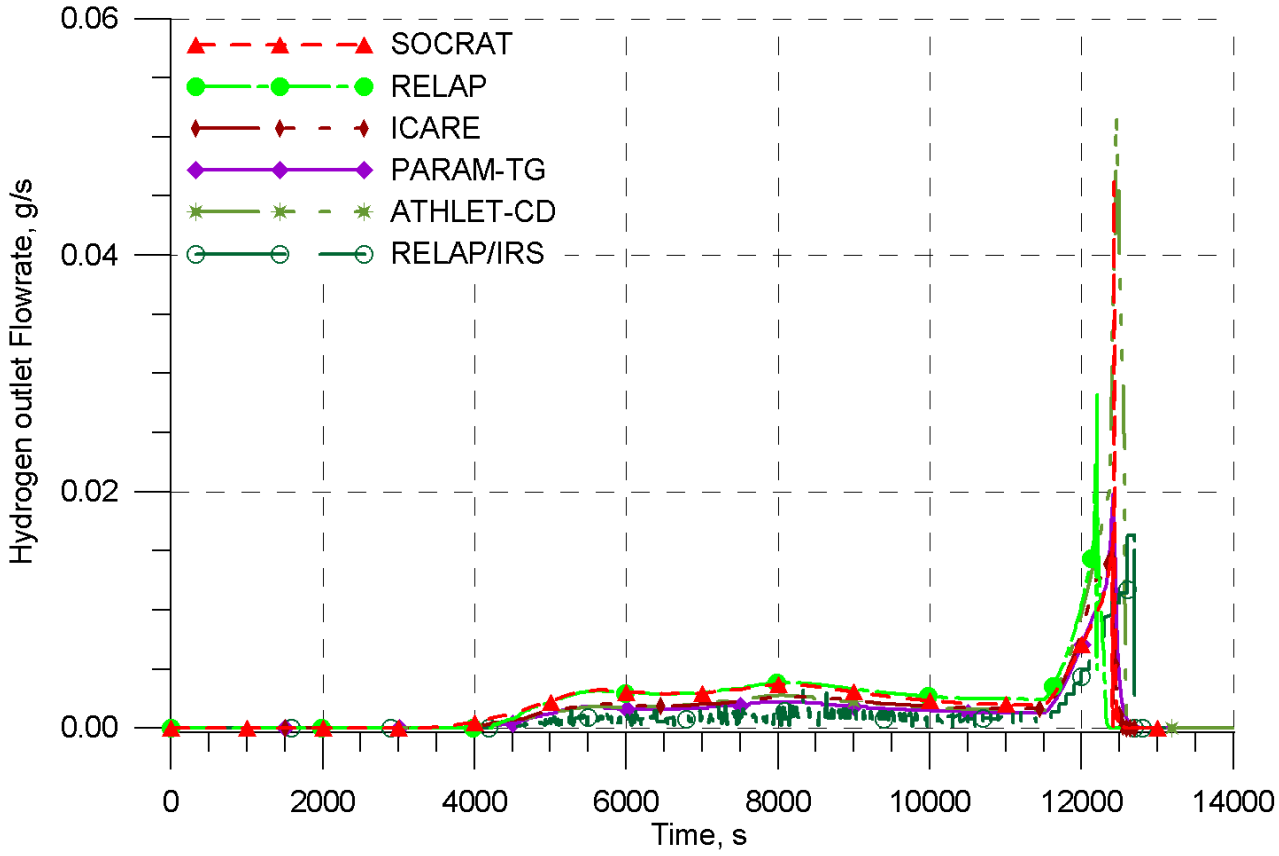

Figure 2.86. Hydrogen flowrate at the test section outlet. PARAMETER-SF3 experiment. Pre-test calculations.

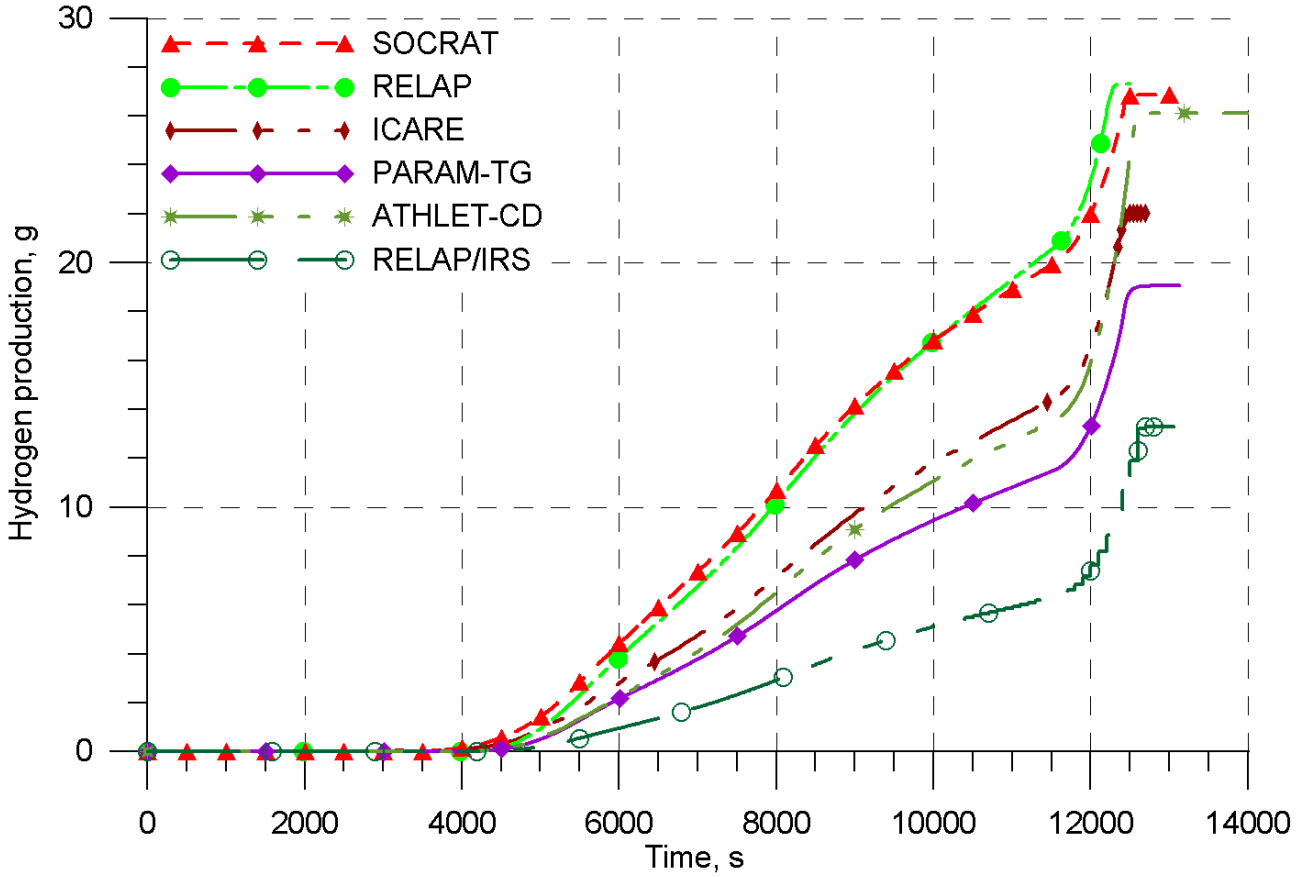

Figure 2.87. Integral hydrogen mass. PARAMETER-SF3 experiment. Pre-test calculations.

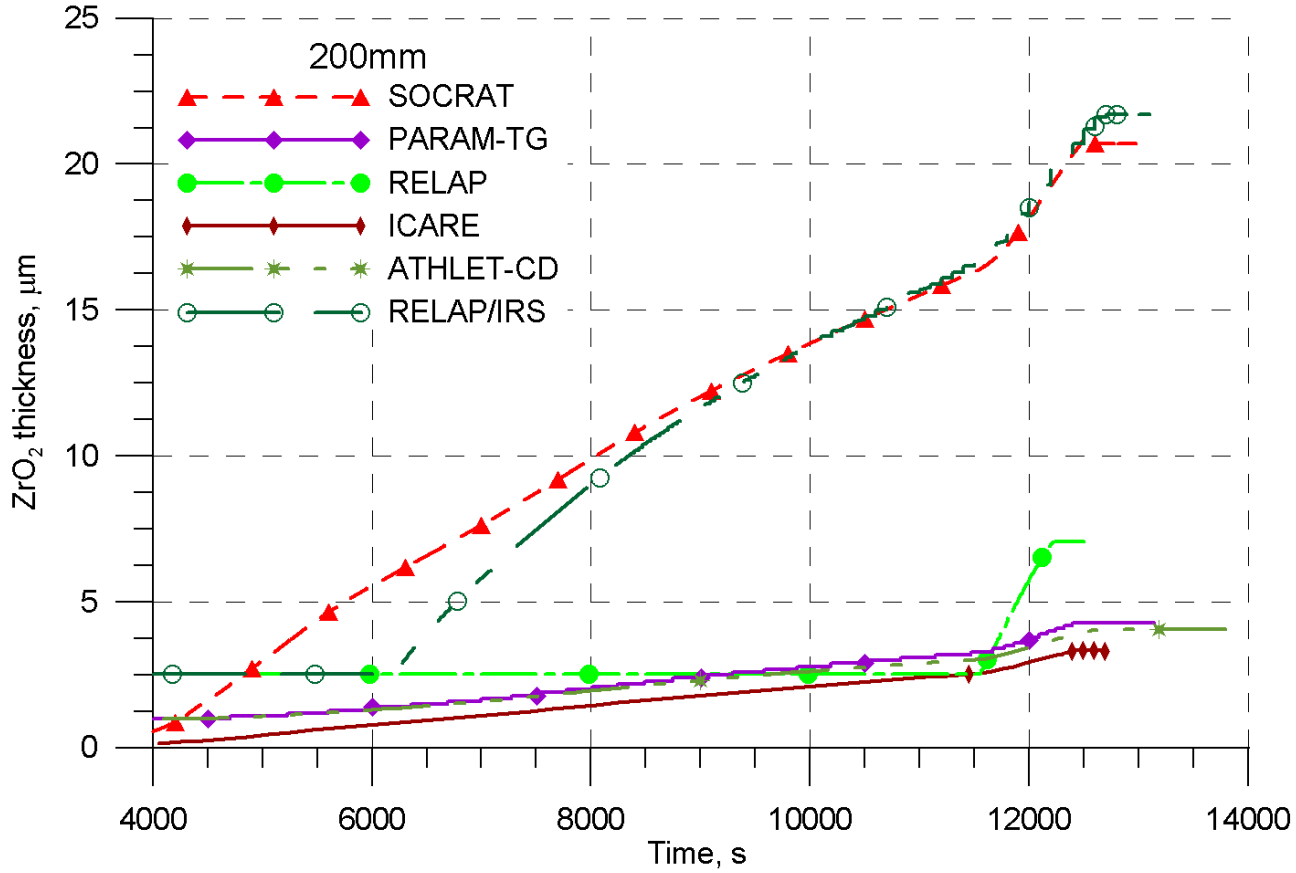

Figure 2.88. Thickness of zirconium oxide scale at the elevation of 200 mm. PARAMETER-SF3 experiment. Pre-test calculations.

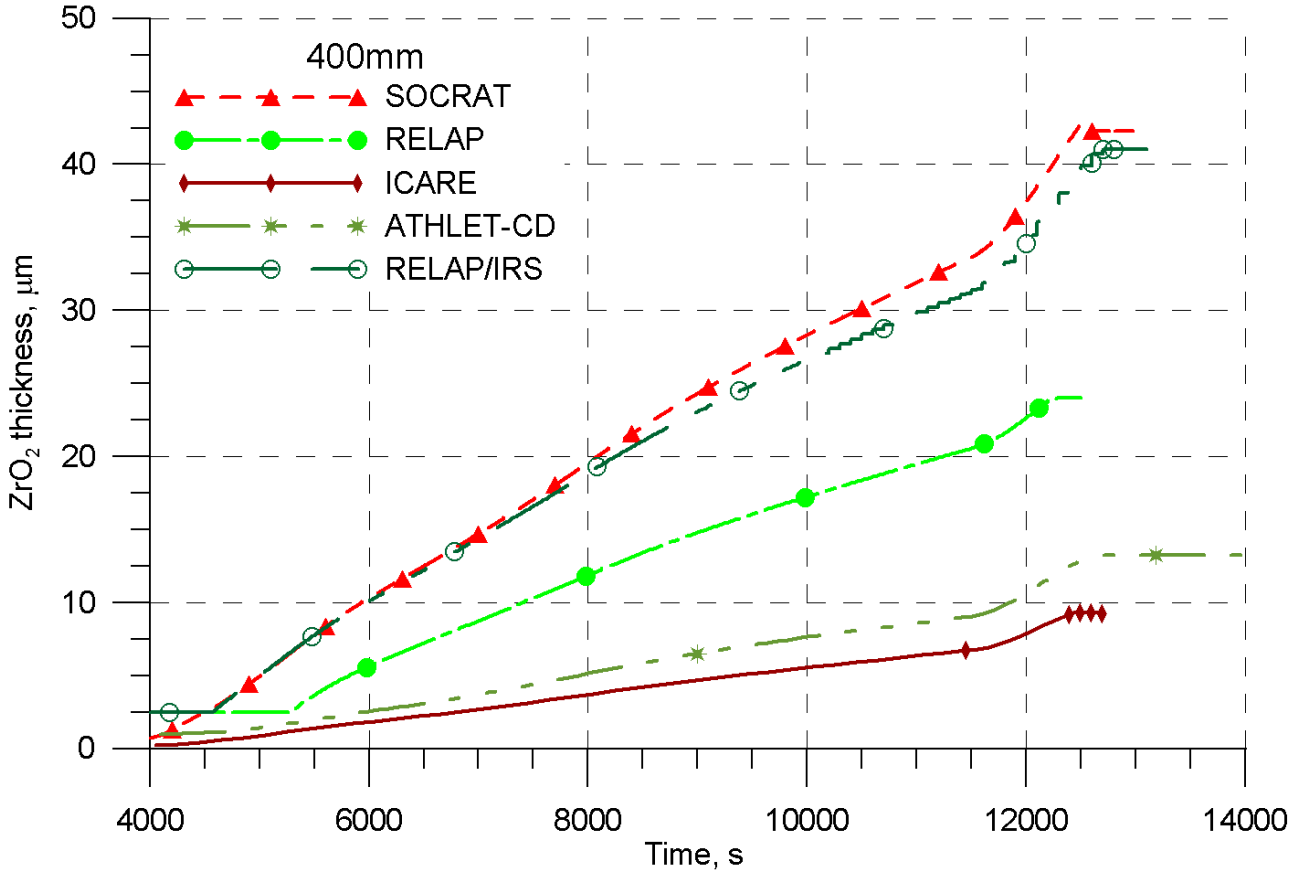

Figure 2.89. Thickness of zirconium oxide scale at the elevation of 400 mm. PARAMETER-SF3 experiment. Pre-test calculations.

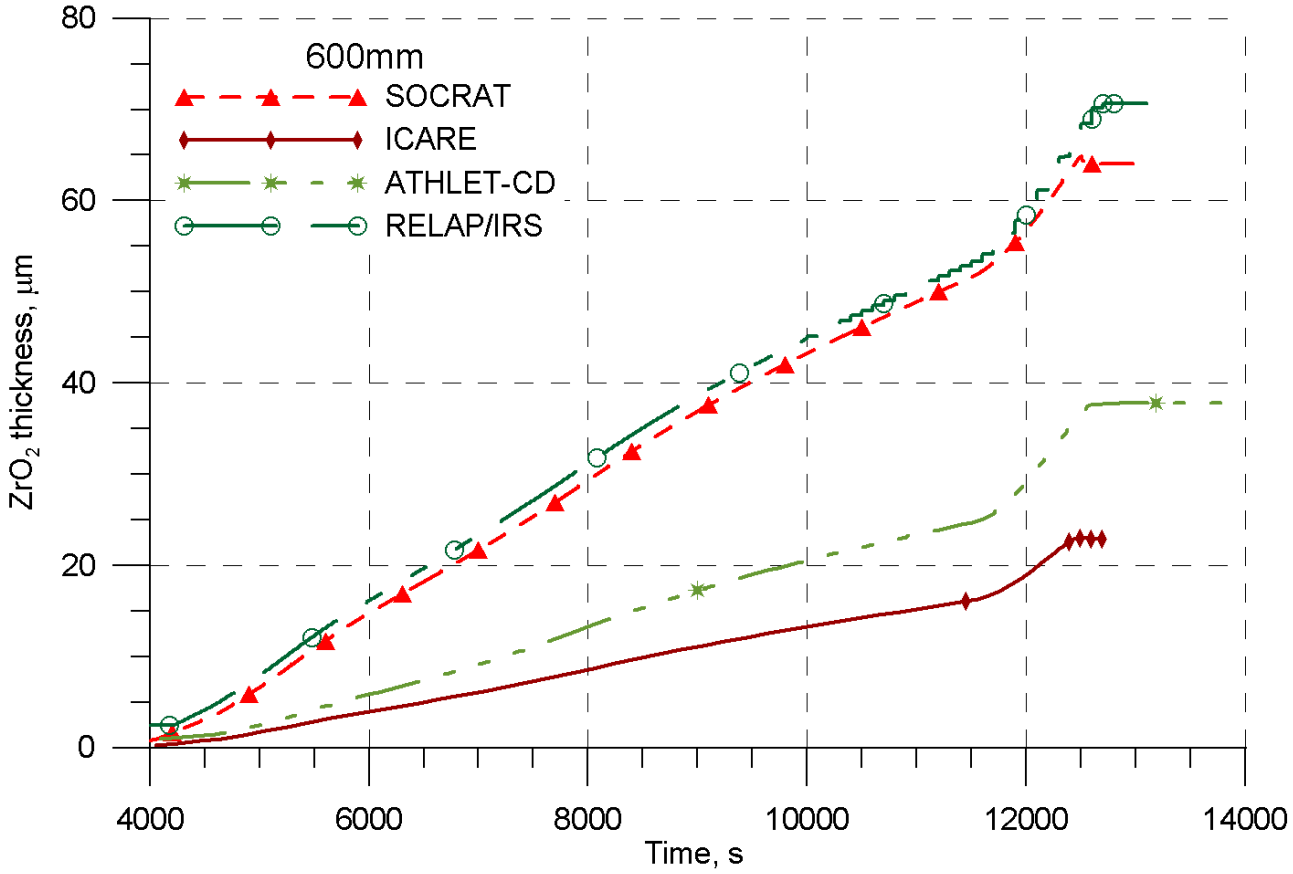

Figure 2.90. Thickness of zirconium oxide scale at the elevation of 600 mm. PARAMETER-SF3 experiment. Pre-test calculations.

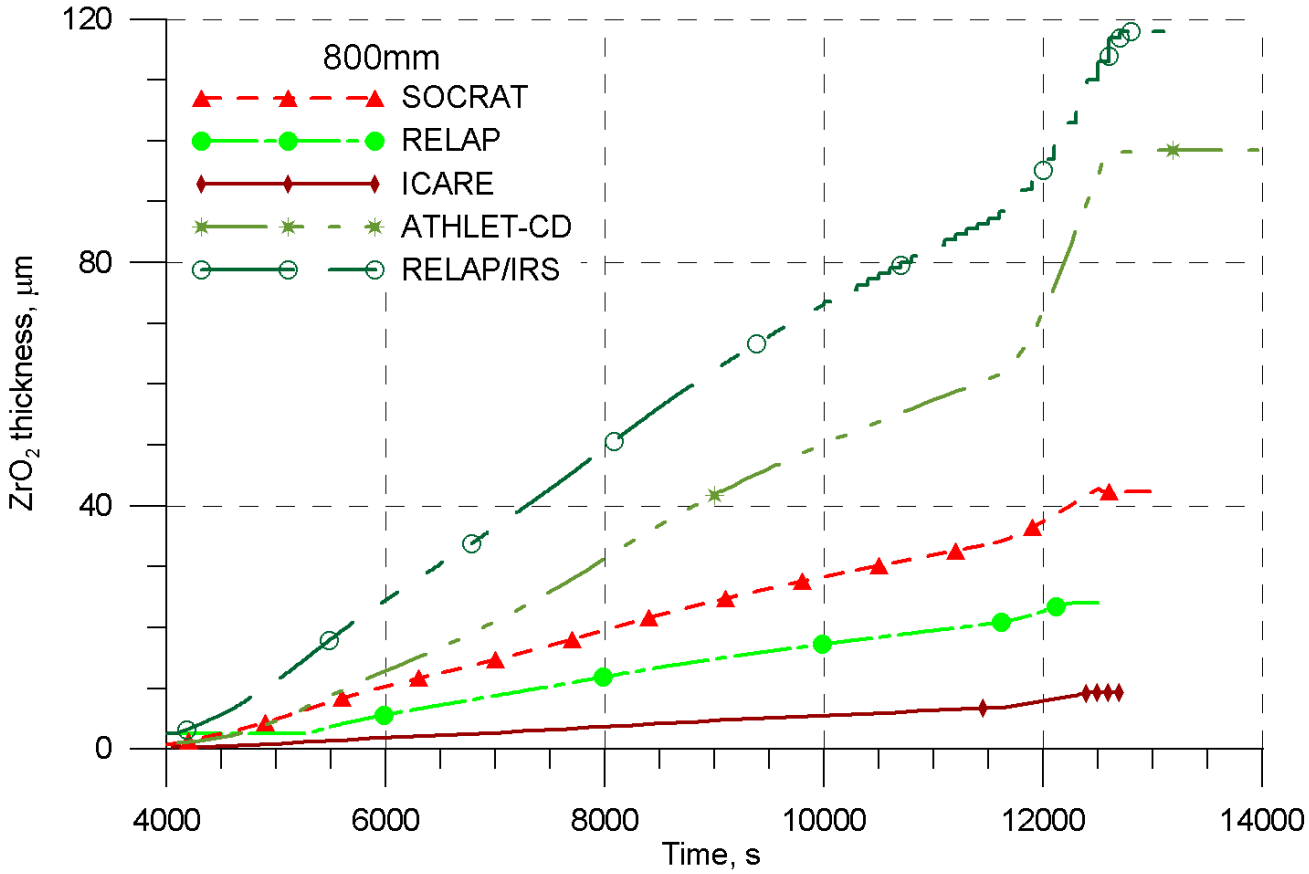

Figure 2.91. Thickness of zirconium oxide scale at the elevation of 800 mm. PARAMETER-SF3 experiment. Pre-test calculations.

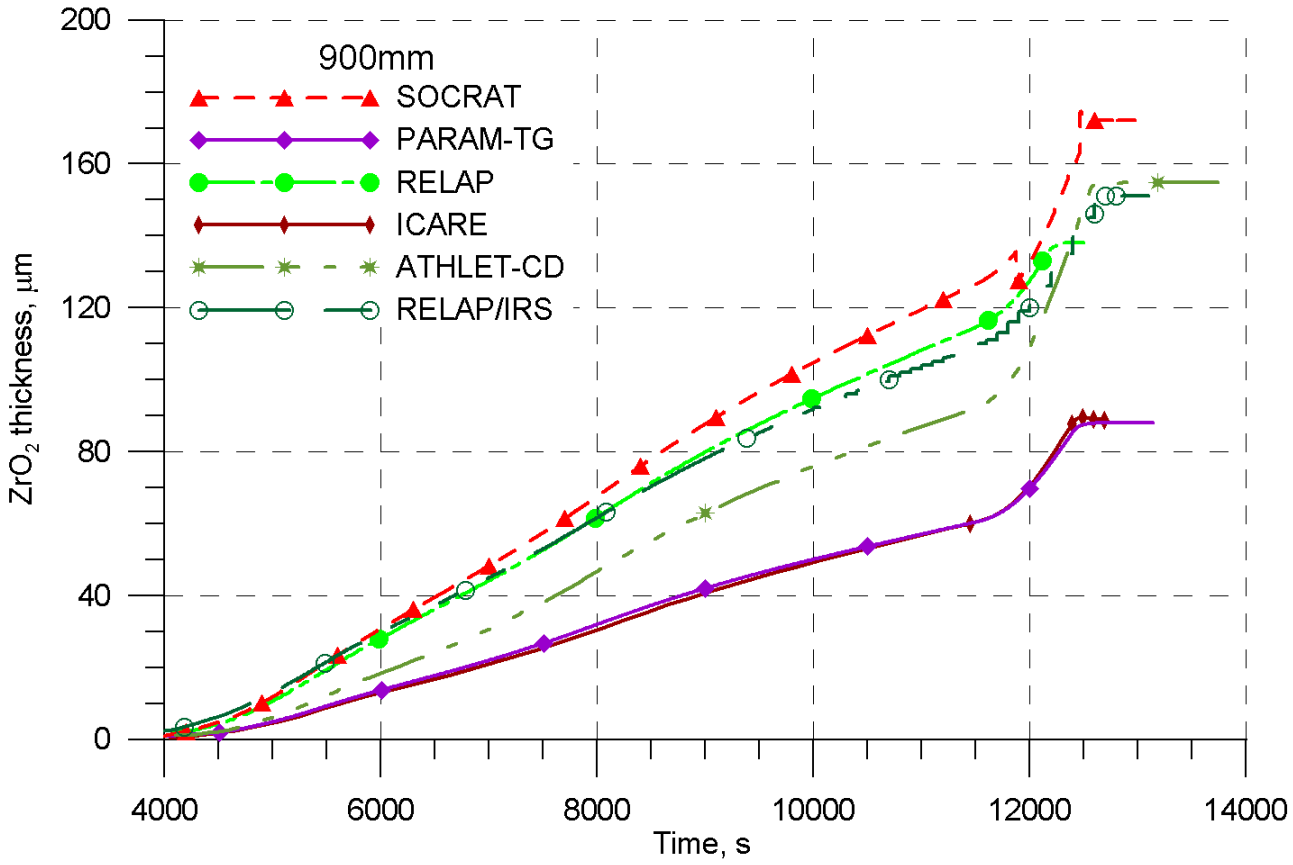

Figure 2.92. Thickness of zirconium oxide scale at the elevation of 900 mm. PARAMETER-SF3 experiment. Pre-test calculations.

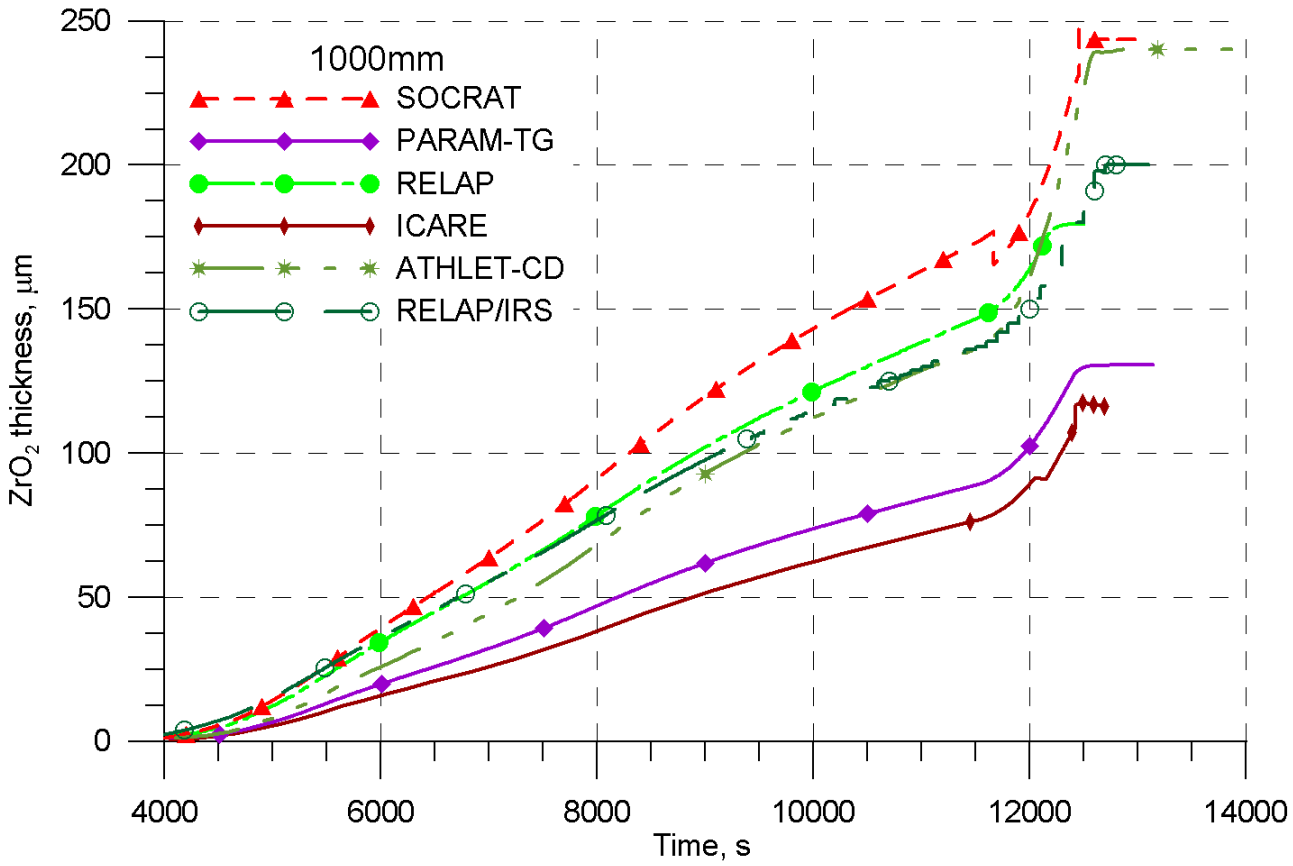

Figure 2.93. Thickness of zirconium oxide scale at the elevation of 1000 mm. PARAMETER-SF3 experiment. Pre-test calculations.

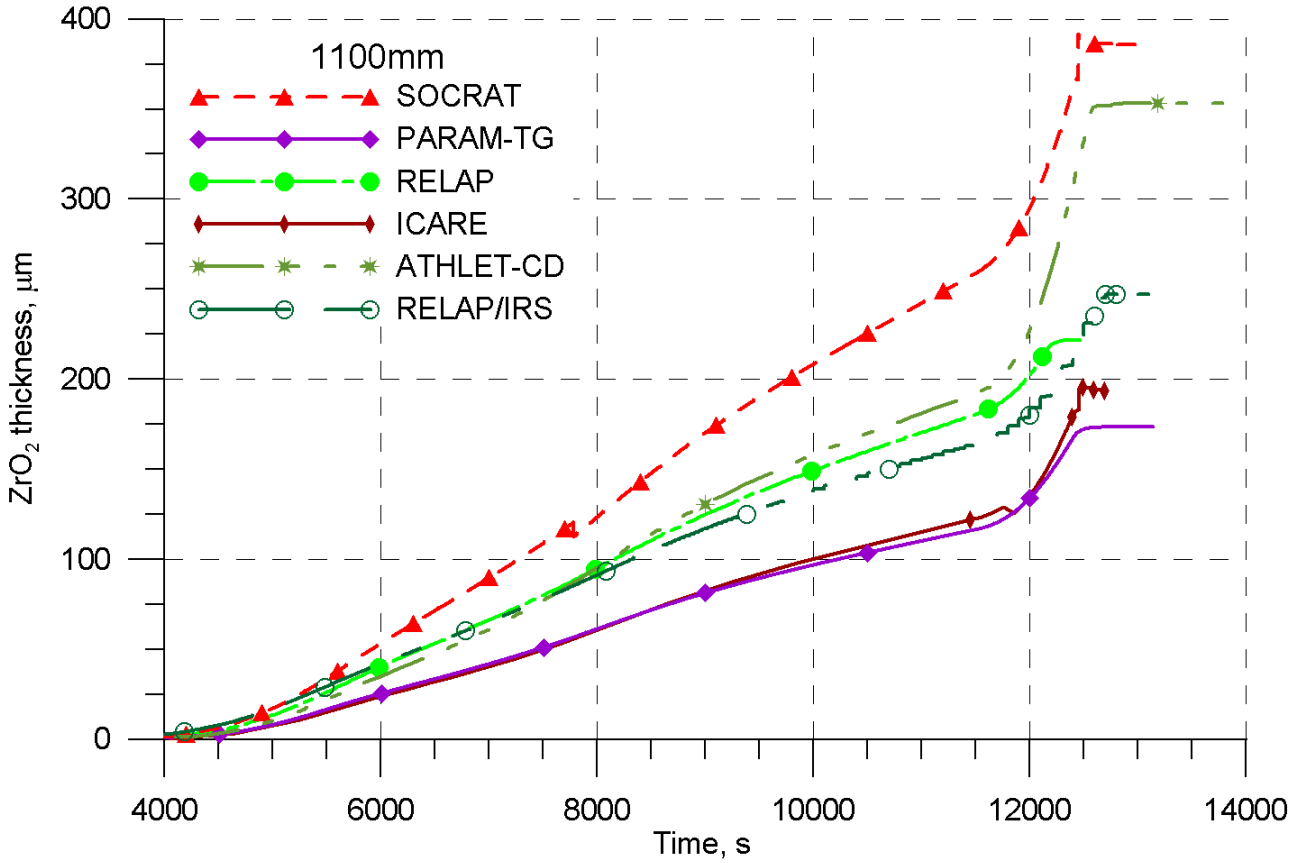

Figure 2.94. Thickness of zirconium oxide scale at the elevation of 1100 mm. PARAMETER-SF3 experiment. Pre-test calculations.

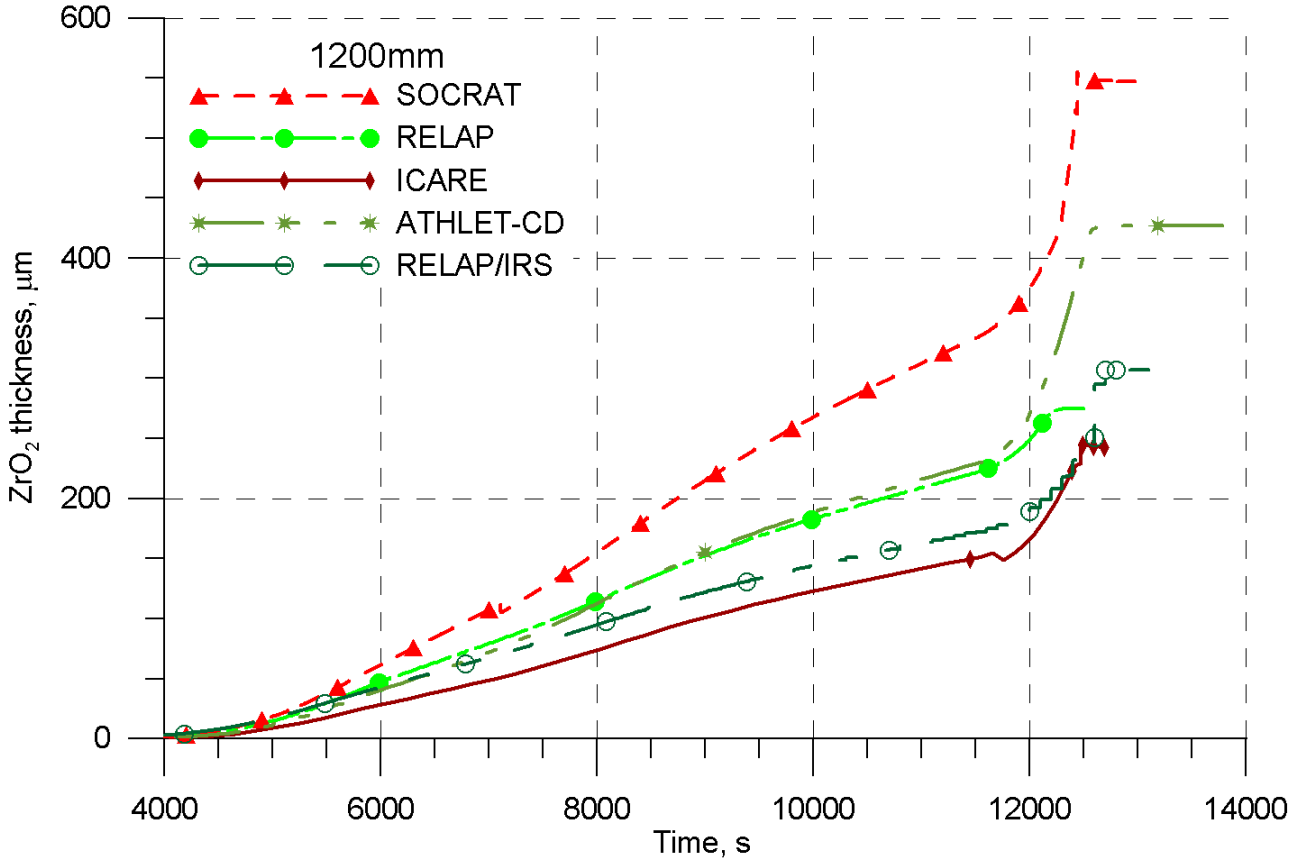

Figure 2.95. Thickness of zirconium oxide scale at the elevation of 1200 mm. PARAMETER-SF3 experiment. Pre-test calculations.

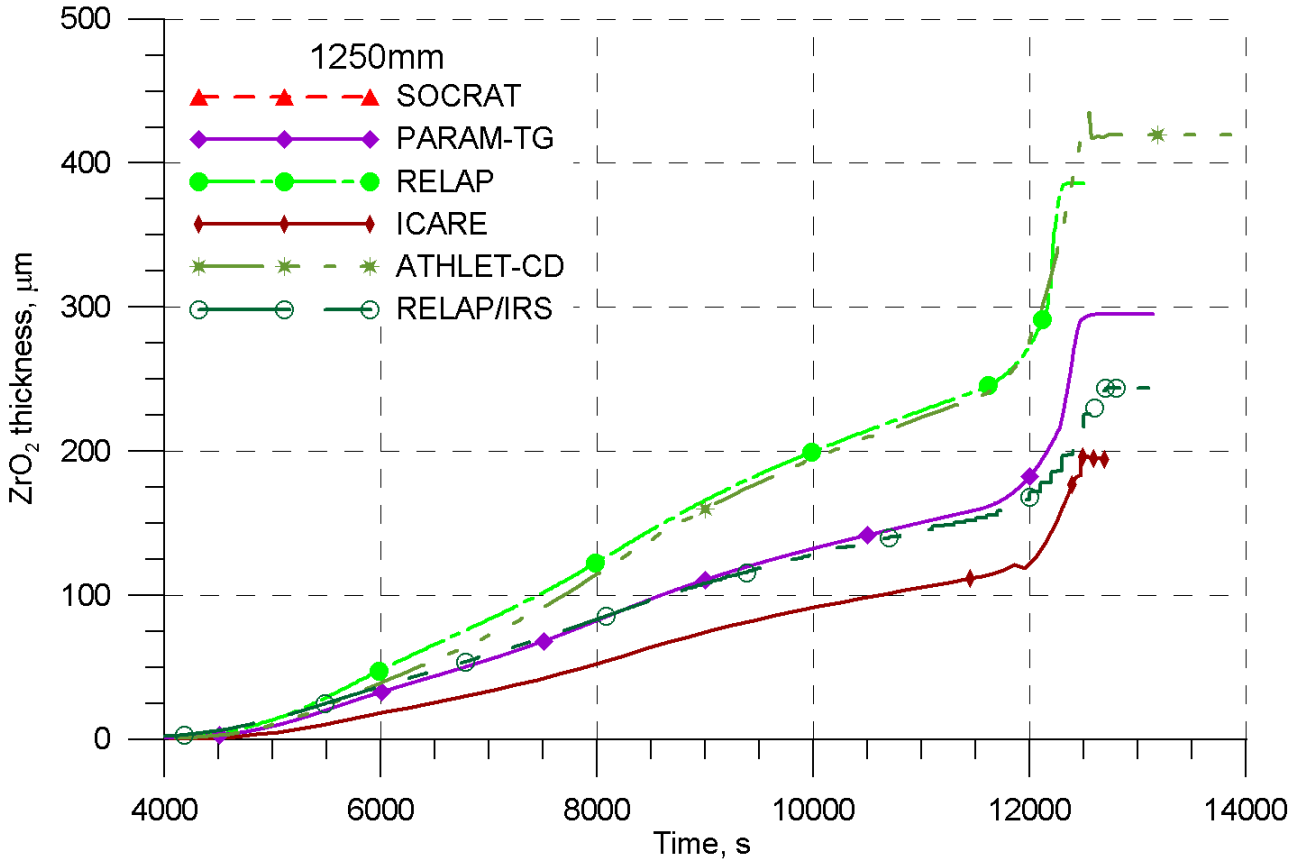

Figure 2.96. Thickness of zirconium oxide scale at the elevation of 1250 mm. PARAMETER-SF3 experiment. Pre-test calculations.

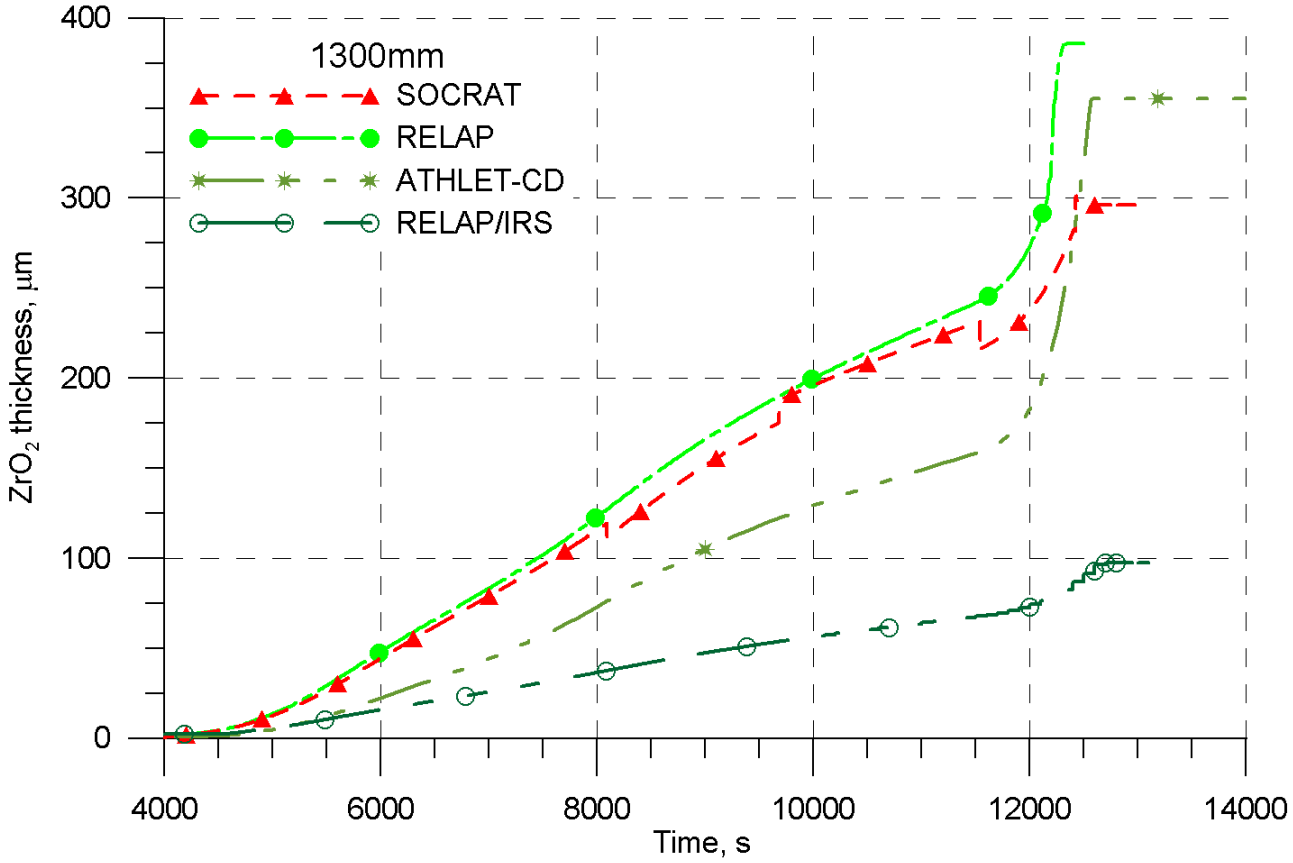

Figure 2.97. Thickness of zirconium oxide scale at the elevation of 1300 mm. PARAMETER-SF3 experiment. Pre-test calculations.

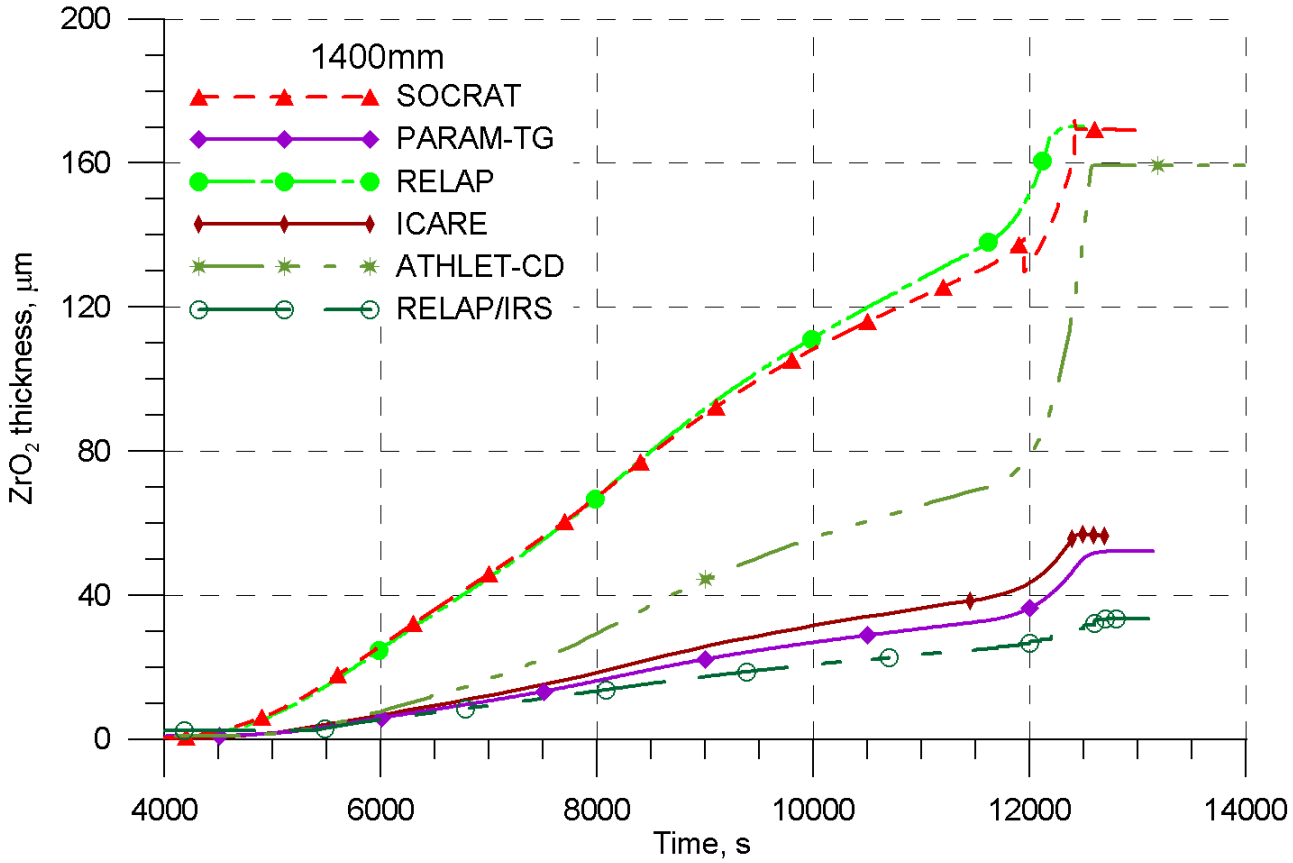

Figure 2.98. Thickness of zirconium oxide scale at the elevation of 1400 mm. PARAMETER-SF3 experiment. Pre-test calculations.

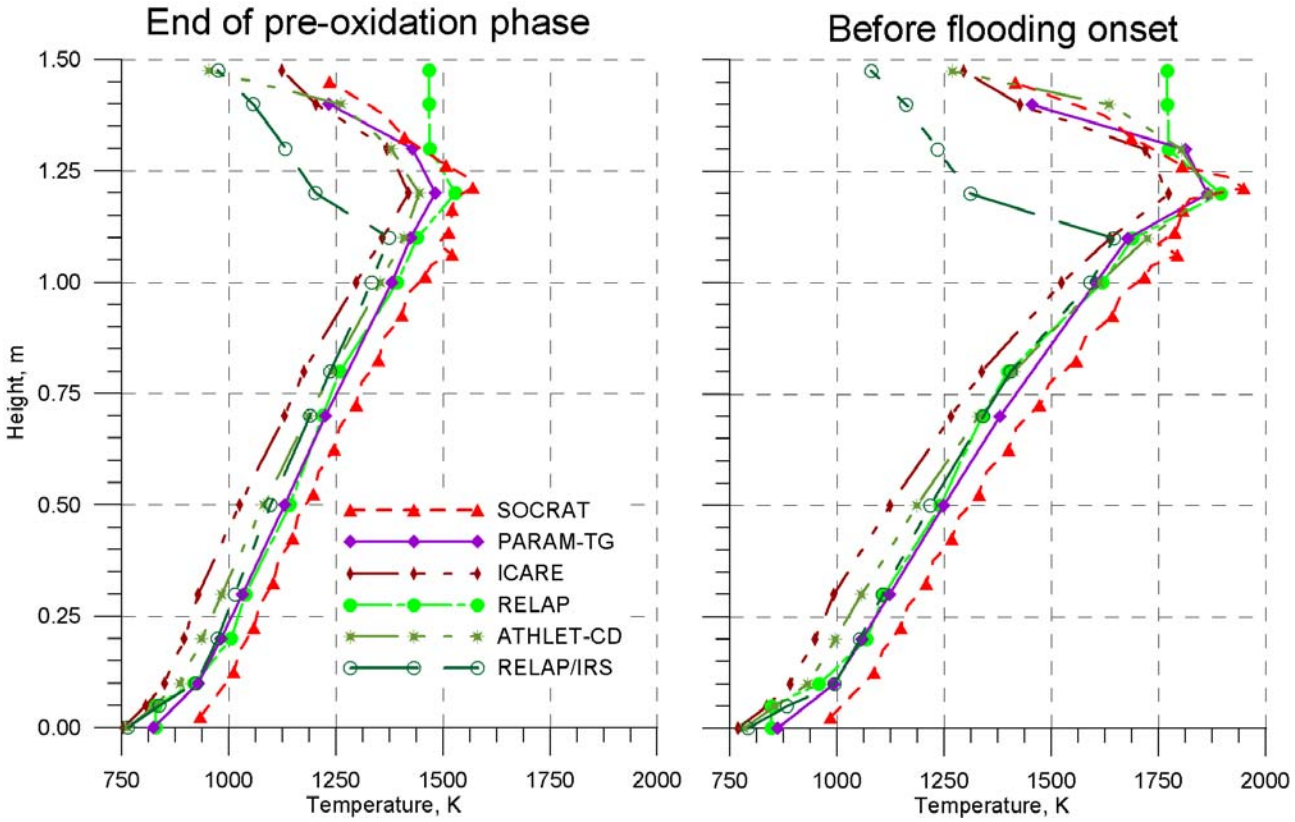

Figure 2.99. Axial temperature profiles. PARAMETER-SF3 experiment. Pre-test calculations.

3 POST-TEST CALCULATIONS OF PARAMETER-SF3 EXPERIMENT

3.1 MAIN RESULTS OF PARAMETER-SF3 EXPERIMENT

3.1.1 Objective of the experiment. Phenomena and processes

PARAMETER-SF3 experiment was conducted on 31 October, 2008, in FSUE SRI SIA "LUCH", Podolsk, at the PARAMETER test facility. In the given experiment the initial phase of severe LOCA was simulated for NPP with VVER-1000 when the core drying occurs, then its heating-up to ~ 1600°C and water top flooding in case of ECCS restoration.

The experiment SF3 was conducted to study the behaviour of a 19-rod model FA of VVER-1000 under simulated conditions of severe accident including the stages of low rate cooling with top flooding, and namely:

– Study of time history of cooling a 19-rod model FA of VVER-1000 overheated to ~ 1600°C with water top flooding;

– Study of behaviour of structural components of 19-rod model FA of VVER-1000 (fuel pellets and claddings, shroud, spacing grids);

– Study of oxidation degree of structural components of 19-rod model FA of VVER-1000;

– Study of interaction and structural-phase changes in the materials of a model FA of VVER-1000 (fuel pellets and claddings);

– Study of hydrogen production time history.

Main parameters of PARAMETER-SF3 experiment are presented in Table 3.1.

Table 3.1. Typical parameters of PARAMETER-SF3 experiment

Steam/argon flow rate, (g/s)	Pre-oxidation temperature, K	Presence of AE with B_4C	Maximum temperature before flooding, K	Formation of substantial melting regions	Flooding type	Hydrogen production, g
3.5/2	1473	no	≈1950	no	top	35*

* No considerable hydrogen production at the flooding stage is revealed

Sequence of events for PARAMETER-SF3 experiment is presented below (Table 3.2).

Table 3.2. Time sequence of main events in SF3 experiment

Stage	Main parameters			
	FA temperature, ºC	Environment	Heating rate, ºC/s	Time, s
FA pre-heating in argon flow	20-100	Argon flow at temperature to 160ºC (argon mass flow rate 2 g/s)	–	0-750
FA heating in steam-gas mixture	100-500	Argon/steam mixture (argon/steam mass flow rate 2/3.5 g/s)	0.1-0.3	750-2500
Stabilization of main parameters	~ 500	Argon/steam mixture (argon/steam mass flow rate 2/3.5 g/s)	-	2500-4500
FA heating to 1100ºC	500-1100	Argon/steam mixture (argon/steam mass flow rate 2/3.5 g/s)	~0.2	4500-7000
FA heating to 1200ºC	1100-1200	Argon/steam mixture (argon/steam mass flow rate 2/3.5 g/s)	~0.1	7000-8000
FA pre-oxidation	~ 1200	Argon/steam mixture (argon/steam mass flow rate 2/3.5 g/s)	-	8000-13750
FA heating to 1600ºC	1200-1600	Argon/steam mixture (argon/steam mass flow rate 2/3.5 g/s)	~0.5	13750-14480
FA top flooding (when FA temperature reaches Tmax=1600ºC)	Till complete FA cooling	Water (mass flow rate 40 g/s to FA)	-	14480-14965

3.1.2 Brief description of PARAMETER facility and its main characteristics

PARAMETER test facility located in FSUE SRI SIA “LUCH”, Podolsk, was designed for studying the VVER FA under the conditions simulating design basis, beyond design basis and severe accidents at VVER reactor.

For performing the SF3 experiment the new test section was developed and fabricated in FSUE SRI SIA “LUCH” [8], in the structure of this test section some effects were taken into account that were revealed in the analysis of results of PARAMETER-SF1, PARAMETER-SF2 experiments, [6], [7]:

The improved test section comprises three sections combined with flange joints (see Figure 3.1).

All fuel rod simulators (except for the central unheated fuel rod) are combined into one heated section.

In the upper part of the model FA the water injection system is arranged comprising 41 tubes ∅4x1 mm and located in the test section upper flange of the test section, the guiding channel and collecting thimble.

Each fuel rod of the assembly is equipped in the upper part with the helium filling device including the capillary tube ∅1.6x0.3 mm with the length of ~1500 mm. All capillary tubes are connected to the common compensation tank with the capacity of ~10 L.

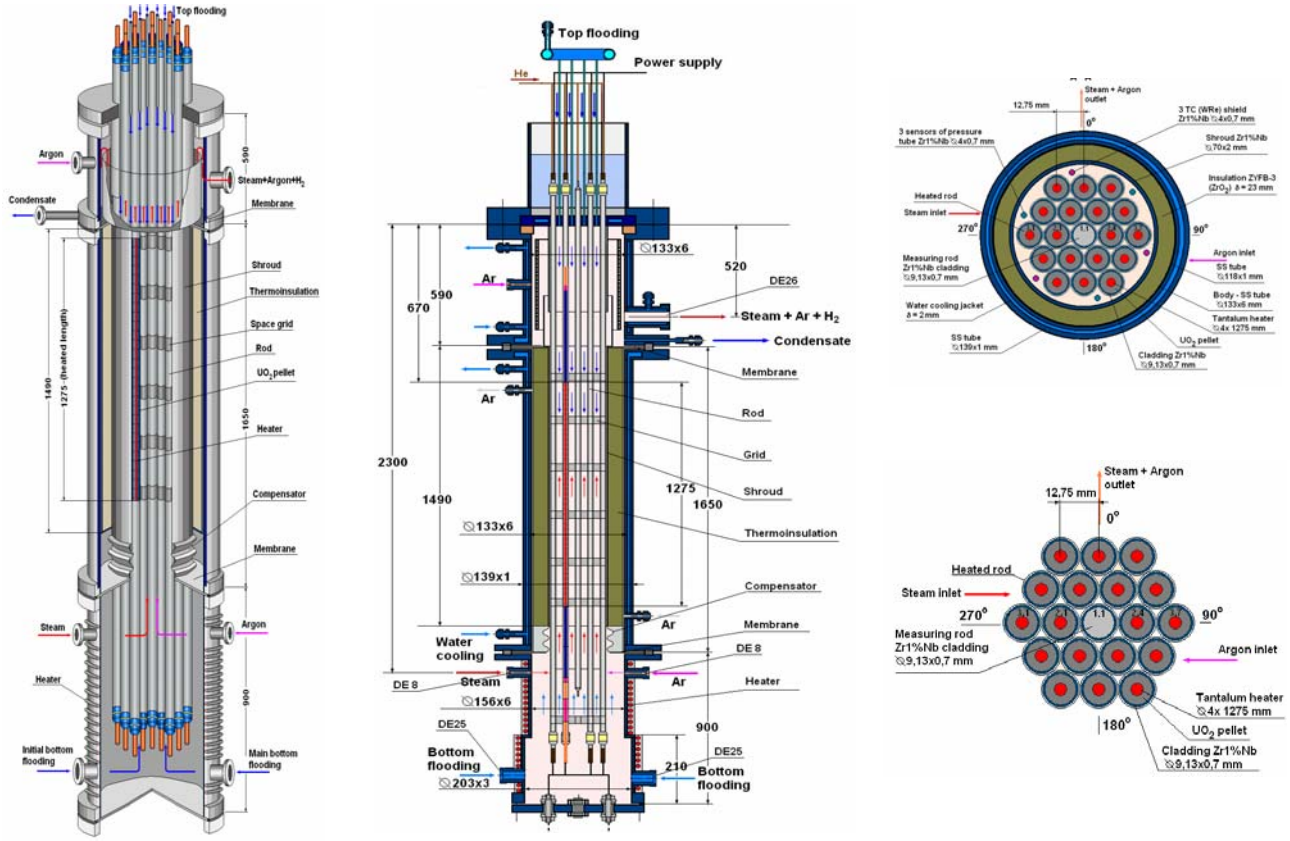

Figure 3.1. General view of the test section and the model FA sectional view.

It should be noted that PARAMETER facility is equipped with the very detailed instrumentation. The measurement system of PARAMETER is intended for measurement and registration of critical parameters and events in the course of experiment.

For measurement of different types of parameters the following types of measuring instruments are used:

- Temperatures are measured with thermocouples (TC) of four types;
- Pressure is measured with pressure pick-ups;
- Mass flow rates of steam, argon and water is monitored with electron flow meters;
- Check of water masses in different tanks is made after experiment by means of weighing on electronic balance;
- For continuous analysis of hydrogen the system of hydrogen detection SOV-3 is used based on electric conductance-measuring method;
- In discrete method of measurement of hydrogen concentration 10 sampling tanks are used with the subsequent analysis of gas mixtures using the gas chromatograph.

Main technical characteristics of the model FA are presented in Table3.3.

Table 3.3. Main technical characteristics of the model FA

Fuel rod simulators and model FA	
Number of heated fuel rods	18
Number of unheated fuel rods	1
FA grid pitch, mm	12.75
Fuel rod cladding external/internal diameter, mm	9.13/7.73
Cladding material	Zr-1%Nb
Height of heated fuel rods, mm	3120
Height of unheated fuel rod, mm	2950
Heater material	tantalum
Sizes of heated fuel rod, mm:	
diameter/height	4/1275
coordinates	from 0 to 1275
Coordinate of the location of steam/argon inlet (radial), mm	-372 (270^o/90^o)
Coordinate of the location of steam/argon outlet (radial), mm	1425 (0^o)
Internal gas (helium) pressure in fuel rods, MPa	0.24
Fuel pellets	
Heated fuel rods external diameter/of central hole/height, mm	UO_2 pellets with holes $7.6^{-0.03}/4.2^{+0.15}/11^{\pm 0.1}$
Unheated fuel rod	UO_2 pellets with holes $7.6^{-0.03}/4.2^{+0.15}/11^{\pm 0.1}$
Spacer grid	
Material	Zr-1%Nb
Height, mm	20
Number, pcs.	6
Distance between grids, mm	255
Coordinates of upper edge of grids, mm:	
of the first (lower)	30
of the sixth (upper)	1305
Shroud	
Material	Zr-1%Nb
Size:diameter/wall thickness, mm	69.7/1.2
Height, mm	1450
Thermal insulation	
Material	ZrO_2 ZYFB-3
Thickness, mm	23
Height, mm	1450
Thermal insulation housing	
Material	Steel 12X18H10T
Thickness, mm	1
Height, mm	1450
Outer diameter, mm	118

3.2 NODALIZATIONS

3.2.1 Nodalization for SOCRAT computer code

In developing the nodalization for the test section of SF3 experiment for SOCRAT code (Table 3.4) the experience in constructing the nodalization for SF2 experiment (see section 1.2.1) was taken into account, as well as the data obtained in simulation of the installation using the finite element method.

Table 3.4. Assumptions in the nodalization for SOCRAT code

Process or phenomenon	Process consideration
Argon and steam mixing	Ideal
Oxidation of spacer grid	Three upper grids are simulated (1300, 1050 and 800 mm)
Assembly flow area irregularity	Not considered
Cross-section steam-argon temperature non-uniformity	Two parallel thermohydraulic channels: - 7 central rods; - 12 periphery fuel rods, 12 displacers, shroud
Availability of thermocouples	One thermocouple is simulated at the elevation of 1250 mm for evaluation of difference in readings of the detector and of actual cladding temperature and also for evaluation of oxidation
Availability of pheripheral rods	Simulated in the form of zirconium rods for evaluation of oxidation
Heater of the lower section	Heat flux is applied to the lower section outside surface
Path upstream of hydrogen detector	Simulated conventionally for effective consideration of transport delay from the assembly to the detector
Radiative heat transfer	In radial and axial direction
Inlet nozzles	Not simulated. The source was assigned directly in LP element. Temperature of steam-argon mixture, starting from the time moment of 6000 s, was assumed equal to 560 K that assured rather good agreement of calculated and experimental cladding temperatures at the elevations of 0÷300 mm

Figures 3.2 и 3.3 present the calculated values of the profile of coolant temperature and argon concentration in the hottest section (~1250 mm), obtained with the use of ANSYS-CFX code. Hydraulic 3D-model of PARAMETER facility included all hydraulic elements of the installation from inlet to outlet nozzles. Availability of thermocouples and spacier grids was not considered. The axial temperature profile for fuel rods and shroud, calculated with the use of SOCRAT code, was assigned to be the boundary conditions for thermal problem. Complete Navier-Stokes equation was solved.

It follows from the Figures that irregularity of argon concentration profile through the assembly section can be neglected.

Nodalization for calculation of PARAMETER-SF3 experiment, developed with regard for the given comments and based on the test section structure, is presented in Figure 3.4. Main difference from the nodalization for SF2 experiment is representation of the test section heated part with two parallel hydraulic channels instead of one. This was caused by considerable irregularity (~ 150 K) of experimental temperatures of claddings in the assembly upper part in SF2 experiment and confirmed by the calculation using finite element method. Simplified simulation of irregularity of simulator temperatures through the section in the assembly upper part in calculation of SF2 experiment did not allow for make the whole regard for edge effects and was the cause of substantial error in solution of thermal problem. This resulted in overestimation of cladding temperature at the elevation of 1100 and 1300 mm (Figures 1.34 and 1.35).

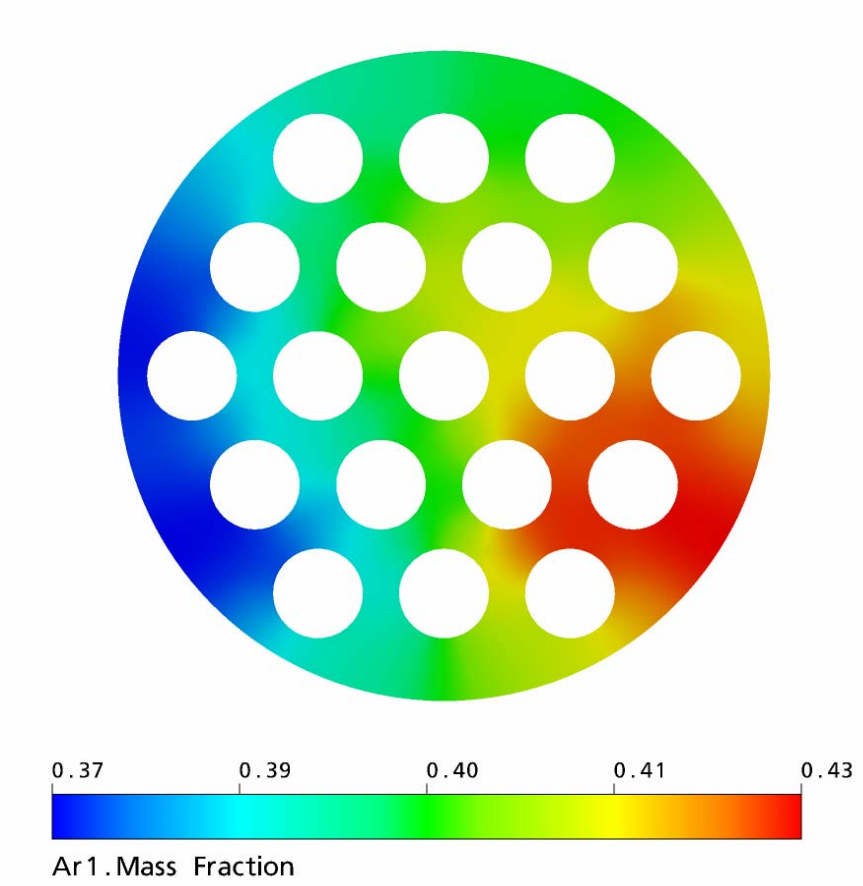

Figure 3.2. Calculated profile of mass argon concentration in the hottest section. The model of PARAMETER facility for ANSYS-CFX code. Test problem.

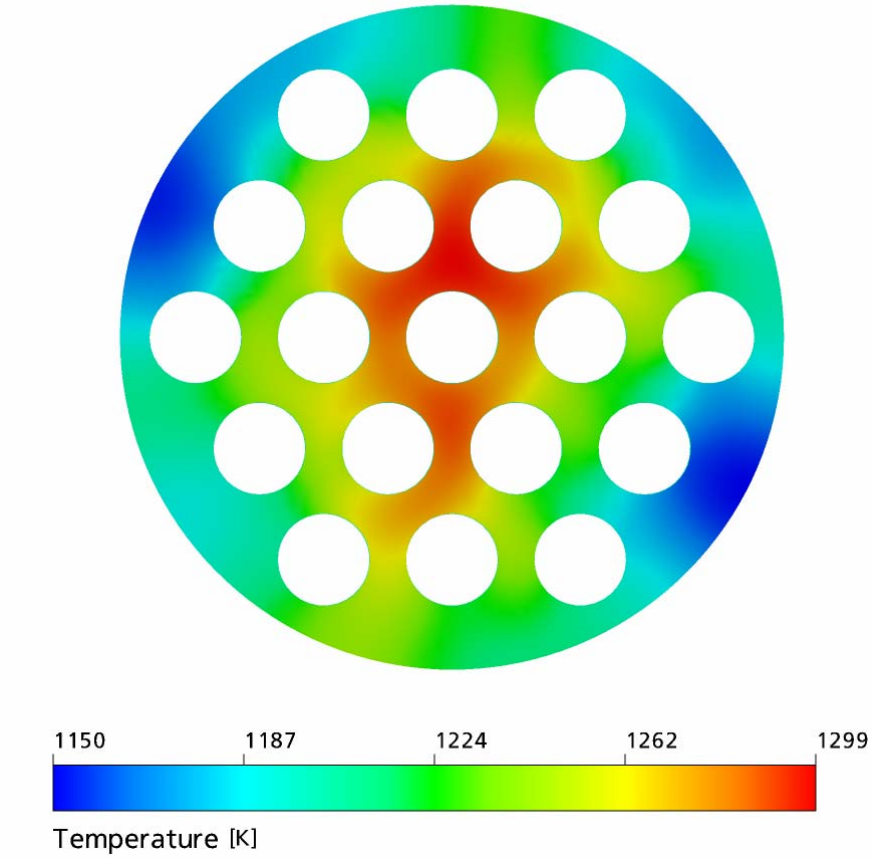

Figure 3.3. Calculated profile of steam-argon mixture temperature in the hottest section. The model of PARAMETER facility for ANSYS-CFX code. Test problem.

Heat elements of the test section (fuel rod simulators, pheripheral rods), shroud, insulation, body) have the conventional axial-circular division. Over the height the elements are represented with 49 calculated cells, over the radius – with five rings:

– HEAT_1 – central rod,
– HEAT_2 – 6 heated fuel rod simulators of the internal (second) row,
– HEAT_3 – 12 heated fuel rod simulators of the external (third) row,
– DISP – 12 pheripheral rods,
– SHROUD – the bundle shroud together with thermal insulation and body.

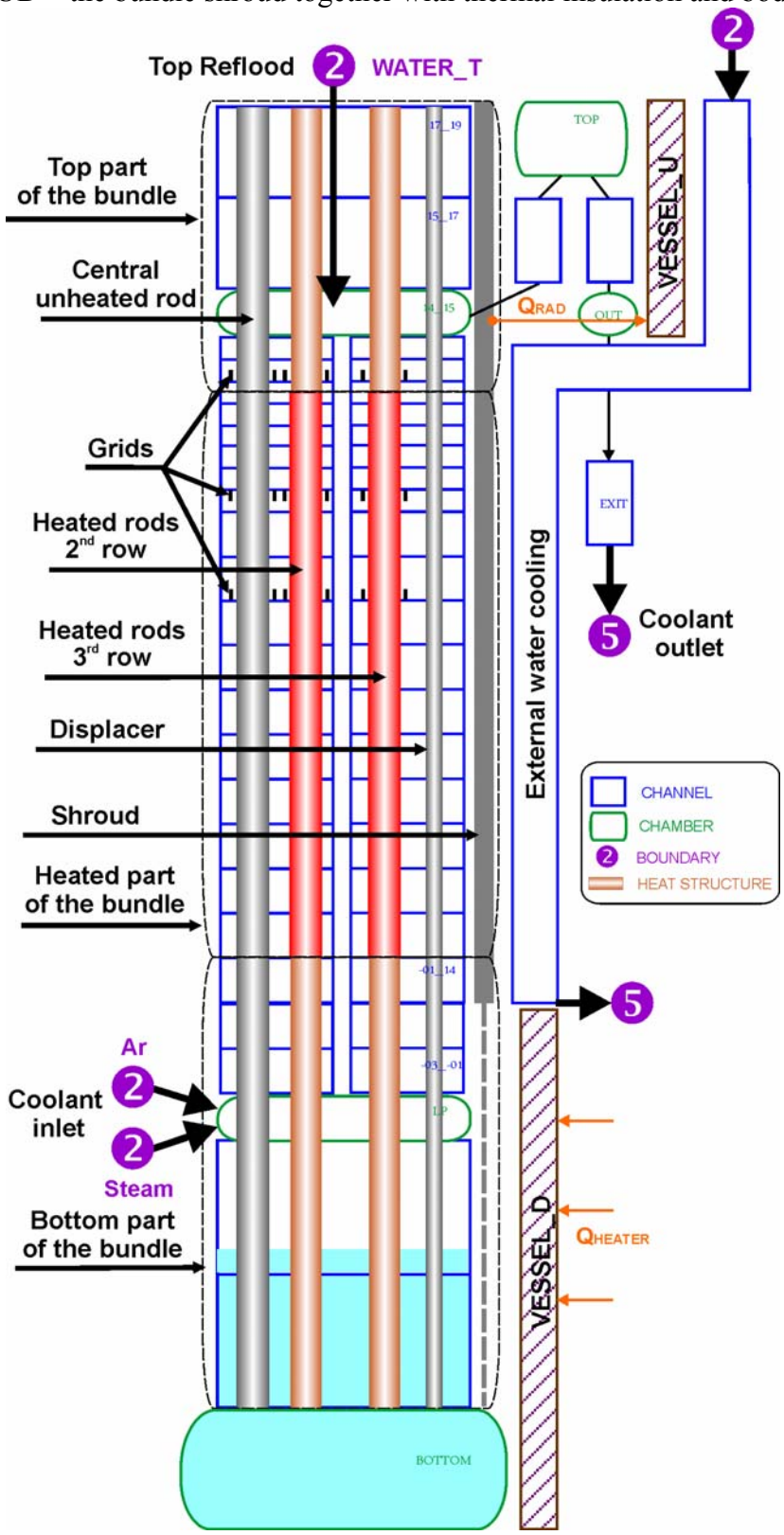

Figure 3.4. Nodalization of the test section for SOCRAT code. PARAMETER-SF3 experiment. Post-test calculations.

For evaluation of hydrogen production one thermocouples and three upper spacer grids are simulated.

The electric heating system was simulated the same way as in PARAMETER-SF2 experiment.

3.2.1.1 Initial and boundary conditions

The initial conditions of PARAMETER-SF3 experiment include the values of temperatures in the bundle, shroud, insulation, vessel at the beginning of the experiment (t=0) corresponding to indoor temperature.

The accurate experimental data of PARAMETER-SF3 on the supplied electric power were used as the boundary conditions (Figure 3.21).

For mass flow rates of steam and argon the averaging was applied (Figures 3.22 и 3.23).

The experimental flow rate of top flooding water was used.

Coolant temperature at the test section inlet was assigned proceeding from the thermal balance (see Table 3.1)

3.2.1.2 Updating of SOCRAT code

The code updating was made with the aim of assigning the spacer grids in the radiation model and consideration of their two-side oxidation.

For adequate consideration of the behaviour of spacer grids the detailed account is required for their reradiation with the surrounding components (fuel rod simulators, shroud, corner rods, steam-gas mixture). As seen from the scheme representing the test section (Figure 3.1), the geometry of radiative heat transfer is rather complicated. The exact location, sizes and mass of spacer grids should be taken into account (Table 3.3).

In the model of radiative heat transfer of SOCRAT code the spacer grids are simulated with the element of SLAB type. The radiative heat transfer is considered with all heat elements available in the test section, moreover, it is three-dimensional. According to the logic of SOCRAT code: if melting and flowing down of spacer grids occur, they stop participation in radiative heat transfer at the given axial level. Continuous change in the grids geometry is also monitored in the code – there is a possibility of calculating the view factors in three options: at each step of the calculation, once – at the beginning of the calculation, and once – within the assigned time interval.

Oxidation of spacer grids is considered using the actual surface area accessible for oxidation. Coincidence of calculated results by SOCRAT code for oxidation of grids with the data of experimental post-test study of the test section showed assuredly the adequacy of operation of new modules integrated into SOCRAT code for simulation of spacer grids.

3.2.2 Nodalization for ICARE/CATHARE code

For simulation in ICARE/CATHARE V1 code the detailed nodalization is applied. With this, separate FA physical elements are fixed to the geometry of meshing into radial and vertical cells. Figures 3.5 and 3.6 present the scheme of FA working region model in two sections.

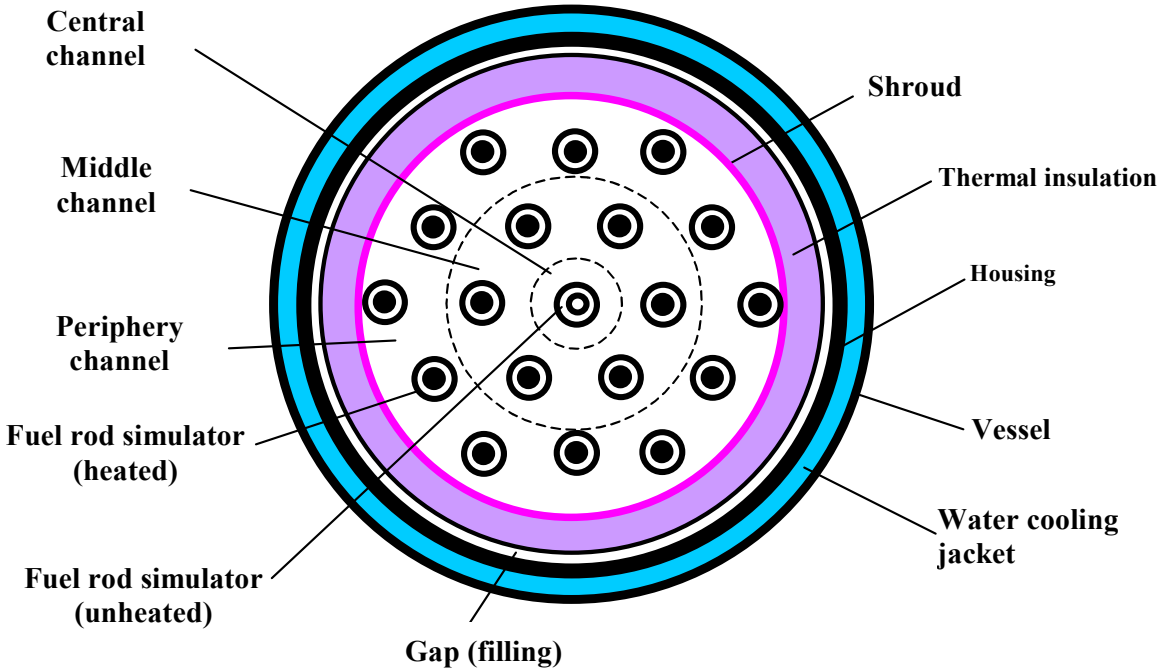

Figure 3.5. Scheme of model FA arrangement in radial section.

Figure 3.5 presents the radial meshing of FA hydraulic channel at PARAMETER facility into three parts (cells) covering the central fuel rod simulator, six middle fuel rod simulators and 12 periphery ones, respectively. With this, among the periphery ones, two groups by six fuel rod simulators are picked out with different distance to the centre for detailed consideration of radiative heat transfer.

The shroud and thermal insulation in the model (see Figure 3.5) are represented with conical rings. In all radial concentric structures the heat conduction transfer is simulated up to the water cooling jacket. Additionally for the region of the gap with filling the model of radiative heat transfer is applied.

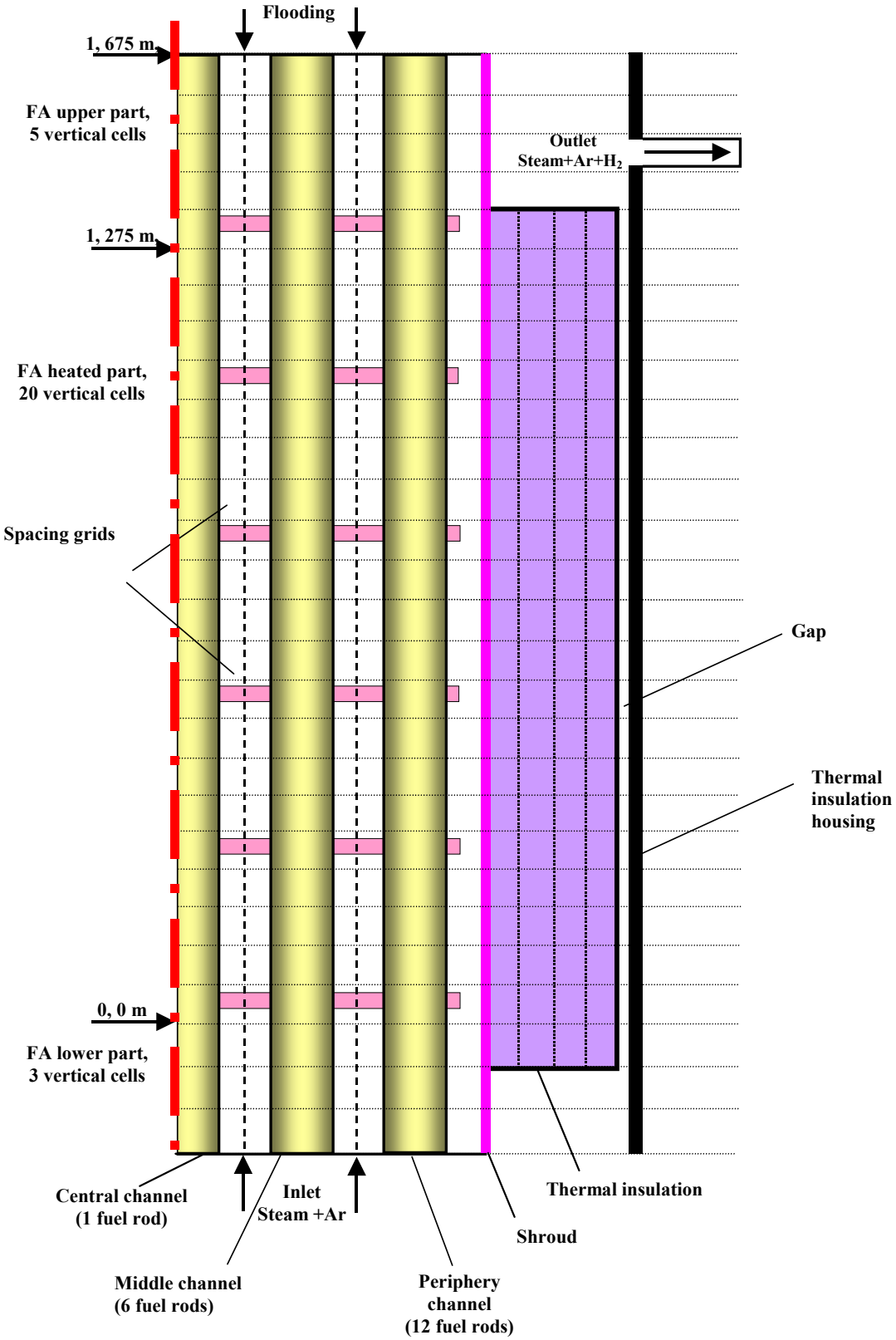

Figure 3.6. Scheme of model FA arrangement in vertical section (right side).

As shown in Figure 3.6, the FA hydraulic channel of PARAMETER facility is divided in vertical direction into 28 cells and there are three typical parts:

– lower part - upstream of the heated zone beginning;

– central part including the heated zone;

– upper part.

During simulation the nodalization is applied with small axial cell spacing (up to 6 cm in the heated zone). Proceeding from the previous calculations of experiments on reflooding using

ICARE/CATHARE V1 code, such meshing provides for satisfactory accuracy of the flooding front motion simulation.

3.2.2.1 Initial and boundary conditions

Time dependences of the electric power supplied, the flow rates of steam. Argon, water of top and bottom flooding in the calculations of SF3 experiment using ICARE/CATHARE code are assigned according to the experimental data. Total external resistance for each fuel rod was $3.5 \cdot 10^{-4}$ Ω.

3.2.2.2 Database on material properties

For the majority of materials the standard database is applied. For zirconium oxidation the correlations are applied that were developed in IBRAE on the basis of processing a number of experimental data and adapted to ICARE/CATHARE code [11].

3.2.3 Nodalization for PARAM-TG code

Nodalization used in post-test calculations of SF3 is the same as that described in section 1.2.4 and presented in Figures 1.8, 1.9. As compared to the pre-test calculations (Table 2.3) only the flow rate for cooling the upper section vessel is changed, it is 40 g/s.

3.2.4 Nodalization for ATHLET-CD code

In the nodalization of ATHLET-CD code, used in post-test calculations of SF3 and coinciding with that presented in section 1.2.5, one of changes, as compared to the pre-test calculation, was increase in the external resistance to 6 mΩ/rod, starting from the time moment of 13700 s. It was done with the aim of description of the external resistance of complete electric circuit due to break of some parallel sections.

One more change was the use of another oxidation model (IOXM=15, Cathcart/Prater-Courtright) to obtain the better agreement with the experimental dependence of hydrogen generation.

3.2.5 Nodalization for RELAP/SCDAPSIM code

Changes in the post-test calculation concerned only the geometry (the shroud was changed according to the protocol of SF3 experiment), flow rates of steam/argon and the assembly power. The simulation of displacers (corner rods) was added. Losses on current leads remained the same as in the earlier SF experiments.

The nodalization is similar to the pre-test of SF3. Boundary conditions were changed as to heat transfer on ends of the heated section by the results of the experiment.

Now in the central part (Figure 3.7) there are five groups of elements: the central rod (element *fuel*), 6 heated simulators of fuel rods of the internal row (element *cora*), 12 heated simulators of fuel rods of the external row (element *cora*), 12 displacers (element *fuel*), SHROUD – the assembly housing.

The scheme of element SHROUD is presented in Figure 3.8. It is seen that there are some changes in comparison with the pre-test calculation.

The shroud was simulated up to the water cooling jacket (inclusive).

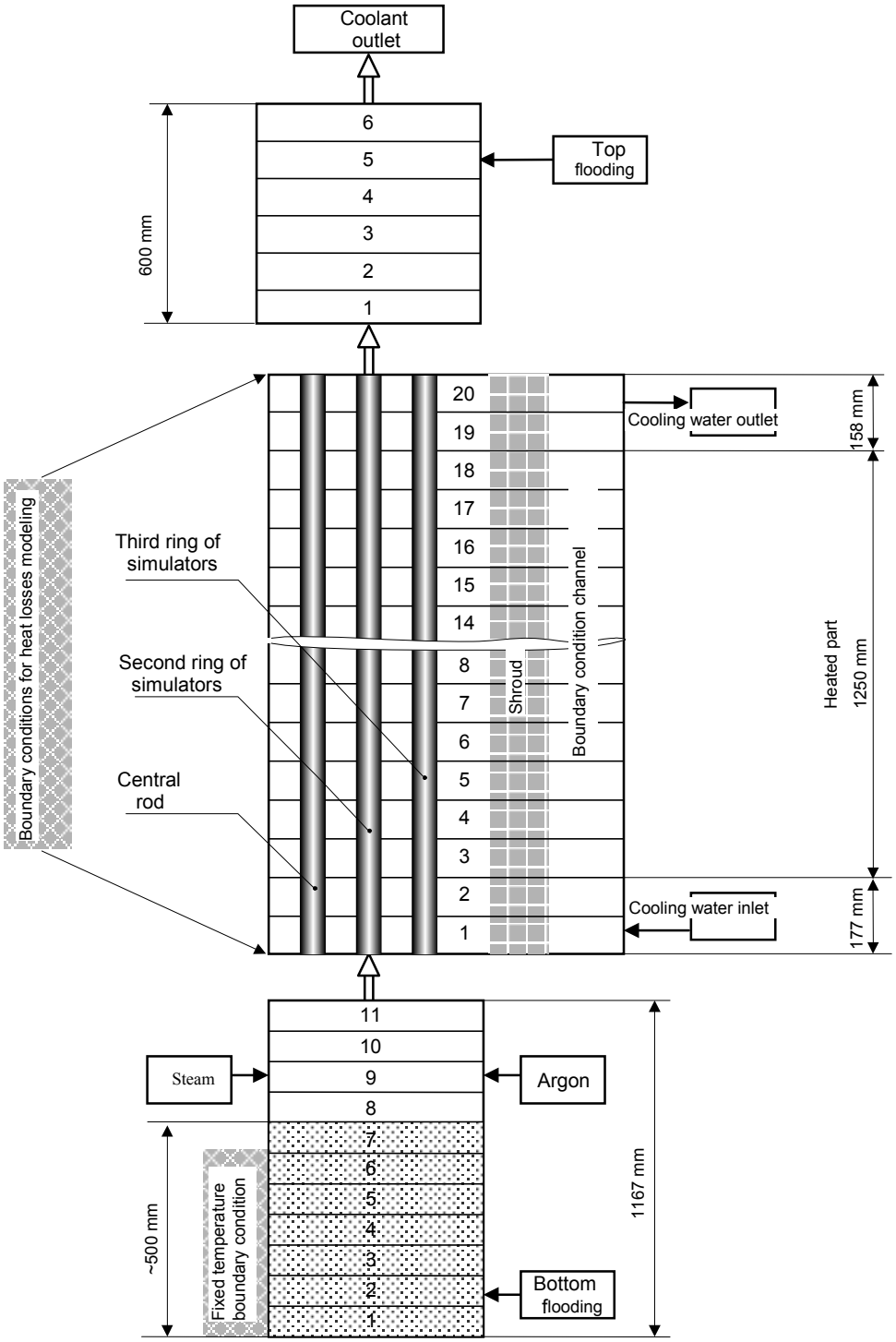

Figure 3.7. Nodalization of PARAMETR-SF facility.

1 - shroud (zirconium);
2 - insulation;
3 - insulation housing;
4 - air gap;
5 - water cooling jacket.

Figure 3.8. Schematic representation of the assembly housing.

3.2.5.1 Initial and boundary conditions

Flow rates of steam, argon, water of top flooding correspond exactly to the experimental ones. Temperature, flow rate of coolant in the channel of housing cooling correspond to the

experimental values. Due to limitation of the code the assembly is divided over the height into 20 elements and 2 types of materials are used for heaters, the simulators are modelled only in the heated part and approximately by 200 mm above and below of the heated zone. Losses on electrodes are simulated with the assigning of the contact resistance. As the input data the total power supplied to the assembly is assigned, and by assigning the contact resistance the losses in current leads are simulated. Thus, the dependence of the simulated section on the temperature are considered automatically.

For simulation of heat conduction the temperature are assigned on the ends of the simulated heated section (1610 mm) in the upper and lower parts.

Beginning of the flooding water supply is assigned not by the time, but by reaching the maximum temperature of claddings that makes possible to avoid the assembly overheating or underheating in the calculations.

In the assembly lower part from the low current leads to the inlet nozzles the wall temperature (heat structure) and water level in this channel are maintained constant.

3.2.5.2 Database on material properties

The following database on material properties is used: for the shroud materials – according to the data on experimental facility (specification SF1), for fuel, heaters and cladding – from the standard library RELAP/SCDAPSIM MATPRO.

3.3 CALCULATIONAL ANALYSIS

3.3.1 Brief description of the results of calculation participants

3.3.1.1 SOCRAT

The main purpose of simulation of SF3 experiment at PARAMETER facility (like for SF2 experiment) was the most possible accurate solution of thermal problem. For consideration of edge effects (heat loss at the end of thermal insulation, presence of water cooled flange) the changes were introduced into the nodalization (section 1.2.1). Calculated values of parameters of chemical interactions were of the secondary character and allowed to evaluate the consistency of measurement of temperatures and hydrogen production (Figure 3.60).

Unlike the SF2 experiment the results of measurements of parameters in SF3 experiment revealed two phenomena that are difficult to consider either due to small number of measurements or due to absence of the phenomenon in the preceding experiments SF2 and SF1.

The measured temperature of fuel rod simulators in the lower sections is indicative of the fact that the steam-argon mixture, entering the facility, was at equilibrium temperature considerably below (by 200 K) than that registered by thermocouples (see Figures 3.32, 3.33). Probably, in the steam flow there was finely dispersed moisture and its amount changed during the experiment.

Fuel rods internal pressure did not correspond to the pressure in the test section (Figures 3.9, 3.24).

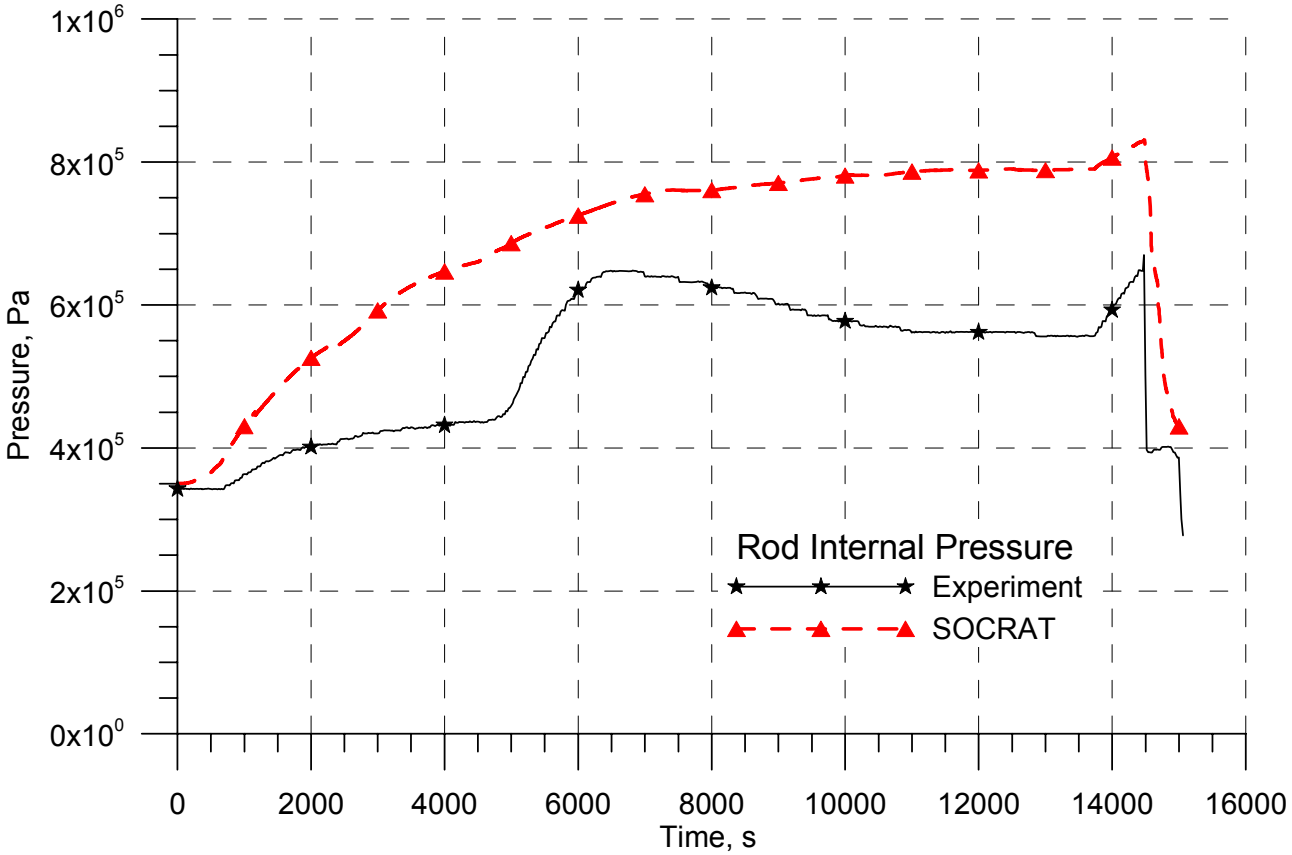

Figure 3.9. Comparison of experimental and calculated pressure in fuel rod simulators. PARAMETER-SF3 experiment post-test calculations.

It is distinctly seen from Figure 3.9 that within the interval of 6000-10000 s on the background of some increase in electric power the pressure decrease is observed in fuel rods that corresponds to their ballooning. The calculated pressure has a slight drop within the interval of 7000-8000 s, but nevertheless the calculated and experimental pressures differ qualitatively. In the calculation the highest ballooning of fuel rods was at the elevation of ~700-1000 mm, where the temperature was comparatively high and oxide scale was not so thick. This resulted in considerable (above 100 K) deviation of the calculated temperature from that measured at these elevations. One of the causes is increase in the heater-cladding temperature difference leading to local rise of power due to electric heating. Another cause is decrease in mutual "visibility" of fuel rods in the radiation model.

Nevertheless the models of SOCRAT code gave a possibility of rather exact description of the assembly temperature behaviour both in time and space, except for the elevation range of 700-1000 mm. It should be noted that temperature behaviour of the shroud (Figures 3.56÷3.59) with the use of two-channel hydraulic scheme is better described by the code than in SF2 experiment.

The calculated value of hydrogen production due to oxidation of the simulated elements was ~37 g. Among them: 28.8 g – oxidation of simulator claddings, 1.6 g – of the shroud, 1.6 g – of the spacing grids, 5.2 g – of 12 displacers (corner rods) with diameter of 4 mm. This is rather good agreement with the experimentally measured mass (34.5 g).

It can be noted that the calculated evaluation of hydrogen production due to oxidation of one thermocouple, located at the elevation of 1250 mm, was ~0.3 g. Taking into account availability of 15 thermocouples in the hottest zone (from 1000 to 1300 mm), the hydrogen mass due to oxidation of thermocouples is evaluated as ~4 g, that is, the total hydrogen production can be obtained at the level of ~40 g.

In the analysis of the code authenticity in description of the reflooding one calculated effect was noted that shall be analyzed and will require the code user's recommendations on decrease in dependence on the nodalization. The matter is that in the calculation the flooding water entered practically only on the periphery of the assembly. Absence of cross-overflows resulted in the smooth cooling down of the central fuel rods at the beginning of cooling only at the expense of

reradiation. Figure 3.10 presents a comparison of calculated values of cladding temperatures and the readings of thermocouples at the flooding phase. It follows form the Figure that SOCRAT code gives rather exact indication of the moment of the beginning of the facility upper part wetting. At the elevations of ~500-1000 mm a difference is observed both in the current values of the central part temperatures, and in the rate of its decreasing. Nevertheless the moment of wetting is predicted by the code with the accuracy of ~40 s that corresponds to an error of less than 20% - specified in the certificate of accuracy.

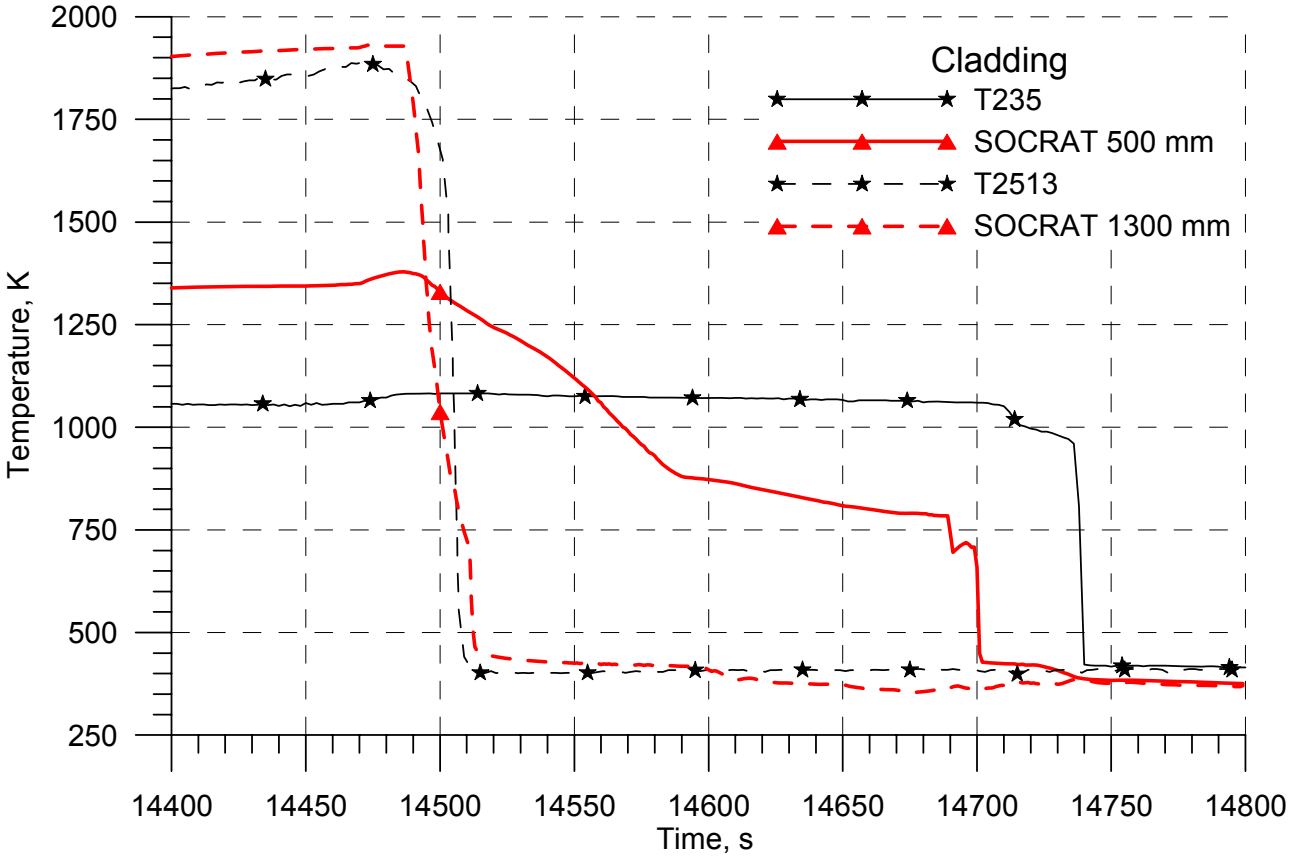

Figure 3.10. Comparison of experimental and calculated flooding motion fronts.
PARAMETER-SF3 experiment. Post-test calculations.

Addition of cross-flows and upgrading of the model of fuel rod ballooning will probably improve the accuracy of simulation of behaviour of test section components, including the reflooding phase.

3.3.1.2 RELAP/SCDAPSIM

The assembly heating-up from indoor temperature to 700 K differs from the experiment because not much attention was paid to this region of rather small significance that is required for obtaining the better agreement with the experiment. The assembly housing model, changed in comparison with SF2 experiment, allowed to obtain better agreement with the experiment as to the temperatures at the first stage, nevertheless this part requires updating. By the moment of reaching the temperature level of 900 K the calculational model is in good agreement with the experiment, as seen in the Figures. Including of flooding into the calculation takes place not by the time but by the maximum temperature reached in the experiment. Reaching this temperature occurs 300 s earlier than in the experiment. Probably this is caused by the fact that switching off the heaters in the simulators was not simulated in the calculation.

Power of steam-zirconium reaction coincides with the calculations made with the use of other codes. Hydrogen production is in agreement with the experiment both integrally (34 g – experiment, 35 g – calculation), and locally. Substantial improvement of results took place due to change in the assembly housing model and the simulation of axial heat losses. The calculation gives a slightly higher rate of oxidation within the interval of 6000-9000 s, probably this is caused by

transport delay in the channels of hydrogen amount measurement. Simulation of displacers (corner rods) gives about 3 g of hydrogen and still more 6 g is given from the shroud oxidation. The difference of less than 5% by hydrogen production practically for the whole oxidation stage allows to expect a good agreement with the experiment also concerning thickness of oxide scale.

On the whole, the temperature field is in agreement with the experiment. Within the large intervals of time and elevations the difference in temperature values in the calculation and experiment does not exceed 100 K. However there are also higher temperature deviations. Mainly they are observed after 10000 s when some heaters are switched off, and, as this process is not simulated, therefore temperatures of such simulators begin to exceed the experimental values. For some thermocouples the coincidence can be called ideal (for instance, T2212.5), for others (for instance, T386) the disagreement with the experiment can exceed 100 K. Temperature maximum is approximately at the same level as in the experiment. Maximum temperature at the pre-oxidation stage is 1570 K, maximum temperature – 1800 K, the hottest zone is located at the elevation of 1250 mm.

On the whole, the best agreement with the experiment is achieved for the simulators with the operating heaters. The rate of temperature rise at the stage of heating-up to 1800 K is in agreement with the experimental value.

Temperature behaviour and the rate of hydrogen production make possible to expect a good agreement with the experiment also concerning thickness of oxide scales. Maximum calculated thickness of oxide scale is 430 μm.

In the calculation the top flooding is started at 14200 s.

In the experiment the non-uniformity of temperatures was observed for fuel rods of one ring that is not reproduced in the calculation due to the code limitations and impossibility to change the portion of power released in different simulators depending on time.

3.3.1.3 ICARE/CATHARE

The calculations with the use of ICARE/CATHARE reproduce satisfactory the main experimental data of PARAMETR-SF3 experiment concerning the following key parameters:

– Temperature behaviour of the simulators and assembly housing under heating and subsequent cooling down;

– Full hydrogen production.

With this, the temperatures of the assembly components correspond, on the whole, to the experimental values, maximum temperatures in the calculation were obtained at the elevation of 1250 mm, and namely: 1925 K at 16459 s for the rods of the internal heated row.

Hydrogen production of 32.8 g is rather close to that measured with some underestimation of the calculated production in the period of reflooding. There is some disagreement in the time history of production within the interval of 7000 – 9000 s that can be caused by the code overestimation of mass gain in weight under Zr oxidation at low temperatures T < 1300 K.

Maximum calculated thickness of zirconium oxide scale (502 μm at 1250 mm) is considerably higher than for SF2 experiment due to elevated temperatures. As for SF2 experiment it was obtained on the very top of the heated zone for the claddings of the internal heated row of simulators. With this, at the given elevation no oxygen free β-phase of zirconium remained that is indicative of high degree of oxidation with possible cracking.

3.3.1.4 PARAM-TG

In the analysis of experimental results we can see the unusual temperature behaviour of claddings of some fuel rods, that is, decrease in temperature not agreed with power behaviour. To reveal the causes of this phenomenon the calculations of the assembly electric resistance were performed.

Figure 3.11 presents the values of the assembly electric resistance calculated by experimentally determined values of voltage and strength of current. The jumps of resistance are seen. These jumps are corresponded by the beginning of temperature drops of fuel rod claddings. Hence a conclusion was made that jumps of electric resistance correspond to breaks of heaters of

those fuel rods at which the jumps of electric resistance are corresponded by temperature drops shown in Figure 3.11. Fuel rods and times of breaks of their heaters are given in Table 3.5.

Table 3.5. Times of break of fuel rod heaters

Fuel rod	3.9	3.6	3.5	3.4	2.5	3.3	3.2
Break No.	1	2	3	4	5	6	7
Time of break, s	9898	10045	10165	10221	10497	11544	12420

Defining of broken heaters by temperature drop is, of course, is not strict. For instance, thermocouples T3310 demonstrates three drops of such a kind on breaks with numbers 4, 6 and 7. Selection of the 6th break is conventional. And behaviour of fuel rod 2.2 at the moment of 12420 s is similar to fuel rod 3.2, i.e. it can be considered broken.

In the calculation the break of heaters in fuel rods, indicated in Table 3.5, was considered. After a break the power was redistributed among the remaining fuel rods.

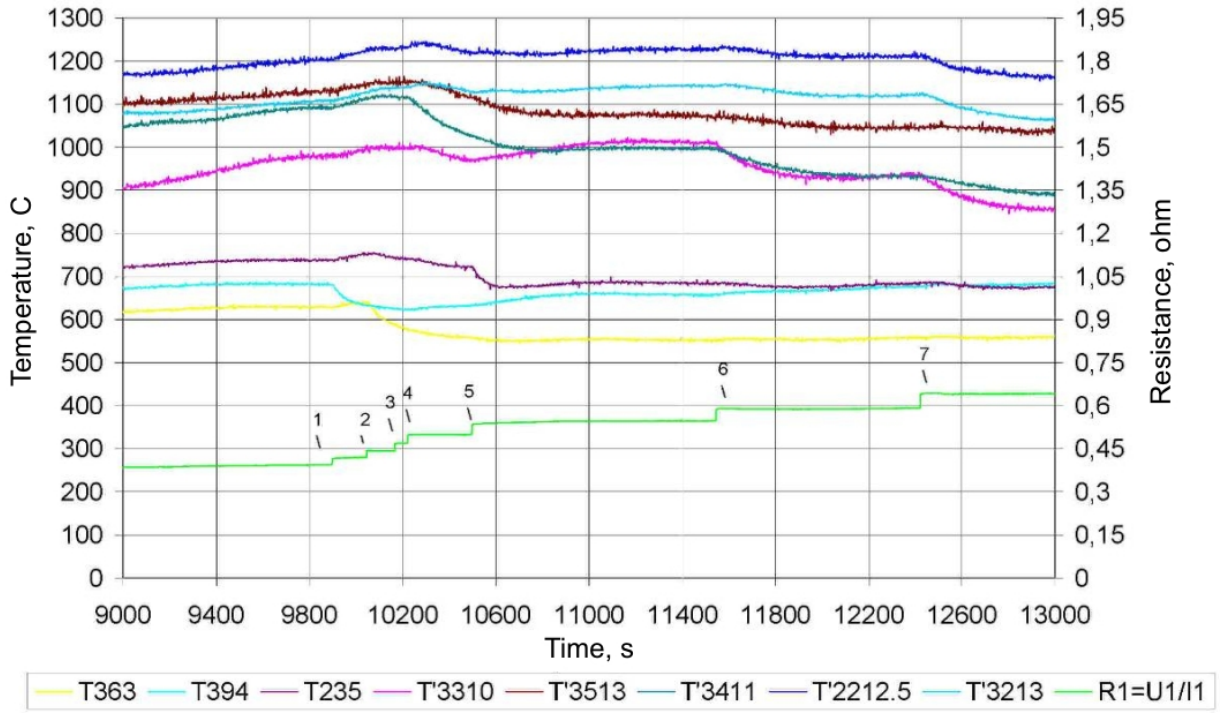

Figure 3.11. Jumps of electric resistance and their connection with temperature drops of fuel rods.

In SF3 experiment, like in SF2, the exceeding of calculated values above the experimental values is observed, especially in the lower core cross-sections. Figure 3.12 presents a comparison of calculation and experiment for fuel rod 2.6 at the core beginning. Comparison with Figure 1.15 shows that here the exceeding is substantially higher: in SF2 it was 70 K, and here – 230 K.

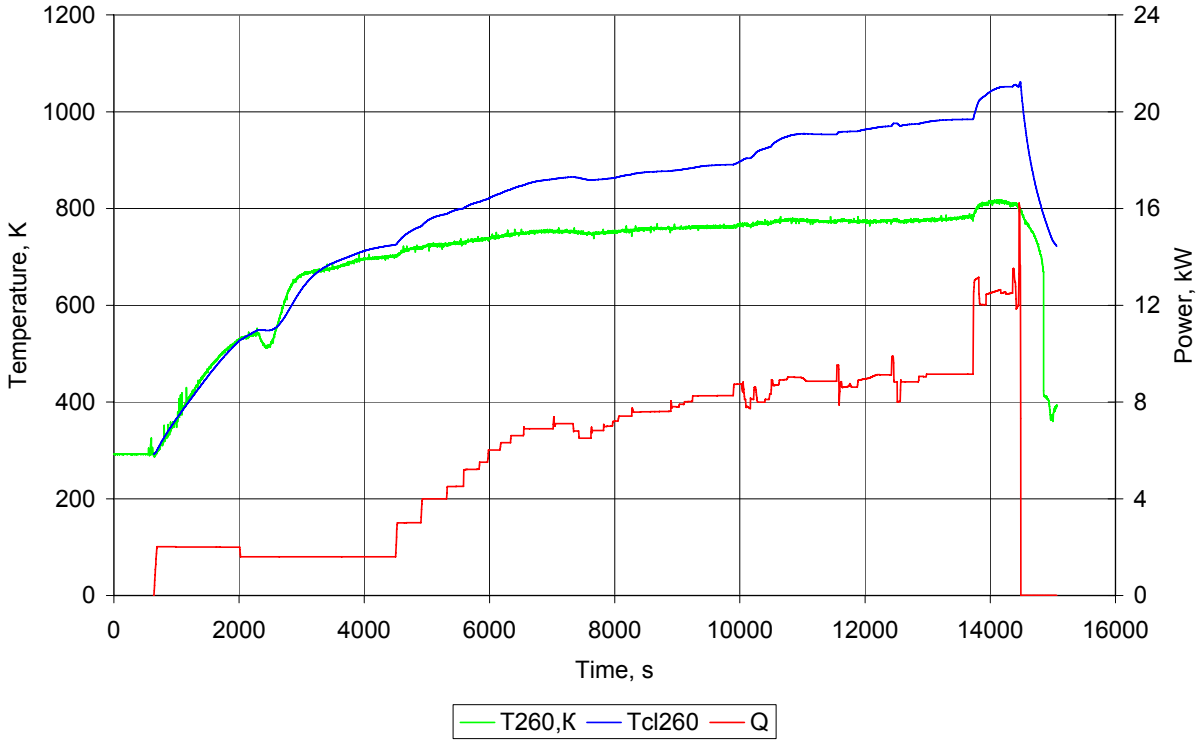

Figure 3.12. Comparison of the cladding temperature calculated value and reading of thermocouple for fuel rod 2.6 in section 0 mm.

Comparison of Figure 1.15 (SF2) and Figure 3.12 (SF3) shows s similar qualitative behaviour of temperature:

– good agreement under cooling with argon,

– substantially greater drop of temperature in the experiment as compared to the calculation under transition to steam (3 – 4 times),

– gradual increase of disagreement in calculation and experiment.

Qualitative explanation of this disagreement is the same as for SF2.

For other elevations the disagreement is also observed. Typical dependence for the fuel rod with the heater break is presented in Figure 3.13, fuel rod 3.6 with break at the moment of 10045 s. Till the time moment of ~ 7500 s the calculated values lay above the experimental values. Then before the break a rather good agreement is observed. And response to the break in the experimental is considerably greater than in the calculation.

Typical dependence for the fuel rod without break of the heater is presented in Figure 3.14. In this case the calculation values are always below the experimental ones, but the difference reduces with increase in temperature.

Figure 3.15 presents the result with the best agreement of calculation and experiment. Here in the interval of good agreement is extended almost to 14000 s. This is also a fuel rod with a break, but in section of 1300 mm the electric power is already low, therefore a break does not produce such effect as in the previous example.

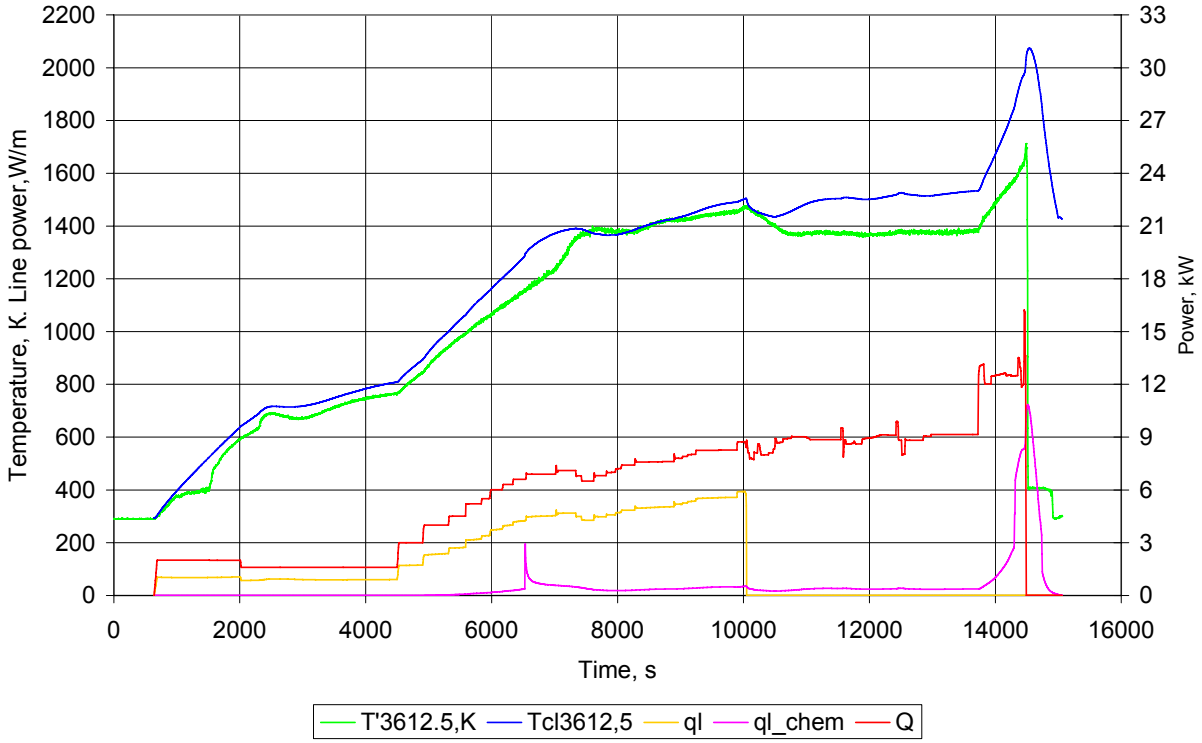

Figure 3.13. Temperature and linear heat rate of fuel rod 3.6 in section of 1250 mm. Experiment: T'3612.5 K, Q – total power. Calculation: Тст 3612,5+, ql=, qlPZr – electric linear heat rate and of steam-zirconium reaction.

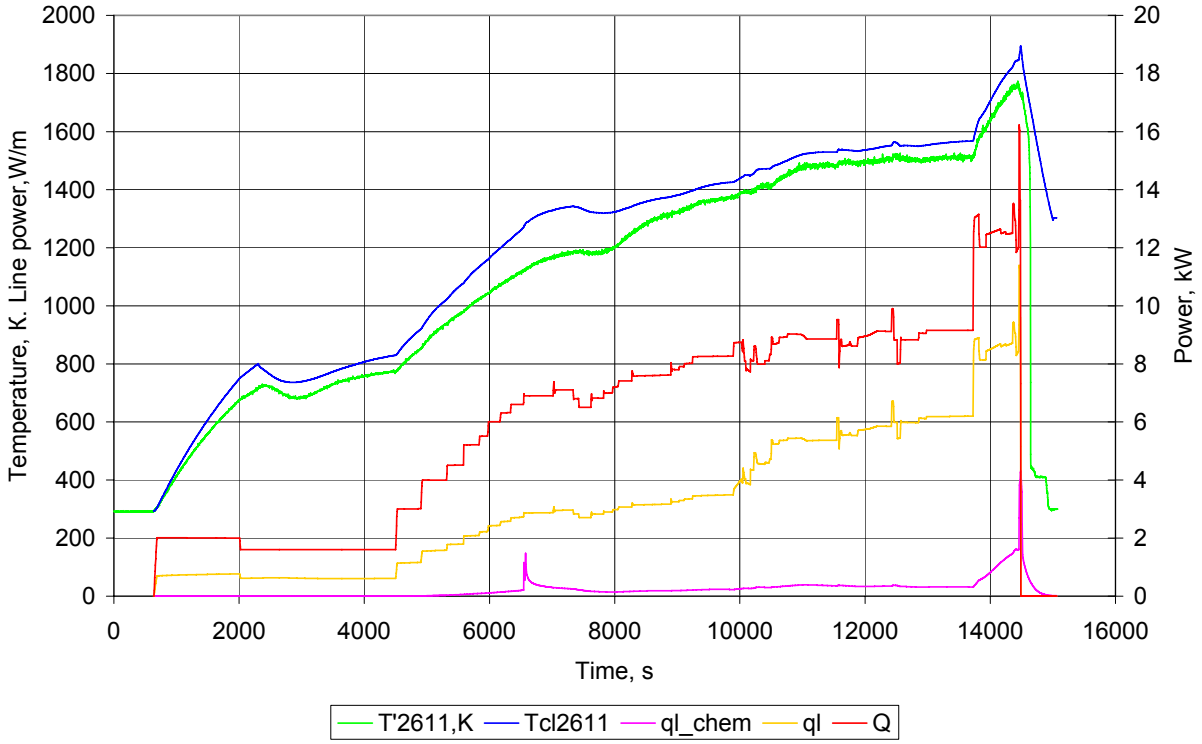

Figure 3.14. Temperature and linear heat rate of fuel rod 2.6 in section of 1100 mm. Experiment: T'3612.5 K, Q – total power. Calculation: Тст 3612,5+, ql=, qlPZr – electric linear heat rate and of steam-zirconium reaction.

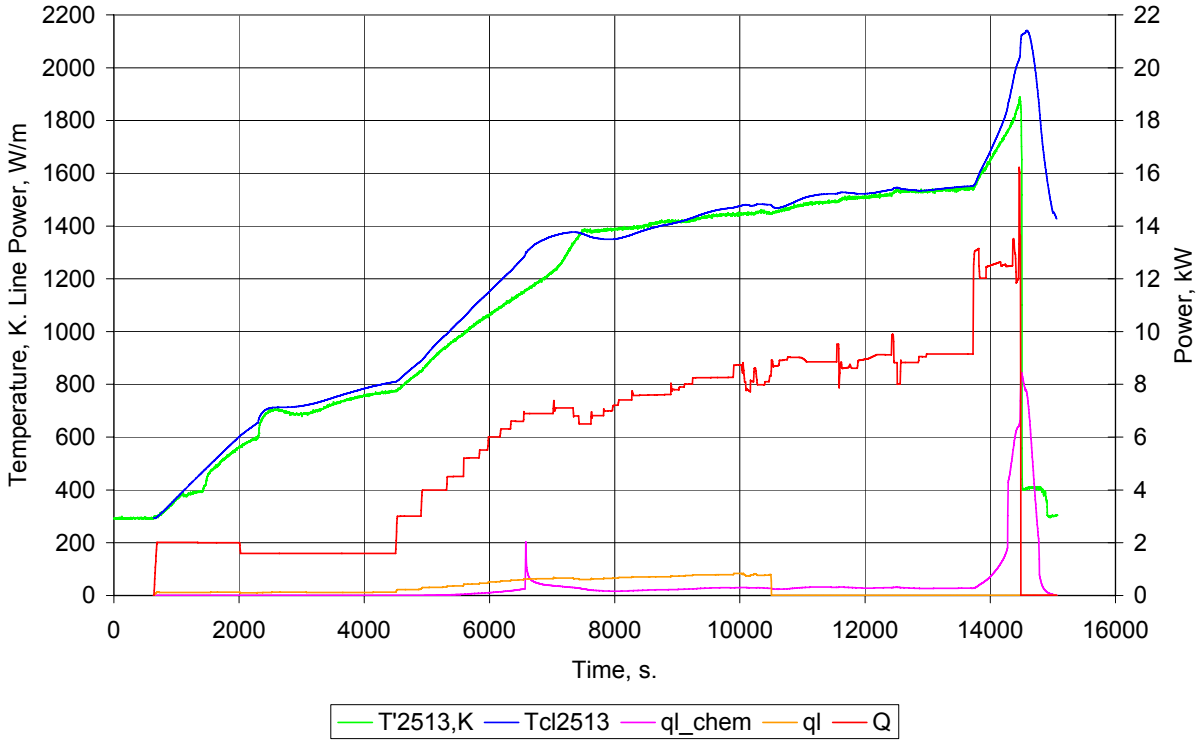

Figure 3.15. Temperature and linear heat rate of fuel rod 2.5 in section of 1300 mm. Experiment: T'2513,K, Q – total power. Calculation: Тст 2513+ , ql=, qlpZr – electric linear heat rate and of steam-zirconium reaction.

Figure 3.16 presents the values of hydrogen flow rate and integral production at the test section outlet. Steam-zirconium reaction is calculated by kinetics of RELAP code. The Figure presents also the experimental data on hydrogen flow rate and integral production by readings of COB. In the calculation the first maximum of reaction rate is observed within the interval of 6000 – 8000 s that is explained by higher calculated temperature in the is region. In the experiment the maximum of reaction rate is within the interval of 8000 – 10000 s that corresponds to temperature of 1300 – 1500 K in the high-temperature region, i.e. approximately to the same temperature interval at which the maximum is observed in the calculations.

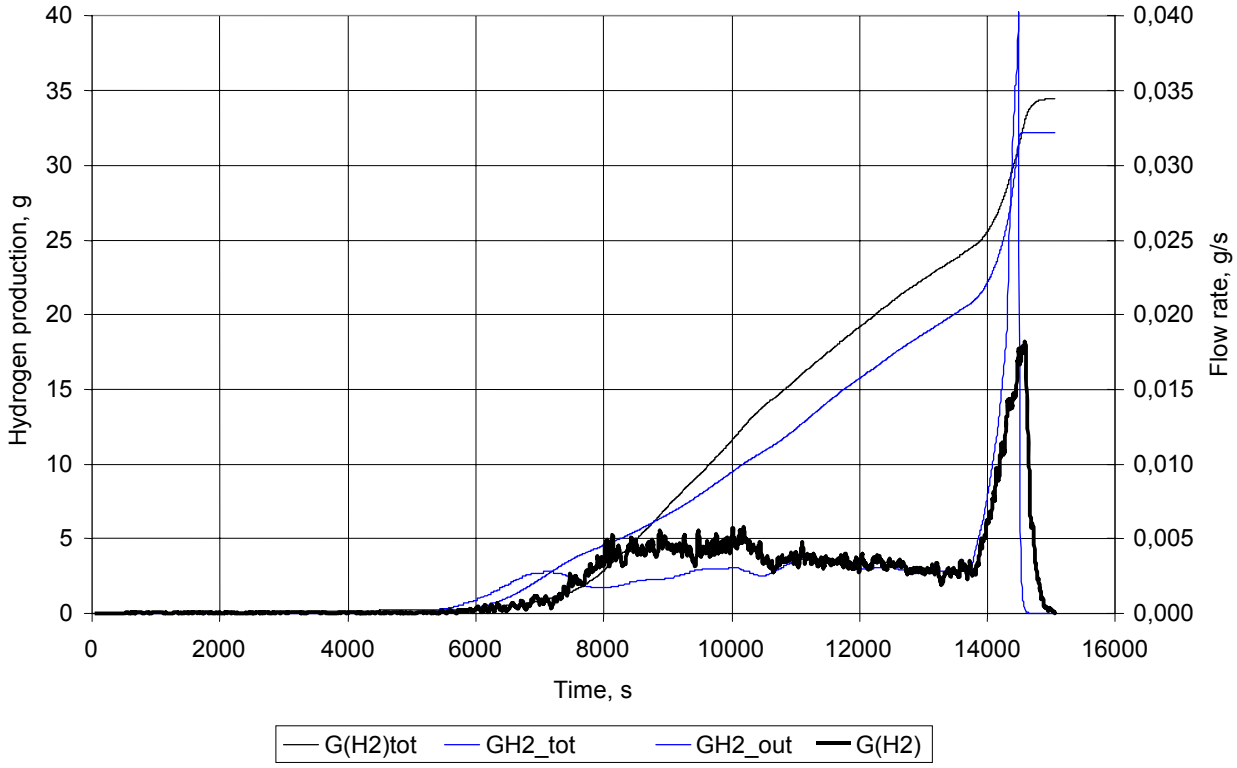

Figure 3.16. Values of hydrogen flow rate and integral production at the test section outlet, H2- calculation, (H2) – experiment, tot – integral production.

3.3.1.5 ATHLET-CD

According to the experiment assignment the top flooding in the calculation was initiated at the time moment corresponding to reaching the maximum temperature of FA - 1600°C. So, in the presented calculation there is time delay of the order of 40 s for flooding switching on. It is seen from the results obtained on flooding that motion of the cooling front is somewhat quicker as compared to the experimental data (motion of the front was calculated at the model standard parameters). Finally, the time of the assembly complete cooling was ~350 s instead of 450 s in the experiment.

In spite of this fact, there is a good agreement between the calculation and experiment for temperatures and especially between the data on the hydrogen integral production.

3.3.2 Analytical justification of the top flooding possibility

Under top flooding the water flow into the assembly is hindered due to presence of steam going upwards over the assembly (Figure 3.17). At reaching the definite mass steam flow rate, called the critical flow rate under counter-current flow limitation, the occurrence of the so-called counter-current flow limitation mode shall be observed when the flows become unstable, the waves of large length are formed on the surface, the pressure differential increases and water starts to move upwards.

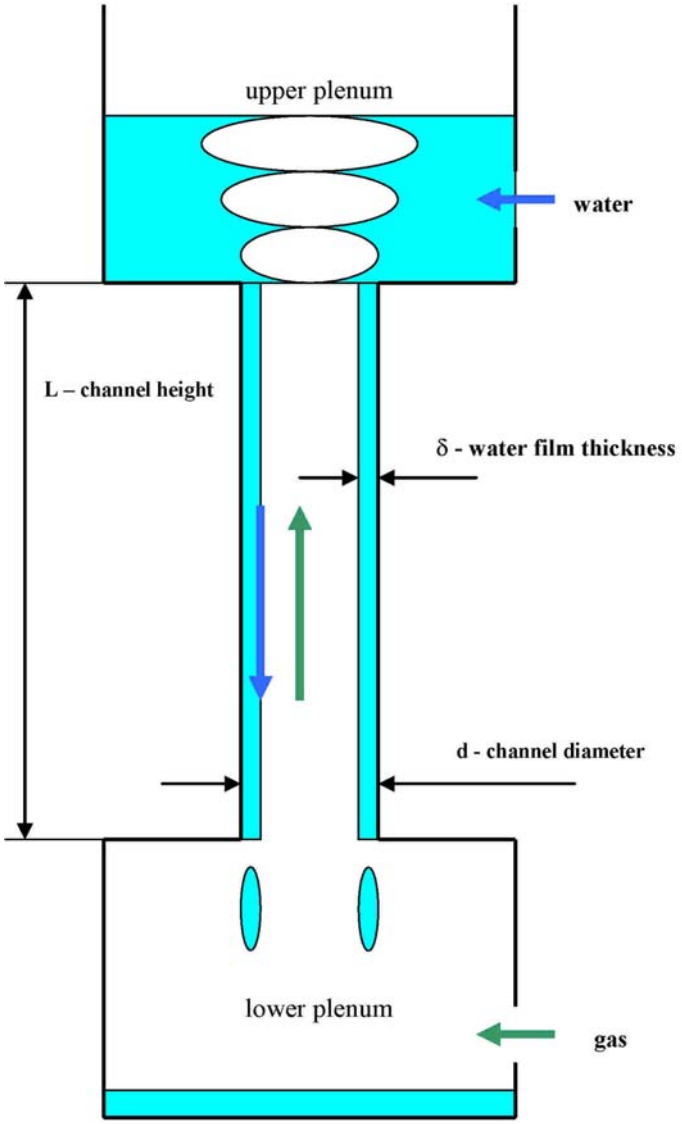

Figure 3.17. Counter-current flow limitation in the test section.

This process called as the phenomenon of counter-current flow limitation (CCFL) is described quantitatively by Wallis correlation of the following type, [22]:

$$j_g^{*1/2} + m j_f^{*1/2} = C, \qquad (3.1)$$

here A_g^* - dimensionless steam flow; A_f^* - dimensionless water flow; C - a constant governing the point of complete counter-current flow limitation (the value A_g^*, when A_f^* = 0); m – a slope of counter-current flow limitation curve.

Thus, the counter-current flow limitation curve in axes of dimensionless flows is of the following classical shape (Figure 3.18).

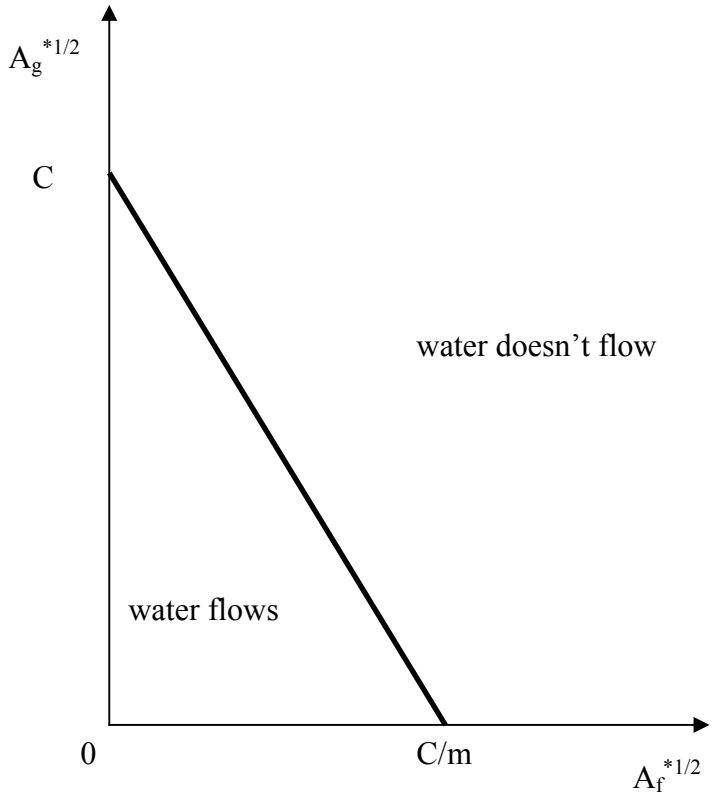

Figure 3.18. Counter-current flow limitation curve.

General correlation relationship for critical heat flux under counter-current flow limitation, describing most of the results obtained for this region, is written down in the following form:

$$q_{CHF} = \frac{C^2 B^{1/2}}{4} \rho_g h_{fg} \left[\frac{g(\rho_f - \rho_g)}{\rho_g} \right] \frac{b}{L(1+(\rho_g / \rho_f)^{1/4})^2}, \qquad (3.2)$$

here b – channel thickness, L – channel length, ρ_f and ρ_g - densities of water and steam, h_{fg} - specific heat of evaporation, C=0,7-1,0 – constant, $B = b^{1-\beta}\alpha^{\beta}$, $\alpha = \sqrt{\sigma / (g(\rho_f - \rho_g))}$ - capillary constant, σ - coefficient of capillary tension, g – free fall acceleration, 0<β<1 – empiric constant. For most of the results obtained the parameter β is equal to zero, so the behaviour of critical heat flux is proportional to $b^{3/2}$.

To begin with, let's imagine that water available on the top and coming downwards under gravity is unlimited by its amount, as it is done during the analysis of the counter-current flow limitation mode. Let's consider one hexagonal cell – one thermohydraulic channel in which the water, washing a hot rod, moves downwards and evaporates continuously (Figures 3.19, 3.20). The steam (both available already in the assembly according to the scenario, and that generated due to water evaporation) and argon will go upwards meeting the water layer.

Following the ideology of the work of [23], for the regions of steam and water in the channel the next two relationships can be obtained from the equation of motion for pressure differences in the lower (p_d) and upper (p_u) parts of the channel with height L:

$$p_d - p_u = \frac{1}{2}\rho_g u_g^2 + f_i \rho_g \frac{2\pi(R+\delta)L}{A(1-X)}(u_g + u_f)^2 + \rho_g g L, \qquad (3.3)$$

$$p_d - p_u = \rho_f g L + \frac{1}{2}\rho_f u_f^2 - f_{wf}\rho_f \frac{2\pi RL}{AX}u_f^2 - f_i \rho_g \frac{2\pi(R+\delta)L}{AX}(u_g + u_f)^2, \qquad (3.4)$$

here

$$A = d^2 \frac{\sqrt{3}}{2} - \pi R^2 \qquad (3.5)$$

is flow area per one rod in the triangle grid, and parameter X is determined from the following relationship $X = \pi\delta(2R+\delta)/A$.

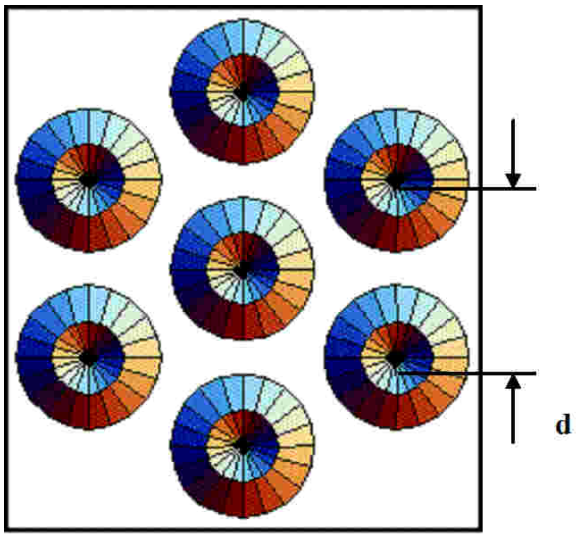

Figure 3.19. Geometry of hexagonal VVER-type FA with absence of flooding. d – grid pitch.

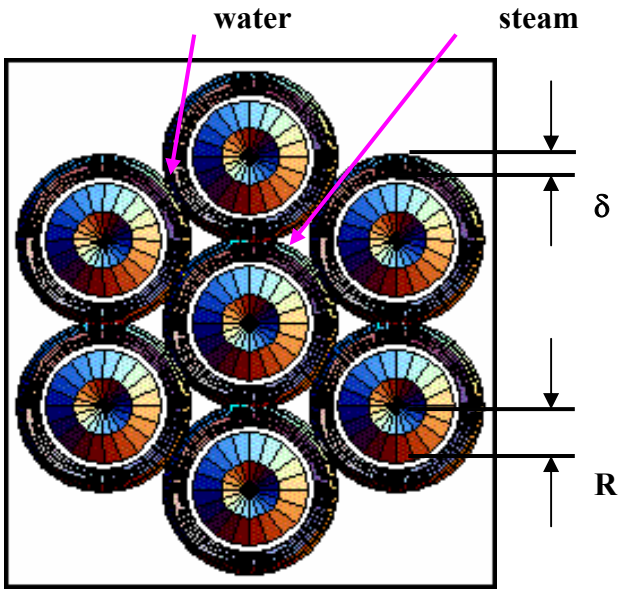

Figure 3.20. Flow geometry under top flooding. R – rod radius, δ - water film thickness.

Coefficients of friction with wall f_{wg} and f_{wf} are estimated by the following correlation relationship for laminar, transient or turbulent modes [23]:

$f_w = A\,\mathrm{Re}^B$

A=16.0, B=-1,0; Re<2000;
A=1.76·10^{-10}, B=2.32; 2000<Re<4000; (3.6)
A=0.314, B=-0.25; Re>4000

Coefficient of friction on steam-water interface is determined from the following relationship [24]:

$f_i = 0.008\left(1 + m(\delta/2d)^n\right)$

$$n = 2.18 + \frac{4.74}{Bo},\ m = 44.38 Bo^n 10^{9.07/Bo},$$

(3.7)

$$Bo = 2d\sqrt{(\rho_f - \rho_g)g/\sigma}\ .$$

Let's pass in equations (3.6, 3.7) to new dimensionless velocities

$$u_g = \frac{A}{A(1-X)} j_g = (gd)^{1/2}\left[\frac{\rho_f - \rho_g}{\rho_g}\right]^{1/2} \frac{j_g^*}{(1-X)},$$

(3.8)

$$u_f = \frac{A}{AX} j_f = (gd)^{1/2}\left[\frac{\rho_f - \rho_g}{\rho_f}\right]^{1/2} \frac{j_f^*}{X}.$$

Then the equations can be rewritten by the following way:

$$p_d - p_u = \frac{(\rho_f - \rho_g)gd}{2(1-X)^2} j_g^{*2} + f_i(\rho_f - \rho_g)gd\frac{2\pi\sqrt{R^2 + AX/\pi}}{A(1-X)}\left[\frac{j_g^*}{(1-X)} + \sqrt{\frac{\rho_g}{\rho_f}}\frac{j_f^*}{X}\right]^2 + \rho_g gL$$

(3.9)

$$p_d - p_u = \rho_f gL + \frac{(\rho_f - \rho_g)gd}{2X^2} j_f^{*2} - f_{wf}\frac{2\pi RL}{AX} gd(\rho_f - \rho_g)\frac{j_g^{*2}}{X^2}$$

$$-f_i(\rho_f - \rho_g)gd\frac{2\pi\sqrt{R^2 + AX/\pi}}{A(1-X)}\left[\frac{j_g^*}{(1-X)} + \sqrt{\frac{\rho_g}{\rho_f}}\frac{j_f^*}{X}\right]^2. \quad (3.10)$$

Then we'll obtain from (3.9-3.10) the following:

$$\frac{j_g^{*2}}{2(1-X)^2} + f_i\frac{2\pi\sqrt{R^2 + AX/\pi}L}{AX(1-X)}\left[\frac{j_g^*}{(1-X)} + \sqrt{\frac{\rho_g}{\rho_f}}\frac{j_f^*}{X}\right]^2 - \frac{L}{d} - \frac{j_f^{*2}}{2X^2} + f_{wf}\frac{2\pi RL}{AX}\frac{j_f^{*2}}{X^2} = 0 \quad (3.11)$$

Then we'll use the conditions of conservation of mass in case of steady-state flow:

$$j_f^* = j_g^*\left[\frac{\rho_g}{\rho_f}\right]^{1/2}. \quad (3.12)$$

As a result, we'll obtain:

$$j_g^{*2} = \frac{1}{\left[\frac{1}{2(1-X)^2} - \frac{1}{2X^2}\right]\frac{d}{L} + f_i\frac{2\pi\sqrt{R^2 + AX/\pi}}{AX^3(1-X)^3} + f_{wf}\frac{2\pi Rd}{AX^3}}. \quad (3.13)$$

Critical value (i.e. the value at which water in its downward motion at a distance L evaporates completely) of linear heat flux per one rod (W/m), according to the considered model, is determined proceeding from the following relationship:

$$q_{CHF} = \rho_g h_{fg} j_g \frac{A(1-X)}{L} = \frac{\rho_g h_{fg}}{F^{1/2}}\left[g\frac{\rho_f - \rho_g}{\rho_g}\right]^{1/2}\frac{d^{3/2}}{L}, \quad (3.14)$$

here the parameter F is determined in the following way:

$$F = f_i(2\pi + AX/R^2) + f_{wf}(\rho_f/\rho_g)2\pi(1-X)^3 + \frac{X^3(1-X)}{2} - \frac{\rho_f X(1-X)^3}{2\rho_g}, \quad (3.15)$$

and as X parameter the value is assumed at which the velocities (or, the critical heat flux, that is identically) the maximum value is assumed.

Maximum value is reached at

$$X = \frac{3\frac{d}{L} + 6f_{wf}\frac{2\pi Rd}{A} - \sqrt{\left(3\frac{d}{L} + 6f_{wf}\frac{2\pi Rd}{A}\right)^2 - 4\left(3\frac{d}{L} + 3f_{wf}\frac{2\pi Rd}{A}\right)\left(\frac{d}{2L_i} - f_i\frac{d}{R}\right)}}{2\left(\frac{3d}{L} + 3f_{wf}\frac{2\pi Rd}{A}\right)} \quad (3.16)$$

Let's make estimations. Heat of vaporization $h_{fg} = 2.25 \cdot 10^6$ J/kg. Then, it turns out that typical value of linear heat flux per one rod of FA will be about 2 10^3 W/m. Generally speaking, we should compare this value with chemical linear heat rate that prevails over the electric rate at later stage.

Gain in the cladding mass under oxidation is determined according to the following empiric relationship [25]:

$\Delta W^2 = Kt$, (3.17)

ΔW - mass gain, mg/cm^2; K – reaction constant, mg^2/(cm^{4}s)

Arrhenius expression is put down in the following form:

$$K = A\exp\left(\frac{-Q}{RT}\right), \quad (3.18)$$

Q - activation energy, J/mole; R – gas constant, J/(mole ·K); T – temperature, K.

Then:

$$\Delta W = \sqrt{Kt} = A^{1/2}\exp\left(-\frac{Q}{2RT}\right)\sqrt{t} \quad (3.19)$$

here

$$K = 9.772 \cdot 10^4 \exp\left(-\frac{19105}{T}\right) \qquad 1073\text{K}<\text{T}<1473\text{K} \quad (3.20)$$

In the work of [26] the following correlations are given for three temperature ranges

$$K = 8.464 \cdot 10^5 \exp\left(-\frac{20820}{T}\right) \qquad 550°\text{C}<\text{T}<1200°\text{C}$$

$$K = 1.59 \cdot 10^6 \exp\left(-\frac{23040}{T}\right) \qquad 1300°\text{C}<\text{T}<1500°\text{C} \quad (3.21)$$

$$K = 9.825 \cdot 10^5 \exp\left(-\frac{20800}{T}\right) \qquad 1500°\text{C}<\text{T}<1600°\text{C}$$

Then the linear chemical heat rate per one rod will be equal to:

$$W = \pi R Q_{oxidation}\frac{K^{1/2}}{\sqrt{t}} \quad (3.22)$$

Comparing (3.22) and (3.14) we'll finally obtain that the flooding will be successful at FA maximum temperature below the value of ~1700°C, otherwise the mechanism of counter-current flow limitation could result in overheating of rods.

Maximum temperatures in PARAMETER-SF3 experiment turned out to be about 1600°C and the flooding was successful. This fact does not contradict the results of the analytical study performed.

3.3.3 Comparison of calculation results and experimental data

3.3.3.1 Approximation of initial and boundary conditions

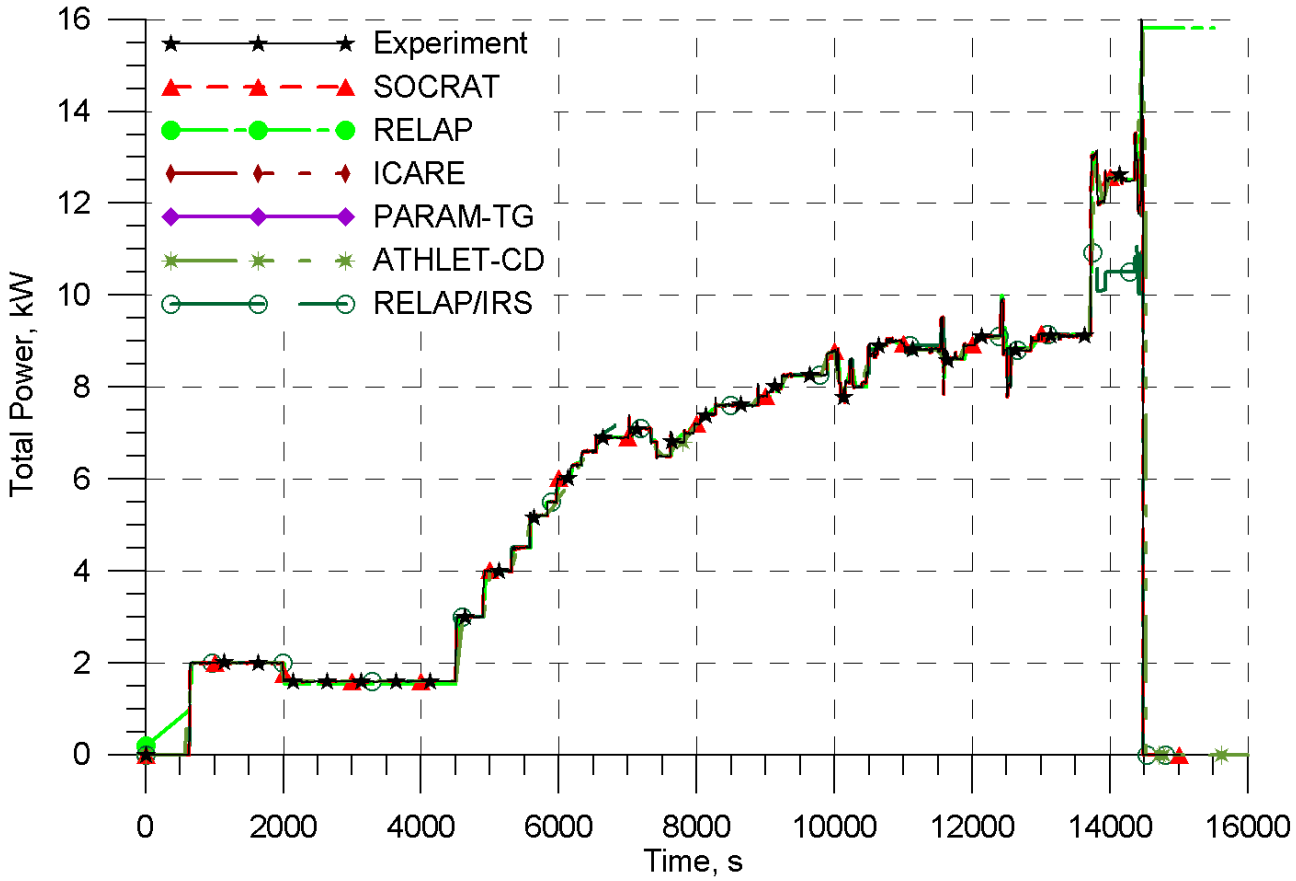

Figure 3.21. Full electric power. PARAMETER-SF3 experiment. Post-test calculations.

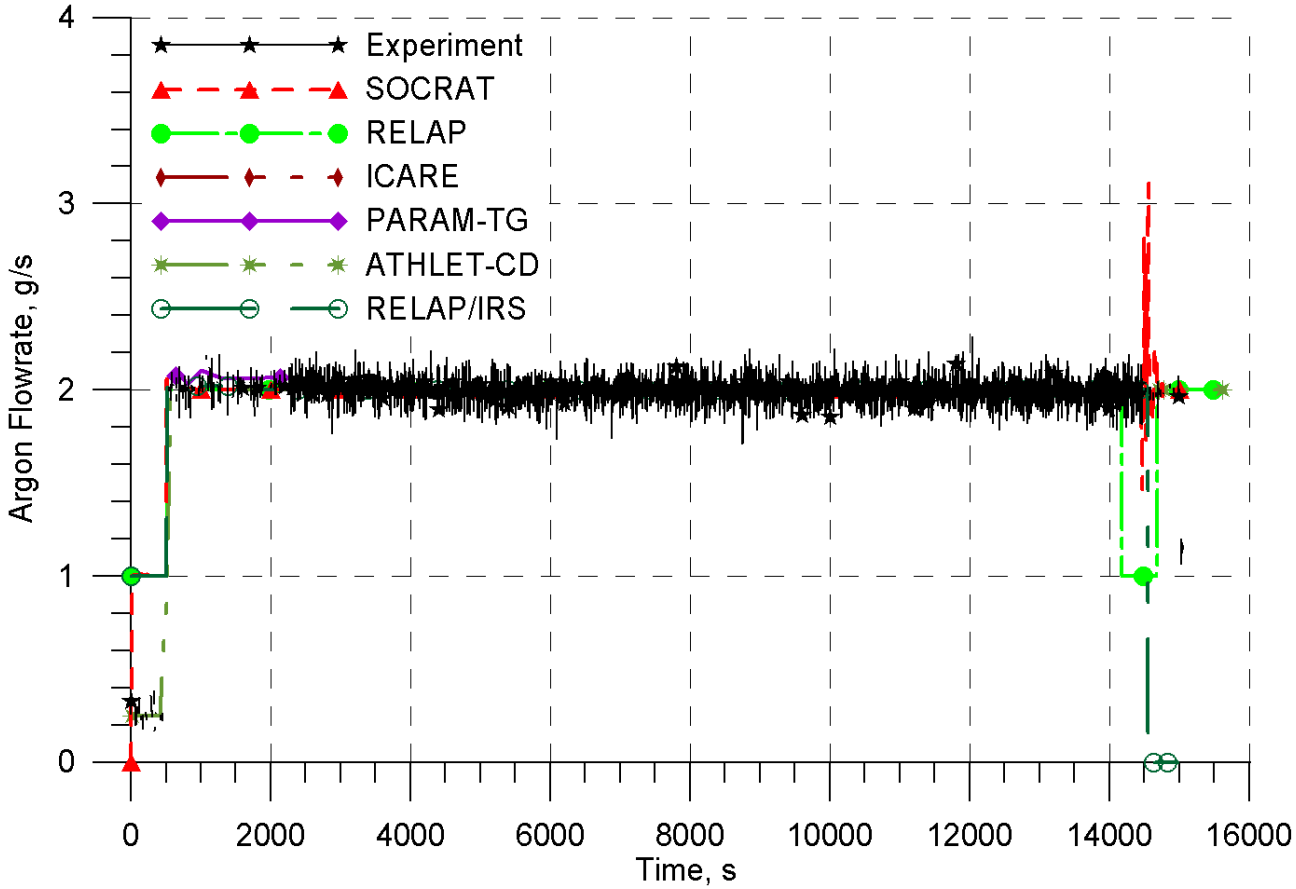

Figure 3.22. Argon flow rate. PARAMETER-SF3 experiment. Post-test calculations.

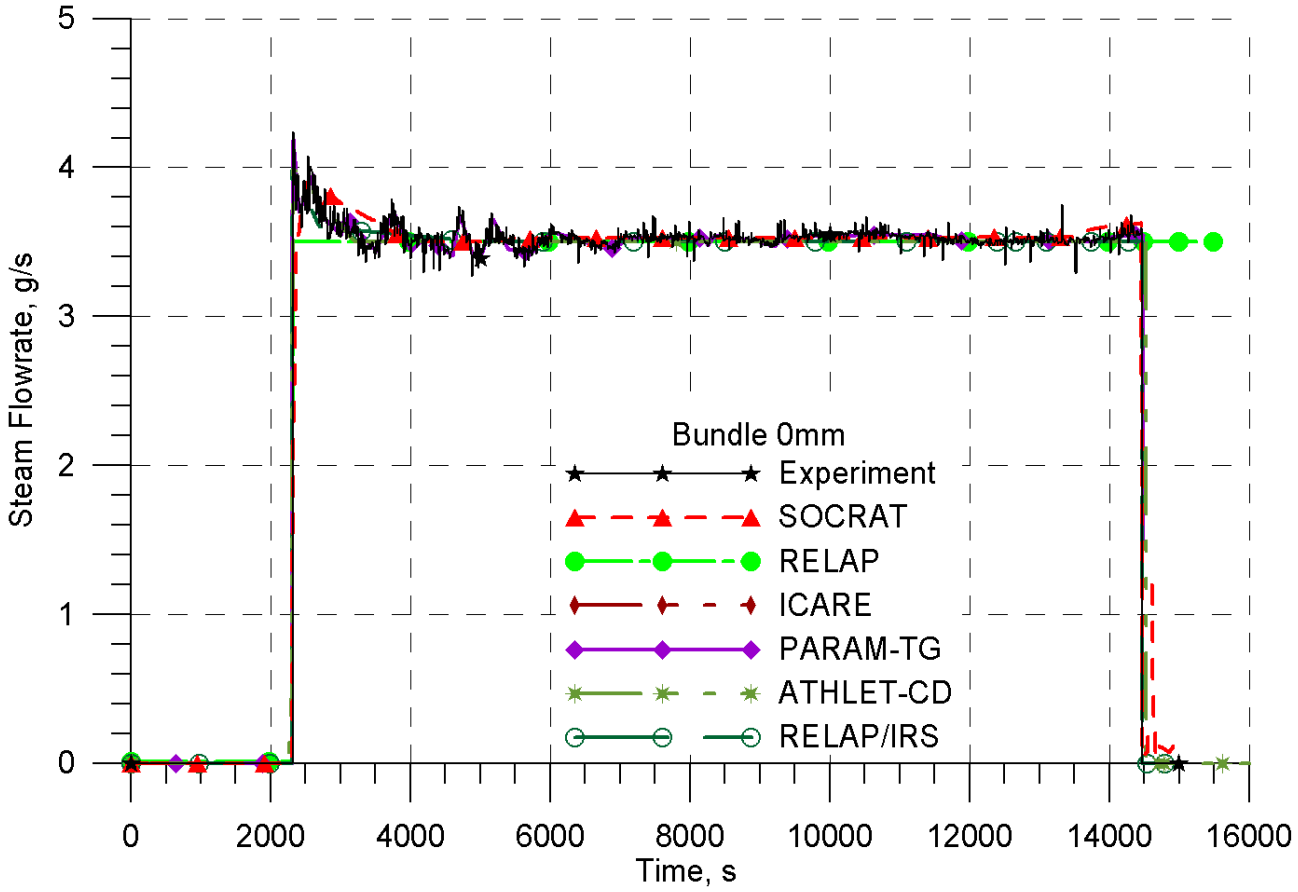

Figure 3.23. Steam flow rate. PARAMETER-SF3 experiment. Post-test calculations.

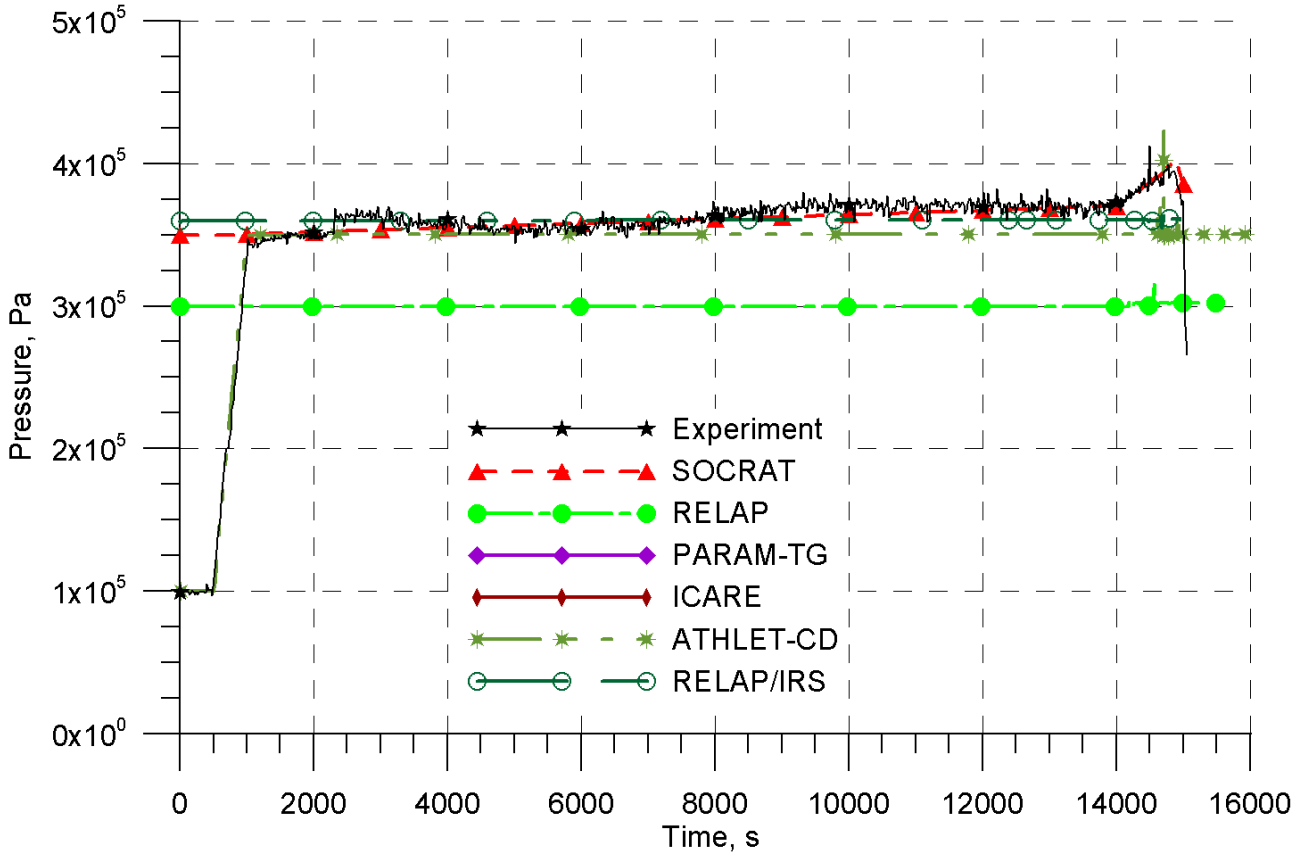

Figure 3.24. Pressure in the test section. PARAMETER-SF3 experiment. Post-test calculations.

3.3.3.2 Heat balance in the facility

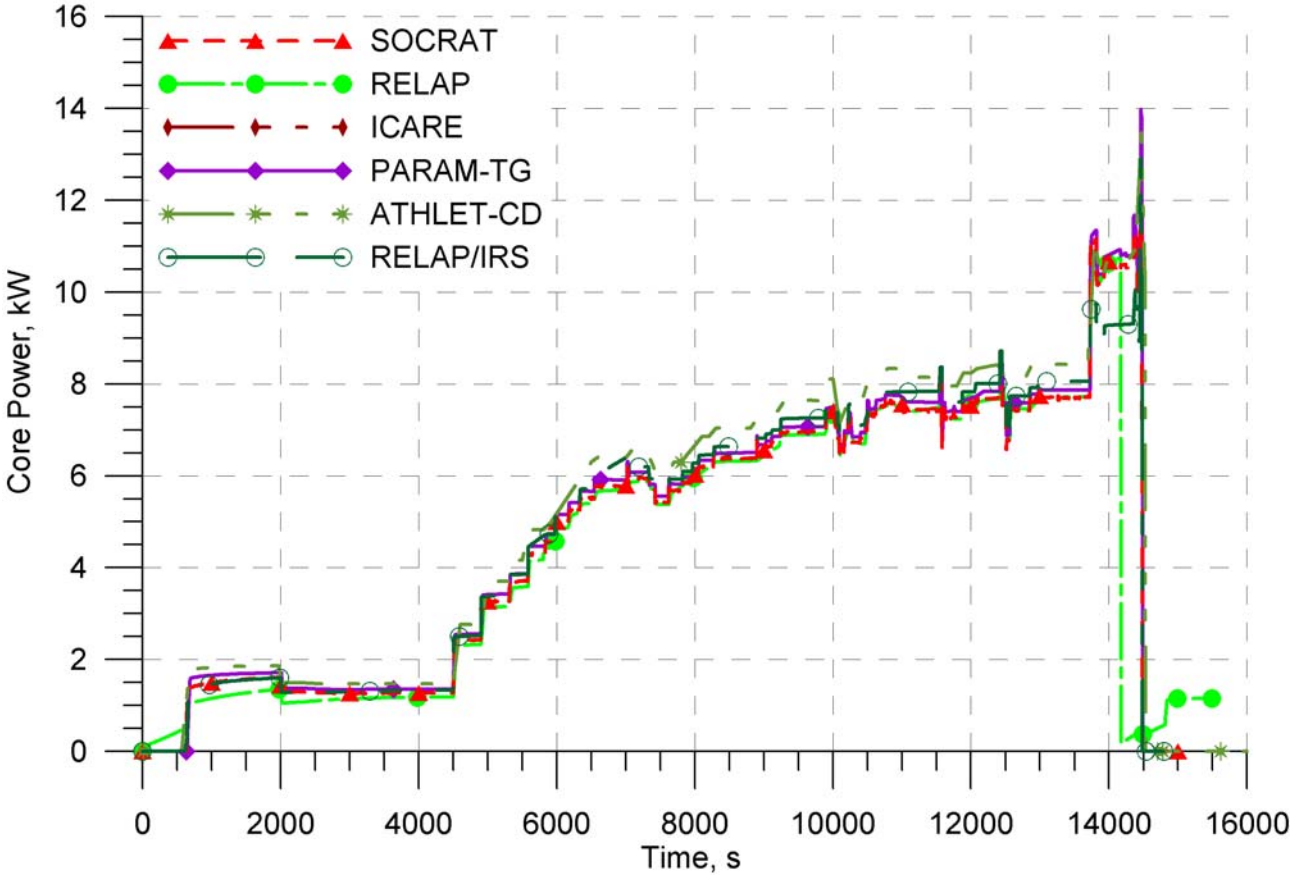

Figure 3.25. Power released in the core. PARAMETER-SF3 experiment. Post-test calculations.

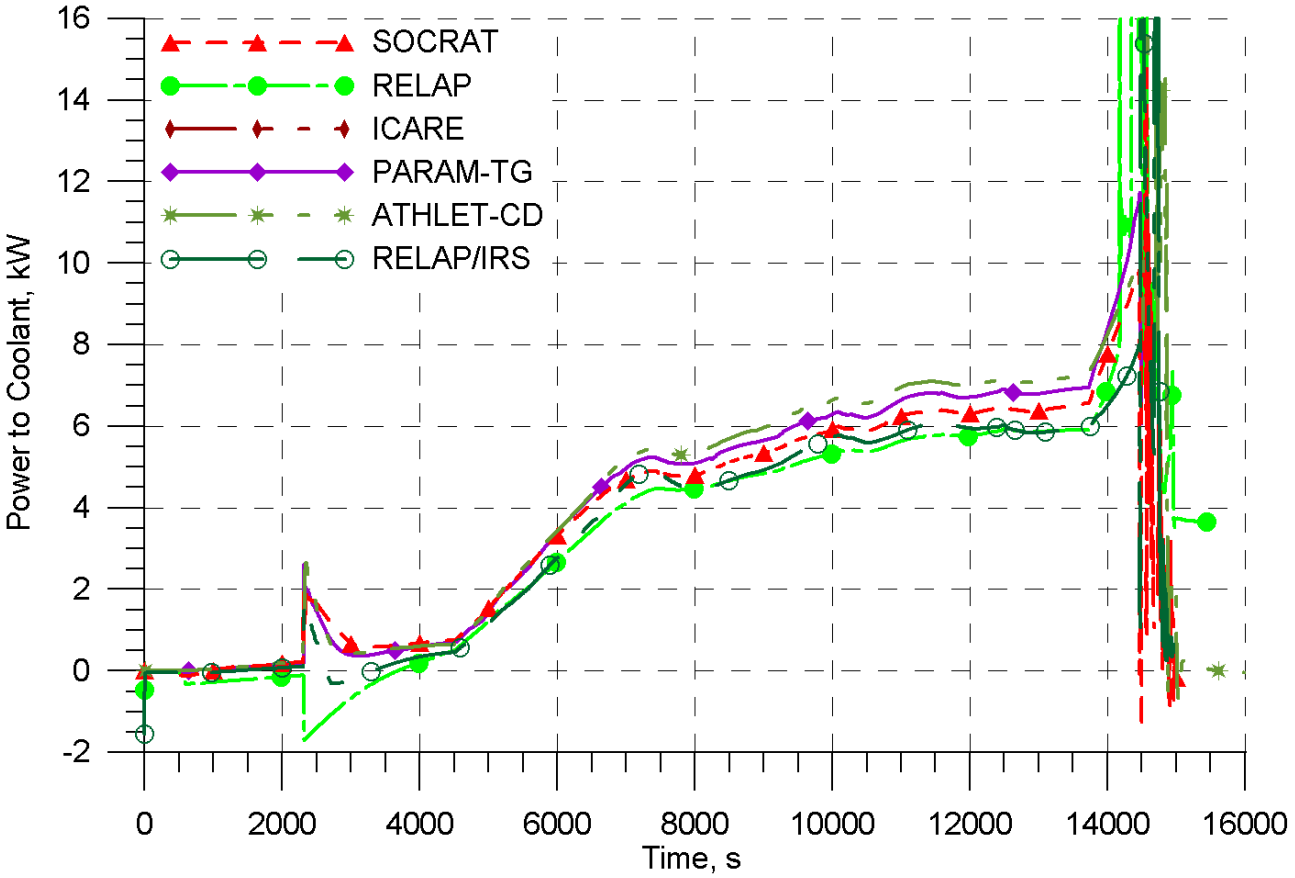

Figure 3.26. Power removed by coolant. PARAMETER-SF3 experiment. Post-test calculations.

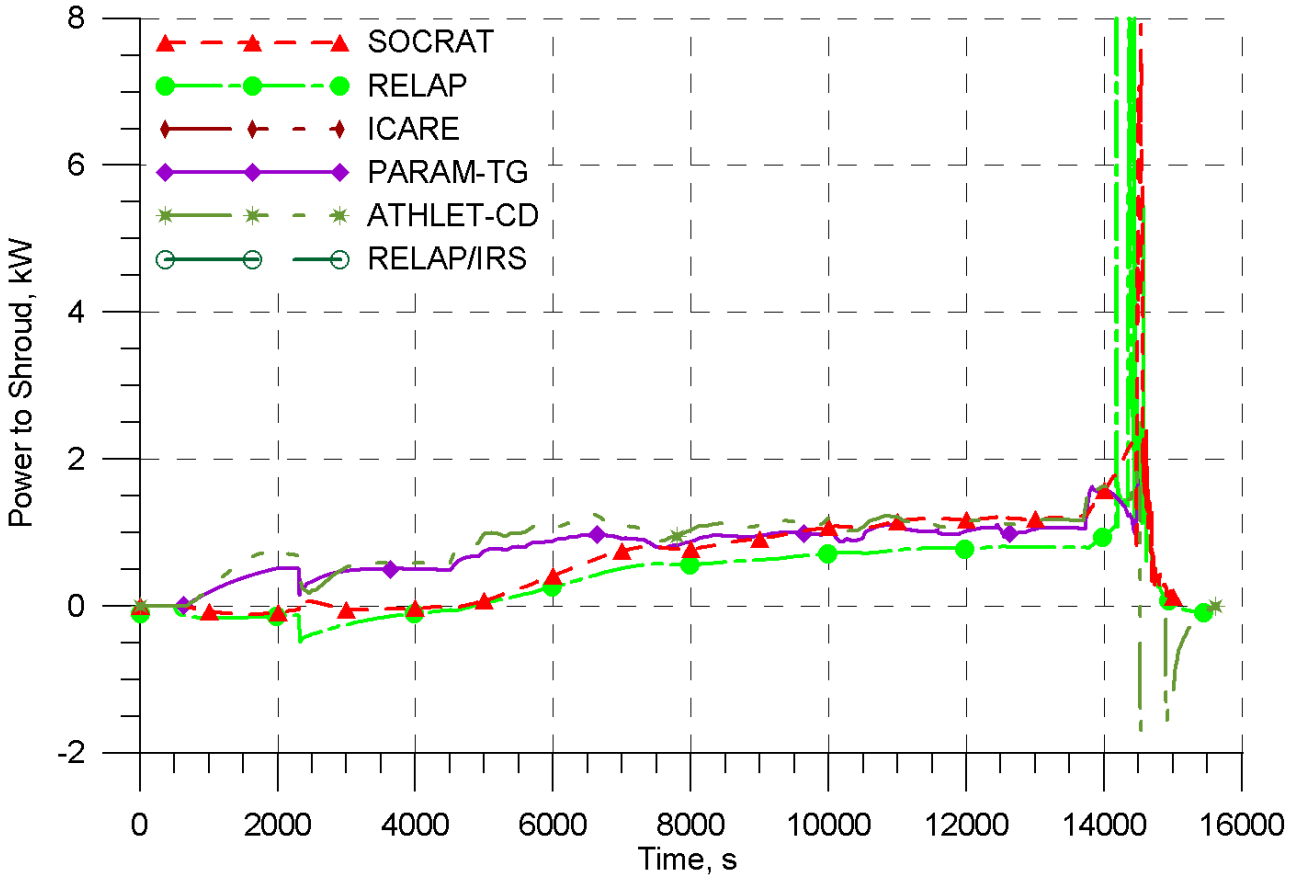

Figure 3.27. Power of heat losses to the shroud. PARAMETER-SF3 experiment. Post-test calculations.

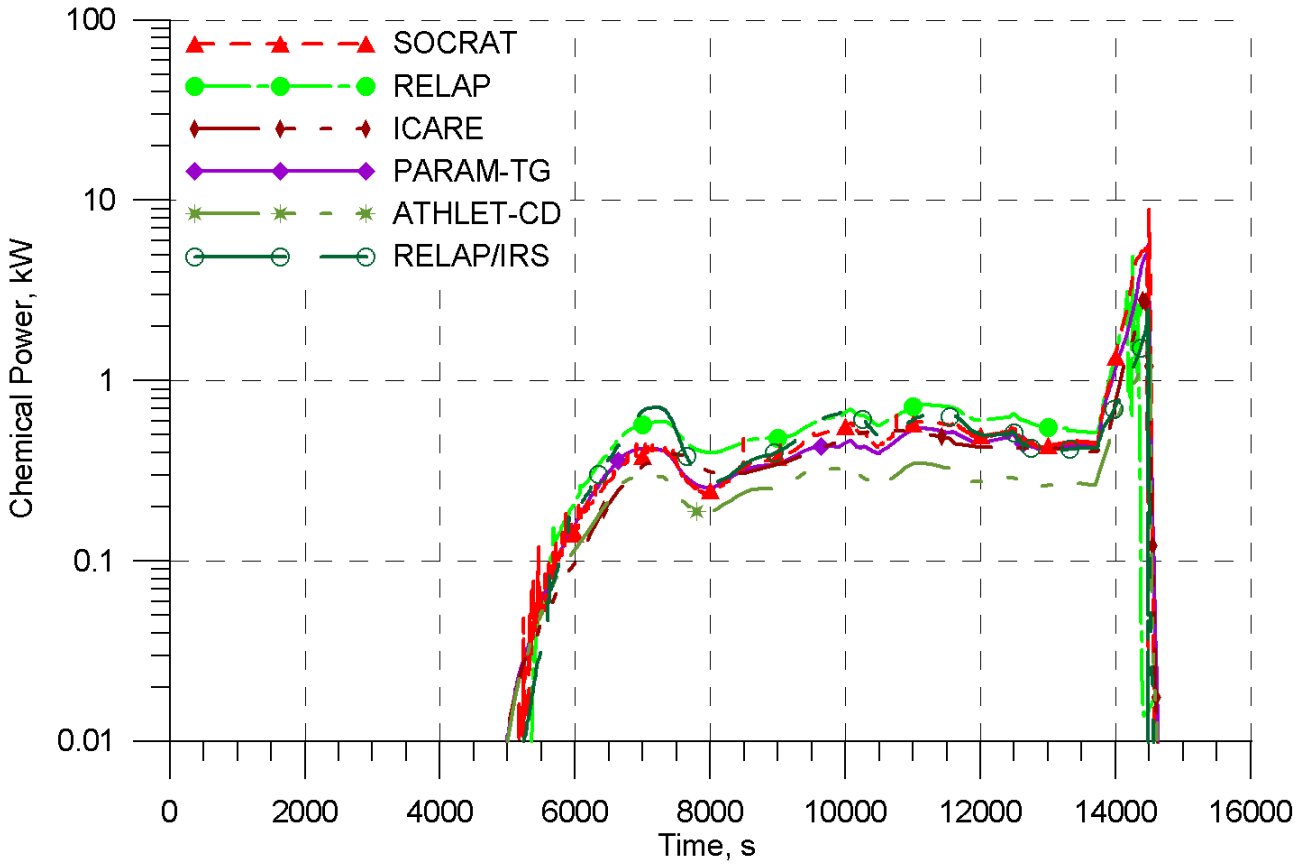

Figure 3.28. Power of chemical reactions. PARAMETER-SF3 experiment. Post-test calculations.

3.3.3.3 Cladding temperatures of fuel rod simulators

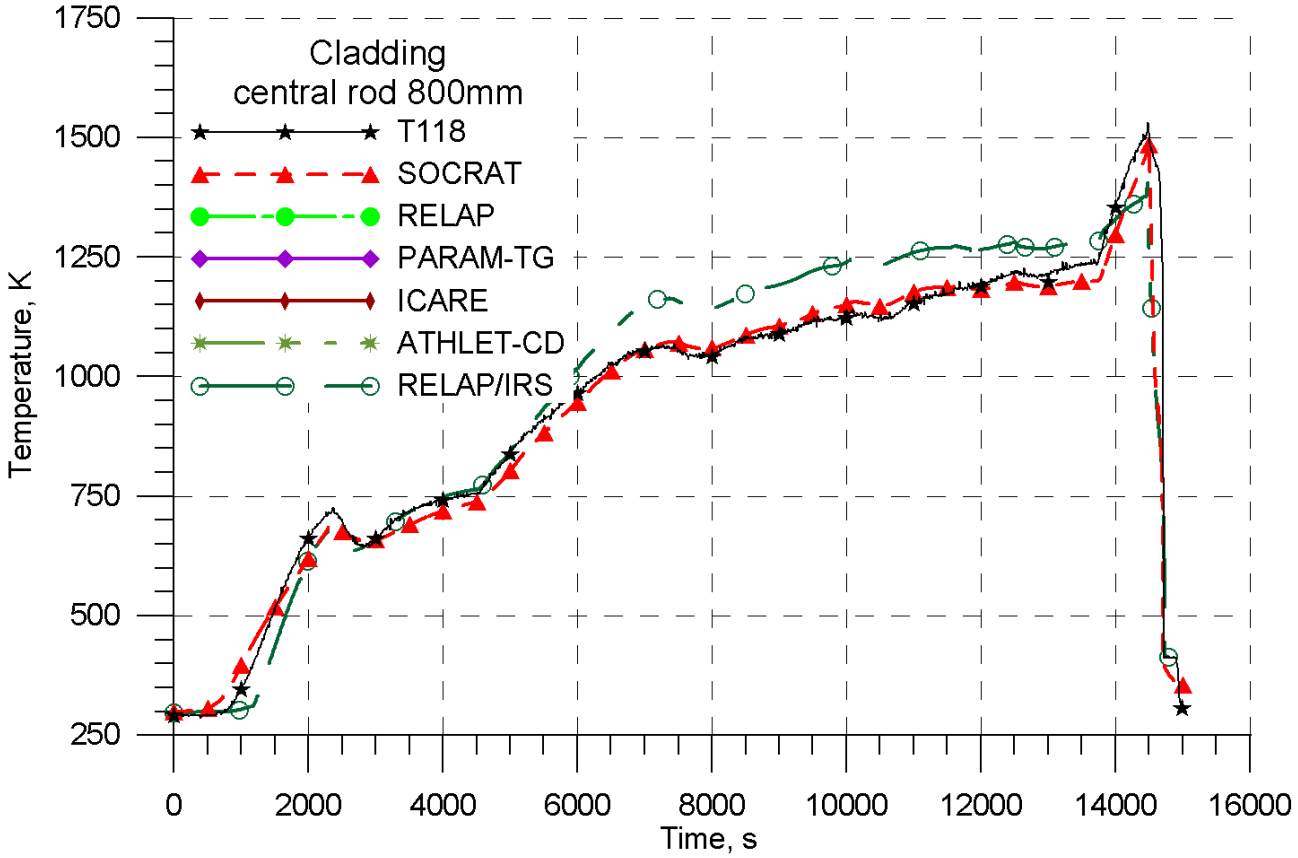

Figure 3.29. Temperature of central fuel rod cladding at the elevation of 800 mm. PARAMETER-SF3 experiment. Post-test calculations.

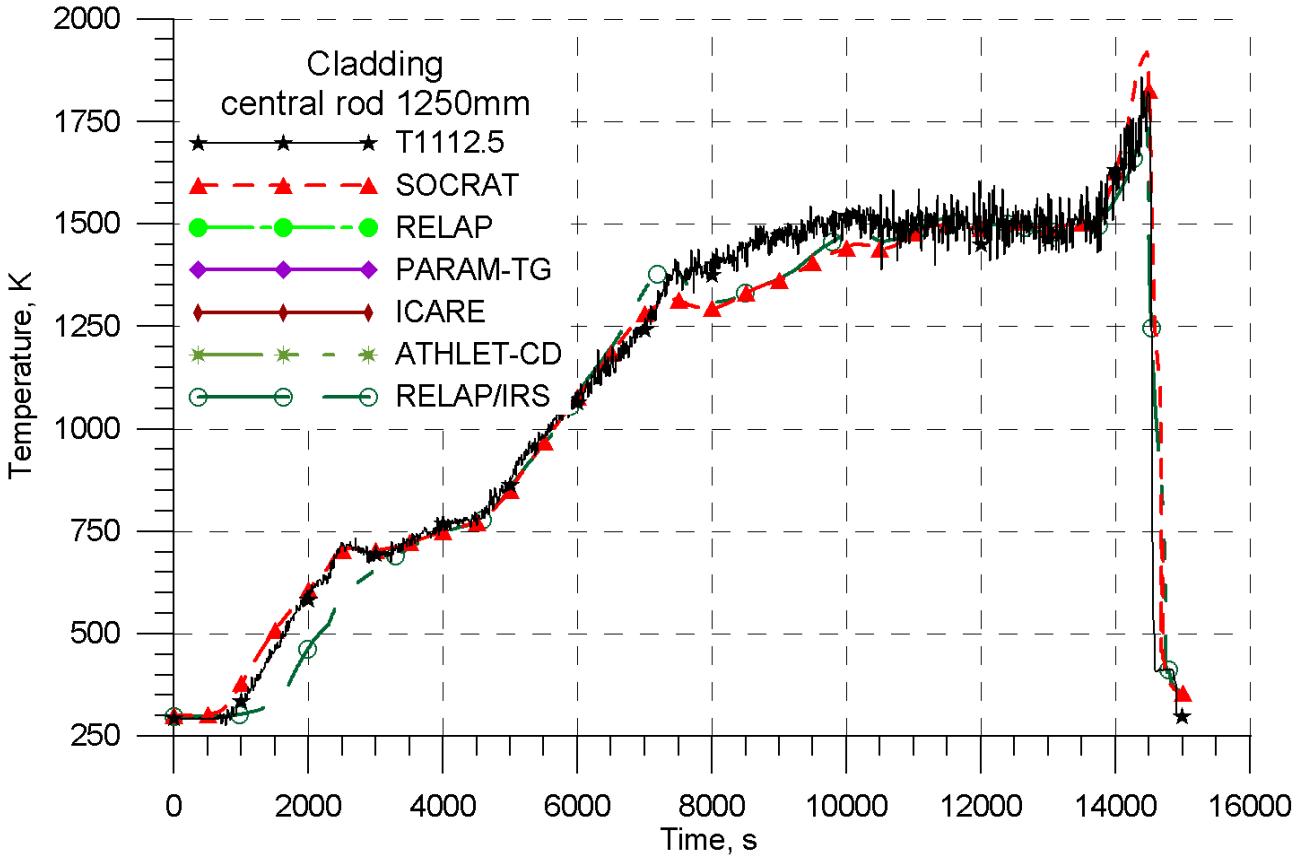

Figure 3.30. Temperature of central fuel rod cladding at the elevation of 1250 mm. PARAMETER-SF3 experiment. Post-test calculations.

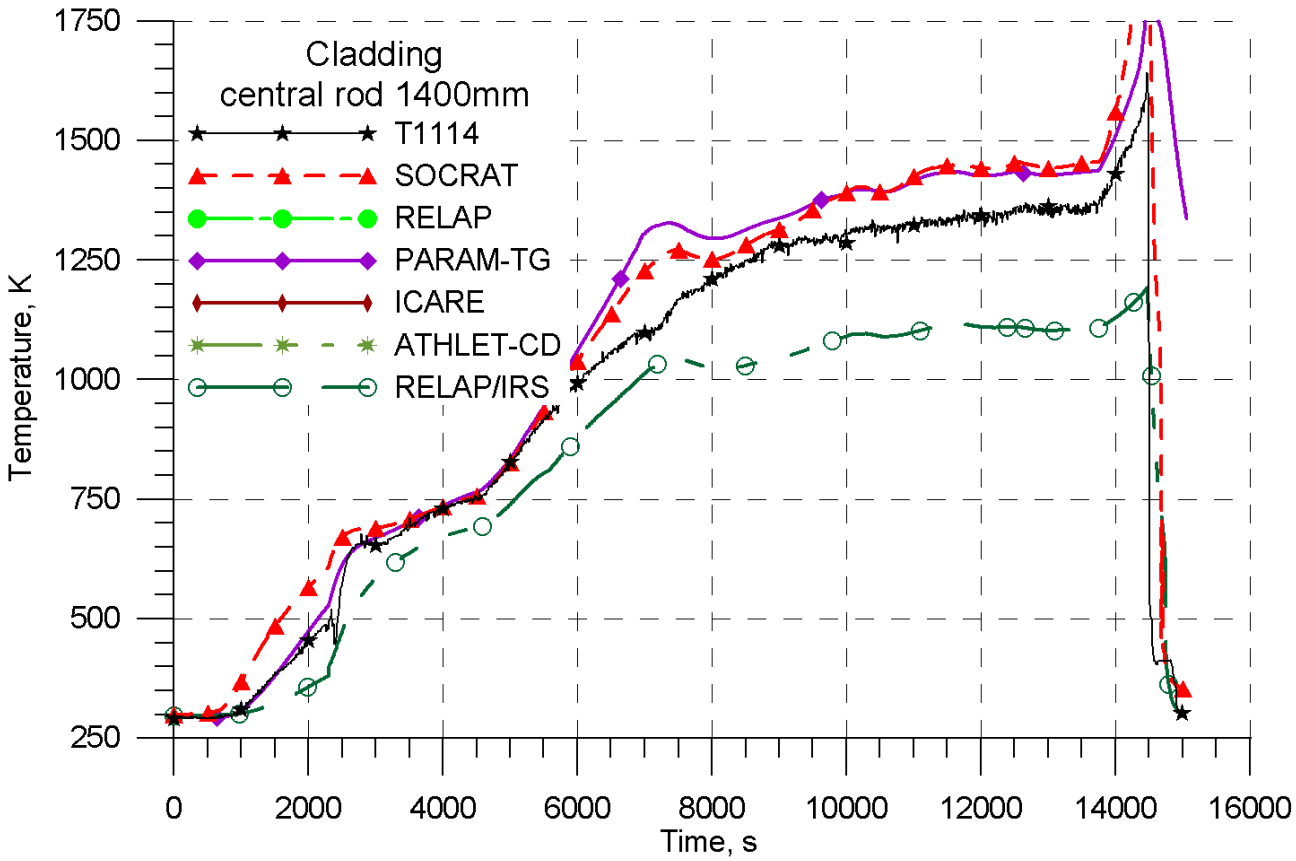

Figure 3.31. Temperature of central fuel rod cladding at the elevation of 1400 mm. PARAMETER-SF3 experiment. Post-test calculations.

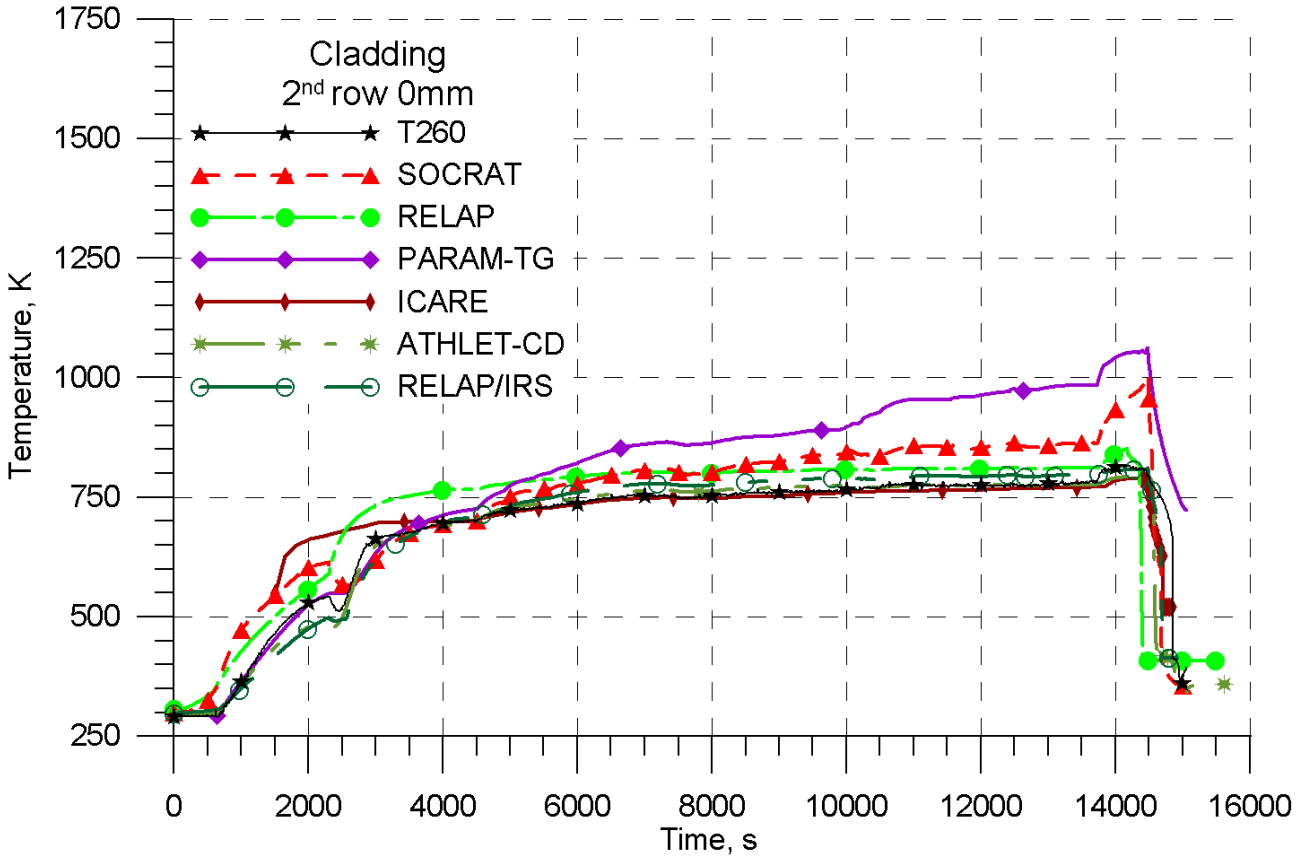

Figure 3.32. Cladding temperature of fuel rod in the second row at the elevation of 0 mm. PARAMETER-SF3 experiment. Post-test calculations.

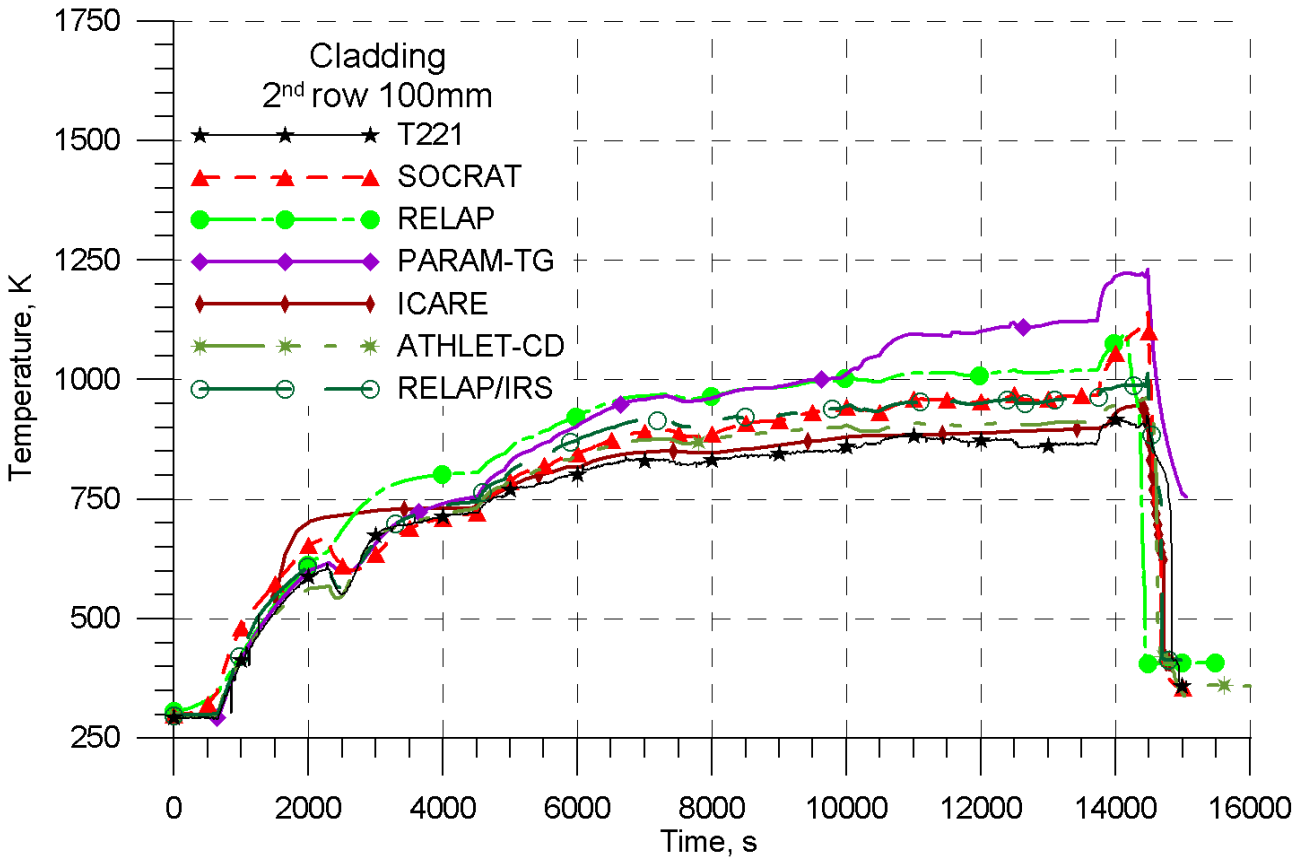

Figure 3.33. Cladding temperature of fuel rod in the second row at the elevation of 100 mm. PARAMETER-SF3 experiment. Post-test calculations.

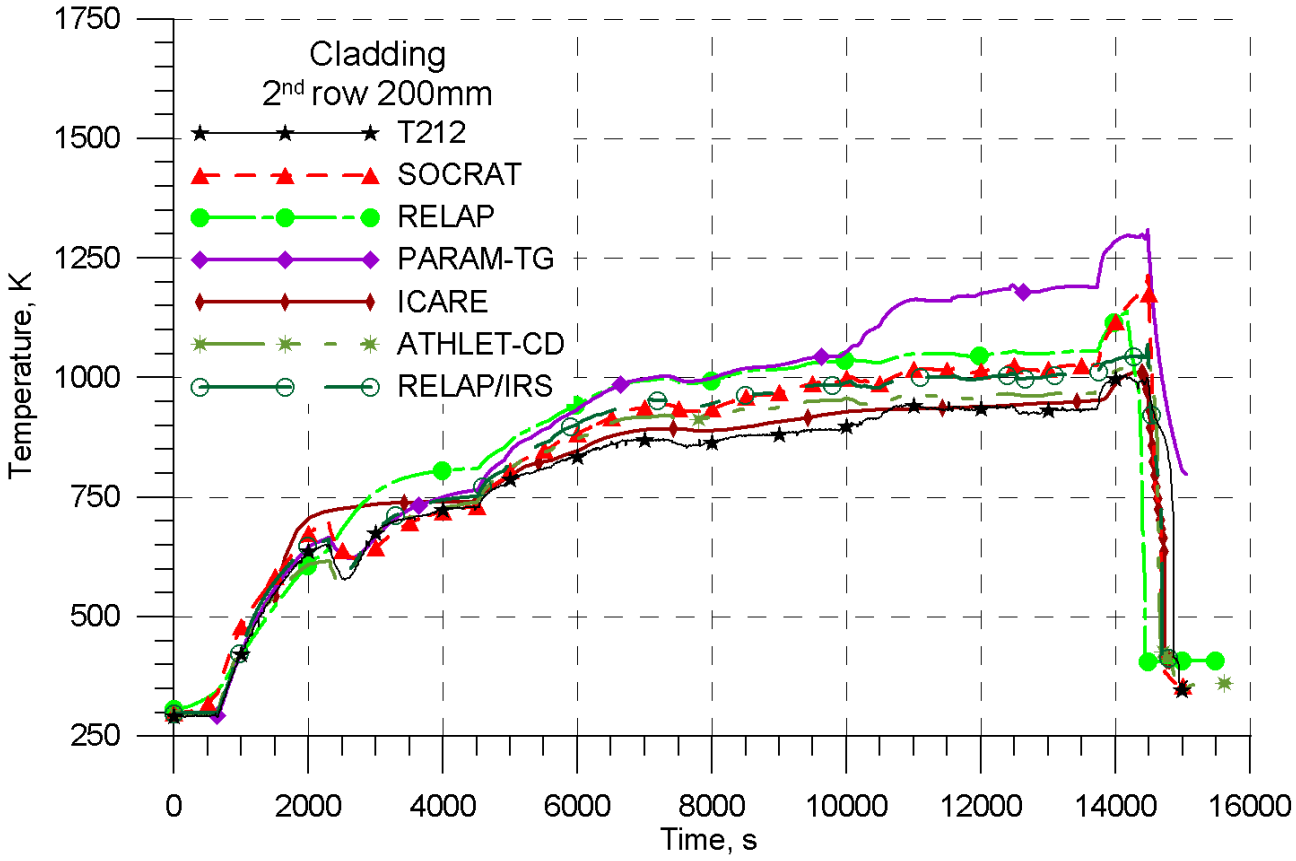

Figure 3.34. Cladding temperature of fuel rod in the second row at the elevation of 200 mm PARAMETER-SF3 experiment. Post-test calculations.

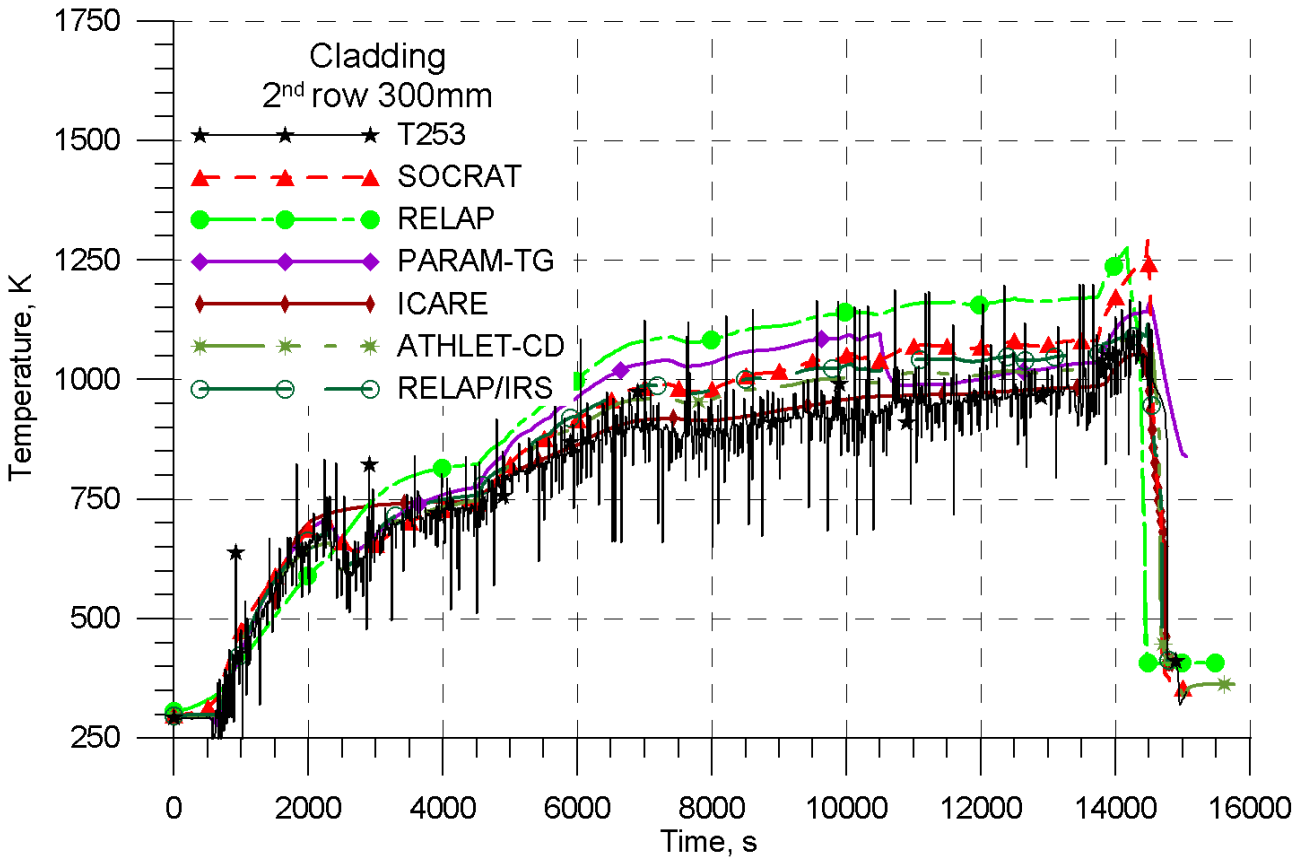

Figure 3.35. Cladding temperature of fuel rod in the second row at the elevation of 300 mm. PARAMETER-SF3 experiment. Post-test calculations.

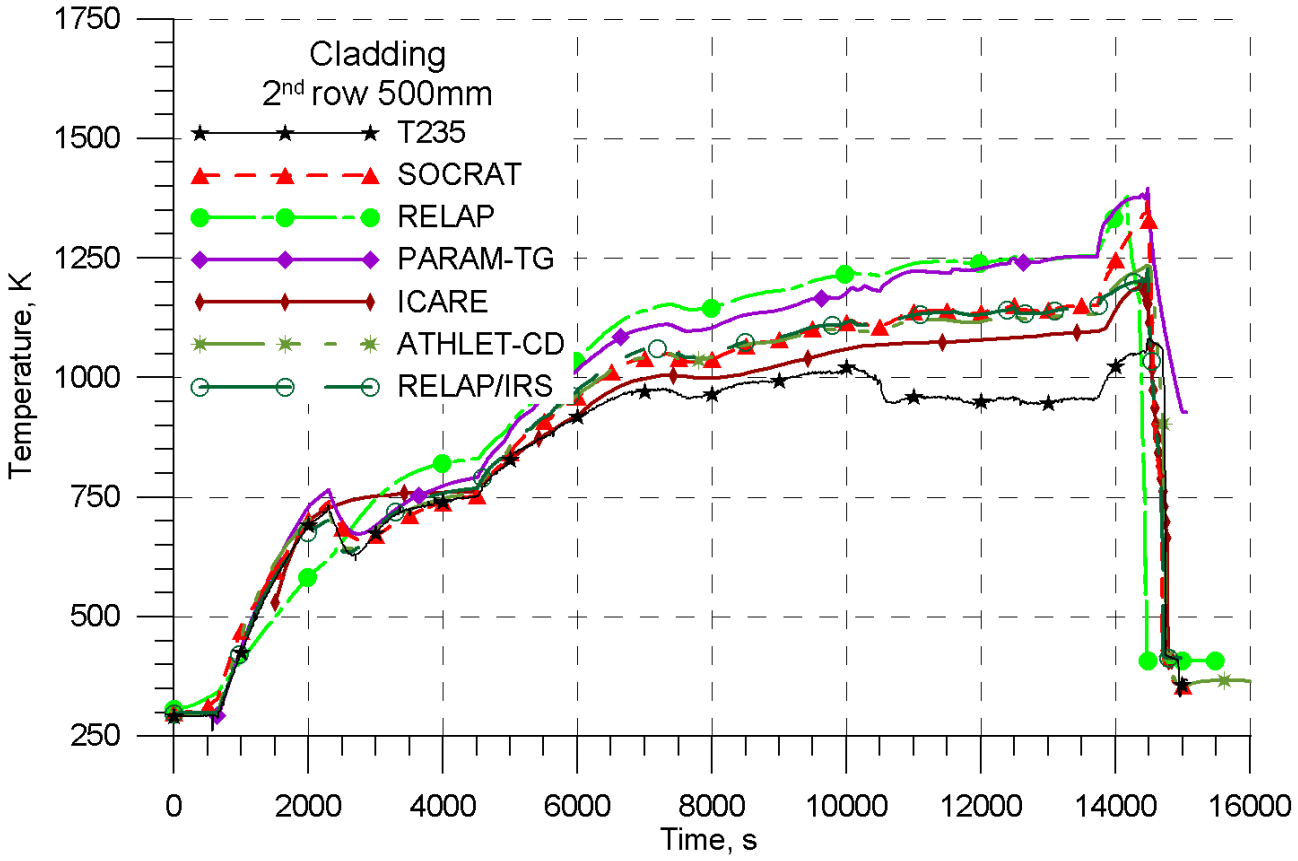

Figure 3.36. Cladding temperature of fuel rod in the second row at the elevation of 500 mm. PARAMETER-SF3 experiment. Post-test calculations.

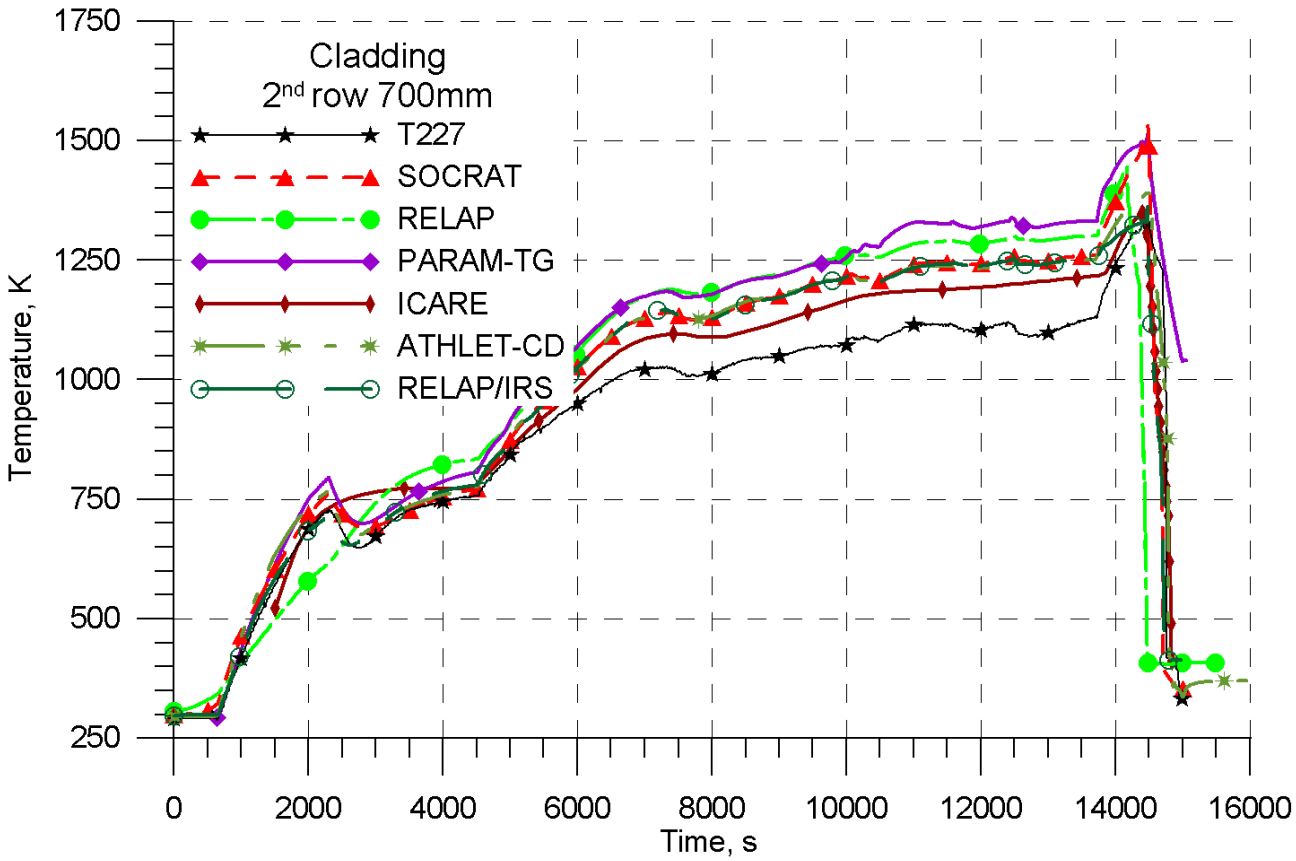

Figure 3.37. Cladding temperature of fuel rod in the second row at the elevation of 700 mm. PARAMETER-SF3 experiment. Post-test calculations.

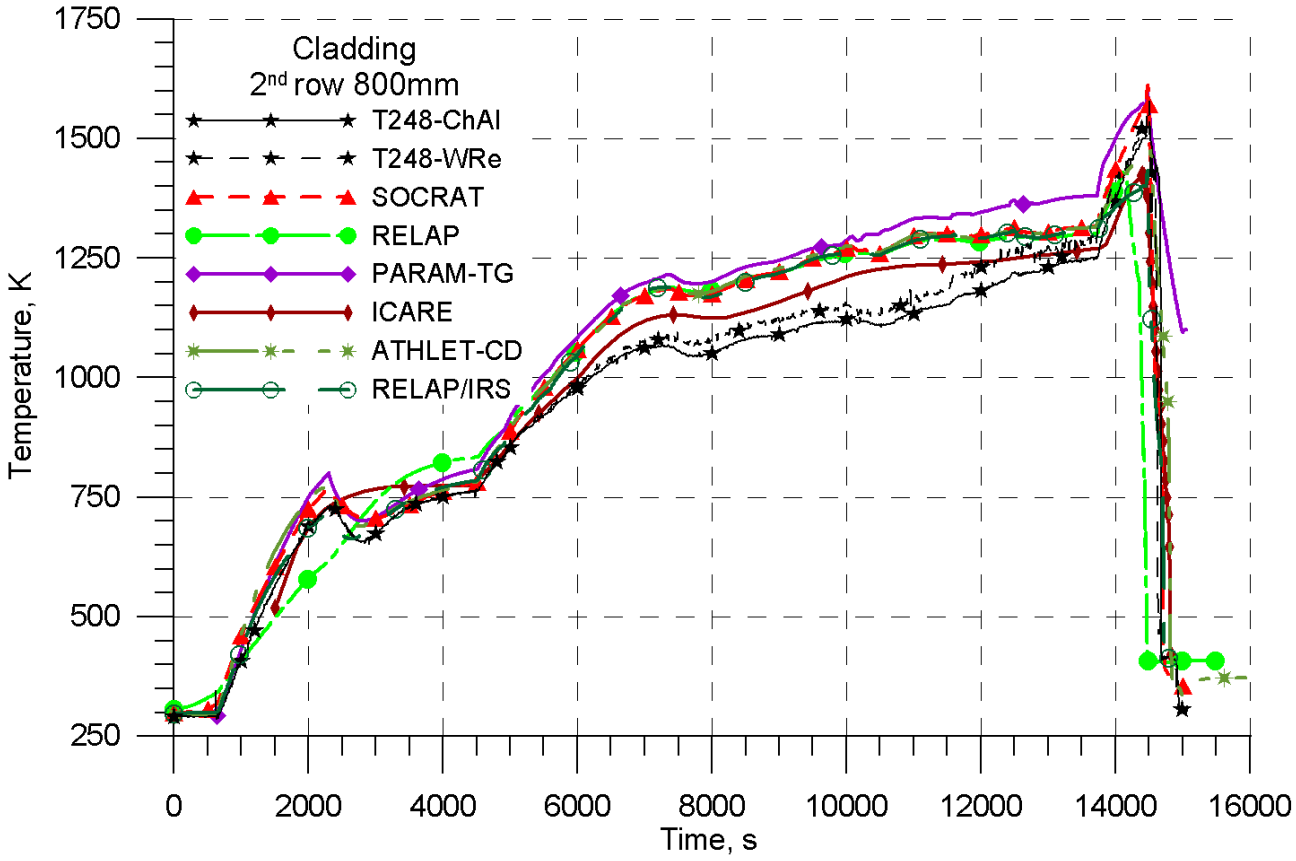

Figure 3.38. Cladding temperature of fuel rod in the second row at the elevation of 800 mm. PARAMETER-SF3 experiment. Post-test calculations.

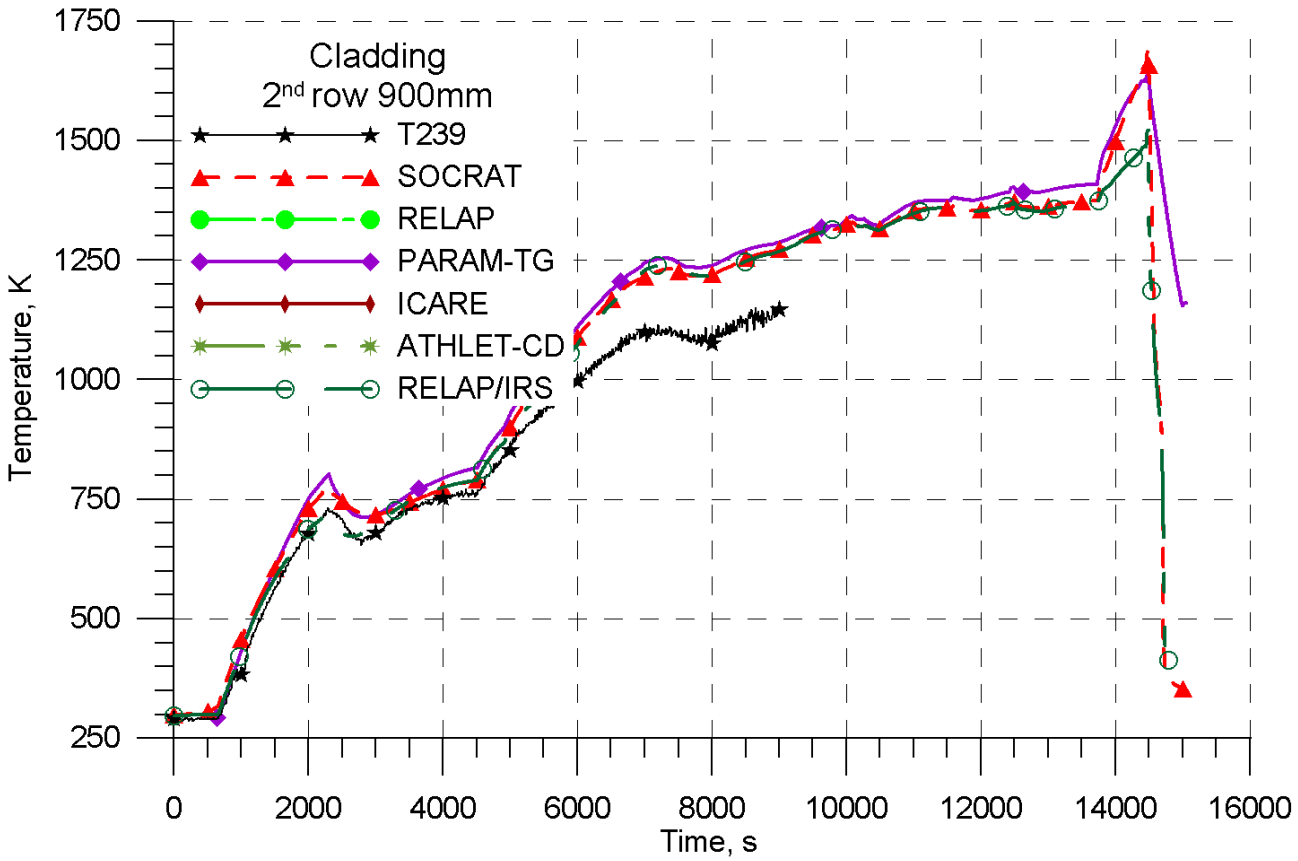

Figure 3.39. Cladding temperature of fuel rod in the second row at the elevation of 900 mm. PARAMETER-SF3 experiment. Post-test calculations.

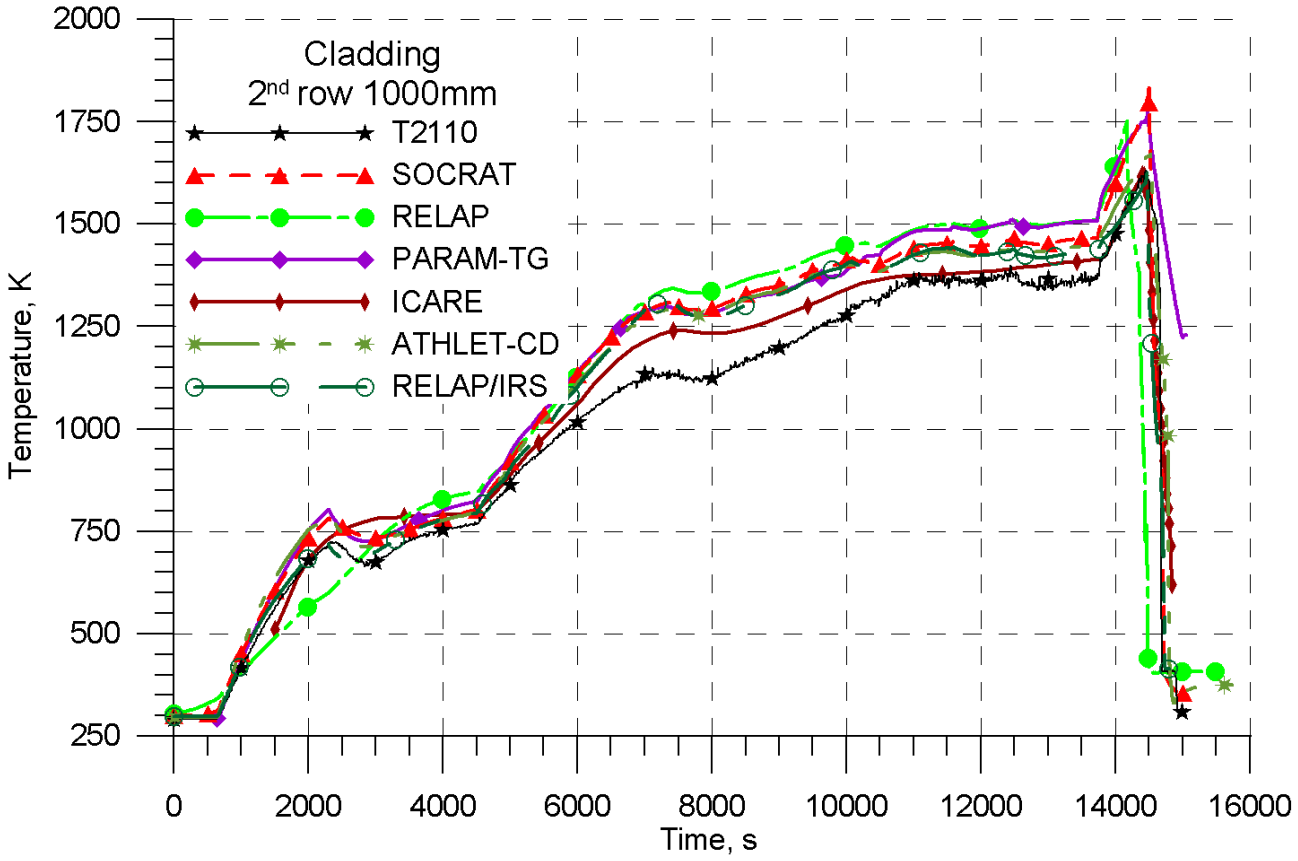

Figure 3.40. Cladding temperature of fuel rod in the second row at the elevation of 1000 mm. PARAMETER-SF3 experiment. Post-test calculations.

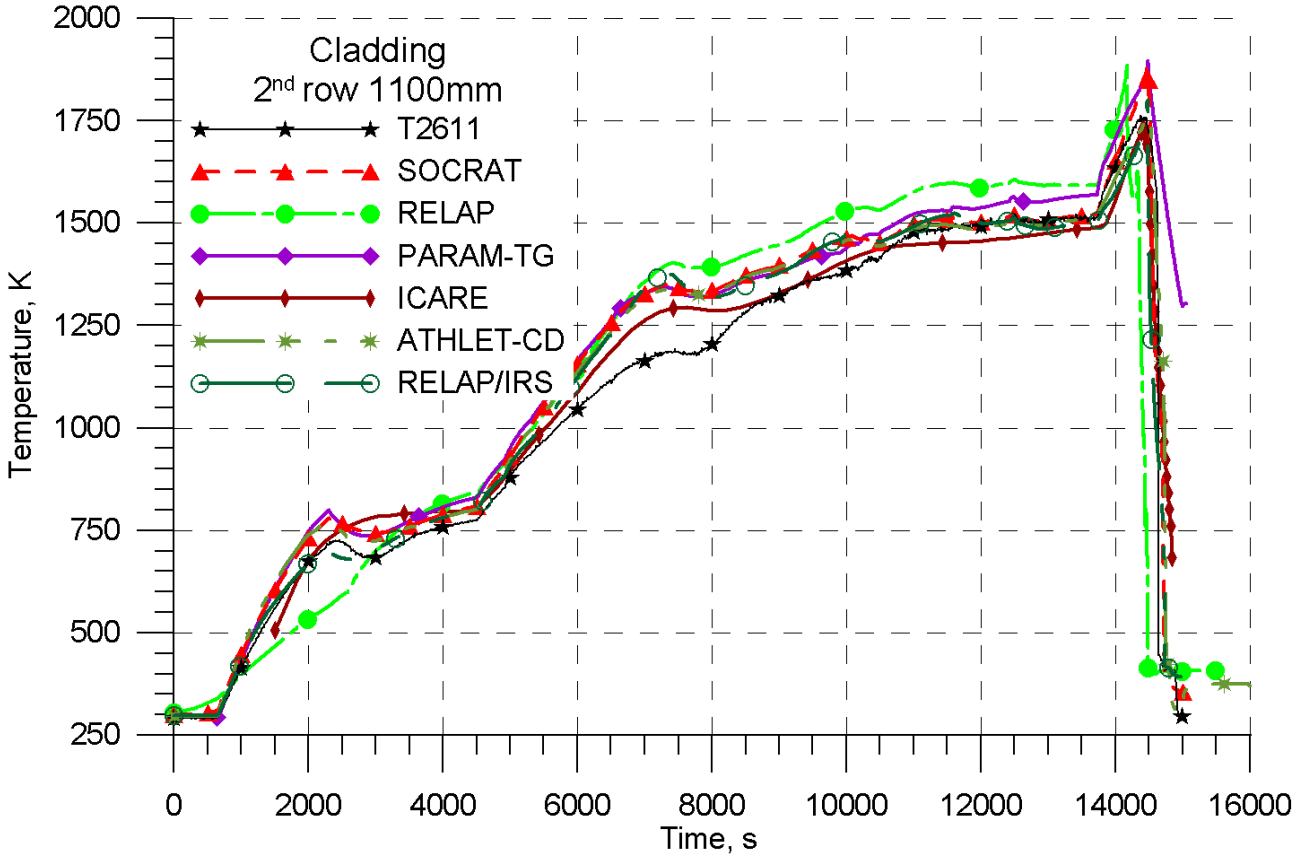

Figure 3.41. Cladding temperature of fuel rod in the second row at the elevation of 1100 mm. PARAMETER-SF3 experiment. Post-test calculations.

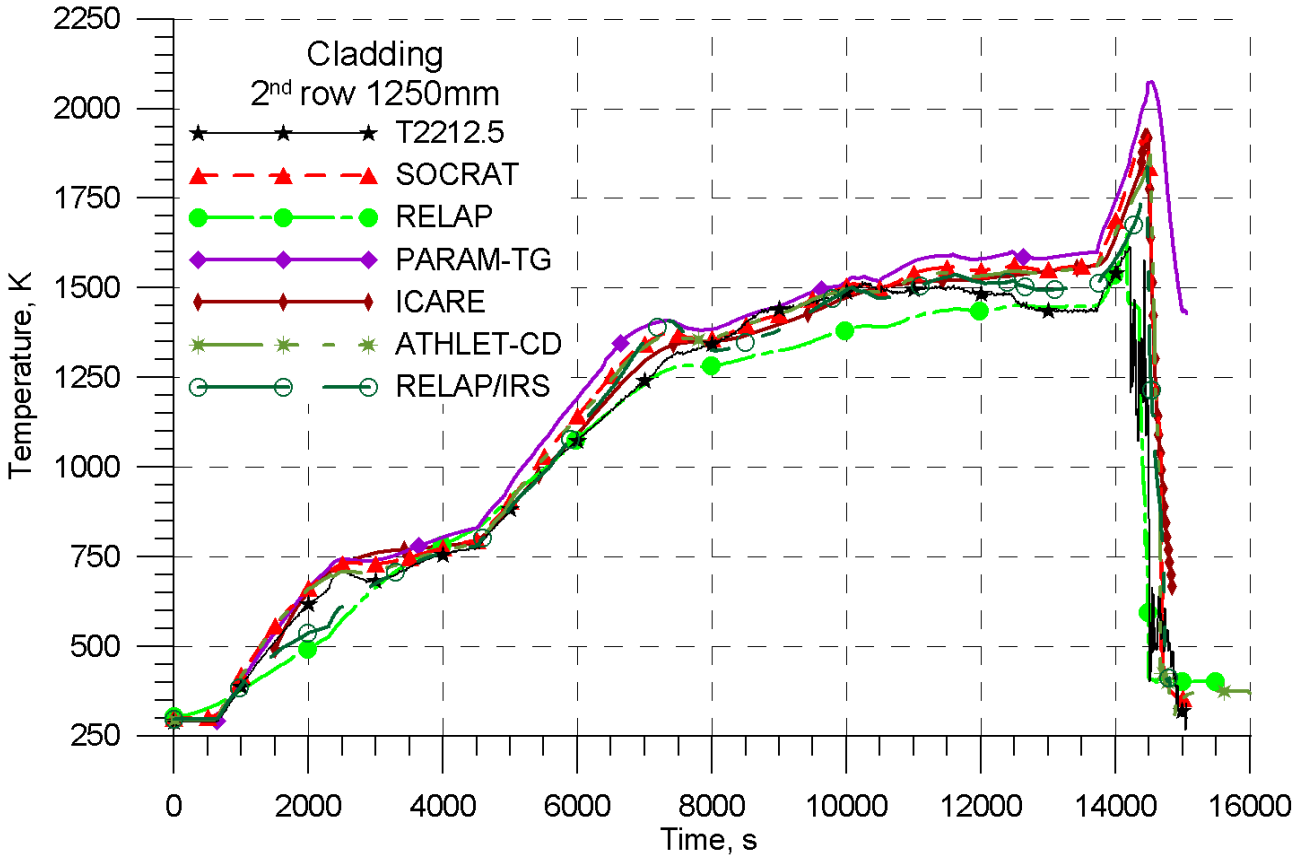

Figure 3.42. Cladding temperature of fuel rod in the second row at the elevation of 1250 mm. PARAMETER-SF3 experiment. Post-test calculations.

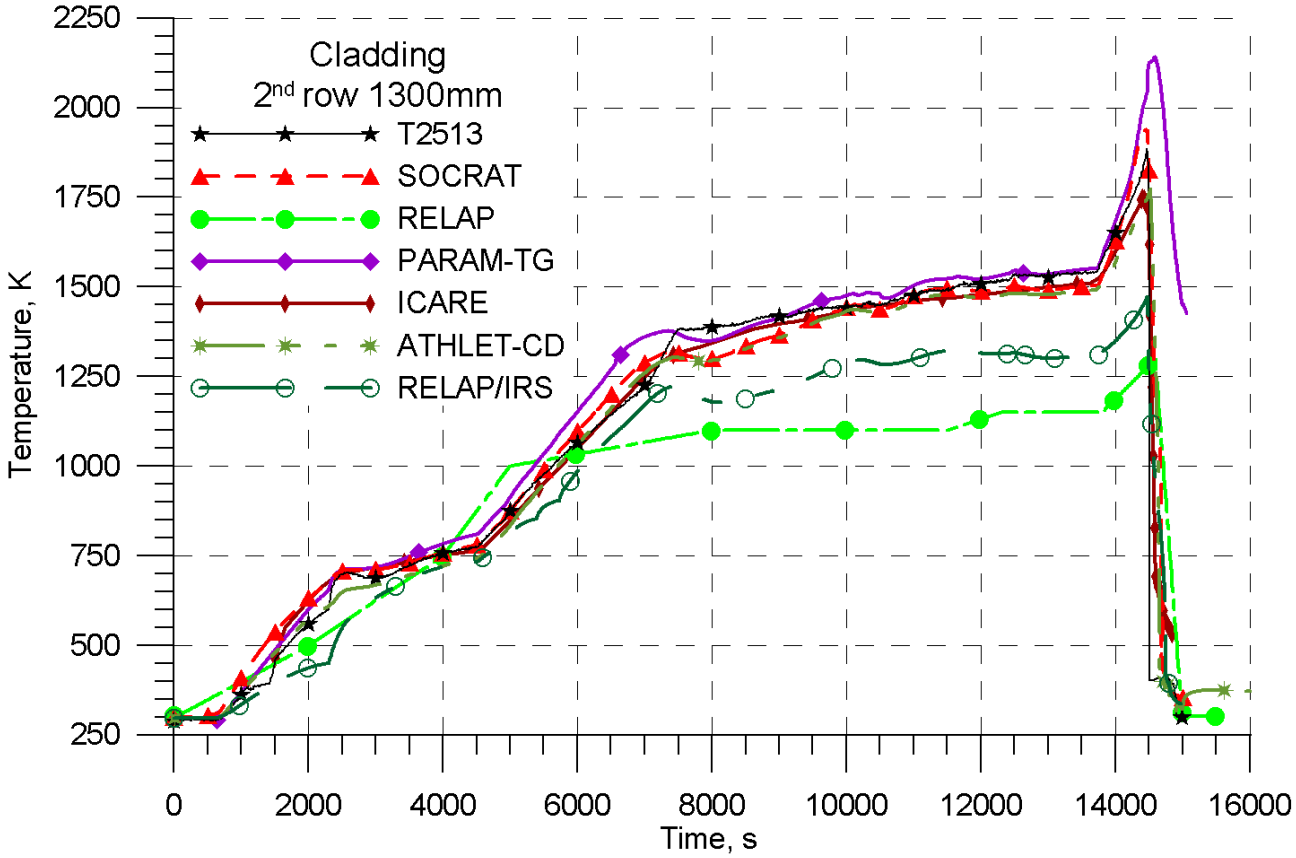

Figure 3.43. Cladding temperature of fuel rod in the second row at the elevation of 1300 mm. PARAMETER-SF3 experiment. Post-test calculations.

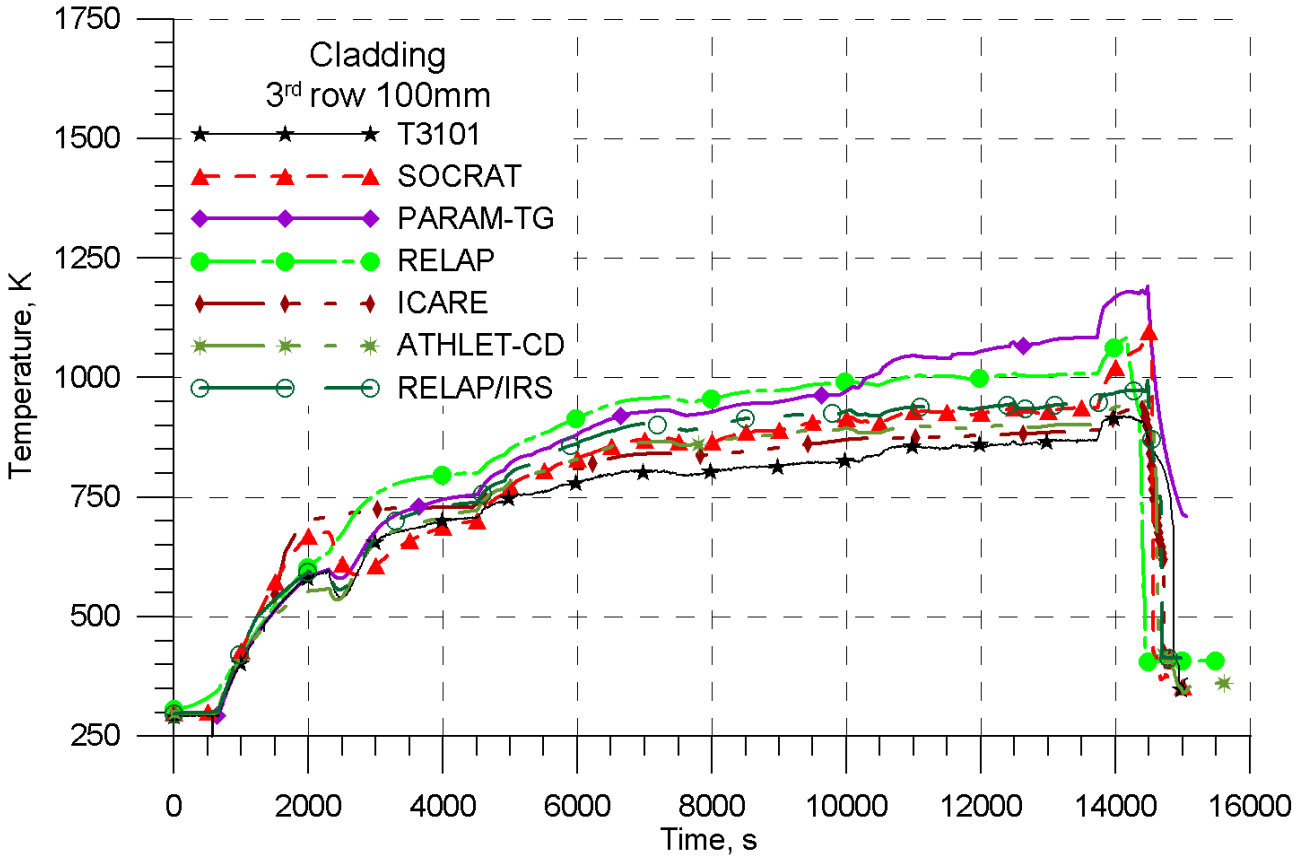

Figure 3.44. Cladding temperature of fuel rod in the third row at the elevation of 100 mm. PARAMETER-SF3 experiment. Post-test calculations.

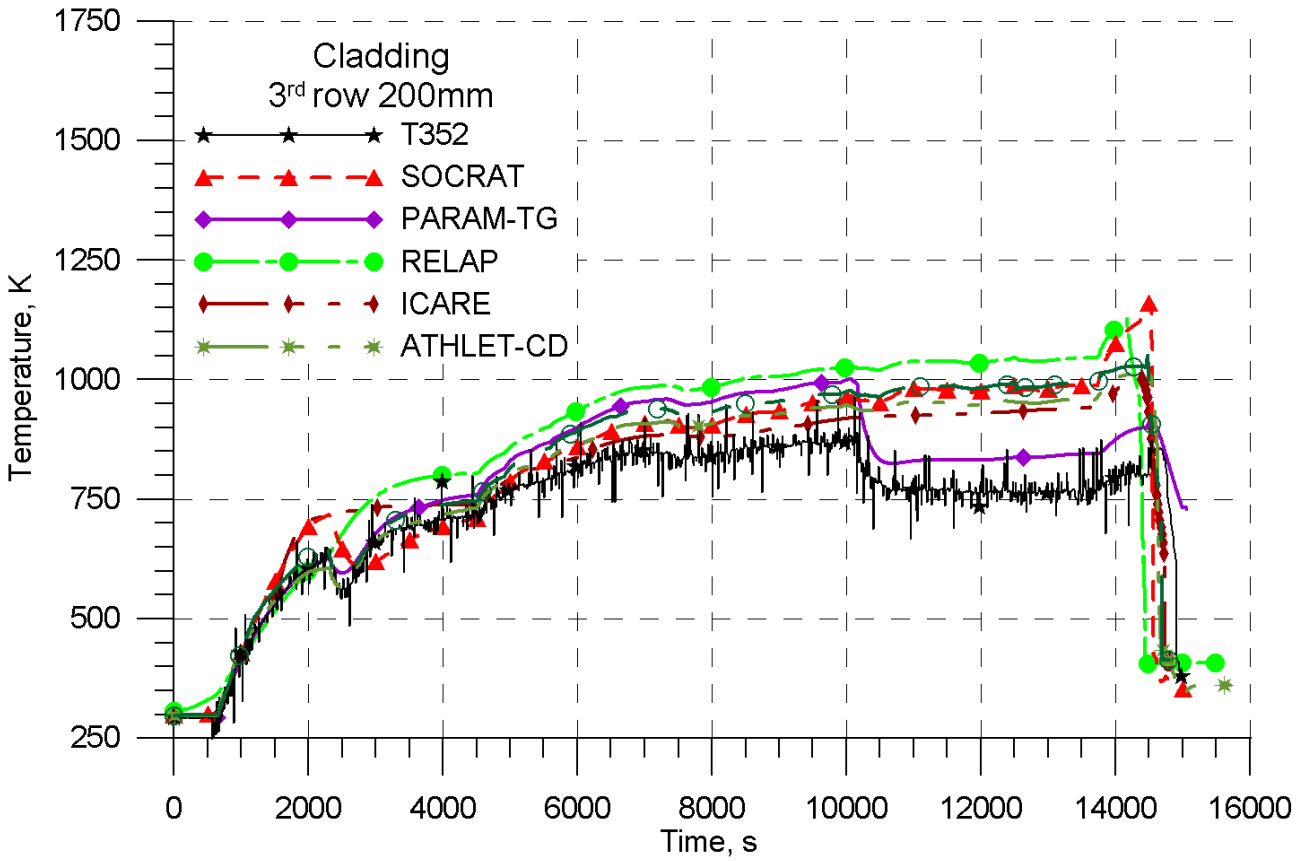

Figure 3.45. Cladding temperature of fuel rod in the third row at the elevation of 200 mm. PARAMETER-SF3 experiment. Post-test calculations.

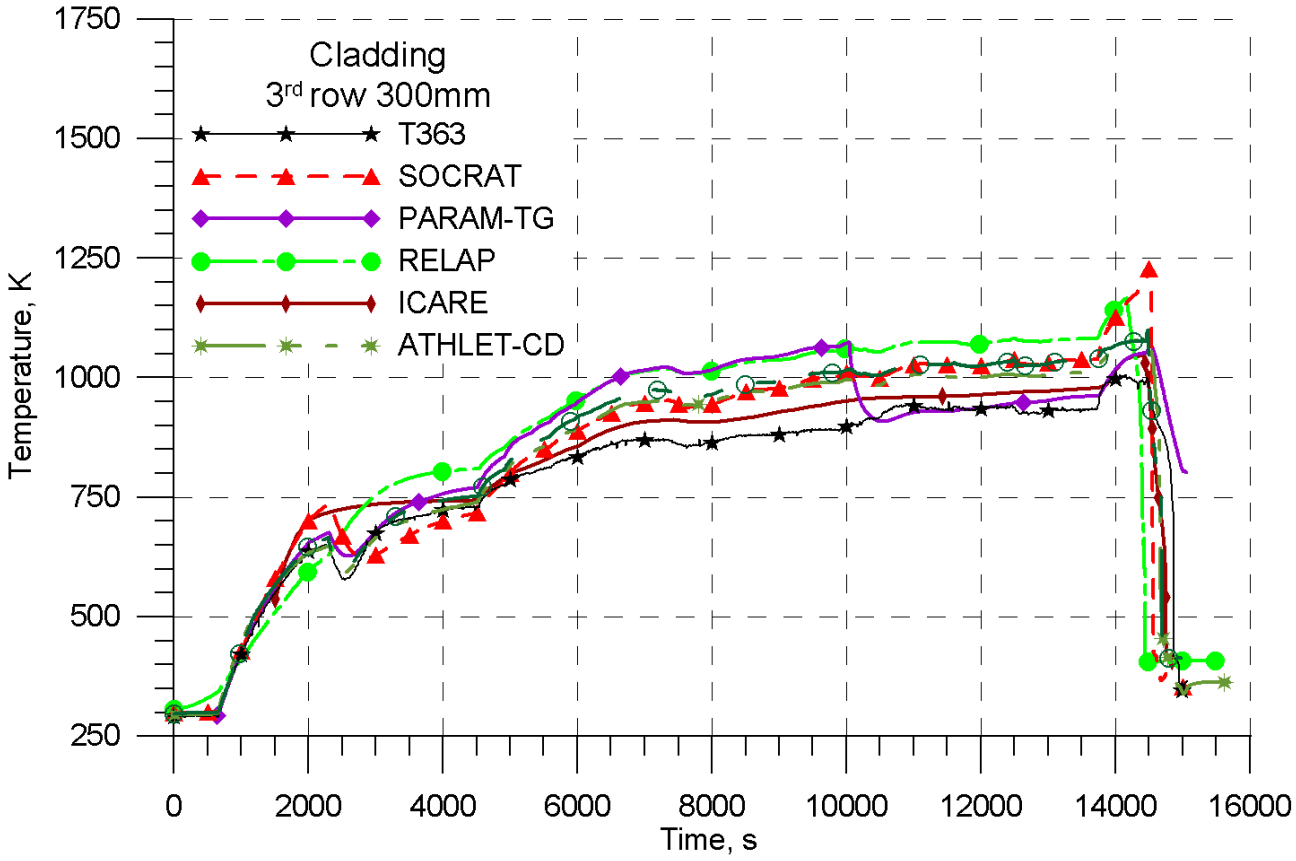

Figure 3.46. Cladding temperature of fuel rod in the third row at the elevation of 300 mm. PARAMETER-SF3 experiment. Post-test calculations.

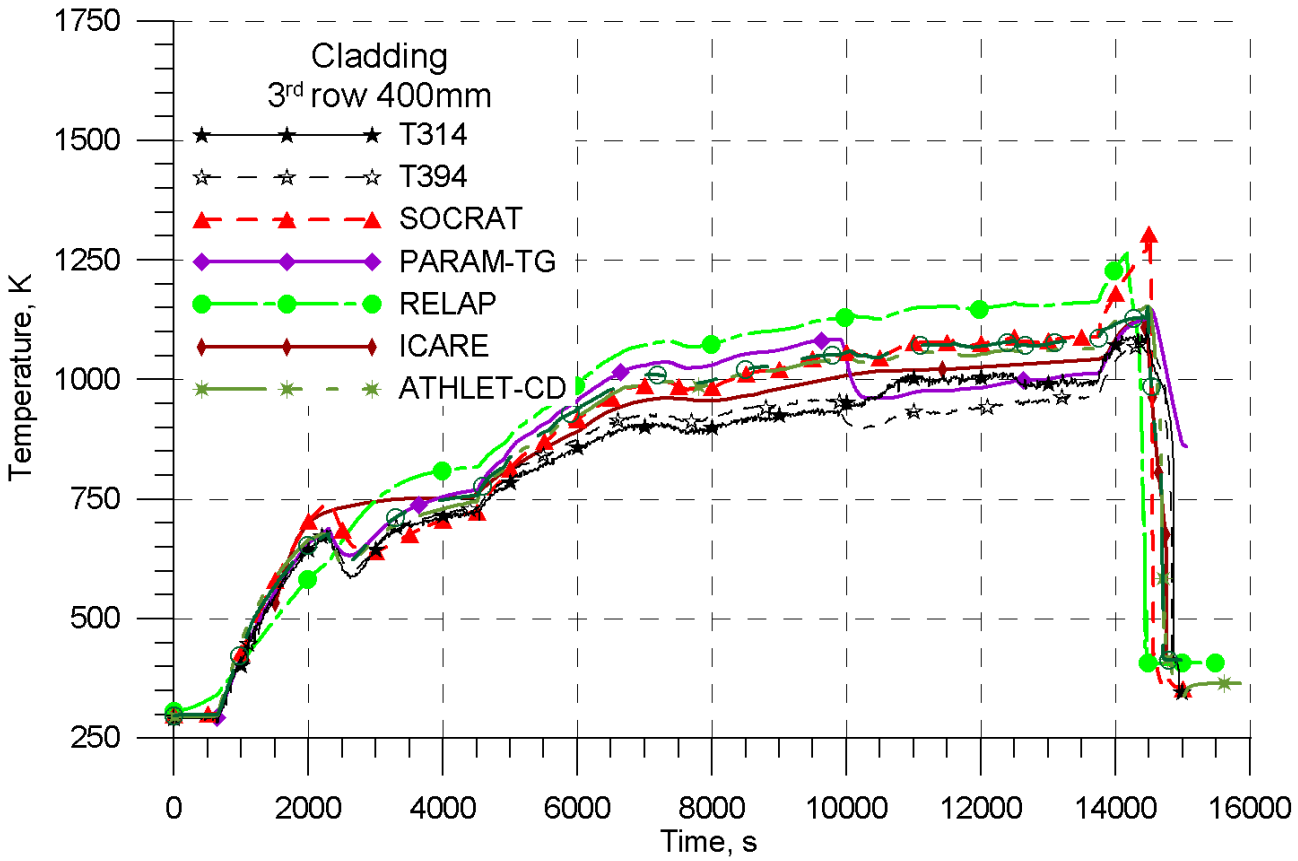

Figure 3.47. Cladding temperature of fuel rod in the third row at the elevation of 400 mm. PARAMETER-SF3 experiment. Post-test calculations.

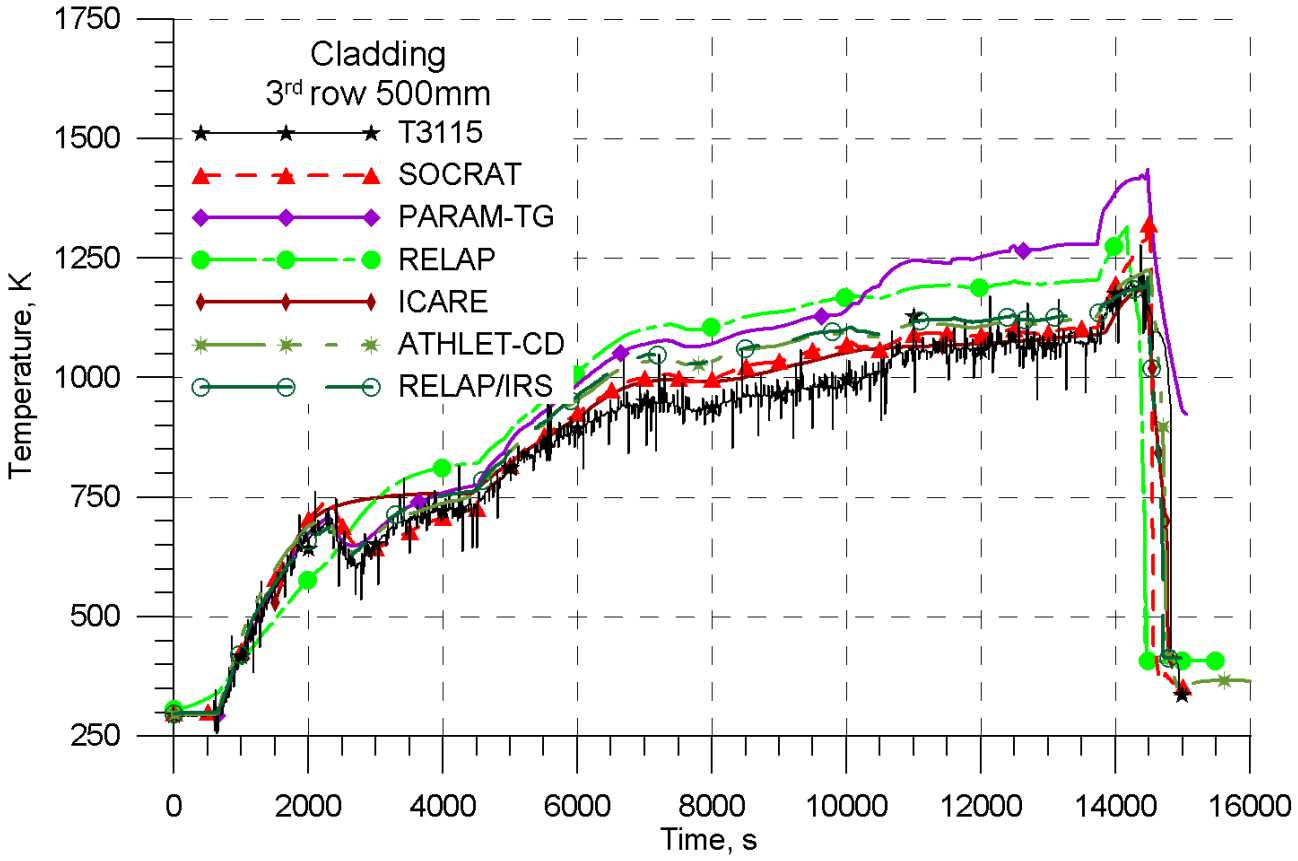

Figure 3.48. Cladding temperature of fuel rod in the third row at the elevation of 500 mm. PARAMETER-SF3 experiment. Post-test calculations.

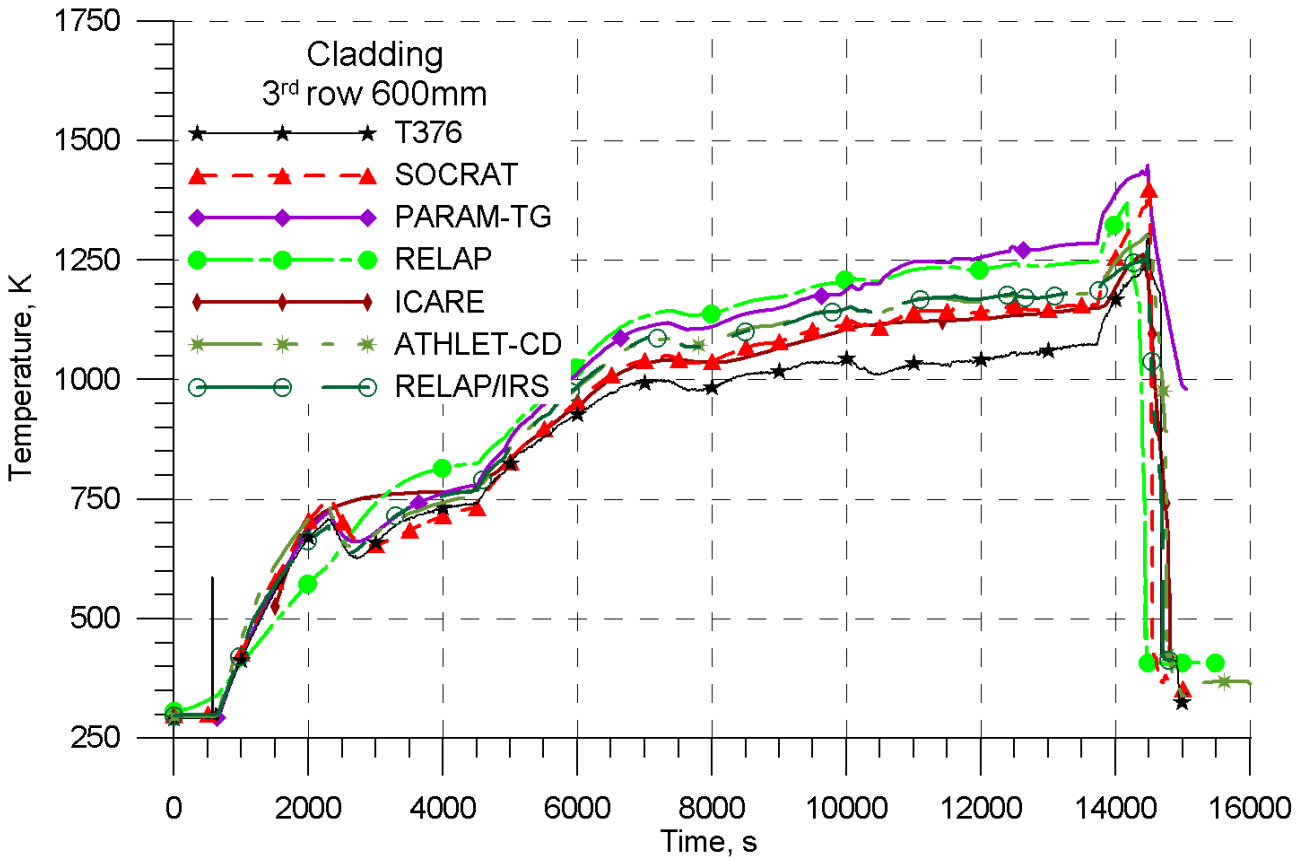

Figure 3.49. Cladding temperature of fuel rod in the third row at the elevation of 600 mm. PARAMETER-SF3 experiment. Post-test calculations.

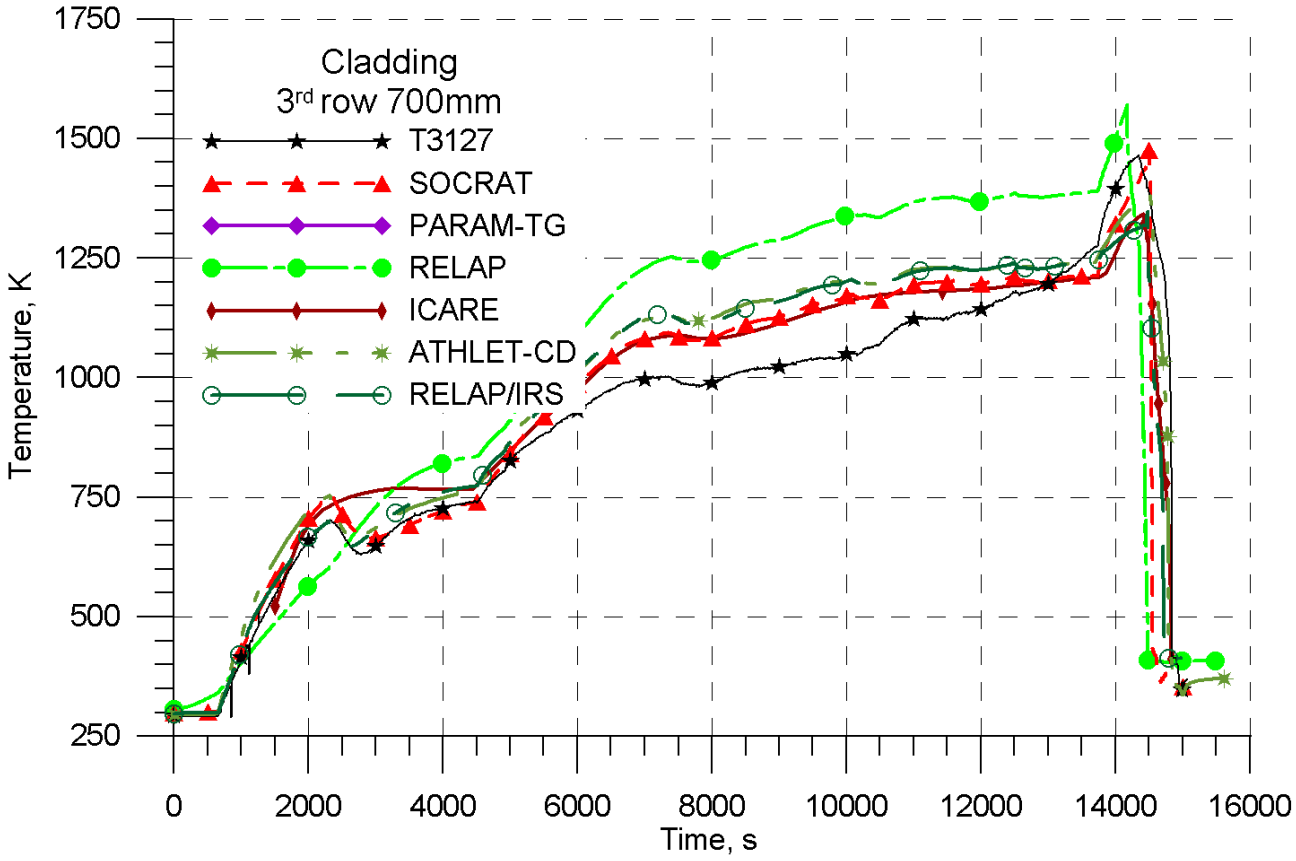

Figure 3.50. Cladding temperature of fuel rod in the third row at the elevation of 700 mm. PARAMETER-SF3 experiment. Post-test calculations.

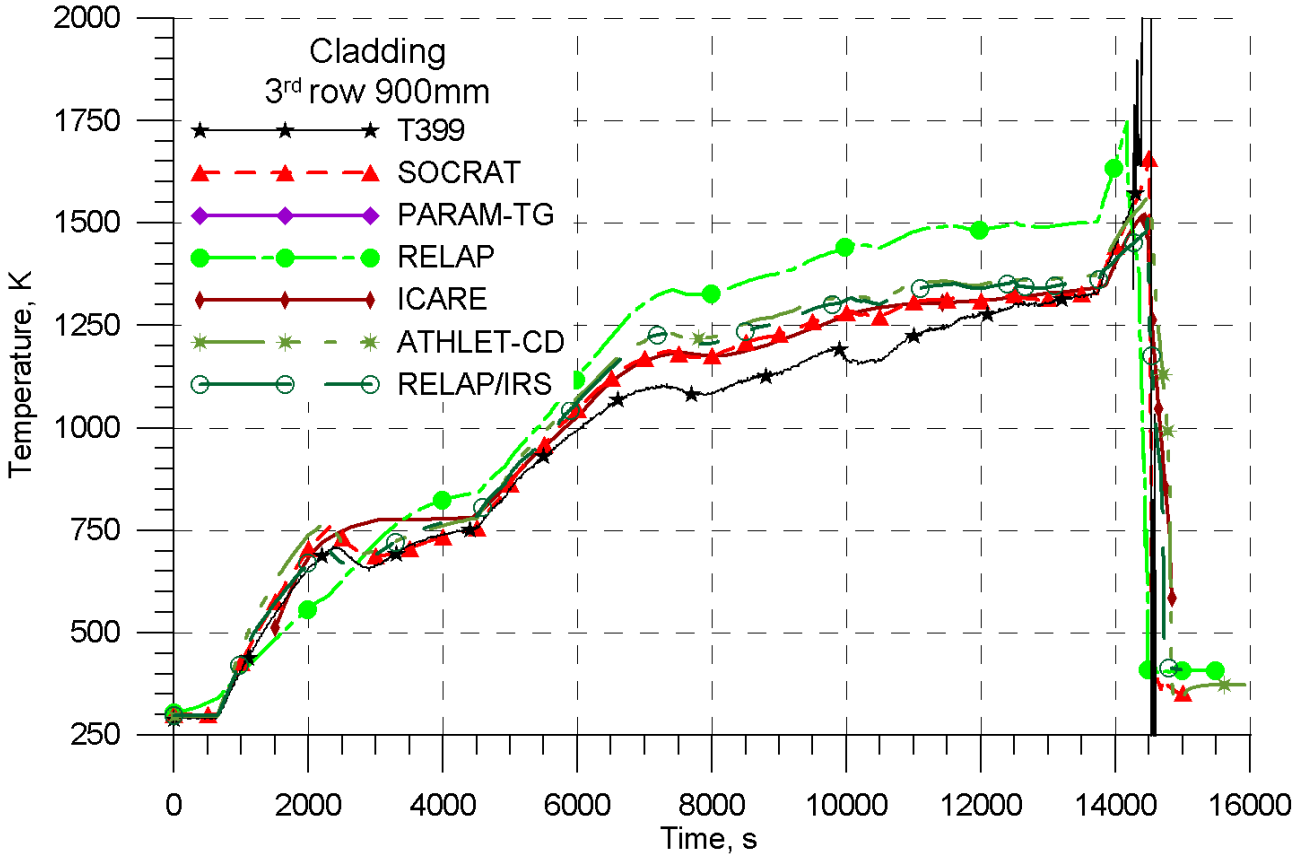

Figure 3.51. Cladding temperature of fuel rod in the third row at the elevation of 900 mm. PARAMETER-SF3 experiment. Post-test calculations.

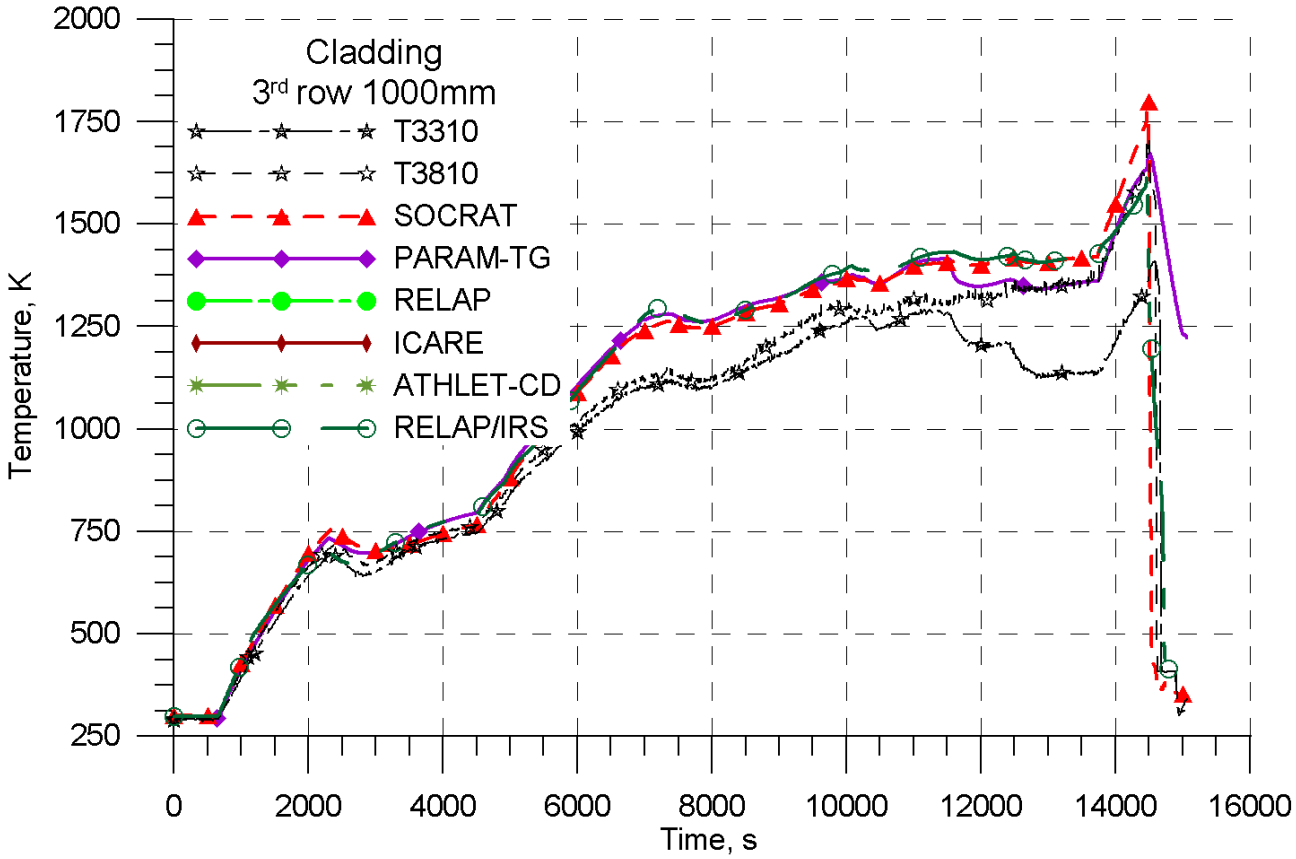

Figure 3.52. Cladding temperature of fuel rod in the third row at the elevation of 1000 mm. PARAMETER-SF3 experiment. Post-test calculations.

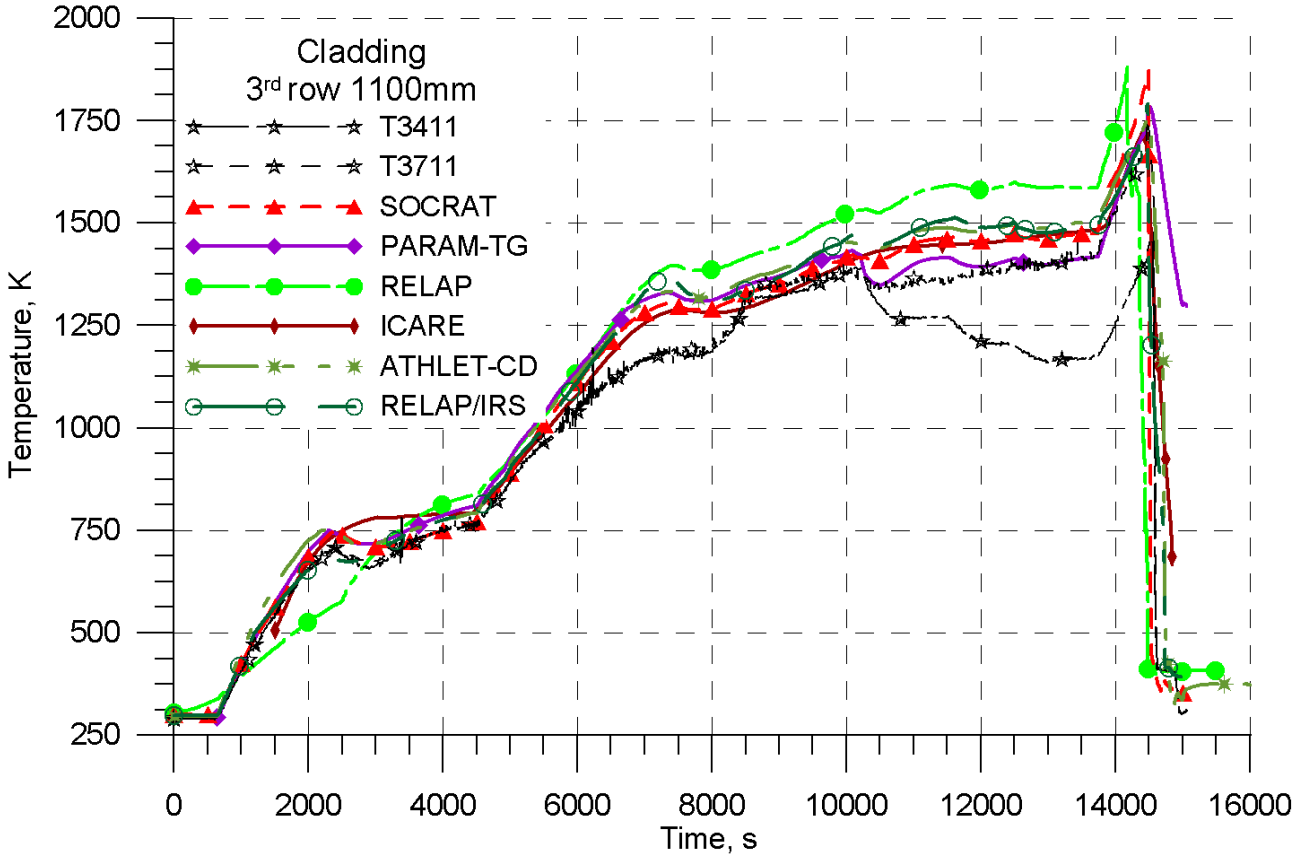

Figure 3.53. Cladding temperature of fuel rod in the third row at the elevation of 1100 mm. PARAMETER-SF3 experiment. Post-test calculations.

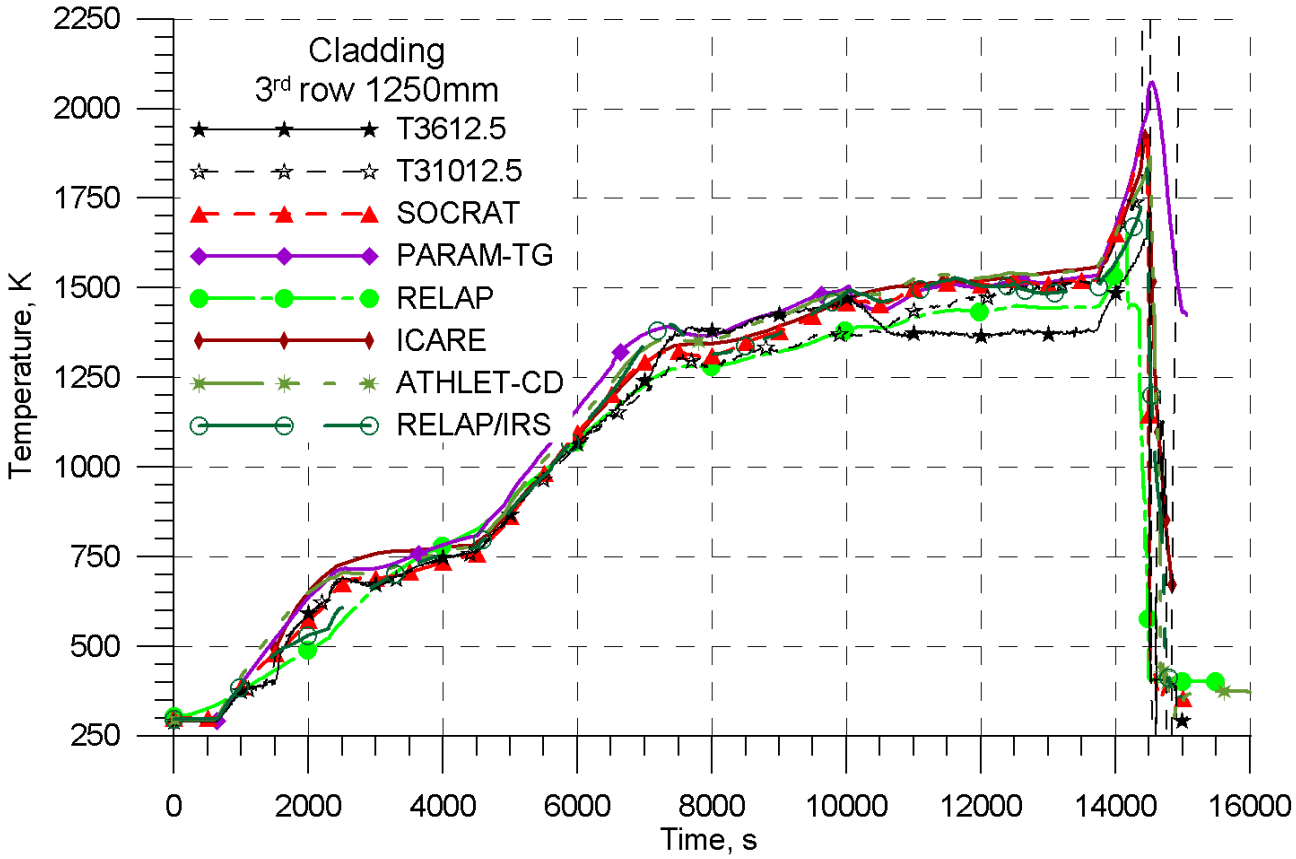

Figure 3.54. Cladding temperature of fuel rod in the third row at the elevation of 1250 mm. PARAMETER-SF3 experiment. Post-test calculations.

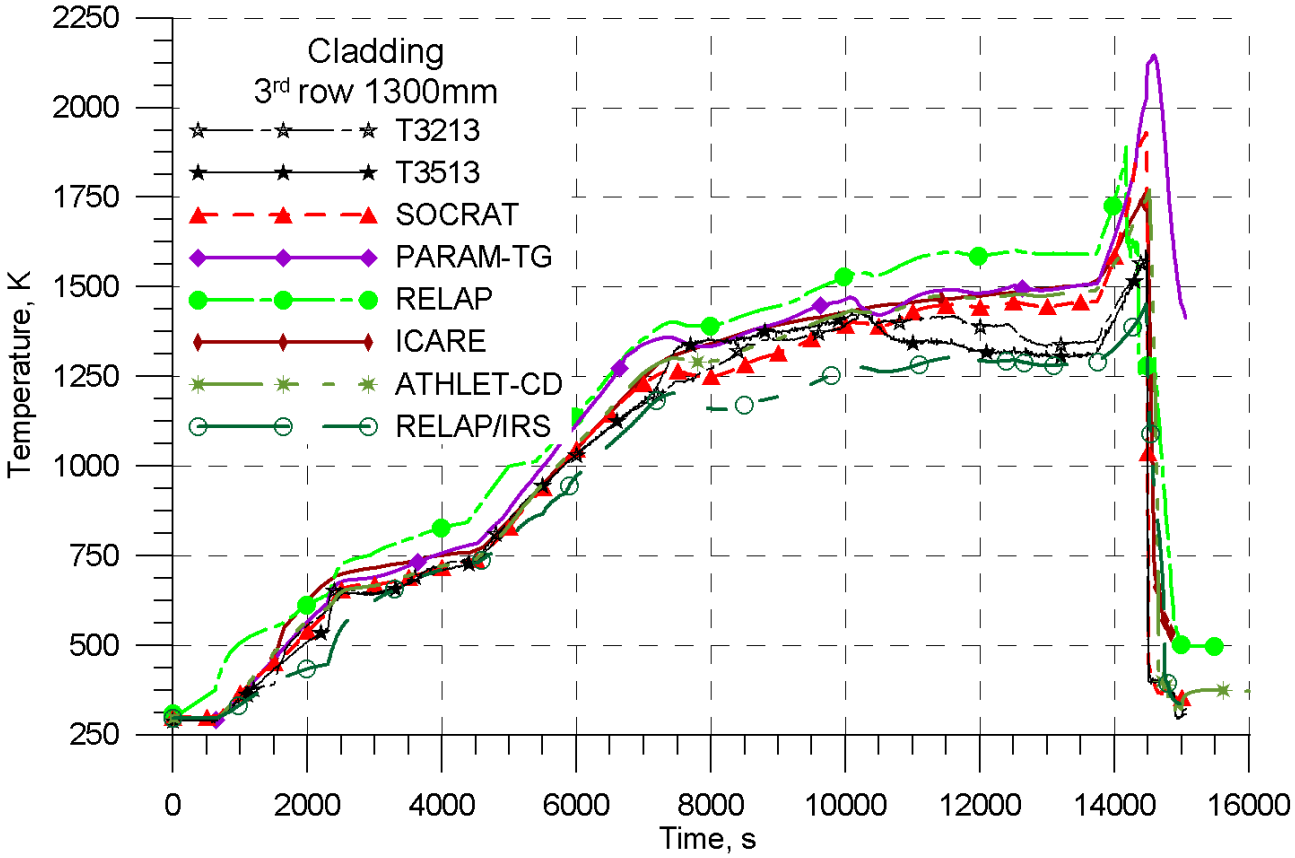

Figure 3.55. Cladding temperature of fuel rod in the third row at the elevation of 1300 mm. PARAMETER-SF3 experiment. Post-test calculations.

3.3.3.4 Shroud temperature

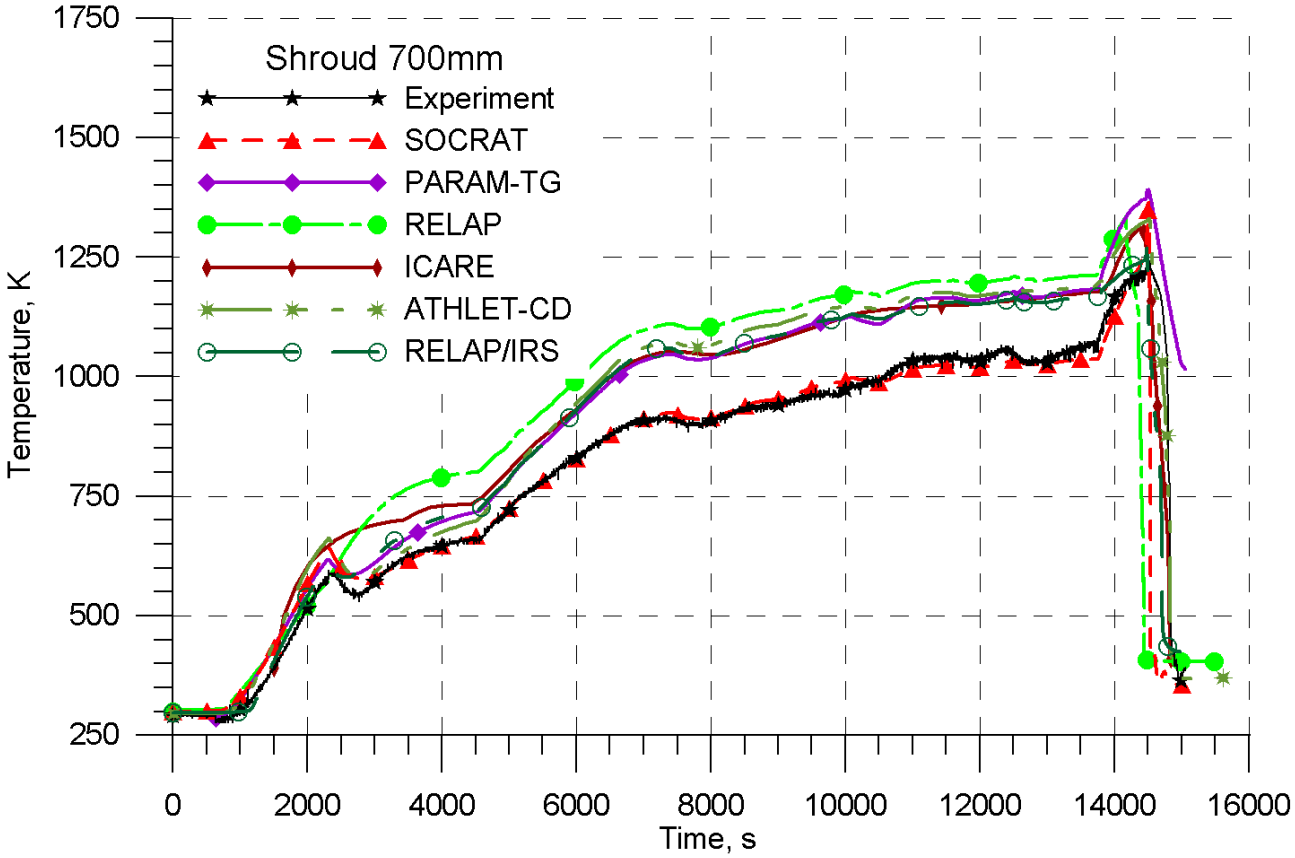

Figure 3.56. Shroud temperature at the elevation of 700 mm. PARAMETER-SF3 experiment. Post-test calculations.

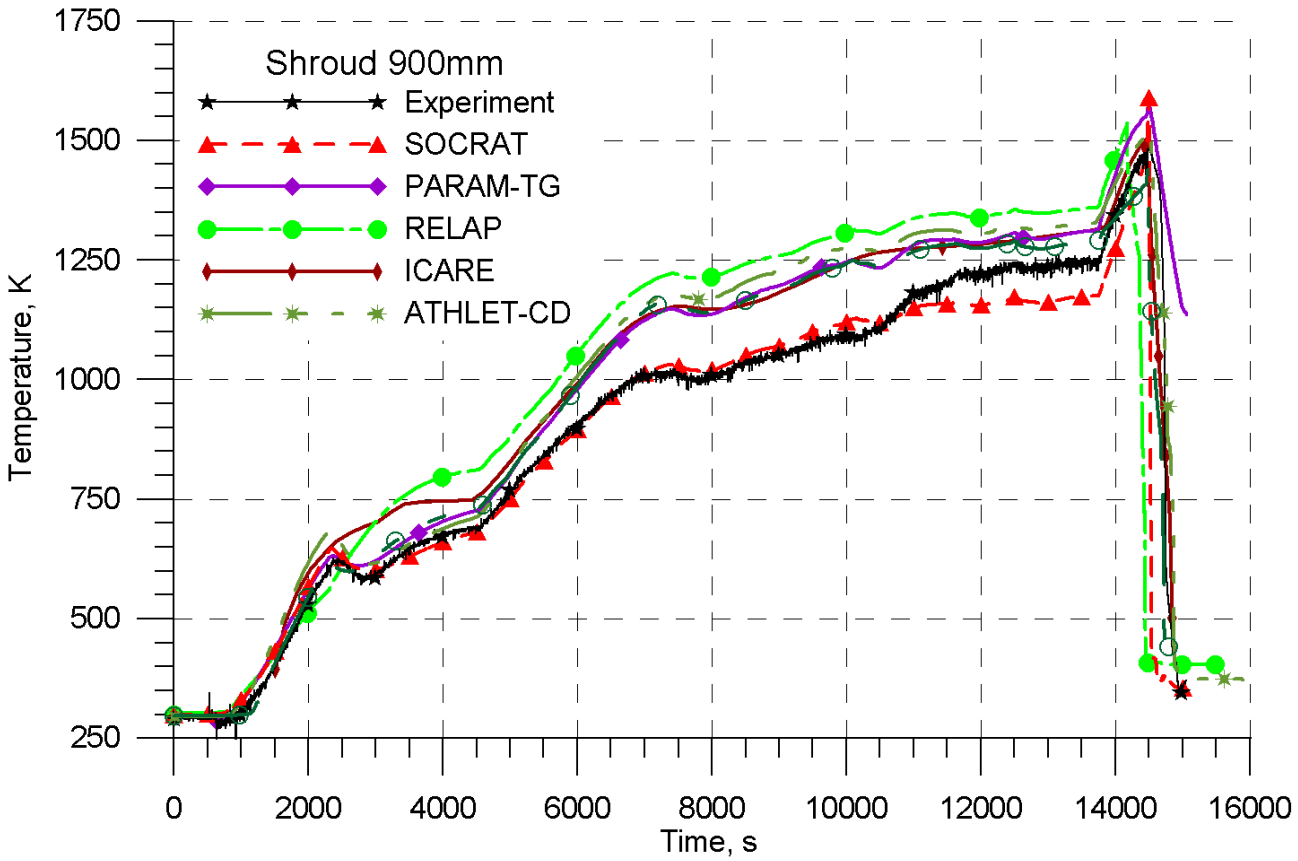

Figure 3.57. Shroud temperature at the elevation of 900 mm. PARAMETER-SF3 experiment. Post-test calculations.

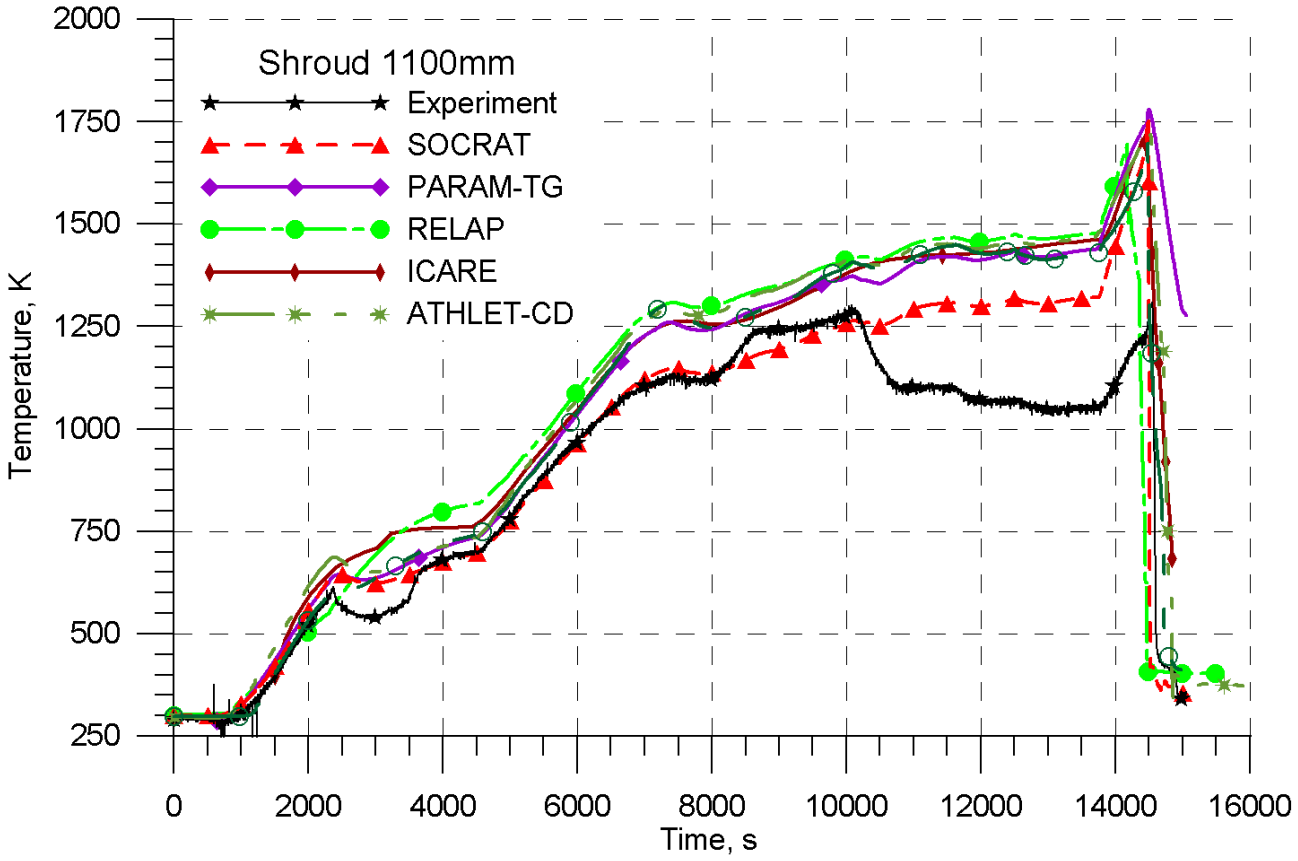

Figure 3.58. Shroud temperature at the elevation of 1100 mm. PARAMETER-SF3 experiment. Post-test calculations.

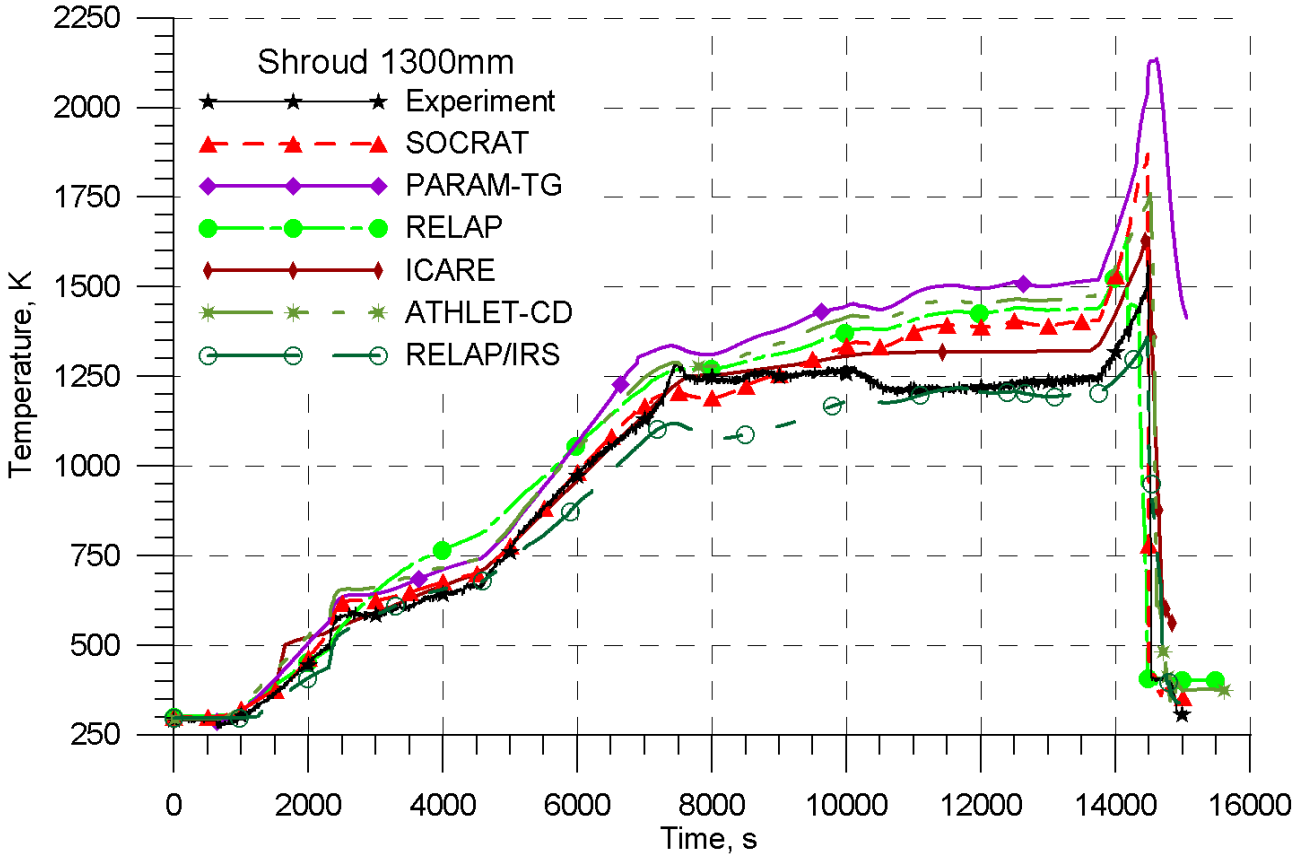

Figure 3.59. Shroud temperature at the elevation of 1300 mm. PARAMETER-SF3 experiment. Post-test calculations.

3.3.3.5 Oxidation of the test section components and hydrogen production

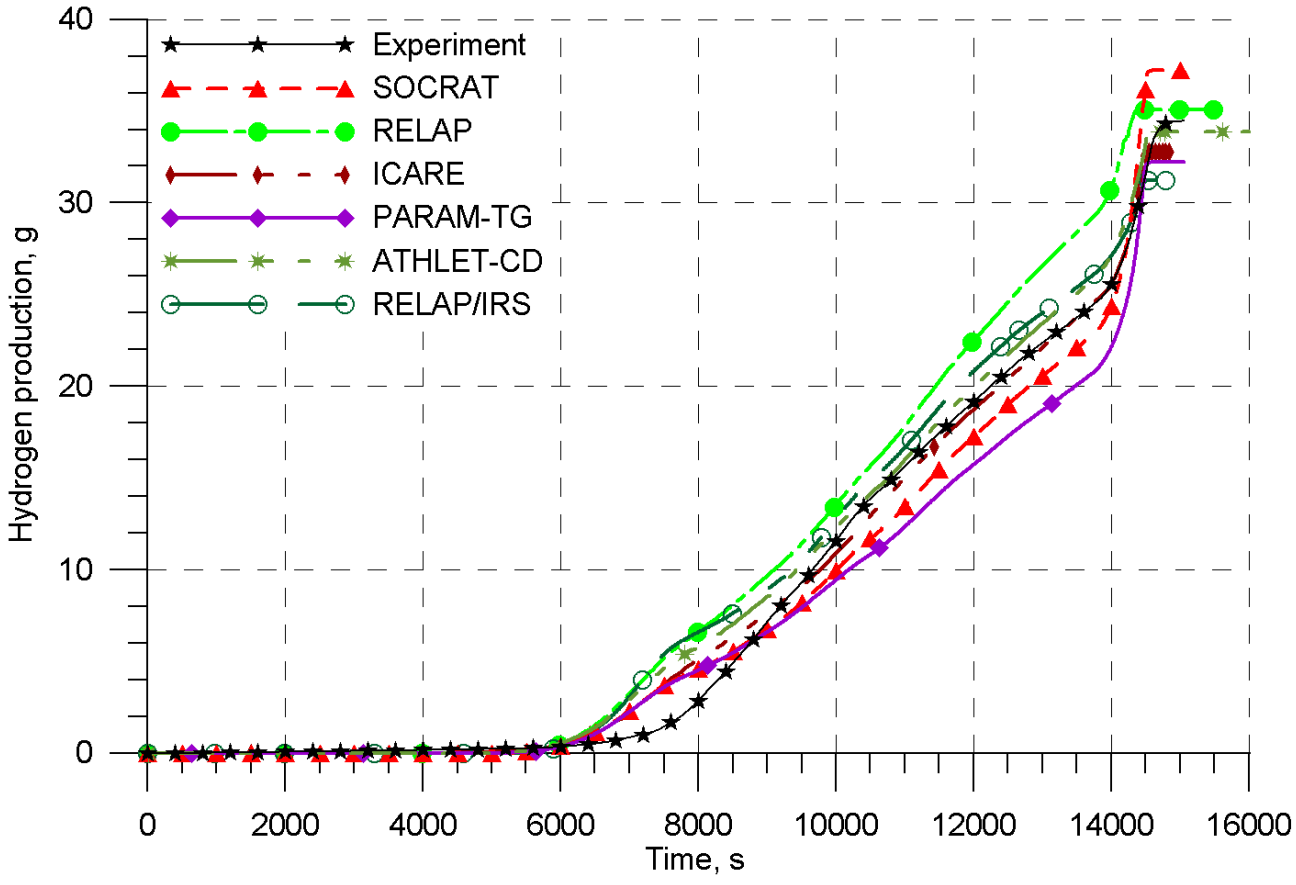

Figure 3.60. Integral hydrogen production. PARAMETER-SF3 experiment. Post-test calculations.

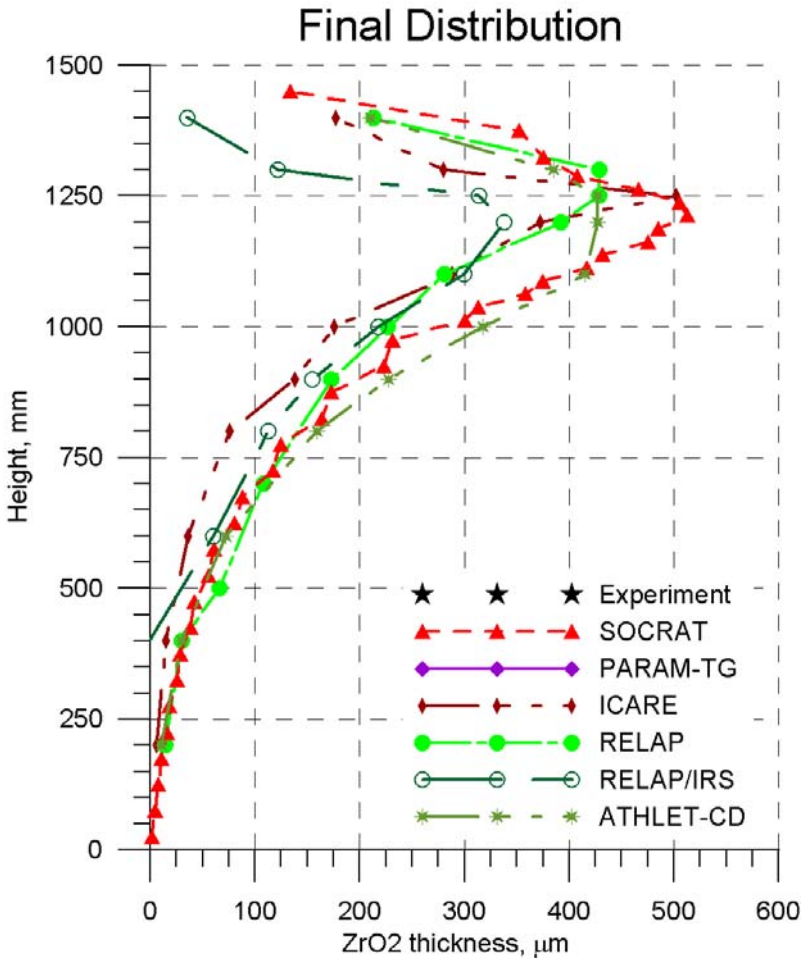

Figure 3.61. Oxide scale distribution on cladding surfaces. PARAMETER-SF3 experiment. Post-test calculations.

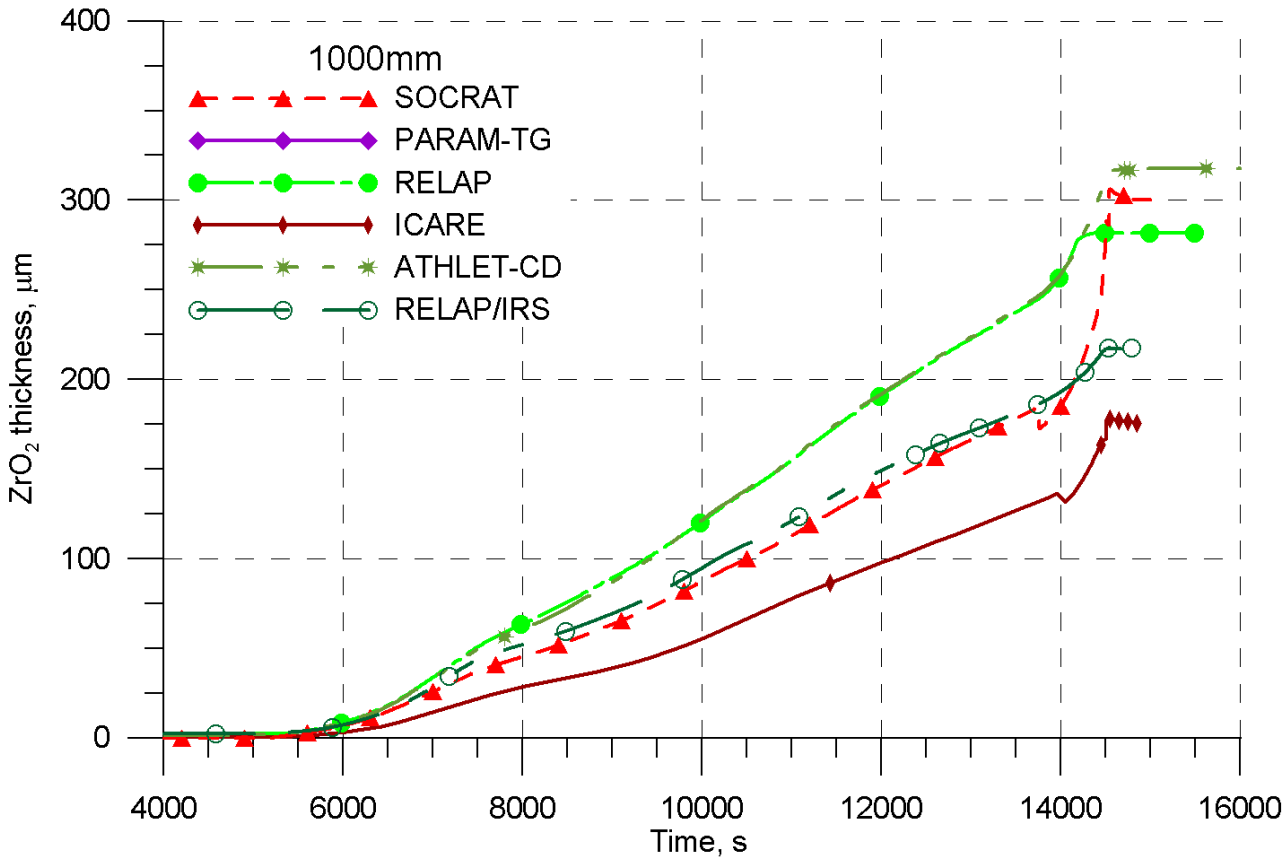

Figure 3.62. Thickness of zirconium oxide scale at the elevation of 1000 mm. PARAMETER-SF3 experiment. Post-test calculations.

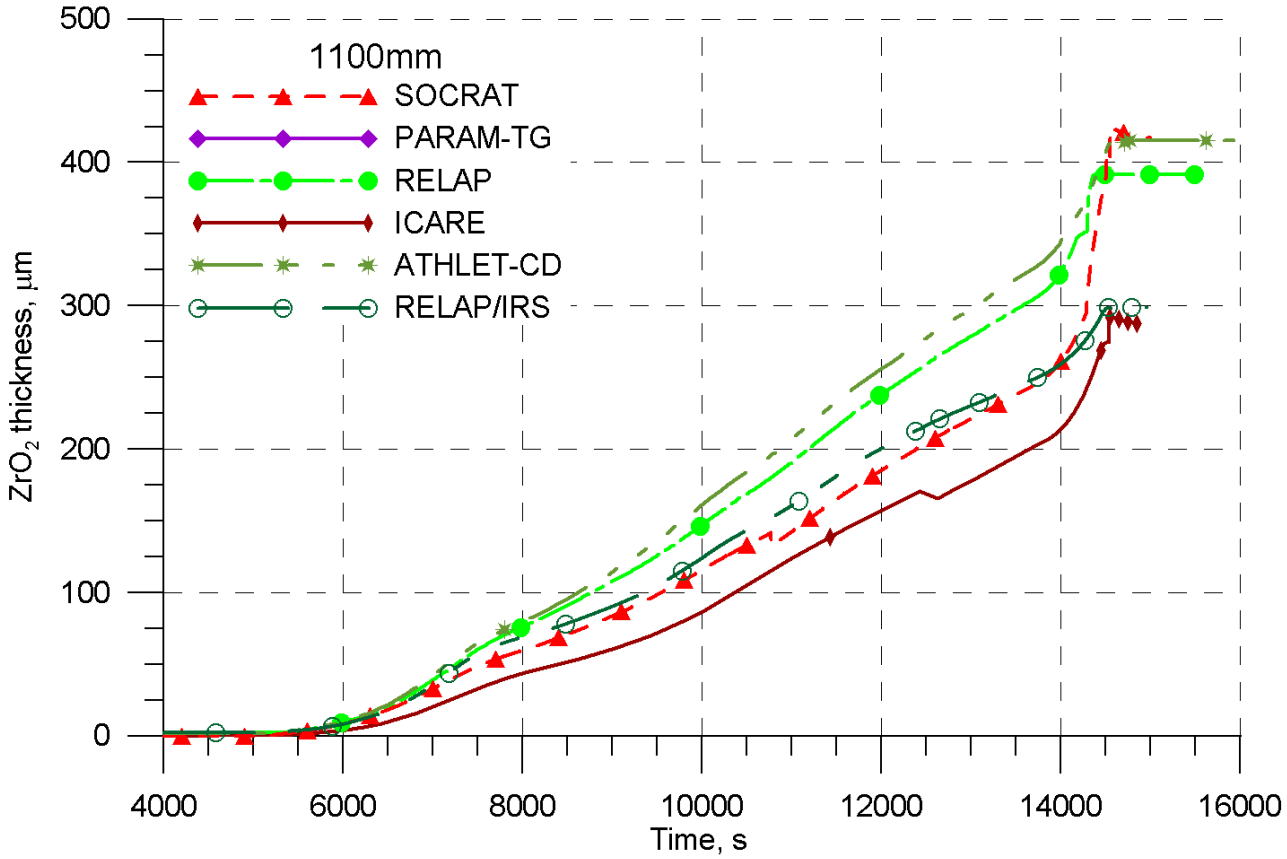

Figure 3.63. Thickness of zirconium oxide scale at the elevation of 1100 mm. PARAMETER-SF3 experiment. Post-test calculations.

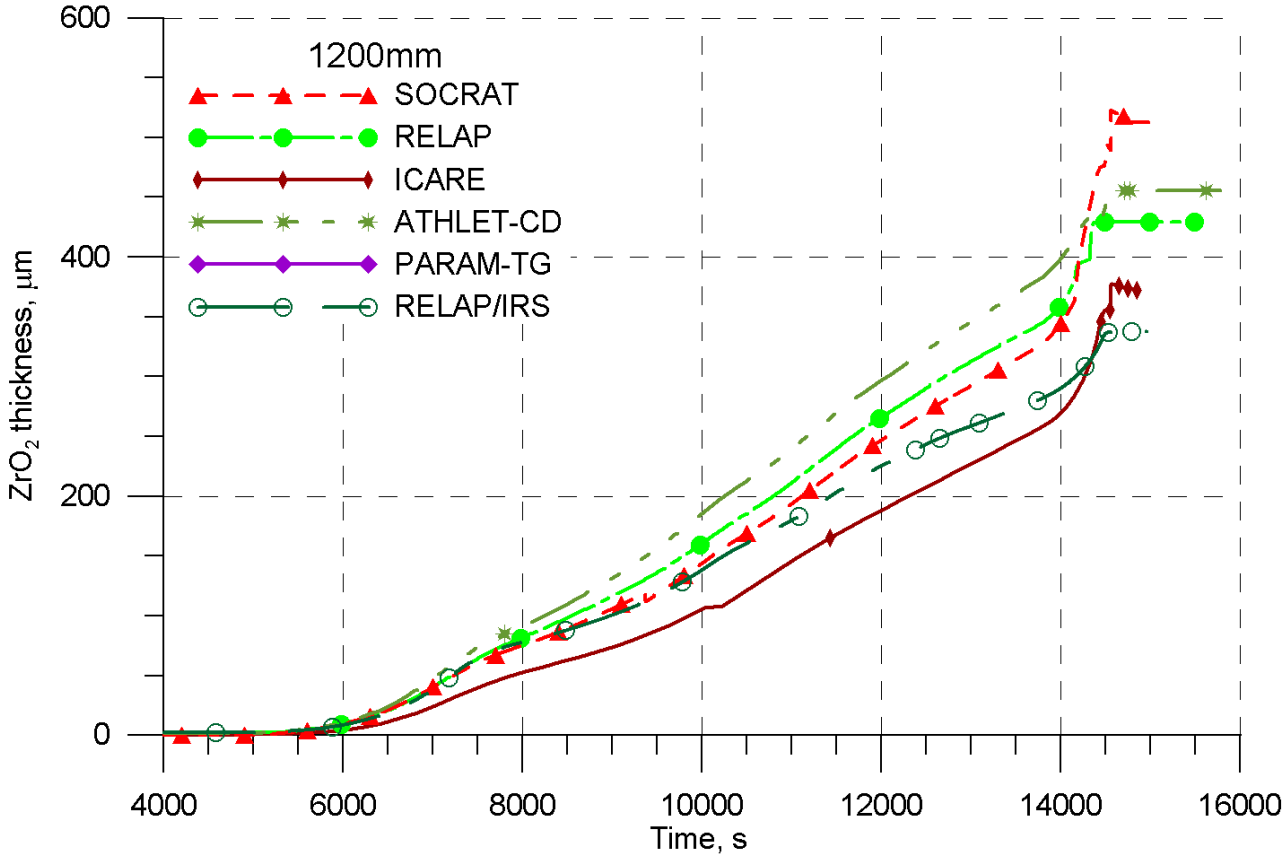

Figure 3.64. Thickness of zirconium oxide scale at the elevation of 1200 mm. PARAMETER-SF3 experiment. Post-test calculations.

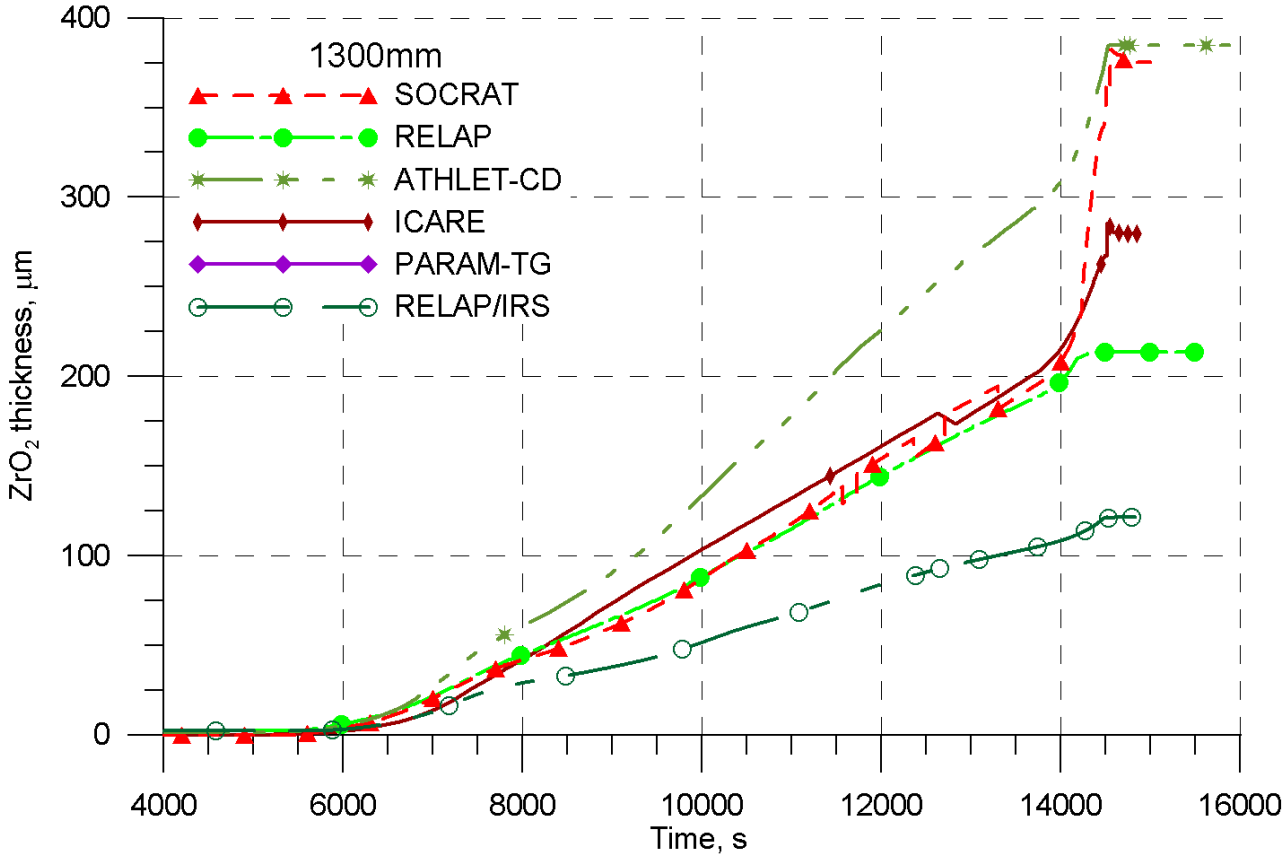

Figure 3.65. Thickness of zirconium oxide scale at the elevation of 1300 mm. PARAMETER-SF3 experiment. Post-test calculations.

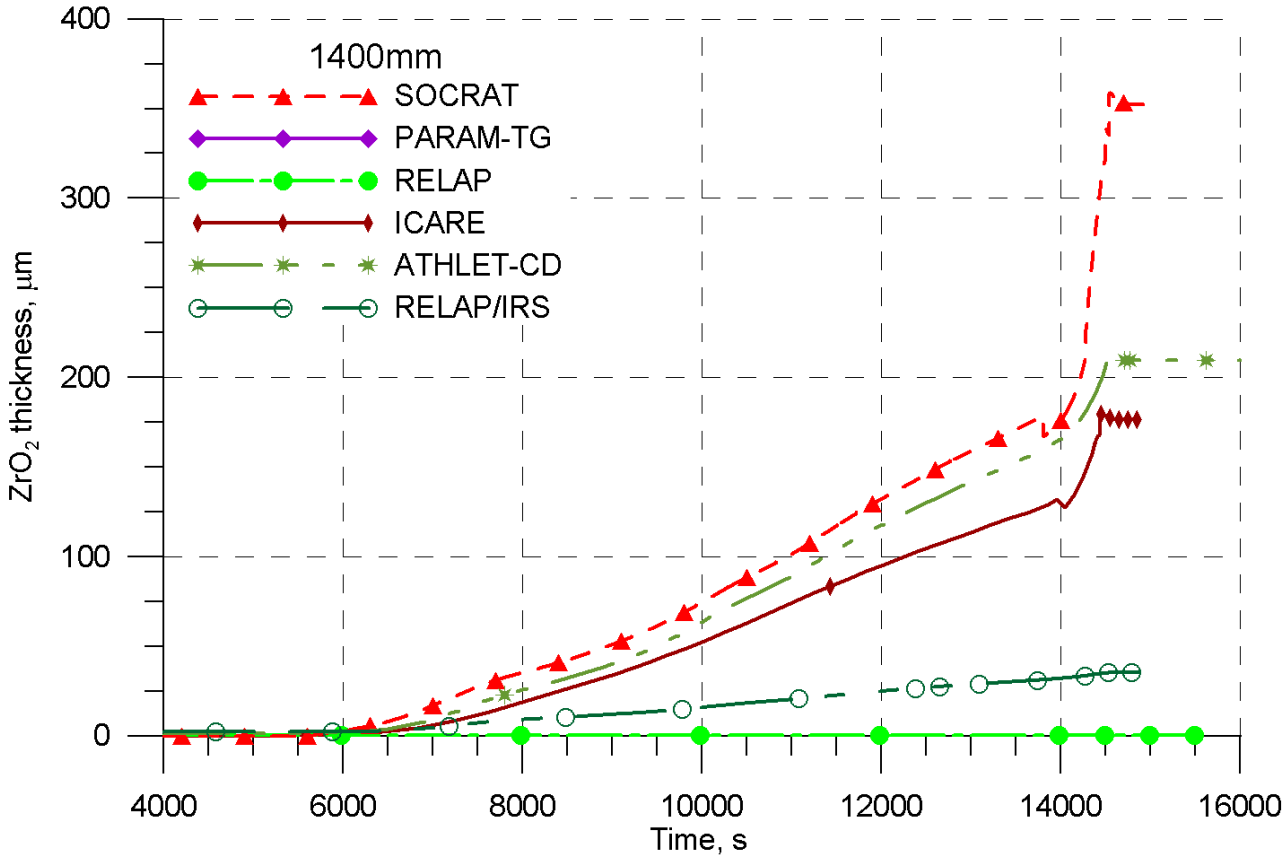

Figure 3.66. Thickness of zirconium oxide scale at the elevation of 1400 mm. PARAMETER-SF3 experiment. Post-test calculations.

4 CONCLUSION

Within the framework of ISTC Project #3690 the pre- and post-test calculations of experiments PARAMETER-SF2 (post-test analysis), -SF3 were performed With this aim the widely used computer code for NPP safety assessment (SOCRAT, ICARE/CATHARE, RELAP/SCDAPSIM MOD3.2) were applied, as well as engineering code PARAM-TG, developed directly for numerical analysis of PARAMETER facility. Collaborators of the Project also took part in calculational studies - GRS (Germany), using ATHLET-CD code, and PSI (Switzerland) with the code SCDAP/RELAP/FZK-PSI.

On the basis of post-test study of PARAMETER-SF2 experiment some limitations were revealed concerning capability of codes to describe definite processes occurring in the course of the experiment, but, on the whole, the calculation results are indicative of the fact that there is a good agreement with experimental data. Experience in SF2 simulation was used in the analysis of PARAMETER-SF3 experiment.

In the course of pre-test numerical analysis the justification was made for the scenario of PARAMETER-SF3 experiment planned in the Work Plan of the Project. Results of pre-test studies, including the analytical work done on revealing the most important factors of uncertainty, allowed to obtain the main initial and boundary parameters of the experiment. In spite of some differences in temperature and physical-chemical behaviour, obtained by various participants of the pre-test studies, we observed, on the whole, a rather consistent time history picture of the experiment.

The pre-test studies made it possible, on the whole, to carry out the heating-up and pre-oxidation phases in PARAMETER-SF3 experiment and to bring the facility to the stage of heating-up at the required rate of temperature rise. The top flooding turned out successful. This is an additional proof of capability of computational means to predict adequately the integral behaviour in the top flooding experiment.

Results of the post-test calculational analysis, performed within the framework of ISTC Project #3690, showed that in spite of complexity of the experiments, the sets of experimental data are in mutual consistency and can be used in verification of the codes, their thermohydraulic models and physical-chemical models under severe accident conditions including the flooding stage.

5 REFERENCES

1 Specification of the PARAMETER-SF3 Experiment (investigation of overheated VVER fuel rods bundle under top flood conditions). ISTC Project #3690.

2 Hofmann P., Homann C., Leiling W., Miassoedov A., Piel D., Schanz G., Schmidt L., Sepold L., Steinbrueck M., Experimental and Calculational Results of the Experiments QUENCH-02 and QUENCH-03, FZKA 6295, Forschungszentrum Karlsruhe, July 2000.

3 Homann C., Hering W., Schanz G., Analysis and Comparison of Experimental Data of Bundle Tests QUENCH-07 to QUENCH-09 about B4C Control Rod Behaviour, FZKA 7101, Forschungszentrum Karlsruhe, July 2006.

4 Schanz G., Heck M., Hozer Z. et al. Results of the QUENCH-10 Experiment on Air Ingress, FZKA 7087, SAM-LACOMERA-D09, Forschungszentrum Karlsruhe, May 2006.

5 Hering W., Groudev P., Heck M., Homann C., Schanz G., Sepold L., Stefanova A., Stegmaier U., Steinbrueck M., Steiner H., Stuckert J. Results of Boil-off Experiment QUENCH-11, FZKA 7247, SAM-LACOMERA-D18, Forschungszentrum Karlsruhe, June 2007.

6 Protocol of PARAMETER-SF1 Experiment results, ISTC Project #3194, 2006.

7 Protocol on the results of PARAMETER-SF2 experiment, ISTC Project #3194, 2007.

8 Protocol on the results of PARAMETER-SF3 experiment, ISTC Project #3690, 2007.

9 "Tests of fuel assemblies under severe accident conditions (PARAMETER-SF series)", Final report on R&A, ISTC Project #3194, FSUE SRI SIA "LUCH", Moscow, 2007.

10 "Analysis of material studies of WWER-1000 model assembly tested at the paraMETER-SF2 experiment under the conditions of severe accident with top and bottom flooding". Report on scientific work under ISTC Project No.3690, FSUE SRI SIA "LUCH", 2008.

11 A. Volchek, Yu Zvonarev, "Modelling improvement of ICARE/CATHARE for VVERs and associated code assessment", Technical Note IRSN/DPAM/SEMCA 2006/247, August 2006.

12 H.Austregesilo, Ch. Bals, "PARAMETER-SF3 pre-test calculation with ATHLET-CD", Meeting of ISTC Project #3690: PARAMETER, Moscow, Russia, 14-16 July 2008.

13 Jon Birchley, Tim Haste, "PSI analytical support for PARAMETER-SF4: Status and Plans", Meeting of ISTC Project #3690: PARAMETER, Moscow, Russia, 14-16 July 2008.

14 A. Volchek, Yu Zvonarev, "PARAMETER-SF2 Analyses using ICARE2 V3 Mod2 and ICARE/CATHARE V2", Third ICARE/CATHARE Users' Club Meeting, Aix-en-Provence, France, April 24-25, 2008.

15 Analysis of behaviour of the model FA temperature measurement system in tests under severe accident conditions in PARAMETER-SF1 experiment, Report of FSUE SRI SIA "LUCH", 2007.

16 Viktorov M.M. Methods of calculation of physical-chemical values and applied calculations. L.: Publishing House "Khimiya", 1977, P. 245.

17 Petukhov B.S., Genin L.G., Kovalev S.A. Heat transfer in nuclear power installations. M.: Energoatomizdat, 1986, P. 472.

18 Labuntsov D.A. Some issues of heat transfer theory under laminar liquid flow in tubes. Teploenergetika, 1958, N 3, c. 87.

19 Bogoslovskaya G.P., Karpenko A.A., Kirillov P.L. Computer code MIF-SKD for thermohydraulic calculation of the core in reactor cooled with water of supercritical pressure. Teploenergetika, 2009, No.3, PP. 34-37.

20 Marcoczy G. Konvektive Warmeubertragung in langsangestromten Stabbundeln bei turbulenter Stromung. Warme- und Stroffubertrag, 1972, Bd. 5, N 4, S. 204-212.

21 Osmachkin V.S. Features of heat transfer in nuclear reactors cooled with incompressible unboiling liquids. Report P/326 (USSR). Third International Conference on Peaceful Utilization of Atomic Energy, Geneva, 1964.

22 Wallis G.B. One-Dimensional Two-Phase Flow. McGraw Hill, 1969.

23 Sudo Y., Kaminaga M. Analytical Study on Mechanism and Predominant Parameter Effects of Countercurrent Flow Limitation in Vertical Channels. Proc. of the 3rd Int.Conf. on Nuclear Engineering ICONE-3. April 23-27, 1995, Kyoto, Japan, v.1, p.223-228.

24 Bharathan D. et al. EPRI Report NP-1165, 1979.

25 Yegorova L., Lioutov K., Jouravkova N., Konobeev A., Smirnov V., Chesanov V., Goryachev A. Experimental Study of Embrittlement of Zr-1%Nb VVER Cladding under LOCA-Relevant Conditions. International Agreement Report, NUREG/IA-0211, IRSN 2005-194, NSI RRC KI 3188, March 2005.

26 Bibilashvili Yu.K., Sokolov N.B., Andreyeva-Andrievskaya L.N., Salatov A.V. High-Temperature Interaction of Fuel Rod Cladding Material (Zr1%Nb Alloy) with Oxygen-Containing Mediums. IAEA-TECDOC-921, Dimitrovgrad, 1995, p.117-128.